

THERMAL CRACKING OF LOW-TEMPERATURE LIGNITE PITCH

John S. Berber, Richard L. Rice, and Delmar R. Fortney

U. S. Department of the Interior, Bureau of Mines,
Morgantown Coal Research Center, Morgantown, West Virginia

INTRODUCTION

The tar used in this study was produced by the Texas Power & Light Company from a Texas lignite carbonized at about 500° C in a fluidized bed. The pitch, as used in this research program, is the tar distillation residue boiling above 350° C. This pitch is about 40 to 50 percent of the crude tar. Pitch is a complex resinous mass of polymerized and polycondensed compounds (1). It is an amorphous solid material and quite brittle at room temperature. The pitch analyses average 84 percent carbon, 8 percent hydrogen, 5 percent oxygen, and 1 percent each of nitrogen and sulfur. It is chemically similar to the tar from which it is prepared, being mainly mixtures of the higher homologs of the compounds contained in the distillable fractions of the tar.

The pitch is potentially useful as a binder in the manufacture of products such as roofing cement, metallurgical electrodes, asphalt paving, and pitch fibre pipe, if its characteristics can be modified by physical and chemical techniques to approximate those of asphalt and bituminous binders (3).

Researchers of the Bureau of Mines, U. S. Department of the Interior, have investigated three methods for changing the lignite pitch characteristics.

Air-blowing, which is used successfully to treat bituminous pitch by lowering the hydrogen content and increasing the softening point and the penetrability, was not too effective with lignite pitch (1, 2).

Catalytic dehydrogenation (6) was found to be effective in reducing the hydrogen content of the pitch, but catalyst cost per pound of treated pitch is high, and the catalyst recovery cost would be prohibitive.

Thermal cracking has proven to be the most effective in changing the pitch characteristics. This report covers the preliminary work done on thermal cracking of pitch and shows the variety of products that may be obtained.

Thermal cracking is widely used in the petroleum industry, particularly for the production of olefins. Thermal cracking has also been used in the treatment of coal tar (4, 5), but seldom has been used in the treatment of pitch. The successful treatment of pitch by this process could upgrade the pitch into metallurgical coke, binders, oxidation feedstock for phthalic and maleic anhydrides, and gases such as hydrogen, methane, and ethylene.

The binding ability of the cracked pitch and oil distillation pitch can be determined by the quality of metallurgical electrodes produced using the pitches as binders. Many factors affect the binding properties of the materials being

used as binders, with different producers and consumers using entirely different standards, so the electrode quality tests were used to help evaluate the effectiveness of thermal cracking of the lignite pitch.

EQUIPMENT

The thermal cracking system is shown in figures 1 and 2. The feed tank (figure 2, A) is made from a 13-in. length of 10-in. diameter schedule 40 pipe, to which a cone has been added for the bottom. The tank is heated by commercial electric heaters. The feed pump (B) is a small gear pump with a variable speed drive. The thermocracker (D) is a 4-1/2 ft-length of 2-1/2-in. diameter schedule 40, type 304, stainless-steel pipe, heated by external electric heaters. The heaters are controlled by outside surface thermocouples welded to the reactor. The receiver (E) is a 20-in. length of 4-in. diameter schedule 40 pipe. The receiver is flanged so that it can be bolted to the bottom of the reactor. The condenser (F) is a 30-in. length of 6-in. diameter pipe, swaged at the bottom end to 1-in. diameter and flanged at the top. The top flange supports a water-cooled tube which inserts into the condenser body in the manner of a cold finger. The knockout (G) is a 34-in. length of a 2-in. diameter pipe having a tangential gas inlet about 8-in. from the bottom. The scrubber (H) is a 30-in. length of a 4-in. diameter pipe having a water-spray nozzle near the top. The water from the scrubber drains into a standpipe water-seal tank (I). The water-seal tank is a piece of 6-in. diameter pipe. The gas meter (J) is a laboratory-type wet-test meter capable of metering 1,000 cu ft of gas at standard conditions.

PROCEDURE

Lignite pitch at 200° C was pumped from the feed tank through electrically heated lines into the top of the thermocracker. The temperature of the thermocracker was maintained at approximately 790° C as indicated by the outside surface thermocouples. At the end of a run, the flow of pitch was stopped and the pump was flushed with a low-boiling tar fraction to keep the impeller of the pump from freezing. Reactions within the cracker produced coke, cracked pitch, oil, and gas. Both the top and bottom of the cracker were removed, and coke was removed from the sides and weighed. Cracked pitch caught in the receiver was weighed and analyzed. The oil removed by the condenser and knockout chamber was weighed and then distilled to 400° C, leaving a pitch residue. This pitch residue was analyzed and, if found to have the desired carbon-to-hydrogen atomic ratio (1.20 to 1.80), was used as a binder for electrodes. Distillate from the oil may be oxidized to phthalic and maleic anhydrides or separated into acids, bases, and neutral oils. Gas from the cracker was cooled and scrubbed, then metered, sampled, and analyzed by gas chromatography.

RESULTS AND DISCUSSION

Results of the thermal cracking tests are given in tables 1 to 4. Of the four major products obtained from the pitch--coke, cracked pitch, oil, and gas--the coke averaged about 15 to 25 percent of the feed to the cracker, the cracked pitch amounted to about 20 to 40 percent, the oil was about 20 to 30 percent, while the balance of the feed to the cracker consisted of gas.

Distribution and yield rates of products (figures 3 to 6) are as expected considering the reaction within the cracker at different crude pitch feed rates. As the pitch is heated it begins to vaporize, and the turbulence of the vapors splashes some of the fluid onto the hot wall where it sticks and is coked. If enough heat is available, the rest of the pitch is vaporized and cracked. As the cracked materials leave the hot zone, heavy high-boiling materials condense immediately and collect in the receiver as cracked pitch; the oil and gas vapors pass on to the condenser. If there is not enough heat available to vaporize all of the pitch fed to the cracker, the unvaporized portion flows through the hot zone and into the receiver without being completely cracked. Such is the case when the crude pitch feed rate is high, the residence time in the cracker being shorter and less time being available for heat to penetrate the interior of the pitch mass. High crude pitch rates also lower the temperature inside the cracker, reducing the amount of coke formed.

Figures 3 and 4 appear to reflect these effects. The coke rate increases more slowly and the cracked pitch rate increases more rapidly than does the crude pitch feed rate. Since the gases are formed by several reactions, each related to the degree of cracking and coking, the gas production rate decreases with the increase in crude pitch feed rate (figure 5). Gases are produced by coking of pitch adhering to the cracker wall, then these gases are cracked to produce hydrogen and olefins. In addition to gas produced from coke, other gases are produced by devolatilization and thermal cracking of the pitch and are also subjected to further cracking. A significant amount of ethylene was produced in the cracker.

Oil produced in the cracker, upon distillation, yielded a pitch residue potentially useful as electrode binder, paving material, pitch fibre pipe, or roofing material, along with a distillate that can be further treated to give valuable chemical intermediates. Table 3 gives characteristics of the pitch residue and some preliminary data on electrodes made with the pitch as binder. The decrease in carbon-to-hydrogen atomic ratio of the pitch residue in relation to the crude pitch feed rate (figure 7) again reflects the inhibition of cracking by relatively high crude pitch feed rates.

The oil is produced in two ways--by cracking of the pitch, the most desirable method, and by devolatilization of pitch without cracking. This is the reason why the oil production rate can increase approximately in proportion to the crude pitch feed rate (figure 6). However, the quality of the oil decreases with decrease in degree of cracking, as is shown by the drop in the carbon-to-hydrogen atomic ratio.

CONCLUSIONS

Thermal cracking of low-temperature lignite tar pitch converted the pitch into a material that served as a satisfactory binder in the manufacture of carbon electrodes. Compressive strength and electrical resistivity of the resulting electrodes fell within acceptable ranges. Crude pitch feed rate to the thermo-cracker significantly affected the rate of formation of products and the composition of the pitch residue from distillation of oil produced in the cracker.

REFERENCES

1. Berber, John S., and Richard L. Rice. Oxidation of a Low-Temperature Lignite Tar Pitch. Preprints, Div. of Fuel Chemistry, Am. Chem. Soc., v. 8, No. 3, Aug. 31-Sept. 3, 1964, pp. 145-151.
2. Chelton, H. M., R. N. Traxler, and J. W. Romberg. Oxidized Asphalts in a Vertical Pilot Plant. Ind. and Eng. Chem., v. 51, No. 11, November 1959, pp. 1353-1354.
3. Greenhow, E. J., and Galina Sugowdz. The Chemical Composition of Coal-Tar Pitch. Coal Research in CSIRO, No. 15, November 1961, pp. 10-19.
4. Montgomery, R. S., D. L. Decker, and J. C. Mackey. Ethylene and Aromatics by Carbonization of Lignite. Ind. and Eng. Chem., v. 51, No. 10, October 1959, pp. 1293-1296.
5. Naugle, B. W., C. Ortuglio, L. Mafrica, and D. E. Wolfson. Steam-Fluidized Low-Temperature Carbonization of High Splint Bed Coal and Thermal Cracking of the Tar Vapors in a Fluidized Bed. BuMines Rept. of Inv. 6625, 1965, 22 pp.
6. Rice, Richard L., and John S. Berber. Catalytic Dehydrogenation of Low-Temperature Lignite Pitch. Presentation, Div. of Fuel Chemistry, Am. Chem. Soc., March 22-31, 1966.

used as binders, with different producers and consumers using entirely different standards, so the electrode quality tests were used to help evaluate the effectiveness of thermal cracking of the lignite pitch.

EQUIPMENT

The thermal cracking system is shown in figures 1 and 2. The feed tank (figure 2, A) is made from a 13-in. length of 10-in. diameter schedule 40 pipe, to which a cone has been added for the bottom. The tank is heated by commercial electric heaters. The feed pump (B) is a small gear pump with a variable speed drive. The thermocracker (D) is a 4-1/2 ft-length of 2-1/2-in. diameter schedule 40, type 304, stainless-steel pipe, heated by external electric heaters. The heaters are controlled by outside surface thermocouples welded to the reactor. The receiver (E) is a 20-in. length of 4-in. diameter schedule 40 pipe. The receiver is flanged so that it can be bolted to the bottom of the reactor. The condenser (F) is a 30-in. length of 6-in. diameter pipe, swaged at the bottom end to 1-in. diameter and flanged at the top. The top flange supports a water-cooled tube which inserts into the condenser body in the manner of a cold finger. The knockout (G) is a 34-in. length of a 2-in. diameter pipe having a tangential gas inlet about 8-in. from the bottom. The scrubber (H) is a 30-in. length of a 4-in. diameter pipe having a water-spray nozzle near the top. The water from the scrubber drains into a standpipe water-seal tank (I). The water-seal tank is a piece of 6-in. diameter pipe. The gas meter (J) is a laboratory-type wet-test meter capable of metering 1,000 cu ft of gas at standard conditions.

PROCEDURE

Lignite pitch at 200° C was pumped from the feed tank through electrically heated lines into the top of the thermocracker. The temperature of the thermocracker was maintained at approximately 790° C as indicated by the outside surface thermocouples. At the end of a run, the flow of pitch was stopped and the pump was flushed with a low-boiling tar fraction to keep the impeller of the pump from freezing. Reactions within the cracker produced coke, cracked pitch, oil, and gas. Both the top and bottom of the cracker were removed, and coke was removed from the sides and weighed. Cracked pitch caught in the receiver was weighed and analyzed. The oil removed by the condenser and knockout chamber was weighed and then distilled to 400° C, leaving a pitch residue. This pitch residue was analyzed and, if found to have the desired carbon-to-hydrogen atomic ratio (1.20 to 1.80), was used as a binder for electrodes. Distillate from the oil may be oxidized to phthalic and maleic anhydrides or separated into acids, bases, and neutral oils. Gas from the cracker was cooled and scrubbed, then metered, sampled, and analyzed by gas chromatography.

RESULTS AND DISCUSSION

Results of the thermal cracking tests are given in tables 1 to 4. Of the four major products obtained from the pitch--coke, cracked pitch, oil, and gas--the coke averaged about 15 to 25 percent of the feed to the cracker, the cracked pitch amounted to about 20 to 40 percent, the oil was about 20 to 30 percent, while the balance of the feed to the cracker consisted of gas.

Distribution and yield rates of products (figures 3 to 6) are as expected considering the reaction within the cracker at different crude pitch feed rates. As the pitch is heated it begins to vaporize, and the turbulence of the vapors splashes some of the fluid onto the hot wall where it sticks and is coked. If enough heat is available, the rest of the pitch is vaporized and cracked. As the cracked materials leave the hot zone, heavy high-boiling materials condense immediately and collect in the receiver as cracked pitch; the oil and gas vapors pass on to the condenser. If there is not enough heat available to vaporize all of the pitch fed to the cracker, the unvaporized portion flows through the hot zone and into the receiver without being completely cracked. Such is the case when the crude pitch feed rate is high, the residence time in the cracker being shorter and less time being available for heat to penetrate the interior of the pitch mass. High crude pitch rates also lower the temperature inside the cracker, reducing the amount of coke formed.

Figures 3 and 4 appear to reflect these effects. The coke rate increases more slowly and the cracked pitch rate increases more rapidly than does the crude pitch feed rate. Since the gases are formed by several reactions, each related to the degree of cracking and coking, the gas production rate decreases with the increase in crude pitch feed rate (figure 5). Gases are produced by coking of pitch adhering to the cracker wall, then these gases are cracked to produce hydrogen and olefins. In addition to gas produced from coke, other gases are produced by devolatilization and thermal cracking of the pitch and are also subjected to further cracking. A significant amount of ethylene was produced in the cracker.

Oil produced in the cracker, upon distillation, yielded a pitch residue potentially useful as electrode binder, paving material, pitch fibre pipe, or roofing material, along with a distillate that can be further treated to give valuable chemical intermediates. Table 3 gives characteristics of the pitch residue and some preliminary data on electrodes made with the pitch as binder. The decrease in carbon-to-hydrogen atomic ratio of the pitch residue in relation to the crude pitch feed rate (figure 7) again reflects the inhibition of cracking by relatively high crude pitch feed rates.

The oil is produced in two ways--by cracking of the pitch, the most desirable method, and by devolatilization of pitch without cracking. This is the reason why the oil production rate can increase approximately in proportion to the crude pitch feed rate (figure 6). However, the quality of the oil decreases with decrease in degree of cracking, as is shown by the drop in the carbon-to-hydrogen atomic ratio.

CONCLUSIONS

Thermal cracking of low-temperature lignite tar pitch converted the pitch into a material that served as a satisfactory binder in the manufacture of carbon electrodes. Compressive strength and electrical resistivity of the resulting electrodes fell within acceptable ranges. Crude pitch feed rate to the thermo-cracker significantly affected the rate of formation of products and the composition of the pitch residue from distillation of oil produced in the cracker.

REFERENCES

1. Berber, John S., and Richard L. Rice. Oxidation of a Low-Temperature Lignite Tar Pitch. Preprints, Div. of Fuel Chemistry, Am. Chem. Soc., v. 8, No. 3, Aug. 31-Sept. 3, 1964, pp. 145-151.
2. Chelton, H. M., R. N. Traxler, and J. W. Romberg. Oxidized Asphalts in a Vertical Pilot Plant. Ind. and Eng. Chem., v. 51, No. 11, November 1959, pp. 1353-1354.
3. Greenhow, E. J., and Galina Sugowdz. The Chemical Composition of Coal-Tar Pitch. Coal Research in CSIRO, No. 15, November 1961, pp. 10-19.
4. Montgomery, R. S., D. L. Decker, and J. C. Mackey. Ethylene and Aromatics by Carbonization of Lignite. Ind. and Eng. Chem., v. 51, No. 10, October 1959, pp. 1293-1296.
5. Naugle, B. W., C. Ortuglio, L. Mafrika, and D. E. Wolfson. Steam-Fluidized Low-Temperature Carbonization of High Splint Bed Coal and Thermal Cracking of the Tar Vapors in a Fluidized Bed. BuMines Rept. of Inv. 6625, 1965, 22 pp.
6. Rice, Richard L., and John S. Berber. Catalytic Dehydrogenation of Low-Temperature Lignite Pitch. Presentation, Div. of Fuel Chemistry, Am. Chem. Soc., March 22-31, 1966.

TABLE 1. - Gas products from thermal cracking of low-temperature lignite tar pitch

Run no.	Crude pitch rate, pph	Gas rate, scfh	Constituents in gas, pct								
			N ₂	O ₂	CO ₂	CO	H ₂	CH ₄	C ₂ H ₆	C ₂ H ₄	C ₃ +
35	2.0	16.7	49.35	0.76	0.45	4.12	21.99	19.67	0.44	2.37	0.85
37	6.0	37.0	8.77	.15	.96	8.38	15.80	42.19	4.30	14.05	5.40
38	9.0	45.2	5.06	.09	.81	7.29	22.63	37.32	4.98	12.63	9.19
43	10.0	51.3	8.35	.09	.80	7.40	20.08	37.94	4.64	12.78	8.12
40	11.0	51.4	1.13	.21	.80	7.49	37.96	35.74	2.64	11.53	2.50
30	13.1	55.1	1.17	.14	.83	7.91	30.52	41.33	3.73	12.08	2.29
42	17.0	66.6	9.84	.08	1.28	7.42	19.96	36.18	5.04	12.76	7.44
41	21.0	76.2	17.28	.13	.92	6.82	14.02	34.88	4.44	14.76	6.75

TABLE 2. - Coke, pitch, and oil products from thermal cracking of low-temperature lignite tar pitch

Run no.	Feed rate, pph	Coke rate, pph	Cracked pitch rate, pph	Oil rate, pph	Distillate from oil, wt pct	Anhydrides from distillate, wt pct		Composition of distillate, vol pct		
						FAA ¹	MAA ²	Acids	Bases	Neutral oil
35	2.0	0.8	0.2	0.8	40.3	16.4	14.5	10.5	6.0	83.5
37	6.0	1.4	1.4	1.4	27.2	17.0	14.4	10.0	8.0	82.0
38	9.0	2.0	2.0	2.2	29.1	11.7	15.2	10.0	7.0	83.0
43	10.0	2.0	3.6	2.6	34.4	10.1	13.9	13.5	5.0	81.5
40	11.0	2.2	3.2	3.6	32.6	11.0	12.8	15.0	5.0	80.0
30	13.1	2.4	3.3	4.1	27.8	14.3	13.8	-----	---	-----
42	17.0	3.0	6.2	5.6	25.9	10.6	14.4	12.5	4.0	83.5
41	21.0	3.8	13.4	7.2	25.9	8.0	12.9	15.0	5.0	80.0

1/ Phthalic anhydride.

2/ Maleic anhydride.

TABLE 3. - Characteristics of pitch and electrodes

Run no.	Crude pitch rate, pph	Oil, wt pct	Pitch from oil, wt pct	Properties of pitch			Properties of electrodes			
				Carbon, wt pct	Hydrogen, wt pct	C/H ratio	Softening point, °C	Coke type	Strength, kg/cm ²	Resistivity, ohm-cm
35	2.0	40.0	56.6	85.63	5.60	1.27	110			
37	6.0	23.3	71.0	88.86	4.69	1.58	145			
38	9.0	24.4	68.5	85.55	5.84	1.22	100	Lignite ^{1/}	183	0.0220
43	10.0	26.0	62.9	85.67	6.00	1.19	115	Petroleum	242	.0076
40	11.0	32.7	66.3	85.60	5.90	1.21	104	Lignite ^{2/}	355	.0180
30	13.1	31.3	68.3	85.81	6.37	1.46	116	Petroleum	323	.0074
42	17.0	32.9	72.6	82.12	7.51	.91	65			
41	21.0	34.3	72.6	81.90	7.57	.90	65			

1/ Uncalcined lignite pitch coke.

2/. Calcined lignite pitch coke.

TABLE 4. - Material balance for thermal cracking of low-temperature lignite pitch

Run no.	Crude pitch rate, pph	Coke rate, pph	Cracked pitch rate, pph	Oil rate, pph	Gas rate, pph	Total, pph	Gain or loss, pph	Recovery, pct
35	2.0	0.8	0.2	0.8	0.9	2.7	+ 0.7	35.0
37	6.0	1.4	1.4	1.4	1.9	6.1	+ .1	1.7
38	9.0	2.0	2.0	2.2	2.2	8.4	- .6	6.7
43	10.0	2.0	3.6	2.6	2.6	10.8	+ .8	8.0
40	11.0	2.2	3.2	3.6	1.9	10.9	- .1	.9
30	13.1	2.4	3.3	4.1	2.2	12.0	- 1.1	8.4
42	17.0	3.0	6.2	5.6	3.4	18.2	+ 1.2	7.1
41	21.0	3.8	13.4	7.2	4.2	28.6	+ 7.6	36.2

- A-Feed tank
- B-Thermocracker
- C-Receiver
- D-Condenser
- E-Scrubber

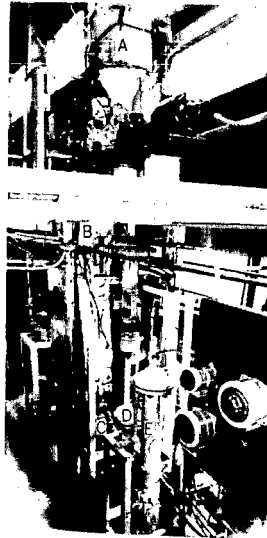


FIGURE 1. - Pitch Thermal Cracking Apparatus.

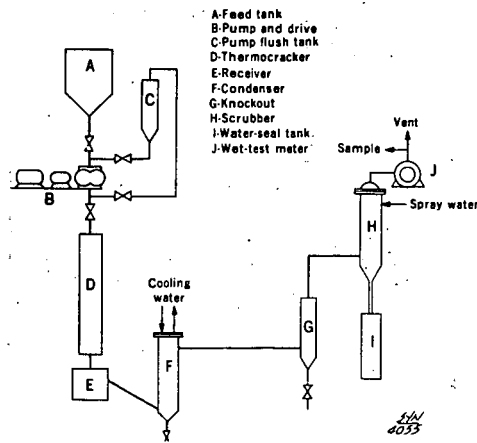


FIGURE 2. - Thermal Cracking System.

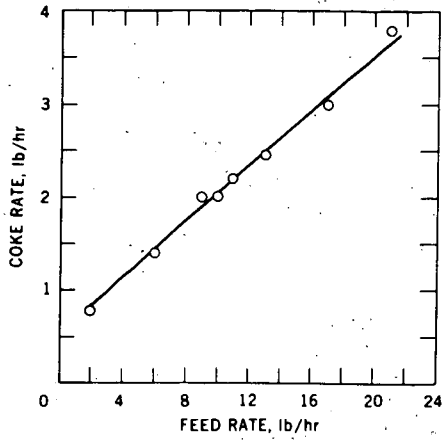


FIGURE 3. - Coke Rate Based on Crude Pitch Feed Rate - Thermal Cracking.

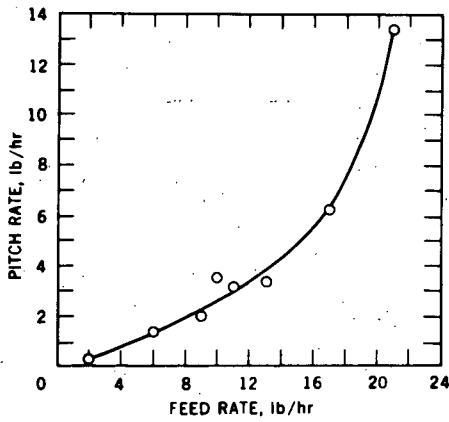


FIGURE 4. - Product Pitch Rate Based on Crude Pitch Feed Rate - Thermal Cracking.

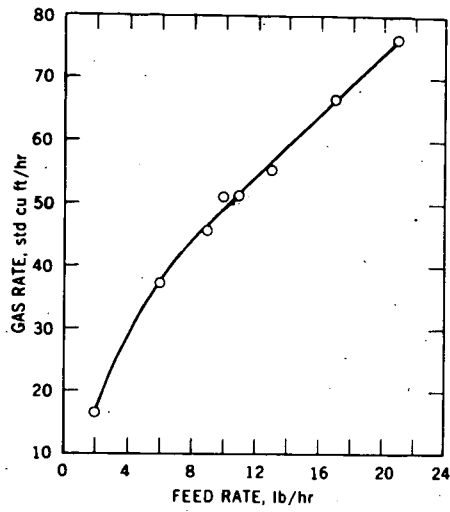


FIGURE 5. - Gas Production Rate Based on Crude Pitch Feed Rate - Thermal Cracking.

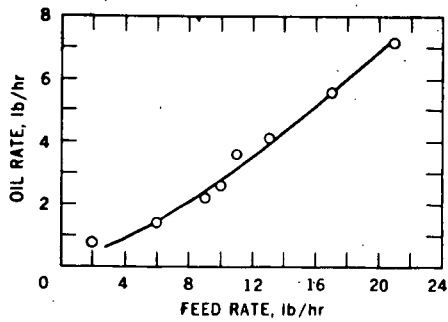


FIGURE 6. - Oil Rate Based on Crude Pitch Feed Rate - Thermal Cracking.

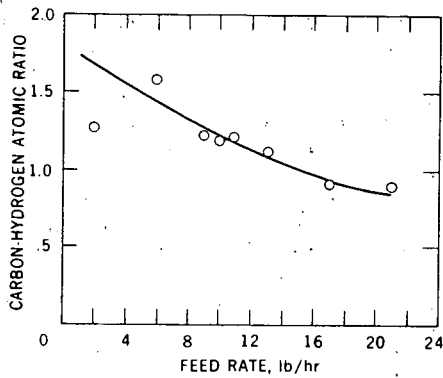


FIGURE 7. - Carbon-to-Hydrogen Atomic Ratio of Oil Distillation Residue Based on Crude Pitch Feed Rate.

378
COAL DEASHING AND HIGH-PURITY COKE

Ward J. Bloomer , The Lummus Company, Newark, N. J. and
F. L. Shea, Great Lakes Research Corp., Elizabethton, Tennessee

Introduction

In 1957, The Lummus Company and Great Lakes Carbon Corporation began a joint investigation into the use of coal as a source of high-purity coke. The process involved the production of a low-ash, low-sulfur deashed coal solution from high volatile bituminous coal, and the conversion of this coal solution into coke using a modification of the Lummus delayed coking operation. (1)

Experimental work on a bench scale was initiated in 1958 and completed in 1961. The experimental scope was expanded to include the production of deashed coal as well as the high-purity coke in either combined or alternate operations.

Bench programs were carried out on several scales of operation. A continuous (block operation) pilot plant was built and operated to confirm the bench work. This unit was capable of processing coal continuously at approximately 200 pounds per hour through the filtration step. At this point, the filtrate was stored for further continuous processing to either deashed coal product (performed in 150-200 pound quantities) or high-purity coke (500 pound quantities).

Summary

A process has been developed to upgrade the quality of coal to a low-ash, low-sulfur, low-chloride product. As a fuel, this material would result in reduced capital and operating costs for power stations. Investment costs would be reduced, due to the higher heating value and cleaner fuel. Operating costs would be reduced by charges associated with the transportation of ash, ash handling and disposal costs, lower maintenance costs, and fly ash removal costs. The substantial reduction in sulfur, ash, and volatile matter would greatly minimize air pollution.

Other potential applications are for use in gas turbines, as a reductant, as a raw material for synthesis gas, as an ingredient in preparing coal blends for metallurgical coke, or for high-purity coke.

The economic potential of the process in its present stage of development is covered in Table 5. The process has certain aspects requiring sustained demonstration efforts to obtain firm economic bases.

Process Description

Figure 1 shows a schematic flowsheet for the production of either deashed coal or high-purity coke as investigated in this program.

Deashed Coal - Crushed, ground and dried raw coal is fed to agitated premix tanks where it is mixed with warm solvent. The slurry is pumped through an extraction heater and thence through either in-line reaction tubes or to agitated digestion tanks. Digestion was investigated over the temperature range of 650 to 850°F and over a pressure range of 75 to 135 psig. Residence times varied from three minutes to two hours. Solvent-to-coal ratios were varied from 1:1 to 4:1

From the digestion tanks, the coal dispersion is fed to a rotary pressure precoat filter designed for operating at 100 psig and 700°F. Washing provisions are included.

The filter cake (2) is discharged into a cake receiver. Filtrate and wash are collected and fed to the product and solvent recovery operations. Vapors from the filtrate receiver are compressed, heated and recycled to maintain pressure on the feed side of the filter drum.

Filtrate flows through the filtrate heaters into a vacuum product recovery unit. Vapors from this unit pass to a flash tower where the bottom stream is all solvent for recycle. A side stream is taken off and in part is used for solvent make-up with the remainder processed for by-product recovery.

Overhead vapors from the flash tower are condensed, and a low boiling fraction recovered as a by-product. Vapors flashing from the filtrate receiver are condensed and introduced as reflux into the bottom section of the flash tower.

Filter cake is calcined and the spent cake used as fuel for the process. Gas and distillate vapors from the kiln combined with gases from the filtrate receiver and flash tower overheads are passed into a light oil scrubber. The absorption oil -- the intermediates cut from the flash tower -- is stripped in the flash tower. Light oil fractions leave the system from a decanter on the flash tower overhead stream. Gas from the light oil scrubber is used for process heat.

High-Purity Coke - For coke product the same flow pattern prevails through the filtrate receiver. The filtrate is pumped to a coking heater and thence to coke drums. Overhead vapors from the coke drums pass to a combination tower where recycle solvent and by-product fractions are recovered. Overhead vapors from the tower pass

through a condenser, gas separator, and thence to a light oil scrubber.

The above operations were investigated on both a bench and pilot plant scale with the exception of cake calcining which was performed only on bench scale. Variables investigated are discussed in the following sections.

Process and Operating Variables for Deashed Coal

A review of our work on solvent deashing indicated the operating conditions necessary to optimize the process. These may be briefly summarized:

1. The development of a stable, high-extractive-efficiency solvent capable of essentially complete recovery in the vacuum recovery unit to yield deashed coal was accomplished by special treatment of a high-boiling coal tar distillate. The required solvent having excellent temperature stability and high solvent power was attained by refractorizing the high-boiling coal tar distillate, employing recycle thermal decomposition and fractionation to eliminate the less refractory and low-boiling constituents. Gratuitously, these are the less effective extraction components.

2. Recovery of from 88 to 95 weight percent of the available carbonaceous matter at extractor pressures in the range of 5 to 8 atmospheres and with solvent-to-coal ratios in the range of 2 or 3:1 was achieved using the refractorized solvent with a boiling range of 600 to 900°F. Typical extraction conditions were 750°F, 75 psig, at a solvent-to-coal ratio of 3:1.

3. Extraction at residence times of 5 to 20 minutes in a stirred solutizer vessel or, preferably, in continuous in-line solution heating coils which would permit a direct circuit from the solvent-coal mixing tank through a conventional heater with a discharge to either a rotary pressure precoat filter or a suitable hydroclone.⁽³⁾ Bench extractions were successfully conducted at holding times of as low as 3 minutes. These were duplicated in a pilot furnace heater coil discharging the hot coal solution continuously through an expanded section of the transfer line to the filter charge tank.

4. Ash removal from the coal solution was accomplished at filtration rates of 200 to 300 lbs/hr/sq. ft. of filter surface. Preliminary rates of 200 to 250 were secured in the pilot rotary precoat pressure filter at low pressure differentials. Small-scale runs on cake washing and calcining were performed to obtain closed-cycle data on solvent and distillate distribution. It was anticipated that the filter cake would be washed with a light oil, calcined and the spent cake used as steam fuel for the process in a full-scale plant.

The bench and pilot plant operations in general closely approached the goals set at the start of the work for the deashed coal production phase of the program. In Table I, there are provided examples of the data relative to the composition of the raw coal, coal-to-solvent ratios, temperatures and pressures and analyses of the coal extract solutions. Yields are shown on the basis of both raw and ash-free coals. Typical coal deashing results are shown in Table 2.

Available Coal Charge Stocks

Extraction of coal with phenanthrene by earlier workers related the degree of extraction to the rank of the coal.⁽⁴⁾ Thus, about 95 percent of the organic material in bituminous coal was dispersed as compared to 27 percent for subbituminous coal and 23 percent for lignite. Bench studies using a preprocessed coal tar distillate solvent matched these extraction efficiencies for the bituminous coal and lignite studied.

The coals extracted ranged in ash content from 5 to 20 weight percent and in sulfur values from 1 to over 4 percent. In each case, it was possible to secure excellent removal of the ash and a substantial portion of the sulfur, chlorides and other contaminants.

Sulfate and pyritic sulfur were fully eliminated with the ash and the organic sulfur forms were noticeably reduced. It was also possible to reduce the volatile matter contents from original values of near 40 percent to around 15 to 25 percent by distillation or by solvent precipitation⁽⁵⁾ of the deashed coal solution.

Improvement of Solvent for Coal Deashing

The wide-range heavy anthracene oil fraction originally used in the coal solution studies boiled between 600°F and 1050°F. Bench delayed coking of the deashed coal solutions gave solvent losses ranging as high as 30 to 60 volume percent through polymerization of the heavy ends and decomposition of the less refractory components of the solvent.

Accordingly, studies were initiated to produce a more stable solvent. As a result, the efficiency of the coal solvent was improved to a point where 85 to better than 90% solution is achieved of the total extractable carbonaceous material of the coal (i.e., excluding the nonsoluble fusain).

This preferred solvent, freed of easily polymerizable material, is capable of essentially complete recovery from either the coal solution by vacuum stripping or from the delayed coking operation at reduced pressure.

Solvent upgrading is the result of two important factors. First, the solvent boiling range has been narrowed and, secondly, the solvent has been stabilized by removal of its less refractory (readily cracked) components. Continued use and recycle of this solvent improve its stability.

A brief discussion of the variables in coal solution and coking of its deashed solution will outline the reasons for the improvements secured by the changes in solvent boiling range and composition noted above:

It is known that the effective solvents for coal are those that have an angular configuration of the rings, and that boil above 300°C (572°F).⁽⁴⁾ Nonangular, or linear, condensed ring systems have a greatly reduced selective solvent action on the constituents of coal that act as binding agents for the micellar portion of the coal. It is this removal of the binding material that leads to the complete disintegration of the colloidal nature of the coal, and peptization of the micelles in the solvent.

Because of the temperatures at which coal dissolution and subsequent recovery of deashed products are effected, it was found that certain high boiling fractions polymerized and were lost from the original solvent. These viscous fractions also decreased filtration rates. They were, therefore, helpfully removed in the course of refractorizing the solvent.

The narrow range solvent first prepared by distillation and employed for solution yielded 83.9 percent of the original ash-free coal. However, by successive heatings of the recovered solvent and redistillations to the original narrow boiling range, the extractive efficiency was increased to 89 to 93% in subsequent extractions.

Use of Other Refractory Aromatic Solvents

Numerous refinery stream fractions such as, for example, thermal-cracked, cat-cracked heavy cycle oils are rich in condensed ring aromatic compounds and their alkylated homologues. For example, a 700° to 1000°F clarified slurry oil has been reported as containing in excess of 70% condensed ring aromatics. Further, thermal cracking of this clarified oil increased the concentration of these aromatics to over 90% and these are predominantly condensed ring types. It is considered that these cracked refinery tars, after further refractorizing, could provide a low-cost coal solvent of high solution efficiency comparable to that of the coal tar solvents.

Removal of Ash

The efficiency of coal solution deashing has been a function of ash particle size distribution rather than of total

ash content of the initial high volatile bituminous coal. Thus, it has been repeatedly demonstrated in the bench and pilot solvent deashing studies on coal samples with ash contents varying from 5 to 20 weight percent that final ash values of 0.1 to 0.3 could be obtained in the treated coal extracts.

Likewise, inorganic chlorides have been largely eliminated with the ash. Coals containing 0.25 and 0.15 weight percent chlorine were reduced to values of 0.004 to 0.003, respectively. It is assumed that coals of considerably higher inorganic chloride contents could be reduced to similar low values. The harmful corrosive effects of ash and chlorides on furnace operation are well known and their effective reduction is obviously very desirable.

Sulfur Reduction

The degree of bituminous coal desulfurization by solvent deashing has proven to be a function of the original ratio of inorganic sulfate and pyritic sulfur to the organic forms. Original total sulfur contents of 1 to 4 percent are reduced to values of 0.4 to 1 weight percent in the extracts.

It is known that this ratio increases with coals of increasing total sulfur content, i.e., in the lower grade coals of correspondingly higher ash. The final sulfur of the deashed coal therefore relates to the original organic sulfur which is only partially removed in the process, whereas the inorganic sulfur is removed substantially quantitatively.

Thus, in Table 1, complete elimination of the pyritic and sulfate sulfurs has been achieved with an accompanying 26 percent reduction in organic sulfur, for an overall sulfur reduction of about 50 percent.

Delayed Coking

The original 1957 concept of the coal deashing process was to prepare a coal solution which, after filtration for removal of its ash, sulfur and other contaminants, would be charged to the conventional Lummus delayed petroleum coking process. The coke drum vapor would pass to the combination fractionation tower for separation of gas and light and medium distillate from a tower bottom cycle oil which would be re-used for fresh coal solution.

The bench and pilot coking of the deashed coal solution proved to be almost routine. This charge stock resembled in many of its characteristics a low temperature carbonization pitch. Lummus had previously in bench scale and pilot plant delayed coking apparatus successfully coked both low and high temperature carbonization pitches as well as Gilsonite and Athabasca tar sand pitches.

The range of temperatures and general operating characteristics proved similar to those employed for the stocks noted above. Reduced pressure is necessary for high solvent (600-900°F) recovery. Thus, it is anticipated that full scale plant operation would produce cokes with volatile matter contents approaching those normally encountered with petroleum stocks. Such cokes would be of low ash and satisfactory sulfur contents and would be secured at high yields.

The product distribution on coal solution and on coal are summarized in Table 3, based on a 2:1 solvent to coal ratio. It was found on examination of the coker total liquid products that the extraction solvent had been recovered without significant change. The properties of the coker feed and product coke are listed in Table 4.

An alternate method of producing high purity coke utilizes the pure coal extract as the raw material. This may be pulverized in a ball and ring or ring roller type mill, such as is used for powdered coal burners. The milled pure coal is then used to form a slurry with a refractory recycle stock, having a boiling range of about 500-700°F. The boiling range of this stock will vary somewhat, depending upon conditions in the heater, the coke drum, and the ratio of solids to liquid, but is selected so that sufficient liquid phase remains in the heater coils so as to convey the milled pure coal without coke build-up in the heater.

A third method of pure coke production considered, particularly where production of pure coke from coal would be conducted in conjunction with the operation of a refinery, involves utilization of petroleum coker feedstock as the liquid in which the slurry of pure coal is formed. Where a low coke yield feedstock is used, the coke produced would be predominantly from pure coal. However, the proportion might be varied, depending upon the type of coker feedstock employed and the ratio of solids to liquid in the slurry charged to the delayed coker.

Alternate Processes for Coal Extract Recovery

As an alternate to the recovery of coal extracts of original or decreased volatile matter contents by distillation, as noted in Tables 1 and 3, it was determined that these products could be recovered readily from solution by precipitation with hydrocarbon solvents. Thus, a paraffinic solvent yielded the complete deashed coal extract, whereas it was possible to recover a deashed coal with a volatile matter content 60 weight percent below that of the original coal with control of intermediate product values by manipulation of the aromaticity of the solvent blends.

References

1. Bloomer, W. J., and Martin, S. W., U. S. Patent 3,109,803 (November 5, 1963).
2. Dicalite 40, General Refractories Company, used for bench and pilot filtrations.
3. Patent pending.
4. Orchin, M., Golumbic, C., Anderson, J. E., and Storch, H. H., U. S. Bur. Mines Bull. 505, 1951.
5. Patent pending.

COAL SOLUTION DEASHING USING A SOLVENT OF VARIOUS RANGES COAL TAR DISTILLATE AND NARROW RANGE SOLVENT

Coal Source	I		II Illinois		III Illinois		IV Penna.		V Illinois		VI Penna.		Lignite
	Raw	Deashed	Raw	Deashed	Raw	Deashed	Raw	Deashed	Raw	Deashed	Raw	Deashed	
Coal Proximate Analysis, Percent by Weight													
Moisture	2.69		Moisture-free basis										
Volatile Matter	37.7	33.6	32.6	33.5	37.2	36.6	36.6	36.6	38.90	36.6	36.6	36.6	45.2
Fixed Carbon	38.9	56.6	67.1	52.5	62.5	56.6	56.6	56.6	53.99	56.6	56.6	56.6	38.0
Ash	19.66	9.8	0.3	14.0	0.3	5.4	5.4	5.4	7.11	5.4	5.4	5.4	15.1
Sulfur	3.72	4.0	1.0	4.3	0.9	1.46	1.46	1.46	1.18(1)	1.46	1.46	1.46	
Chlorine		0.15	0.003	0.25	0.004								
Solvent													
	Wide Range	Narrow Range			Narrow Range	Wide Range	Wide Range	Narrow Range	Narrow Range	Narrow Range	Wide Range	Wide Range	
Refractorized	No	Yes			Yes	No	No	Yes	Yes	Yes	No	No	
Deashed Coal Recovery													
On crushed coal	67.3	83.6			75.4	67.5	67.5	85.3	90.0	90.0	21.3	21.3	
On ash-free coal	83.8	92.7			89.8	71.3	71.3	91.8	95.2	95.2	25.2	25.2	

(continued on next page)

TABLE I (cont'd)

COAL SOLUTION DEASHING USING AS-RECEIVED WIDE-RANGE COAL TAR DISTILLATE
AND NARROW RANGE REFRACTORIZED SOLVENT

Coal Source	I		II		III		IV		V		VI	
	Illinois		Illinois		Illinois		Penna.		Illinois		Penna.	
Filtrate	Raw	Deashed	Raw	Deashed	Raw	Deashed	Raw	Deashed	Raw	Deashed	Raw	Lignite
Sp. Gravity(100°/100°F)	1.2516	1.2250	1.2208		1.2523		1.2140		1.2355		1.2140	1.2355
Softening Point, °F(B&R)	147	131.5	111.0		212				121.5			121.5
Sulfur, Wt. %	0.63				0.44		0.51				0.51	0.57
Carbon Residue, Wt. %	32.7						23.9				23.9	28.0
Ramsbottom Conradson					35.9							
CS ₂ Solubility, Wt. %												
Bitumen	76.81	78.56	80.71		68.35		81.01		85.13		81.01	85.13
Ash	0.06	0.08	0.03		0.07		0.05		0.02		0.05	0.02
Difference	23.13	21.36	19.26		31.58		18.93		14.85		18.93	14.85

(1)	Raw Coal		Coal Extract	
	Raw Coal	Coal Extract	Raw Coal	Coal Extract
Organic S. %	0.799	0.593	0.593	
Pyritic S. %	0.370	Not Detected	Not Detected	
Sulfate S. %	0.012	Not Detected	Not Detected	
Total	1.181	0.593	0.593	

TABLE 2

TYPICAL COAL DEASHING RESULTS

Bench Scale

Coal Source:	Pennsylvania		Illinois		Pennsylvania	
	As Charged	Product	As Charged	Product	As Charged	Product
Proximate Analysis						
Moisture	1.4					
Volatile Matter	36.6	22.3-30.3	33.62	25.2	33.53	37.3
Fixed Carbon	56.6	77.4-69.4	56.56	74.5	52.54	62.5
Ash	5.4	0.02-0.5	9.79	0.3	13.93	0.3
Sulfur	1.46	0.3 - 0.6	3.95	1.0	4.32	0.9
Chlorine			0.15	0.003	0.25	0.004

Pilot Plant

Coal Source:	Illinois	
	As Charged	Product
Proximate Analysis		
Moisture	2.75	
Volatile Matter (Dry Basis)	38.90	20.9+
Fixed Carbon (Dry Basis)	53.99	78.4+
Ash	7.11	0.65
Sulfur	1.18	0.593

TABLE 3

DELAYED COALING RUN - PRODUCT DISTRIBUTION

Basis: Run PF-15
2000 lbs. Southern Illinois Coal (Moisture Free)
4000 lbs. Coker Recycle 500-700°F

<u>Product</u>	<u>Wt. lbs.</u>	<u>Solution Basis</u>		<u>Solvent-free Basis</u>	
		<u>Wt. %</u>		<u>Wt. %</u>	
Gas	134	2.2		6.7	
Liquor & Lt. Oil	60	1.0		3.0	
Coke	1256	20.9		62.8	
Solvent	4000	66.7			
Distillate	46	0.8		2.3	
Spent Cake	<u>504</u>	<u>8.4</u>		<u>25.2</u>	
Total	6000	100.0		100.0	

TABLE 4

DELAYED COKING OF DEASHED COAL SOLUTIONRESULTS OF COKER TEST RUN DC-13

Properties of Feed (1)	Coke Drum No. 1	Coke Drum No. 2
Specific Gravity, 100/60°F	1.1928	1.1811
Softening Point, °F (R&B)	158	108.5
Benzene Insoluble, Wt. %	22.2	19.6
Properties of Coke		
Wt. Percent of Feed	25.7	22.3
Density, lbs/ft ³		
By Weight of Volume Occupied in Coke Drum	50.1	38.5
By Weight of Water Displaced by Sample	66.7	51.3
Volatile Matter, Wt. %	9.17	10.06
Fixed Carbon, Wt. %	90.22	89.28
Ash, Wt. %	0.61	0.66
Sulfur, Wt. %	0.37	0.38
Heating Value, BTU/lb.	14,520	
(1) Weight percent coal extract		-26.2
Benzene insoluble, weight percent-		21.0

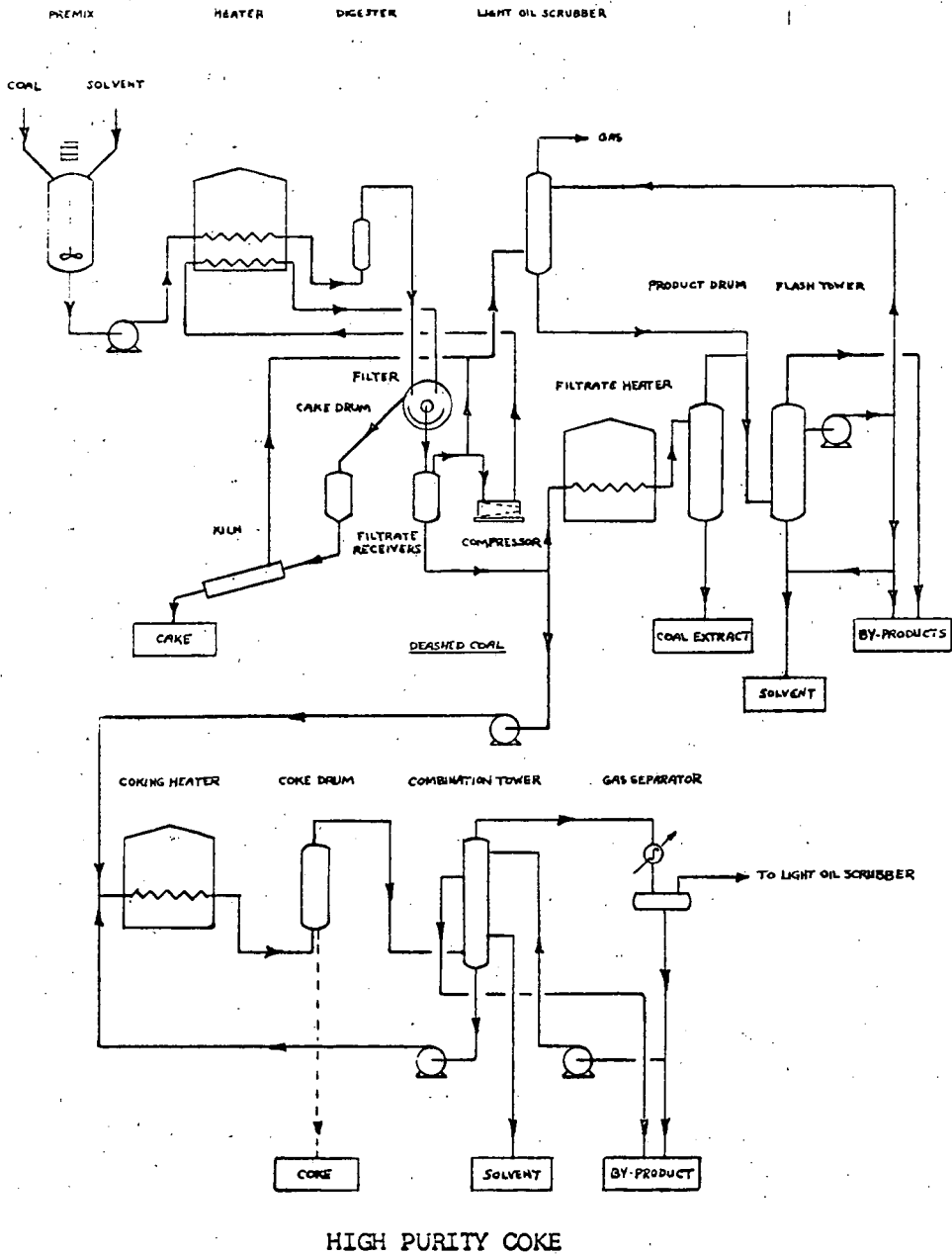
TABLE 5

ECONOMIC STUDY - DEASHED COAL PRODUCT

Plant Capacity, Tons/year	750,000		1,500,000	
Plant Cost	\$13,400,000		\$24,000,000	
	<u>Cost/Ton Product</u>	<u>¢/MM BTU</u>	<u>Cost/Ton Product</u>	<u>¢/MM BTU</u>
Raw Material (Coal)	\$6.50	21.6	\$6.50	21.6
Labor, Supervision, & Overhead	1.14	3.8	.98	3.2
Utilities	1.30	4.3	1.30	4.3
Depreciation	1.19	3.9	1.06	3.5
Maintenance	.54	1.8	.48	1.6
Insurance & Interest	.89	2.9	.80	2.7
Sales Costs	<u>.15</u>	<u>.5</u>	<u>.15</u>	<u>.5</u>
Gross Operating Costs	\$11.71	38.8	\$11.27	37.4
By-Product Credits	<u>(2.60)</u>	<u>(8.6)</u>	<u>(2.60)</u>	<u>(8.6)</u>
Net Operating Costs	\$9.11	30.2	\$8.67	28.8
Pre-tax Investment Return	<u>2.24</u>	<u>7.4</u>	<u>2.00</u>	<u>6.6</u>
Sales Price, (Coal @ \$4.00/ton)	\$11.35	37.6	\$10.66	35.3
Sales Price, (Coal @ \$3.00/ton)	\$9.72	31.9	\$9.03	29.6

- Notes: 1. Plant is a 'grass-roots' facility capable of handling run-of-mine coal from stockpile.
2. Labor - \$5.00/man hour including supervision and overhead.
3. Utilities - Electricity @ \$.006/KWH
Steam @ \$.50/M lbs.
Cooling Water @ \$.02/M Gallons
4. Depreciation - Straight Line over 15 year period.
5. Maintenance - 3% of investment.
6. Insurance & Interest - 5% of Plant cost.
7. By-Product Credits - \$.01/pound average for net excess distillate.
8. Pay-Out - 8 Years.

FIGURE 1
SCHEMATIC FLOW DIAGRAM
DEASHED COAL OR HIGH PURITY COKE



THE HEAT OF REACTION OF ³⁹³HYDROGEN AND COAL

A. L. Lee, H. L. Feldkirchner, F. C. Schora, and J. J. Henry*

Institute of Gas Technology
Chicago, Illinois

INTRODUCTION

This investigation is a part of the study conducted at the Institute of Gas Technology (1,2,4,5,6,7,9,10,11) to obtain the necessary information for designing an efficient coal hydrogasification plant. A thorough literature search reveals that there is no reported data on the heat of reaction of hydrogen and coal. Therefore, two calorimeters were designed, constructed, and operated, one to measure the heat of reaction and the other to measure heat capacity by the drop method. The heat-of-reaction calorimeter can be operated at temperatures up to 1500°F and pressures up to 1500 psia; the drop calorimeter operates at atmospheric pressure and temperatures up to 1500°F. This paper reports the results of the following investigations:

1. The heat of reaction of hydrogen with coals and coal chars after various degrees of gasification.
2. The heat of reaction of coal pretreatment.
3. The heat capacity of coals and coal chars.

APPARATUS

The heat-of-reaction calorimeter built by Dynatech Corporation is shown in Figure 1. The sample is placed in the upper portion of the neck which is cold. The calorimeter body is filled with hydrogen and heated. The temperature of the calorimeter body is measured by four thermocouples and two platinum resistance thermometers. The sample is lowered into the body after the temperature has remained steady for 2 hours. The change in temperature due to a reaction is then measured as a function of time.

The drop calorimeter, which was also built by Dynatech, is shown in Figure 2. The sample is placed in the top furnace until it reaches the desired temperature. It is then dropped into the copper receiver, and the heat capacity of the sample is determined from the temperature rise and heat capacity of the copper receiver.

EXPERIMENTAL RESULTS

The major problem encountered in determining the heat of coal reactions at high temperature and high pressure is prereaction, since coals decompose when heated. Meaningful results can be obtained only if the coal and hydrogen react at conditions at which the desired temperature and pressure are stabilized. Therefore, the method of introducing the sample to the reaction conditions is critical. The coal must not react before the conditions are set, and the pressure must not be disturbed when the coal is introduced.

* Dynatech Corp., Cambridge, Massachusetts.

The present method is to keep the sample at room temperature inside the calorimeter drop tube so that the reaction will not take place prematurely. Convection shields are installed to prevent a large heat loss from convection and to ensure that the sample is in a cold zone while the calorimeter is being stabilized at the reaction conditions.

Establishing a heat balance around the calorimeter was necessary in order to calculate the heat of reaction from experimental data. The heat balance is best expressed by:

$$\Delta\bar{H}_R + h_{in} = (mC_p\Delta T)_{\text{calorimeter}} + (mC_p\Delta T)_{\text{shield}} + (mC_p\Delta T)_{\text{chain}} + (mC_p\Delta T)_{\text{basket}} + (mC_p\Delta T)_{\text{coal}} \quad (1)$$

where: $\Delta\bar{H}_R$ = heat of reaction
 h_{in} = heat input from the neck heater
 m = mass
 C_p = heat capacity
 ΔT = temperature change

Each term in Equation 1 must be either established by calibration or accurately measured. The heat capacity of the calorimeter metal was determined in the drop calorimeter. These data are shown in Figure 3.

The effective mC_p of the reaction calorimeter was calibrated by a constant-heat-input technique in a hydrogen atmosphere at 1000 psia and temperatures from 840° to 1460°F. The results are presented in Figure 4. After the calorimeter constants were determined, the effective $(mC_p\Delta T)$'s of the convection shield, the chain, and the empty sample basket were calibrated in the calorimeter to determine the change of heat input with time, as shown in Equation 2:

$$K(\theta) = \int_0^{\theta} (mC_p\Delta T)_{\text{empty calorimeter}} d\theta = \int_0^{\theta} [(h_{in} - (mC_p\Delta T)_{\text{shield}} - (mC_p\Delta T)_{\text{chain}} - (mC_p\Delta T)_{\text{basket}})] d\theta \quad (2)$$

where: $K(\theta)$ = a constant dependent only on time
 θ = time

Combining Equations 1 and 2, we have:

$$\Delta\bar{H}_R = (mC_p\Delta T)_{\text{calorimeter}} + (mC_p\Delta T)_{\text{coal}} - K(\theta) \quad (3)$$

Equation 3 was used to calculate the heat-of-reaction data reported in this paper.

Design of a hydrogasification plant requires data on the heats of reaction of raw coal in the coal pretreatment process, the pretreated coal in the low-temperature gasifier, the residue from the low-temperature gasifier in the high-temperature gasifier, and the residue from the high-temperature gasifier (4,6). The heat-of-reaction and heat capacity measurements are given in Tables 1 and 2. Figure 5 shows the temperature and pressure profiles of a typical experimental run.

DISCUSSION

Until now, the heat of the coal hydrogasification reaction has only been determined by calculation. These calculations have become more precise as more data became available, but no measurements were made to check the validity of the calculated data.

Initially (in the absence of accurate pilot plant yield data), the heat of reaction was estimated by assuming that coal and carbon were equivalent and that the hydrogasification reaction could be approximated by (5,8):



This approach, of course, is very crude and could not be expected to give a reliable answer, but it could be useful for comparing the thermal efficiencies of various gasification processes.

The next approach, using pilot plant data (7), was to calculate the heat of reaction from the heats of combustion of the reactants and products. The heats of combustion of various coals could be obtained by a Parr-bomb calorimeter or calculated by the modified Dulong formula. But if one attempts to calculate the heat of reaction of hydrogen and coal from heats of combustion, there are two drawbacks. First, because the calculation involves taking the differences of large numbers of the same order of magnitude, chemical analyses of all reactants and products must be very accurate and pilot material balances must be quite close to 100 percent or else the balance must be forced. If this is not the case, large errors can be made in this calculation. This makes the calculated heat of reaction dependent on the quality of the analytical data and on the method used to force the balance. The second drawback is that the calculated heat of reaction is determined for 25°C, so no information is obtained on the reaction heat at actual reaction temperatures.

Of course, if the heat of reaction could be determined at one temperature, the heat of reaction at various temperatures could be calculated from heat capacity data. Some heat capacity data are available in the literature for coals and cokes, but none are available for the particular coals used here. Moreover, the measurement methods used so far are not very accurate. In most cases the gaseous decomposition products were allowed to escape from the calorimeters during coal heatup, and, consequently, the heat capacity data are rather doubtful.

A comparison of the heats of reaction of hydrogen and coal obtained from the heat of formation data for $C + 2H_2 \rightarrow CH_4$ and the pilot plant data with that obtained from the calorimetry studies is shown in Figure 6. Note that the pilot plant data were based on a 77°F reference

temperature, while the present experimental data were obtained at operating conditions. Moreover, the experimental data were obtained from coals at four different stages of reaction: raw coal, pretreated coal, low-temperature gasification residue, and high-temperature gasification residue. Ash balances were used to put these results on a common basis. The ash balance calculations gave the percent of carbon gasified in each coal or char. Raw coal was assumed to have 0% carbon gasified. Thus Figure 6 shows the general trend of the heat of reaction.

Accurate heat-of-reaction data are given in Table 1. Although the pilot plant data are considerably scattered, the average value is not too different from that obtained by the other methods. The calorimetry data also show some scattering, which is due to the heterogeneous nature of the coal, and the characteristics of the calorimeter and the sensing instruments. Examinations of the temperature measurement, the pressure measurement, the temperature distribution in the calorimeter, the total mass balance, and the calibration results obtained from the constant-heat-input method and experimental runs on hydrogen and n-decane reactions indicate that the data reported in Table 2 should not have a deviation greater than 10%.

ACKNOWLEDGMENT

This work is jointly sponsored by the American Gas Association and the U.S. Department of the Interior, Office of Coal Research. Their support is gratefully acknowledged. Valuable advice and discussions were provided by Drs. B. S. Lee, S. A. Weil, and C. W. Solbrig of the Institute of Gas Technology. J. R. DeSando assisted in the experimental work.

1. Feldkirchner, H. L. and Huebler, J., "Reaction of Coal With Steam-Hydrogen Mixtures at High Temperatures and Pressures," Ind. Eng. Chem. Process Design Develop. 4, 134-42 (1965) April.
2. Huebler, J. and Schora, F. C., "Coal Hydrogasification," Chem. Eng. Progr. 62, 87-91 (1966) February.
3. JANAF Thermochemical Tables. Distributed by: Clearinghouse for Federal Scientific and Technical Information, Springfield, Va.
4. Kavlick, V. J. and Lee, B. S., "Coal Pretreatment in Fluidized Bed," Amer. Chem. Soc. Div. Fuel Chem. Preprints 10, No. 4, 131-39 (1966) September.
5. Linden, H. R., "Pipeline Gas From Coal: Status and Future Prospects," Coal Age 71, 64-71 (1966) January.
6. Pyrcioch, E. J., Lee, B. S. and Schora, F. C., "Hydrogasification of Pretreated Coal for Pipeline Gas Production," Amer. Chem. Soc. Div. Fuel Chem. Preprints 10, No. 4, 206-23 (1966) September.
7. Pyrcioch, E. J. and Linden, H. R., "Pipeline Gas by High-Pressure Fluid-Bed Hydrogasification of Char," Ind. Eng. Chem. 52, 590-94 (1960) July.
8. Rossini, F. D. et al., Selected Values of Physical and Thermodynamic Properties of Hydrocarbons and Related Compounds. Pittsburgh: Carnegie Press, 1953.
9. Tajbl, D. G., Feldkirchner, H. L. and Lee, A. L., "Cleanup Methanation for Hydrogasification Process," Amer. Chem. Soc. Div. Fuel Chem. Preprints 10, No. 4, 235-45 (1966) September.
10. Tsaros, C. L. and Feldkirchner, H. L., "Production of High Btu Gas," Chem. Eng. Progr. 62, 49-54 (1966) August.
11. von Fredersdorff, C. G. and Vandaveer, F. E., "Substitute Natural Gas From Coal," in Segeler, C. G., Ed., Gas Engineers Handbook, Section 3, Chap. 9, 3/100-3/123. New York: The Industrial Press, 1965.

Table 1. ANALYSIS OF COAL AND COAL CHARS

	<u>Raw Coal</u>	<u>Pretreated Coal</u>	<u>Low-Temp Residue</u>	<u>High-Temp Residue</u>
Proximate Analysis, wt %				
Moisture	1.3	0.5	0.6	0.6
Volatiles	34.6	23.3	4.6	3.3
Fixed Carbon	52.0	63.5	77.6	71.6
Ash	12.1	12.7	17.2	24.5
Total	100.0	100.0	100.0	100.0
Ultimate Analysis, wt %				
Carbon	71.2	70.1	76.9	72.6
Hydrogen	5.14	3.70	2.05	1.08
Nitrogen	1.23	1.37	1.01	0.54
Oxygen	6.03	8.30	0.65	0.00
Sulfur	4.19	3.80	2.09	1.24
Ash	12.21	12.73	17.30	24.62
Total	100.00	100.00	100.00	100.00
Reaction Temperature, °F	1300	1300	1300	1300
Reaction Pressure, psia	1000	1000	1000	1000
Coal Reacted (Avg), %	49.7	47.2	27.3	28.8
Carbon Gasified (Avg), %	50.6	41.0	29.5	26.0
Avg ΔH_R , Btu/lb coal reacted	1817	1919	2432	3078

Table 2. HEAT OF REACTION OF COAL

<u>Material</u>	<u>Temperature, °F</u>	<u>Pressure, psia</u>	<u>Coal Reacted, %</u>	<u>Carbon Gasified, %</u>	<u>ΔH_R, Btu/lb coal reacted</u>
Raw coal	1000	1000	41.5	--	1300
Raw coal	1300	1000	52.4	50.7	1951
Raw coal	1300	1000	52.2	52.0	1723
Raw coal	1300	1000	48.1	55.6	1788
Raw coal	1300	1000	46.1	44.2	1807
Raw coal	1400	1000	51.7	52.3	1775
Pretreated coal	1300	1000	46.1	37.6	1935
Pretreated coal	1300	1000	47.3	41.2	1717
Pretreated coal	1300	1000	47.3	41.5	1844
Pretreated coal	1300	1000	47.1	40.0	2476
Pretreated coal	1300	1000	48.3	45.0	1625
Low-temp residue	1300	1000	27.3	29.5	2432
Low-temp residue	1300	1000	--	--	2566
High-temp residue	1300	1000	28.8	26.0	3078

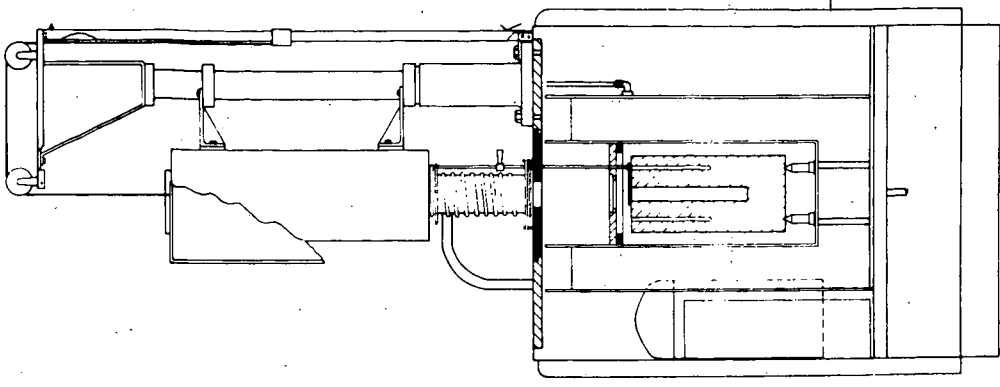


Figure 2. DROP CALORIMETER

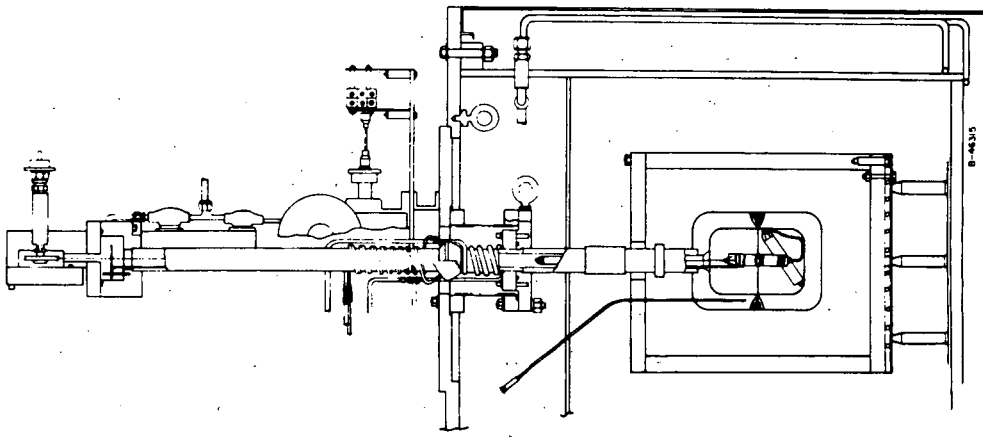


Figure 1. HEAT-OF-REACTION CALORIMETER

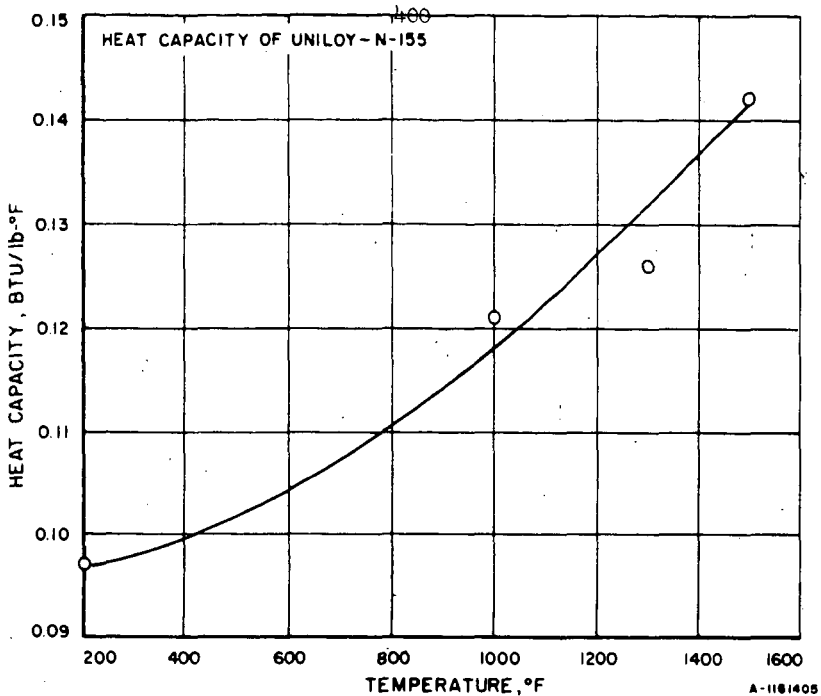


Figure 3. MEAN HEAT CAPACITY OF CALORIMETER
(From 70°F to Temperatures Indicated)

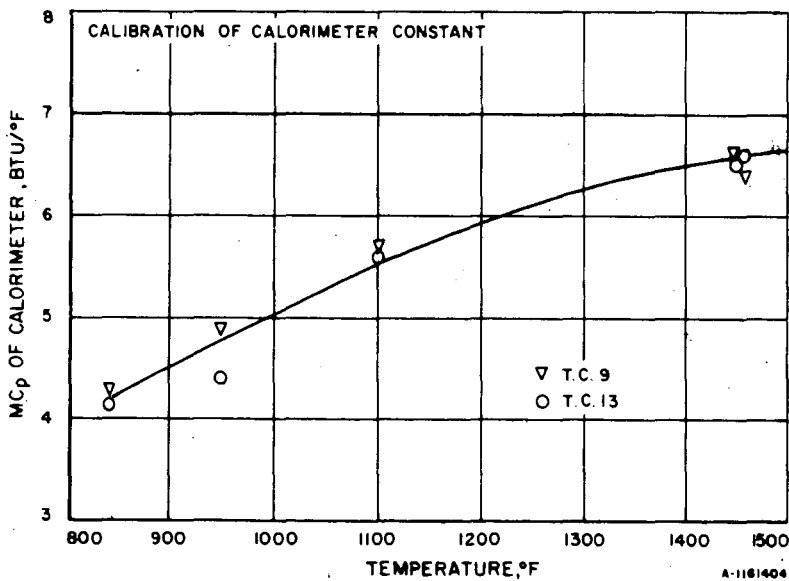


Figure 4. CALIBRATION OF HEAT-OF-REACTION CALORIMETER

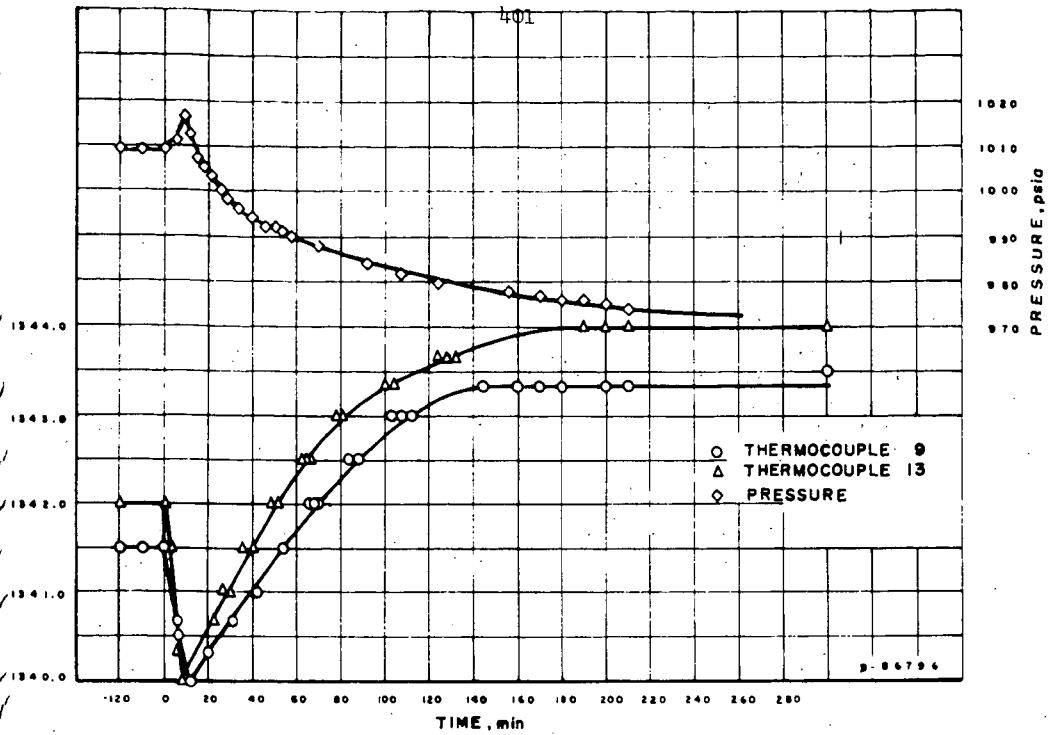


Figure 5. TIME-TEMPERATURE DATA FOR HEAT OF REACTION OF HYDROGEN AND COAL

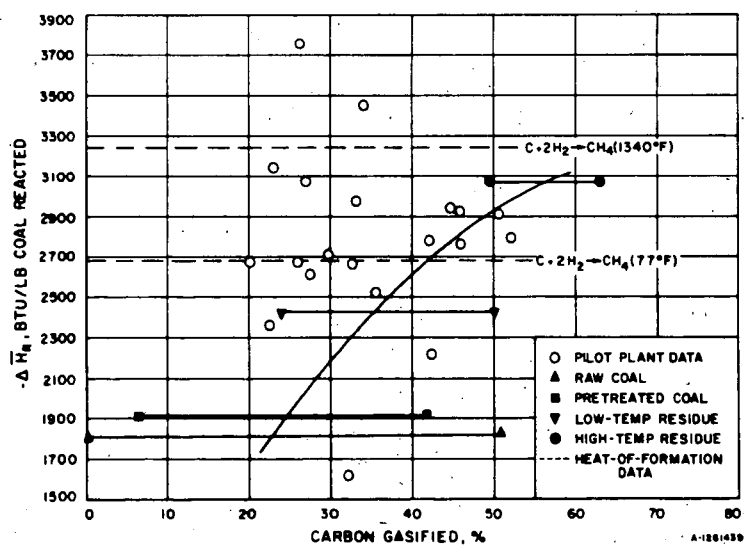


Figure 6. COMPARISON OF DATA FOR HEAT OF REACTION OF HYDROGEN AND COAL

HYDROGEN CYANIDE PRODUCED FROM COAL AND AMMONIA

G. E. Johnson, W. A. Decker, A. J. Forney, and J. H. Field
Pittsburgh Coal Research Center, U. S. Bureau of Mines,
4800 Forbes Avenue, Pittsburgh, Pennsylvania 15213

INTRODUCTION

Hydrogen cyanide (HCN) has been one of the country's strongest growth petrochemicals in recent years. U. S. production has increased from 174 million pounds in 1960 to 350 million pounds in 1964, a 100-percent increase over the 4-year period. The growth of production of hydrogen cyanide has been directly related to the expansion in production of synthetic textiles from acrylonitrile. Relative growth and production of hydrogen cyanide and acrylonitrile is as follows:

Production of Hydrogen Cyanide and Acrylonitrile

Year	Hydrogen cyanide, ^{5/} million lb	Acrylonitrile, million lb
1960	174	229 ^{10/}
1961	211	250 ^{10/}
1962	266	360 ^{10/}
1963	293	455 ^{10/}
1964	350	593 ^{10/}
1965	---	371 (6 months) ^{4/}

About 50 percent of the total output of hydrogen cyanide goes into the production of acrylonitrile; most of the remainder is used in production of adiponitrile and the manufacture of methyl methacrylate.^{7/} However, in recent years acrylonitrile and adiponitrile are being produced by processes which generate hydrogen cyanide as a byproduct.^{3/} The bulk of acrylonitrile is used in production of acrylic fiber (Orlon, Acrilan, Dynel, Zefran, etc.),^{a/} a smaller amount in production of nitrile rubber, the adiponitrile in manufacture of Nylon.

The manufacture of sodium cyanide utilizes about 7 percent of hydrogen cyanide production. The remaining hydrogen cyanide goes to a large number of relatively small uses including ferrocyanides, acrylates, ethyl lactate, lactic acid, chelating agents, optical laundry bleaches, and pharmaceuticals.

The Andrussow process is the major commercial process used for producing hydrogen cyanide. It involves the reaction of methane, ammonia, and air over a platinum catalyst at 1,000° to 1,200° C.^{9/} The platinum catalyst is usually alloyed with rhodium (10 to 20 percent).

Conversion by the Andrussow process in a single pass is limited to about 69 percent of the ammonia (about 75 percent with gas recycle) and 53 percent of the methane. A typical analysis of the reaction gases leaving a catalytic reactor is as follows in volume-percent: Nitrogen 56.3, water vapor 23.0, hydrogen 7.5, hydrogen cyanide 6.0, carbon monoxide 4.4, ammonia 2.0, methane 0.5, carbon dioxide 0.2, and oxygen 0.1.

^{a/} Reference to trade names is made for identification only and does not imply endorsement by the Bureau of Mines.

In the catalytic Degussa process which is not in general use but is similar to the Bureau of Mines method in that heat is provided externally, the offgas from the ammonia-methane reaction contains more than 20 percent hydrogen cyanide. Utilization of methane and ammonia are reported as 91 and 85 percent, respectively.

In its search for new uses for coal the Bureau of Mines has been investigating the production of hydrogen cyanide from coal. Although hydrogen cyanide is present in coke oven gases, and at one time was recovered as a byproduct, this source of the gas has not been commonly used in the United States since the development of the newer methane-ammonia processes. Although the production of hydrogen cyanide from coal is technically feasible, production in yields that could be competitive is a problem of major concern.

EQUIPMENT AND PROCEDURE

Figure 1 is a flowsheet of the experimental unit. Coal ground to minus 300 mesh is dropped in free-fall through a heated reaction zone in the presence of ammonia at rates up to 1.10 lb/hr. A revolving-disk feeder especially designed by the Bureau of Mines to feed coal at low rates was constructed; it delivered to within ± 5 percent of the desired feed rate.

A special coal feed system is used to prevent agglomeration and possible plugging of the reactor by heating the coal rapidly through its plastic range (about 400° C).

The reactor itself is a 4-foot length of vitreous refractory mullite, 1-1/8 inches ID and 1-3/8 inches OD, jacketed with two electrical resistance heaters. The top heater (maximum temperature 850° C) is 12 inches long and is wound with Nichrome wire. It serves as preheater for the coal and gas. A Kanthal heater (Al-Cr-Co-Fe alloy, maximum temperature 1,250° C) encloses the center 20 inches of the tube, or the reaction zone. The bottom section of the reactor is exposed to the atmosphere for rapid cooling of the product gases.

The bottom of the reactor tube fits into a 4-liter side-arm flask or char receiver in which the heavier solids are collected. The fine solids and carbon black produced are collected in an electrostatic precipitator. After the product gases leave the precipitator they pass through a cooler, then they are either metered or sent through absorbers to remove the hydrogen cyanide for analysis.

All of the piping and vessels are stainless steel or glass in order to counteract the corrosive nature of the gases. Since the gases are toxic, the unit is completely enclosed, and the enclosure is well ventilated to prevent any accumulation of escaped gases. The whole structure (6 ft x 6 ft x 15 ft high) is covered with steel sheeting. It has an exhaust blower (400 cfm) on the roof and access doors at both ground and 8-foot levels. Figure 2 shows the exterior of the unit and figure 3 shows its interior.

Product gas can be recycled to the top of the reactor adjacent to the cooled feed tube along with part of the feed gas. This flushes away any tar vapors which might adhere to the walls and cause plugging. The remainder of the feed gas (0 to 10 scfh) enters the reactor with the coal. Ammonia, helium, methane, nitrogen, or air, or mixtures of these gases fed from cylinders have been used as feed gas.

Before startup, the system is purged with inert gas. After the reactor has been heated to 1,250° C the desired flows of coal and gas are started. Ammonia and nitrogen or helium are the gases usually used. The gas flow is generally split, part entering the top of the reactor adjacent to the cooled feed tube, and the remainder entering with the coal.

The powdered coal is fed through a steam-jacketed tube (5/16-inch OD) which extends into the preheat zone of the reactor. The coal leaves the end of the feed tube which is at the temperature of the steam to enter the preheat zone of 850° C. The temperature of the coal rises very suddenly to 850° C because of the high heat-transfer rate to the small particles. The carrier gas (usually helium, an inert gas) fed with the coal keeps the particles in motion and helps prevent agglomeration as the coal rapidly passes through its plastic range.

Proximate and ultimate analyses^{2, 6/} are made of the char and heavier solids collected in the char receiver and of the lighter solids collected by the electrostatic precipitator. Mass spectrometric and chromatographic analyses are made on spot samples of the product gas. For cyanide determinations, metered amounts of product gas are bubbled through two scrubbers in series containing solutions of sodium hydroxide. Titration with silver nitrate solution determines the total cyanide present.^{1/}

EXPERIMENTAL RESULTS AND DISCUSSION

The initial tests were made with a metallic reactor tube, but because of low yields of hydrogen cyanide and failure of the metal at the temperatures employed, the metal tube was replaced by a ceramic reactor tube.

In all the tests of this report with hvab coal, Pittsburgh seam coal from Bruceton, Pa., was used. Its ultimate analysis is as follows in percent: Carbon 75.6, ash 8.4, oxygen 8.0, hydrogen 5.1, nitrogen 1.6, and sulfur 1.3.

The effect of varying the coal-ammonia feed rates is illustrated in table 1. Hydrogen cyanide yields were computed from the wet-chemical method of analysis which is considered the more reliable method since it was determined from proportionated gas samples taken continuously throughout the test (sample volume of 0.2 to 2 cu ft). Only spot gas samples (sample volume 0.01 cu ft) were used for the chromatograph and mass spectrograph analyses.

In test C-241 the coal-feed rate was 0.37 lb/hr and the ammonia-feed rate was 1 cu ft/hr. (All process gas volumes reported are corrected to standard conditions of 0° C and 760 mm mercury pressure.) A hydrogen cyanide yield of 0.6 cu ft per cu ft of ammonia reacted was obtained, corresponding to about 12 percent hydrogen cyanide in the product gas.

In test C-243 the hvab coal-feed rate was reduced to 0.19 lb/hr, while the ammonia-feed rate was increased to 2.3 cu ft/hr. A yield of 0.4 cu ft hydrogen cyanide per cubic foot of ammonia consumed was obtained, corresponding to about 13 percent hydrogen cyanide in the product gas.

The yield of hydrogen cyanide per pound of coal was approximately doubled when the coal-feed rate was halved and the ammonia-feed rate doubled (tests C-241 to 243), while the hydrogen cyanide yield per cubic foot of ammonia consumed decreased by one-third.

Table 1.- Data from Tests with hvab Coal and Ammonia with Helium at 1,250° C

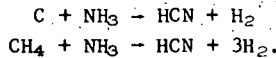
Test	Product gas, percent											
	HCN ^{1/}	H ₂ S	NH ₃	H ₂	O ₂	N ₂	CO	CO ₂	CH ₄	C ₂ H ₄	C ₃ H ₈	C ₈ H ₁₀
C-241	11.8	0.0	0.0	77.7	0.1	6.7	9.6	0.3	5.1	0.4	0.1	0.0
C-243	13.1	.0	17.5	68.6	.9	6.8	4.0	.1	1.0	.0	.0	1.1
C-239	13.2	.1	.5	75.9	.1	4.4	10.6	.5	6.9	.6	.1	.3
C-198	5.4	.3	.0	78.3	.3	3.5	11.1	.3	5.7	.5	.0	.0

	Feed				Yield, cu ft			
	He, cu ft/hr	NH ₃ , cu ft/hr	Coal feed, lb/hr	Total off gas He-free, cu ft/hr	Length of run, min	HCN/lb coal	HCN/cu ft NH ₃ feed	HCN/cu ft NH ₃ consumed
C-241	1.00	1.00	0.37	5.06	30	1.59	0.60	0.60
C-243	0.49	2.35	.19	4.90	30	3.31	.27	.40
C-239	.98	1.00	.73	5.59	15	1.01	.74	.76
C-198	2.12	0.20	.37-.40	3.61	15	0.51	.98	.98

^{1/} Wet-analytical method of analysis for HCN only; other components are the average of 2 chromatograph and 2 mass spectrometer analyses, HCN-free basis.

In test C-239 (table 1) the coal-feed rate was increased to 0.73 lb/hr, while the ammonia flow was maintained at 1 cu. ft/hr. A hydrogen cyanide yield of about 0.8 cu ft per cubic foot ammonia reacted was obtained, equivalent to about 13 percent hydrogen cyanide in the product gas.

In the next listed test, C-198, the coal-feed rate was 0.37 to 0.40 lb/hr, while the ammonia flow was only 0.2 cu ft/hr. The hydrogen cyanide content in the product gas was only 5 percent, table 1, but conversions of about 100 percent of the ammonia were obtained with 1 cu ft of hydrogen cyanide formed per cubic foot of ammonia used. This yield of hydrogen cyanide approximates the stoichiometric yield according to the following reactions:



In typical commercial units using catalysts for the methane-ammonia reaction, the ammonia conversion attained is about 75 percent. Yield values include the slight amount of hydrogen cyanide that may be formed when coal is heated to high temperatures without adding ammonia.

In general, the tests of table 1 indicate that an excess coal feed is desirable in order to attain maximum utilization of the ammonia since the ammonia is by far the more expensive raw material.

Tests With Coals of Different Rank

In addition to the hvab coal, lignite, subbituminous, low-volatile bituminous, and anthracite coals, coal char, and activated carbon were tested as raw materials for producing hydrogen cyanide. It is thought that the volatile matter in coal reacts with the ammonia to form hydrogen cyanide, therefore coals with higher volatile content should produce more hydrogen cyanide. The volatile-matter contents on a moisture-free basis of the various materials tested are as follows:

Test	Identification of coal	Source of coal	Volatile matter, percent
C-123, 124, 125, 198, 239, 241, 243	Hvab, Pittsburgh seam	Bruceton, Pa.	34.0
C-207	Activated carbon, Grade SXWC	Union Carbide and Carbon Corp.	2.0
C-210	Anthracite	Anthracite Research Center, Schuylkill Haven, Pa.	7.6
C-246	Subb, Laramie seam	Erie, Colo.	38.5
C-249	Lvb, Pocahontas #3 seam	Stepheson, W. Va.	17.5
C-252	Lignite, unnamed seam	Beulah, N. Dak.	41.1
C-254	Pretreated hvab, ^{1/} Pittsburgh seam	Bruceton, Pa.	32.6

^{1/} Treated with air at 200° C.

Table 2 shows the results of these tests. Lignite with 41 percent volatile matter produced the most hydrogen cyanide, 0.4 cu ft per cubic foot of ammonia consumed; activated carbon, containing the least volatile matter (2.0 percent), produced the least hydrogen cyanide, 0.007 cu ft per cubic foot of ammonia consumed.

The chemical nature of the volatile matter and the oxygen content of the coal may also affect the hydrogen cyanide yield. The ratio of H₂ to CO in the off gases varied from 2.3 to 1 for subb coal and 2.4 to 1 for lignite to 7 to 10 to 1 for hvab. The higher carbon monoxide values obtained with subb coal and lignite are due to the higher oxygen contents of these coals, being 17.1 and 20.3 percent, respectively, compared with 8.0 percent for the hvab coal.

Table 2.- Data from Tests with Various Coals and Ammonia with Helium at 1,250° C

Test	Product gas, percent										
	HCN ^{1/}	H ₂ S	NH ₃	H ₂	O ₂	N ₂	CO	CO ₂	CH ₄	C ₂ H ₄	C ₃ H ₈
C-246 Subb	5.4	0.0	0.0	64.2	0.0	4.9	28.0	0.5	2.4	0.0	0.0
C-249 Lvb	4.2	.0	.0	78.9	.1	14.2	3.6	.0	3.0	.2	tr.
C-252 Lignite	6.4	tr.	.0	64.6	.1	6.1	26.3	.5	2.4	.0	.0
C-254 Pretreated, hvab	3.8	.1	.0	72.3	.8	10.6	14.3	.0	1.9	.0	.0
C-210 Anthracite	0.2	.0	.0	73.4	.3	21.4	2.9	.4	1.5	.0	.0
C-207 Activated carbon	.25	.0	.0	70.0	.0	23.0	6.6	.1	0.3	.0	.0

	Feed				
	He, cu ft/hr	NH ₃ , cu ft/hr	Solids feed, lb/hr	Total off gas He-free, cu ft/hr	Length of run, min
C-246 Subb	0.91	1.00	0.42	6.88	30
C-249 Lvb	.97	1.00	.47	3.92	30
C-252 Lignite	1.06	1.00	.37-.40	6.38	15
C-254 Pretreated, hvab	1.04	1.00	.35	5.80	30
C-210 Anthracite	1.02	1.15	.37-.40	4.15	15
C-207 Activated carbon	1.06	1.15	.62	3.23	15

	Yield, cu ft		
	HCN/lb coal	HCN/cu ft NH ₃ feed	HCN/cu ft NH ₃ consumed
C-246 Subb	0.88	0.37	0.37
C-249 Lvb	.34	.16	.16
C-252 Lignite	1.05	.41	.41
C-254 Pretreated, hvab	.63	.22	.22
C-210 Anthracite	.021 _{2/}	.007	.007
C-207 Activated carbon	.013 _{2/}	.007	.007

- 1/ Wet-analytical method of analysis for HCN only; other components are the average of 2 chromatograph and 2 mass spectrometer analyses, HCN-free basis.
 2/ Per pound of carbon.

Tests With Air in the Feed Gas

Tests were made to determine the effect that oxygen in the treating gas would have on the yield of hydrogen cyanide. It was thought that the heat for raising the temperature of the reactants to reaction temperature could be supplied by direct contact with a hot flue gas containing oxygen instead of by electric heating (table 3). In test C-125, a maximum yield of hydrogen cyanide was produced for tests with air in the treating gas--0.12 cu ft of hydrogen cyanide per cubic foot of ammonia consumed, or 9.2 percent hydrogen cyanide in the product gas. When more than 0.5 percent air was fed into the reactor, moisture condensed on the walls of the solids-collection flask; the yield of hydrogen cyanide decreased. The moisture could have been absorbing the hydrogen cyanide since hydrogen cyanide is highly soluble in water. This approach was abandoned.

Table 3.- Product Gas Analyses and Yields of Hydrogen Cyanide from Tests with hvab Coal, Ammonia, and Air at 1,250° C

Test	Product gas, percent						Length of run, min	Feed		
	HCN ^{1/}	CH ₄	NH ₃	H ₂	N ₂	CO		NH ₃ , cu ft/hr	Air, cu ft/hr	Coal, lb/hr
C-123	10.3	1.1	10.2	62.8	16.2	9.7	20	5.90	0.52	0.17-0.20
C-124	10.9	0.6	6.9	62.1	17.2	13.2	20	2.96	.53	.17- .20
C-125	9.2	.4	9.6	48.4	31.5	10.1	20	3.08	1.08	.17- .20
	Total off gas, cu ft/hr		Yield, cu ft HCN/lb coal			HCN/cu ft NH ₃ feed	HCN/cu ft NH ₃ consumed			
C-123	4.18		2.30			0.073	0.078			
C-124	3.05		1.77			.112	.120			
C-125	3.70		1.82			.110	.123			

1/ Wet-analytical method of analysis for HCN only; other components are the average of 2 chromatograph and 2 mass spectrometer analyses, HCN-free basis.

Tests With Methane and Ammonia

Tests were made without coal feed but with ammonia and methane to determine the resulting hydrogen cyanide yields for comparison. In one series of tests 2.0 cu ft/hr of methane was reacted with ammonia in flows varying from 0.3 to 2.5 cu ft/hr at 1,250° C. As illustrated in figure 4, yields of 0.18 to 0.61 cu ft of hydrogen cyanide per cubic foot of ammonia consumed were obtained, equivalent to 1.2 to 13.8 percent hydrogen cyanide in the product gas. The yield of hydrogen cyanide reached a maximum at a feed ratio of methane to ammonia of about 1 to 1.

A series of tests was made in which the methane and ammonia flow rates were maintained at 2 and 1 cu ft/hr, respectively, while the reactor temperature was increased from 1,000° to 1,275° C. Hydrogen cyanide yields are plotted with temperature in figure 5, indicating increased hydrogen cyanide yields with increased temperature. Maximum yields of about 0.6 cu ft of hydrogen cyanide per cubic foot of ammonia consumed were obtained at the higher temperatures, while at 1,000° C only 0.07 cu ft of hydrogen cyanide per cubic foot of ammonia consumed was formed.

To explore the use of coal-derived gases in the formation of hydrogen cyanide from ammonia, synthetic mixtures of a low-temperature carbonization gas, a coke oven gas, and a producer gas were prepared and reacted with ammonia at 1,250° C. Gas flows were adjusted to give a minimum methane-to-ammonia ratio of 1 to 1. In figure 6 the hydrogen cyanide yields obtained are plotted with the methane contents of the coal gases. Increasing hydrogen cyanide yields were produced with increasing methane contents of the feed gas.

ECONOMIC EVALUATION

The Bureau of Mines Process Evaluation Group, Morgantown, W. Va., made a preliminary cost study of an integrated plant to produce hydrogen cyanide by reaction of ammonia with coal. The cost study was based on experimental results including a yield of 0.6 cu ft of hydrogen cyanide per cubic foot of ammonia. Electrical heating was assumed as in the bench-scale tests; a plant capacity of 40 million pounds per year was chosen. The total estimated capital investment was \$12,930,000 including costs for power generation.

Based on a coal cost of \$4.00 per ton and an ammonia cost of \$100.00 per ton, the operating costs before profit and taxes would be 5.82 cents per pound of hydrogen cyanide product allowing byproduct credit. Addition of 12-percent gross return on investment would give production costs of 9.7 cents per pound of product when \$4.00 per ton coal is used. The current market price is 11.5 cents per pound.^{8/}

Credit has been allowed in the cost figures for a 7.6-percent yield of carbon black and the excess char produced in the process. Some of the char and the scrubbed product gas (containing about 75 percent hydrogen) are consumed in the steam plant for power generation. Electrical heating, which was used in the test unit and also in the cost figures, is one of the most expensive types of heating, accounting for greater than 40 percent of the capital costs in the estimate. If cheaper conventional heating could be used, production costs would be lowered considerably.

CONCLUSIONS

Hydrogen cyanide has been produced from coal and ammonia at 1,250° C in bench-scale studies. The use of a metal reactor was unsuccessful because the metal failed at the temperatures required, and the yield of hydrogen cyanide was low. The yield was improved greatly when a refractory ceramic reactor was used.

Hydrogen cyanide yields approximating stoichiometric of 1 cu ft of hydrogen cyanide per cubic foot of ammonia reacted were obtained at low flows of ammonia. At higher ammonia flows, ammonia conversion of about 75 percent was obtained, which is the usual conversion attained in commercial units using natural gas and a platinum catalyst.

The low-volatile coals gave low yields of hydrogen cyanide; the high-volatile coals gave the best yields. The results indicated that the hydrogen cyanide is produced by reaction of ammonia with the hydrocarbons in the coal. Yields of hydrogen cyanide from reaction of ammonia with gas mixtures containing methane are directly related to the methane content of the gas.

Cost studies indicate that hydrogen cyanide can be produced from coal and ammonia at a price approximating the posted sales price.

BIBLIOGRAPHY

1. American Public Health Association, Inc. Standard Methods for the Examination of Water and Wastewater. 11th ed., 1960, pp. 355-356.
2. A.S.T.M. Standards with Related Material. Gaseous Fuels, Coal and Coke. Part 19, 1966, 470 pp.
3. Chemical Week, Market Newsletter, v. 99, No. 23, Dec. 3, 1966, p. 65.
4. Chemicals, Quarterly Industry Report, U.S. Business and Defense Services Admin., v. 12, No. 4, Dec. 1965, p. 40.
5. Current Industrial Reports, Inorganic Chemicals and Gases 1964. U. S. Commerce Department, Series M-28A, Released Jan. 28, 1966, p. 6.
6. Fieldner, A.C., and W. A. Selvig. Methods of Analyzing Coal and Coke. BuMines Bull. 492, 1951, 51 pp.
7. Fugate, W.O. Hydrogen Cyanide, pp. 574-585 in v. 6 Encyclopedia of Chemical Technology. Interscience Publishers, New York, N.Y., 1962, 2d ed., ed. by R. E. Kirk and D.O. Othmer.
8. Oil, Paint and Drug Reporter. V. 189, No. 23, June 6, 1966, p. 20.
9. Sherwood, Peter W. Synthesis of Hydrogen Cyanide by Autothermic Reaction. Refining Engineer, v. 31, No. 2, February 1959, pp. C-22-26.
10. U. S. Tariff Commission, Synthetic Organic Chemicals, U.S. Production and Sales:

1960 -	Tariff Commission Publication No. 34,	p. 53,	published 1961.
1961 -	ditto	72,	p. 53, published 1962.
1962 -	do.	114,	p. 56, published 1963.
1963 -	do.	143,	p. 55, published 1964.
1964 -	do.	167,	p. 55, published 1965.

All published in Washington, D. C.

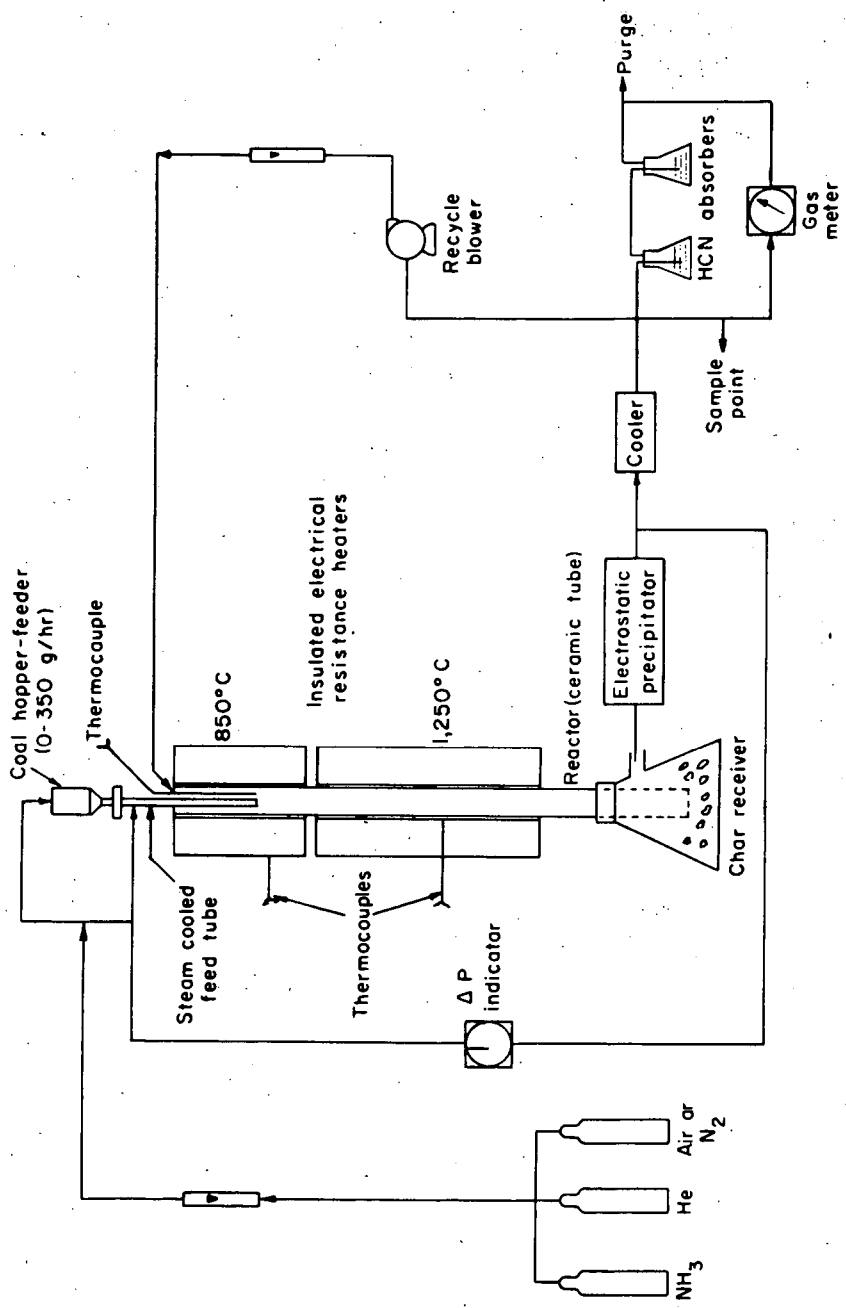


Figure 1. Flowsheet of hydrogen cyanide unit.

6-1-66

L-9365

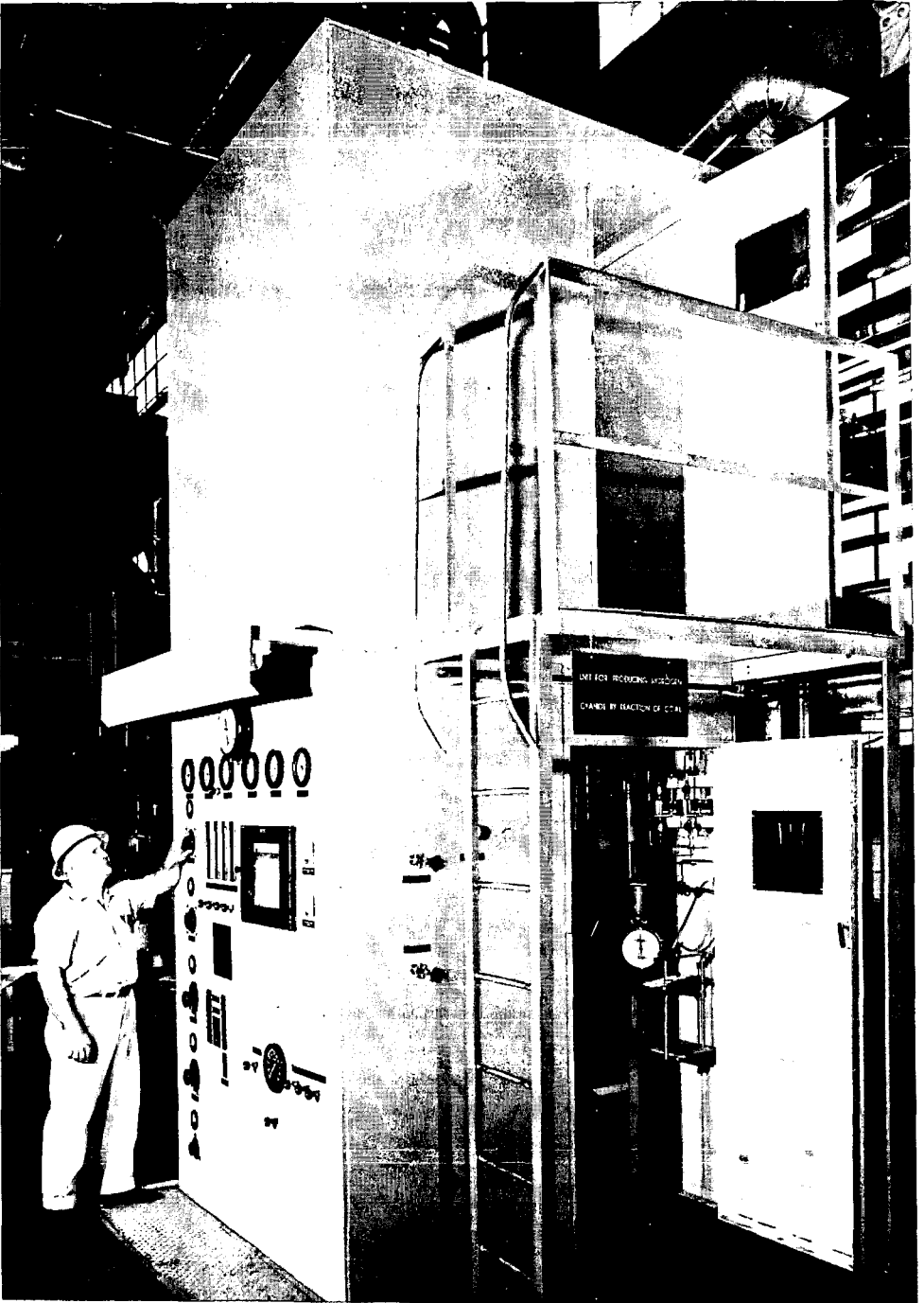


Figure 2. Enclosure surrounding hydrogen cyanide unit.



Figure 3. Hydrogen cyanide reactor.

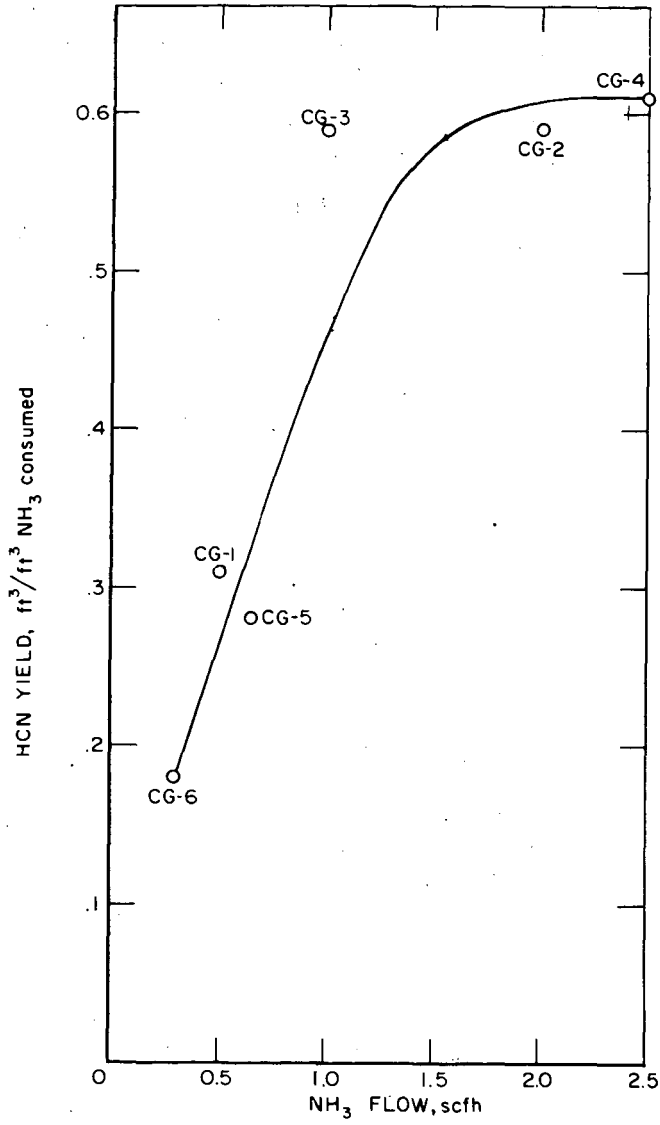


Figure 4. Effect of ammonia flow rate on yield of hydrogen cyanide from methane-ammonia reaction at 1,250° C. (Methane flow 2 scfh).

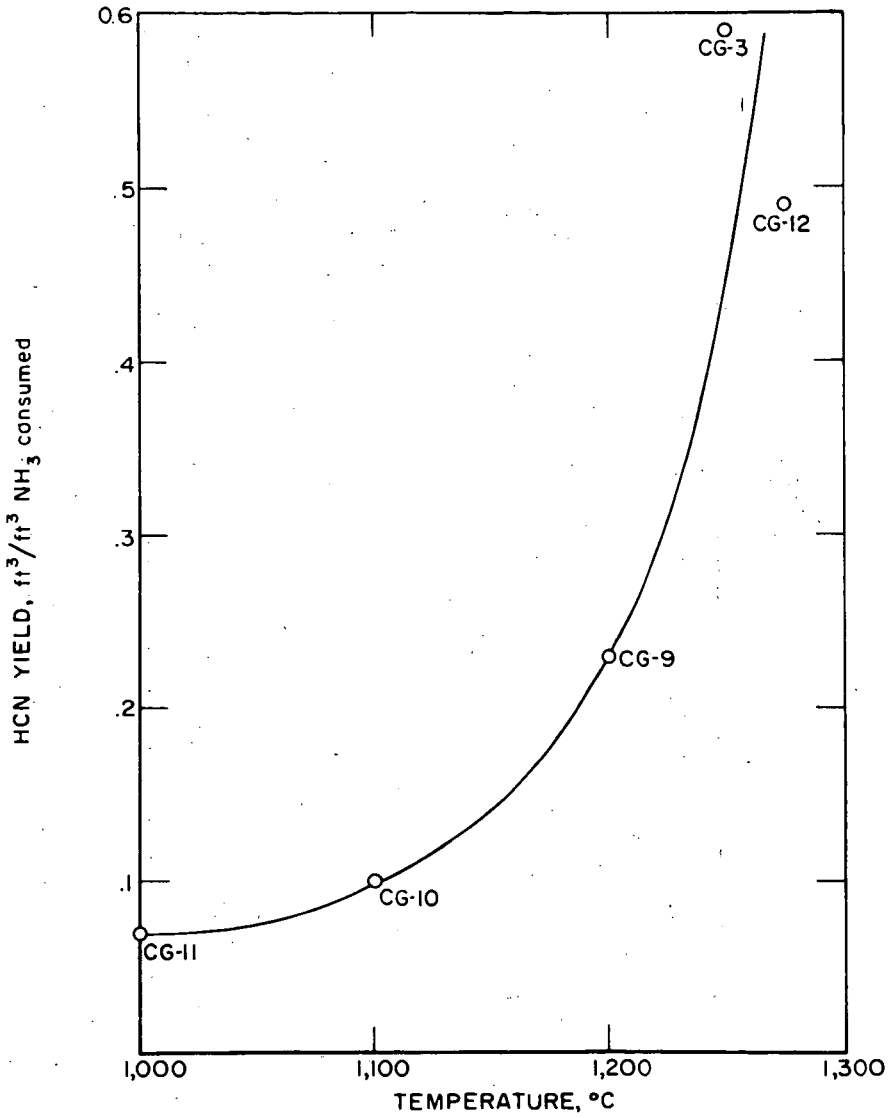


Figure 5. Effect of temperature on yield of hydrogen cyanide from reaction of methane (2 scfh) and ammonia (1 scfh).

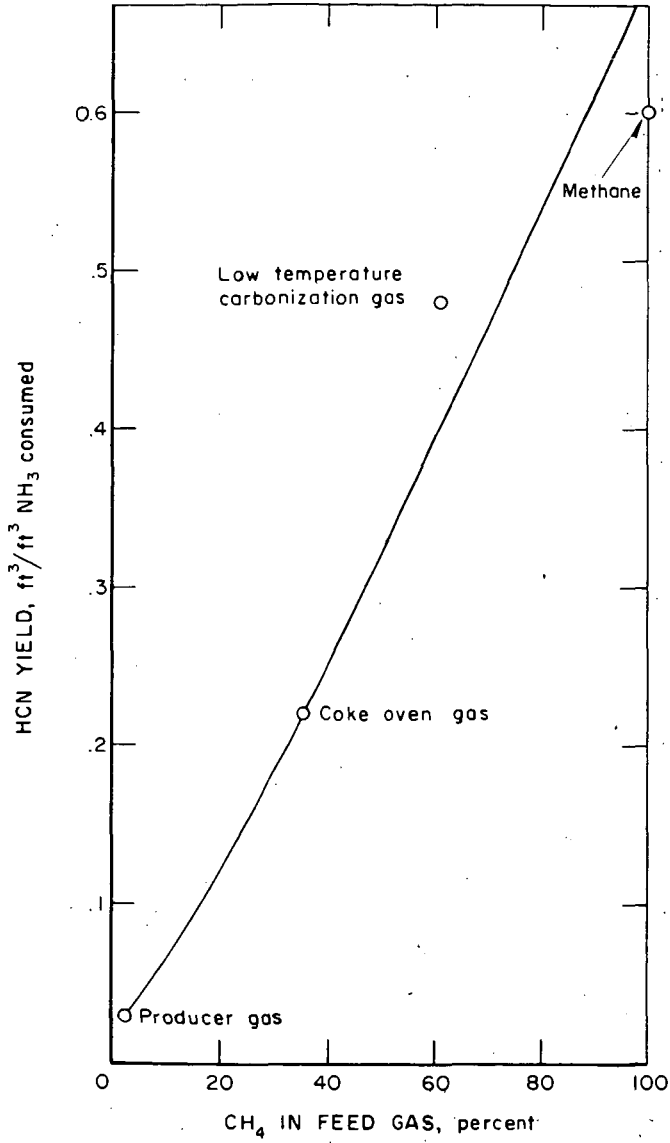


Figure 6. Variance of hydrogen cyanide yield with methane content of feed gas in reaction with ammonia at 1,250° C.

MÖSSBAUER SPECTROSCOPY OF IRON IN COAL

John F. Lefelhocz*, Robert A. Friedel[†], and Truman P. Kohman*

*Department of Chemistry, Carnegie Institute of Technology
 †Pittsburgh Coal Research Center, Bureau of Mines, U.S. Department of the Interior
 Pittsburgh, Pennsylvania 15213

INTRODUCTION

Metallic elements (Na, Mg, Al, Si, K, Ca, Ti, Fe) which occur abundantly in the ash obtained from the combustion of coals are present in the original coals partly as inorganic constituents or minerals. The identification of minerals present usually does not account quantitatively for several of these elements, and it is supposed that some sort of organic bonding with the coal is involved. The nature of this bonding in most coals has not been determined. Changes in the infra-red spectra of lignites and brown coals following acid and alkali treatment indicate the presence of metallic salts of carboxylic acids (1,2,3). For higher rank coals, little or nothing is known about the structures of the metallic elements "organically bound". In the case of iron, for example, it has not been determined whether the so-called "organic" iron is in the ferrous or ferric state, to what element or elements the iron is bonded, or whether there is more than one form of "organic" iron. The term "organic" must be interpreted with care; the nature of the bonding is uncertain; and presumably could be ionic, coordinate, or organo-metallic.

Mineral components containing iron can often be identified petrographically. Pyrite (FeS_2) is common, both as distinct nodules and as veins, often intertwined with carbonaceous macerals. An electron microprobe study of several coals (4) revealed, however, many examples which lacked a correlation between Fe and S distributions. In some cases Fe was distinctly associated with Si and Al, suggesting incorporation in an aluminosilicate gel or kaolinite. A strong parallelism of Fe and Ca (but not Si, Al, K, or S) in one specimen suggested the presence of Fe as carbonate or possibly oxide. In some cases the Fe showed fairly uniform distribution with no apparent correlation with other ash-forming elements. This presumably could be "organic" iron.

Mössbauer spectroscopy has been employed to study the chemical properties of iron in a great variety of natural materials: oxides and oxyhydroxides (5,6), sulfides (7,8), numerous silicate minerals (5,6,9,10,11,12), ilmenite and related titanium minerals (5,13), siderite (6), jarosites (5,14), löllingite (15), ordinary chondrite meteorites (16), carbonaceous chondrites (17), an achondrite (16), and several tektites (11).

Recent general articles on Mössbauer spectroscopy (18,19,20,21,22) discuss the interpretation of spectra in terms of the chemical state of iron, including its oxidation state, bonding, and environmental symmetry. The isomer shift (δ), quadrupole splitting (Δ), line width (Γ), line intensities, and a comparison of the spectra obtained at room temperature and at liquid- N_2 temperature are useful.

We have undertaken Mössbauer studies to characterize non-mineral iron in

coal. A major advantage of the Mössbauer technique is that the iron is observed without altering its chemical state or environment. The relatively low atomic number of the major elements present makes it possible for small amounts of iron to be observed in rather large amounts of coal. Samples of whole coal and vitrain as free as possible from minerals were selected in order to minimize mineral-iron interference, and a few samples whose chemical analysis indicated "organic" iron were included.

EXPERIMENTAL PROCEDURES

Nine specimens, vitrain or whole-coal, of seven coals with rank from lignite (72% C) to anthracite (95% C) were used. Their designations and geographic origins are given in Table 1, in order of increasing carbon content.

Table 2 is a compilation of the analytical data for C, H, N, S, Fe, ash, and O (by difference) on samples of these materials, as determined by the Coal Analysis group at the Bureau of Mines. The total iron in the coal was determined by ash analysis. HCl-soluble iron was determined by treating a separate powdered sample with 25% HCl to extract any iron present as carbonates, oxides, sulfates, etc. Pyrite iron was then removed by treating the HCl-leached coal with 25% HNO₃ to dissolve the iron combined with sulfur; the extract was evaporated to dryness to expel oxides of nitrogen, and the residue was dissolved in HCl. In each case the iron was reduced with SnCl₂, the slight excess of which was eliminated with HgCl₂. The reduced iron was titrated with potassium dichromate. "Organic" iron was then calculated by subtracting the two acid-soluble iron contents from the total iron. The resulting iron contents are listed in Table 2 as: total, HCl-soluble, pyrite, and "organic".

Mössbauer spectra were obtained on coal samples that were ground in a mortar and pestle. A cylindrical cell, open on one end with a circular aperture of 7.14 cm², was made by gluing a sheet of lucite 1/32" thick with Duco cement to the bottom of a circular wall made from a paper card. A 3.50-g sample was then placed into this cell. The top window, also 1/32" lucite, was then cemented in place. The sample mass per unit area was thus held constant at 0.490 g cm⁻². Inorganic iron compounds and mineral samples were ground and mounted either between two lucite sheets held together with Duco cement, or by mixing the solid with acetone and Duco cement and allowing this mixture to harden on a lucite sheet. This latter method was used only when the sample would not interact with acetone or the cement. The area for these samples was also 7.14 cm². All of the materials used in this investigation contained natural iron with presumably 2.19 atom % Fe⁵⁷.

The Mössbauer spectrometer incorporates a Nuclear Science and Engineering Corporation Model-B lathe-type drive modified in this laboratory for automatic operation. The operating mode employs constant velocity, advanced in increments of 0.05 mm s⁻¹. The detector of the 14.4-keV Co⁵⁷ → Fe⁵⁷ gamma radiation is a Reuter-Stokes proportional tube containing 10% methane in krypton, feeding through a single-channel analyzer set at 11 - 17 keV. Absorbers were mounted on the moveable table perpendicular to the radiation beam. The stationary source consists of ~ 5 mCi of Co⁵⁷ diffused into chromium metal. A Baird-Atomic scanning count integrator and Varian chart recorder plot the number of counts in a constant time interval at each velocity in succession.

Powdered samples of sodium nitroprusside gave an isomer shift, relative to the Co⁵⁷-Cr source, of -0.11 mm s⁻¹, and a quadrupole splitting of 1.68 mm s⁻¹. With this source a line width of 0.25 mm s⁻¹ was observed with an absorber containing 5 mg cm⁻² of Fe as K₄Fe(CN)₆·3H₂O. The estimated uncertainty in the velocity setting is about 2% of the velocity and the estimated uncertainty in derived spectral parameters is ~ 0.05 mm s⁻¹. The counting time at each velocity was ~ 5

Table 1. Designations, geographic origins, and adjusted* carbon contents of coal samples used.

Code #	Designation†	Geographic Origin	Mass fraction C* (%)
A	Indian Head lignite	Zap Bed, Indian Head Mine, N. Dakota	72.2
B	Harmatten vitrain, hvcb	No. 7 Bed, Harmatten Mine, Illinois	76.5
C	Corbin coal, hvab	High Splint Bed, Lynch Mine, Corbin Plant, Ky.	84.3
D	Bruceston vitrain, hvab	Pittsburgh Bed, Bruceston Mine, Pa.	84.2
E	Bruceston coal, hvab	Pittsburgh Bed, Bruceston Mine, Pa.	84.7
F	Jewell Valley coal, mvb	Jewell Bed, Jewell Valley Coal Co., Va.	90.3
G	Pocahontas No. 4 vitrain, lvb	Pocahontas No. 4 Bed, McAlpine No. 2 Mine, W.Va.	90.3
H	Pocahontas No. 4 coal, lvb	Pocahontas No. 4 Bed, McAlpine No. 2 Mine, W.Va.	90.4
I	Dorrance anthracite vitrain	Dorrance Mine, Lehigh Valley Coal Co., Pa.	92.7

* Adjusted to moisture- and ash-free basis. Calculated from C and ash contents of Table 2.

† h = high; m = medium; l = low; v = volatile; b = bituminous; a, c = sub-classifications of high-volatile coals.

Table 2. Analytical data on coal samples used.

Sample No.	Mass Fraction Fe (%) [*]			Mass fraction (moisture-free basis) (%) [†]						
	Total	HCl-sol.	Pyrite	"Organic" [†]	Ash	C	H	N	S	O [†]
A (a)	0.13	-	-	-	5.6	68.2	4.6	0.6	0.6	20.2
B (a)	0.81	0.40	0.27	0.14	1.0	75.8	5.3	1.3	1.8	14.8
C (a)	0.23	0.06 [§]		0.17	3.8	81.1	5.3	1.6	0.5	7.7
D (a)	0.62	-	0.33	(0.29) [#]	1.4	83.0	5.4	1.6	0.8	7.8
(b)	0.33	0.02	0.21	0.11						
E (a)	4.18	-	3.85	(0.33) [#]	1.9	83.1	5.6	1.6	0.7	7.1
(b)	0.32	0.06	0.20	0.06						
F (a)	1.39	0.24 [§]		1.16	1.8	88.7	4.6	1.4	0.5	3.0
(b)	0.47	0.37	0.08	0.02						
G (a)	0.46	0.03	0.00	0.44	1.2	89.2	4.6	1.5	0.8	2.7
H (a)	0.43	0.15	0.00	0.28	2.6	88.1	4.3	1.3	0.6	3.1
(b)	0.39	0.21	0.04	0.14						
I (a)	0.41	0.00	0.03	0.38	1.8	91.0	2.5	1.0	0.8	2.9
(b)	0.57	0.11	0.20	0.26						

[†] By difference.

^{*} In sample as received, before drying.

[§] Includes both HCl-soluble and pyrite iron.

[#] Includes both "organic" and HCl-soluble iron.

[†] Determined on samples other than those used for Mössbauer and iron determinations.

minutes, yielding ~ 600,000 counts and a relative standard deviation < 0.15%. The velocity region scanned for each sample was from -2.00 mm s^{-1} to about $+4.00 \text{ mm s}^{-1}$.

Most measurements were made a room temperature. A cryostat made from styrofoam was mounted on the moveable table of the instrument for low-temperature measurements. The sample was placed in this and submerged in liquid N_2 . The spectrum of each coal sample was run twice at room temperature, before and after the spectrum was taken at liquid- N_2 temperature.

Spectral parameters were generally read from plotted spectra. The data from sample F(a) were fitted to a double Lorentz curve by a least-squares program using an IBM 7040 computer. Isomer shifts are reported (in mm s^{-1}) with respect to the isomer shift of sodium nitroprusside. Quadrupole splittings are reported (in mm s^{-1}) as the velocity differences between the minima of two associated absorption lines.

DATA

Room-temperature spectra for the nine coal samples are illustrated in Figure 1. Each spectrum shows neither, either, or both of just two components: (1) a close doublet similar to those of pyrite and marcasite, and (2) a wide doublet similar to those of many ferrous compounds. Table 3 lists the Mössbauer parameters, including the fractional peak absorptions, for what we will call respectively the pyrite and non-pyrite resonances. Isomer shifts and quadrupole splittings obtained with our instrument on some powdered iron compounds and minerals which were regarded as possibilities for the non-pyrite spectrum appear in Table 4.

The parameters observed for the pyrite iron are: isomer shift (δ) = $+0.54 \text{ mm s}^{-1}$; quadrupole splitting (Δ) = 0.58 mm s^{-1} . All of the coals having a non-pyrite absorption as shown in Figure 1 have: $\delta = +1.38 \text{ mm s}^{-1}$; $\Delta = 2.62 \text{ mm s}^{-1}$. The computer analysis of sample F(a) indicated both lines in the spectrum had widths (Γ) of 0.39 mm s^{-1} ; their intensity ratio is within 5% of unity.

Liquid- N_2 spectra showed the same absorption peaks as at room temperature, with $\delta = +0.65 \text{ mm s}^{-1}$ and $\Delta = 0.58 \text{ mm s}^{-1}$ for pyrite and $\delta = +1.47 \text{ mm s}^{-1}$ and $\Delta = 2.78 \text{ mm s}^{-1}$ for the non-pyrite iron.

INTERPRETATION

The isomer shift is a function of nuclear properties and the electron density at the absorbing nucleus relative to that of the source or a standard absorber, such as sodium nitroprusside (23,24). As the electron density at the iron nucleus, due essentially only to s electrons, increases, the isomer shift decreases algebraically. Thus, ferrous compounds have a more positive isomer shift than ferric compounds, as the additional 3d electron of the former increases the shielding effect on the 3s electrons and thereby decreases their density at the nucleus (18). For ferric iron, isomer shifts (relative to sodium nitroprusside) have been observed in the range -0.1 to $+1.1 \text{ mm s}^{-1}$, and for ferrous iron from -0.1 to $+1.6 \text{ mm s}^{-1}$.

Quadrupole splitting into a two-line spectrum occurs when the iron nucleus is in an asymmetric electric field. The field consists of two parts, (1) that produced by the electrons of the iron atom, including those shared with adjacent atoms, and (2) that resulting from charges of the surrounding atoms; each part can contribute to asymmetry at the nucleus. Ferric compounds show quadrupole splittings from zero to about 2.3 mm s^{-1} ; here the asymmetry is caused chiefly by charges of the surrounding atoms. Ferrous compounds show larger values, from zero to $\sim 3.3 \text{ mm s}^{-1}$. Ferrous iron can exist in either a high-spin or a low-spin

Table 3. Room-temperature Mössbauer spectral parameters for coal samples*

Sample No.	Pyrite iron ²⁺			Non-Pyrite iron		
	Isomer shift [†] (mm s ⁻¹)	Quadrupole splitting (mm s ⁻¹)	Fractional absorption (%)	Isomer shift [†] (mm s ⁻¹)	Quadrupole splitting (mm s ⁻¹) [‡]	Fractional absorption (%)
A (a)	-	-	N.O.†	-	-	N.O.†
B (a)	0.59	0.55	1.6	-	-	N.O.
C (a)	-	-	N.O.	1.39	2.65	2.3
(b)	-	-	N.O.	1.30	2.65	2.1
D (a)	0.51	0.55	3.6	-	-	N.O.
(b)	0.53	0.48	3.6	-	-	N.O.
E (a)	0.50	0.58	22.7	1.41	2.70	2.6
(b)	0.50 _±	0.53	2.3	-	-	N.O.
(c)	0.50	0.53	1.7	-	-	N.O.
F (a)	-	-	N.O.	1.38	2.62	11.0
(b)	-	-	N.O.	1.39	2.65	5.5
G (a)	-	-	N.O.	1.38	2.65	1.5
(b)	-	-	N.O.	1.38	2.65	1.0
H (a)	0.54	0.60	1.3	1.39	2.65	1.5
(b)	0.59	0.60	1.7	1.36	2.60	1.7
I (a)	-	-	N.O.	-	-	N.O.
(b)	0.56	0.65	1.0	-	-	N.O.

* Weighing 3.50 g and distributed evenly over 7.14 cm².

‡ May include marcasite.

† With respect to center of sodium nitroprusside spectrum.

‡ Zero-point uncertain by 0.10 mm s⁻¹.

† N.O. = not observed; in general, < 0.5%.

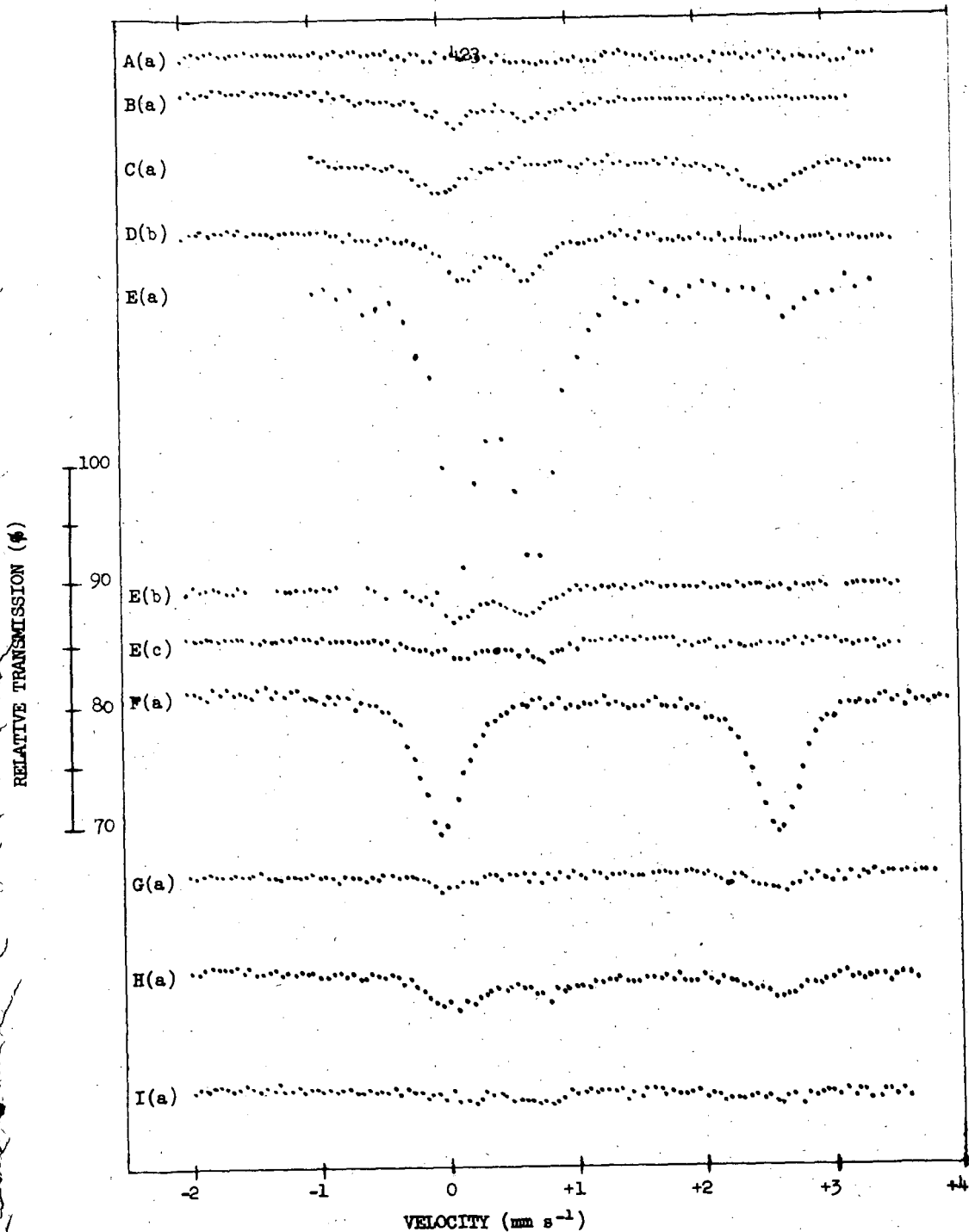


Figure 1. Mössbauer spectra of coal samples. In most cases, each point represents ~ 600,000 counts. The source was Co^{57} diffused into chromium metal. To convert the velocity scale to the sodium nitroprusside scale, add 0.11 mm s^{-1} to the indicated values.

state, depending on the strength of the ligand field around the central iron atom. In the high-spin configuration the large asymmetry of the valence shell results in considerable asymmetry at the nucleus; low-spin ferrous compounds have smaller field asymmetries, which are due chiefly to the external environments only.

Pyrite and marcasite, respectively stable and metastable forms of FeS_2 , are low-spin ferrous compounds. Isomer shifts and quadrupole splittings observed in this laboratory (Table 4) are in agreement with those of Temperley and Lefevre (8). The parameters of the two minerals are so similar that the spectra cannot be resolved when both are present. A comparison of the data in Tables 3 and 4 confirms the conclusions from petrographic (25) and x-ray diffraction (26) studies that the iron sulfide in coal consists mainly of pyrite.

From the Mössbauer data on the non-pyrite iron observed in several coal samples (Figure 1 and Table 3), it can safely be concluded that this iron is in a high-spin ferrous state. Furthermore, the combination of such high values of both isomer shift and quadrupole splitting has been reported only in octahedrally-coordinated high-spin ferrous compounds, so it is highly probable that the non-pyrite iron in coals is in octahedral coordination. Neither the analytical nor the Mössbauer data yields a distinction between inorganic or organic minerals or compounds.

The natural line width (Γ_0) of the Fe^{57} gamma radiation corresponds to a velocity difference of 0.0973 mm s^{-1} (27), and the minimum observable line width (Γ) in a Mössbauer spectrum is twice this, 0.195 mm s^{-1} . Inhomogeneities in the source and absorber, instrumental "noise", unresolved quadrupole splitting, and atomic spin-spin relaxation effects (22,28,29) increase the apparent line widths, and further widening occurs with thick absorbers (30). The minimum width we have observed with our instrument is 0.25 mm s^{-1} for a very thin absorber. The value of $\Gamma = 0.39 \text{ mm s}^{-1}$ observed for the strongest non-pyrite iron spectrum (sample F(a)) indicates that this doublet is caused by a fairly well-defined iron compound or mineral, though some inhomogeneity may be present.

A large number of iron compounds have strong Mössbauer absorptions (large recoil-free fractions) at room temperature. Some ferrous compounds show little or no absorption at room temperature, but at liquid- N_2 temperature the intensity is strongly enhanced (31,32). We have observed this effect with ferrous stearate, which must be cooled to liquid- N_2 temperature before resonant absorption is detected. Herzenberg and Toms (5) have observed that samples of $\gamma\text{-Fe}_2\text{O}_3$ and $\delta\text{-FeOOH}$ give nonresonant absorption at room temperature. These would probably exhibit an effect at liquid- N_2 temperature. Lack of such an effect in the coals is interpreted to mean that there are no compounds present in significant amounts that do not have appreciable resonant absorption at room temperature.

Isomer shifts and quadrupole splittings depend on the temperature. A second-order Doppler effect (22) decreases the isomer shift as the temperature is increased. Quadrupole splittings for high-spin ferrous compounds are affected by temperature much more strongly than those of other iron compounds because the population of the d_{σ} levels of iron in an octahedral field is determined by a Boltzmann distribution (18,22). For example, $\text{FeSO}_4 \cdot 7\text{H}_2\text{O}$ shows a change of δ from $+1.53$ to $+1.56 \text{ mm s}^{-1}$ and of Δ from 3.19 to 3.47 mm s^{-1} in going from room to liquid-nitrogen temperature (18). The observed change in the non-pyrite iron spectrum in coal of δ from $+1.38$ to $+1.47 \text{ mm s}^{-1}$ and of Δ from 2.62 to 2.78 mm s^{-1} is in agreement with our assignment to this class of compounds.

In some iron compounds where the Mössbauer absorption ordinarily shows a 6-line hyperfine structure as a result of a magnetic field at the nucleus, very

finely comminuted samples show instead a two-line pattern at room temperature as a result of thermal disruption of the macroscopic magnetic domains. Kündig et al. (33) observed this effect in $\alpha\text{-Fe}_2\text{O}_3$ in particles of $\sim 50\text{-\AA}$ diameter, but at liquid- N_2 temperature the 6-line pattern was observed. The absence of any magnetic splitting in the coal spectra at room- or liquid- N_2 temperatures probably rules out the possibility that the non-pyrite doublet is caused by a magnetically ordered material (such as Fe_2O_3 , Fe_3O_4 , FeC_3 , FeS , or metal) present as very small particles.

Inequality in the intensity of the components of a doublet may result from the anisotropy of the absorption cross section relative to the crystal axes when (1) a single-crystal absorber is oriented preferentially with respect to the optical axis, or (2) there is anisotropy in the recoilless fraction of the split $3/2$ state; the latter condition results in unequal absorption even with powdered samples (Goldanskii effect) (20,21). Most of the samples used in this work were powdered, so only the second effect could be operative, except for biotite, which was mounted as a sheet. The essential equality of intensity of the two non-pyrite coal spectrum lines would eliminate any compounds showing unequal absorption in powdered samples as possible causes of this absorption.

At the present state of Mössbauer spectroscopy, the identification of an unknown compound from its spectrum can only be made by finding a known compound having the same spectrum and temperature dependence. We have been unable to find any published combination of spectral parameters, for either natural or synthetic iron compounds, which match that of the non-pyrite iron in coal. Ankerite (Table 4), which has not been reported previously, likewise does not match.

In Figures 2 and 3 we have plotted Δ versus δ for all single- or two-line iron spectra for which we have been able to obtain data (5,6,8,9,10,11,14,18,31,34,35,36,37,38,39,40). Attention is called to the variations in δ and Δ within isomorphous silicate series (olivines, pyroxenes) in which the Fe/Mg ratio varies. Many silicate minerals show two or more coupled Mössbauer doublets, eliminating from consideration many points near the coal point on the plots. Biotite gives an apparent 2-line spectrum with δ and Δ similar to the coal spectrum, but with decidedly unequal intensities (our measurement), which persist in powdered samples (6), and which can be resolved into a coupled doublet (9), whereas the coal spectrum is symmetrical. Even considering the compositional variations and the uncertainties of measurement, it is apparent that the non-pyrite iron in coal is distinct from any compound whose Mössbauer spectrum is known. Minerals excluded include oxides and oxyhydroxides, sulfides and related compounds, the carbonates siderite and ankerite, titanian minerals, and the many silicates examined.

Some ferrous complexes of pyridines (35) and 1,10-phenanthrolines (37) have similar though non-matching δ and Δ values. These comparisons suggest that the non-pyrite iron could be bound to heterocyclic nitrogen aromatic groups in the coal macerals, or possibly in a clay-like silicate mineral or gel.

An attempt was made to correlate the Mössbauer absorption intensities in the coals with the analytical data. Mössbauer spectra were determined on mixtures of pyrite in carbon, and the fractional peak absorption was plotted against the mass fraction of pyrite iron. In a few coal samples the Mössbauer absorption and the analytically determined amount of iron as "pyrite" did agree with the above plot, but in others the agreement was poor. This may be due to the inadequacy of the chemical method for determining pyrite iron, and to differing matrix effects in the coals and the standards. Likewise, a poor correlation was found between the non-pyrite iron absorption in coals and the amount of "organic" iron deduced from the chemical analyses, although the sample with the highest "organic" iron, Jewell Valley coal F(a), showed the strongest non-pyrite Mössbauer spectrum.

Table 4. Room-temperature isomer shifts and quadrupole splittings for polycrystalline iron compounds and minerals

Compound or Mineral	This Work		Other Work		Ref.
	$\delta^*\S$	$\Delta\S$	$\delta^*\S$	$\Delta\S$	
Pyrite, FeS_2	0.54	0.60	0.55	0.61	8
Marcasite, FeS_2	0.51	0.50	0.52	0.51	8
Siderite, $(\text{Fe},\text{Mg})\text{CO}_3$	1.47	1.78	1.47	1.80	6
Ankerite, $(\text{Ca},\text{Mg},\text{Fe})\text{CO}_3$	1.46	1.50	-	-	-
Olivine, $(\text{Mg},\text{Fe})_2\text{SiO}_4$	1.39	2.95	1.39	3.04	10
Biotite, $\text{K}(\text{Mg},\text{Fe})_3(\text{AlSi}_3\text{O}_{10})(\text{OH})_2$	1.36	2.50	1.27 1.46	2.41 2.81	9
Tourmaline, $\text{Na}(\text{Mg},\text{Fe})_3\text{Al}_6(\text{BO}_3)_3(\text{Si}_6\text{O}_{18})(\text{OH})_4$	1.30	2.38	Fe^{+2} 1.19 Fe^{+2} 1.44 Fe^{+3} 0.99	2.10 2.61 0.91	10
Ferrous sulfate, $\text{FeSO}_4 \cdot 7\text{H}_2\text{O}$	1.56	3.05	1.53	3.19	18
Ferrous acetate, $\text{Fe}(\text{C}_2\text{H}_3\text{O}_2)_2$	1.45	2.23	-	-	-
Ferrous stearate, $\text{Fe}(\text{C}_{18}\text{H}_{35}\text{O}_2)_2$	0.66†	0.70†	-	-	-
Non-pyrite iron in coal	1.38	2.62	-	-	-

* Respect to center of sodium nitroprusside spectrum.

† At liquid nitrogen temperature; no resonant absorption observed at room temperature.

§ In mm s^{-1} .

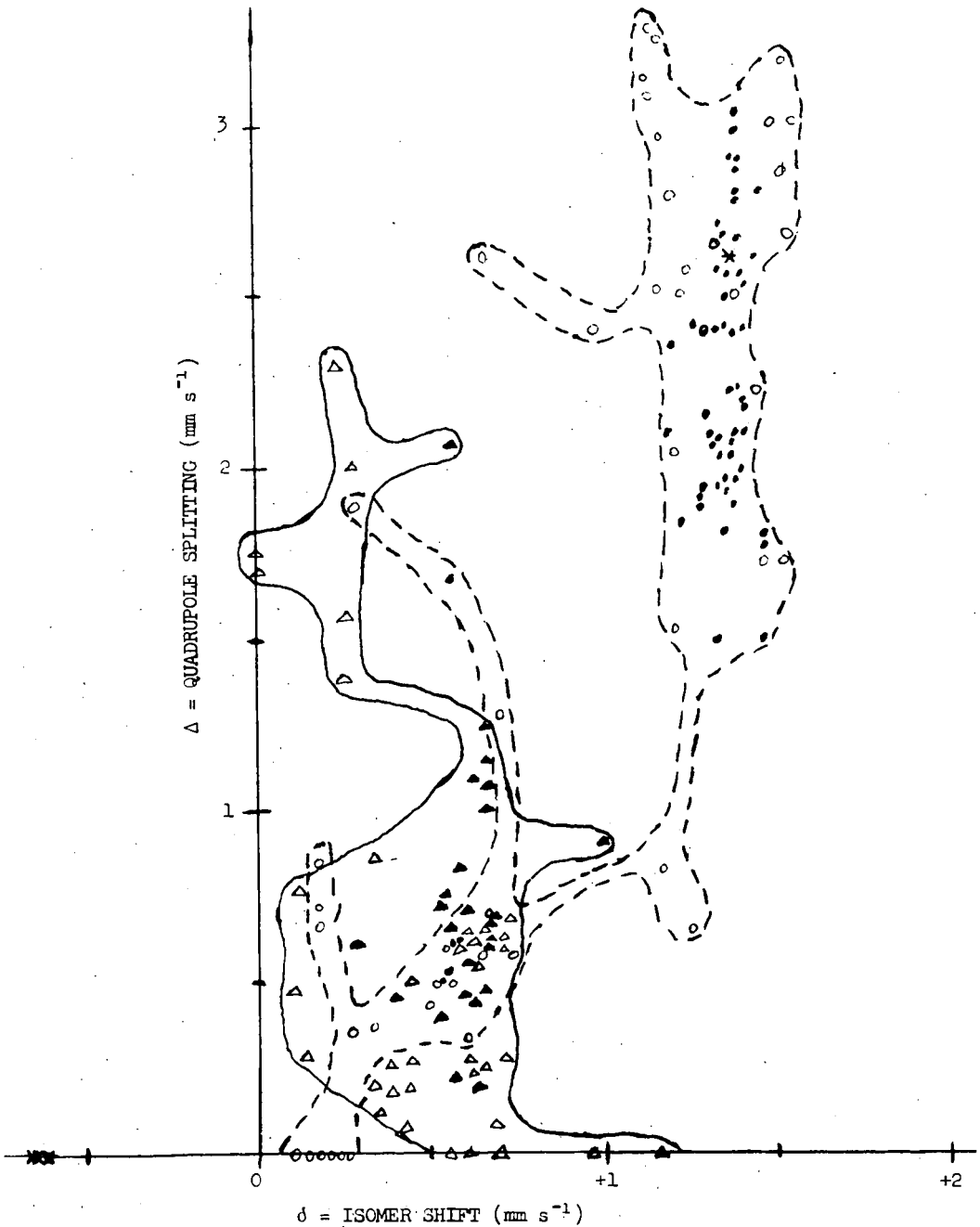


Figure 2. Representative plot of quadrupole splitting versus isomer shift (relative to sodium nitroprusside) for: — ferric compounds (Δ) and minerals (\blacktriangle); ---- ferrous compounds (\circ) and minerals (\bullet); ferrate compounds (\times), and the non-pyrite iron found in coal (*).

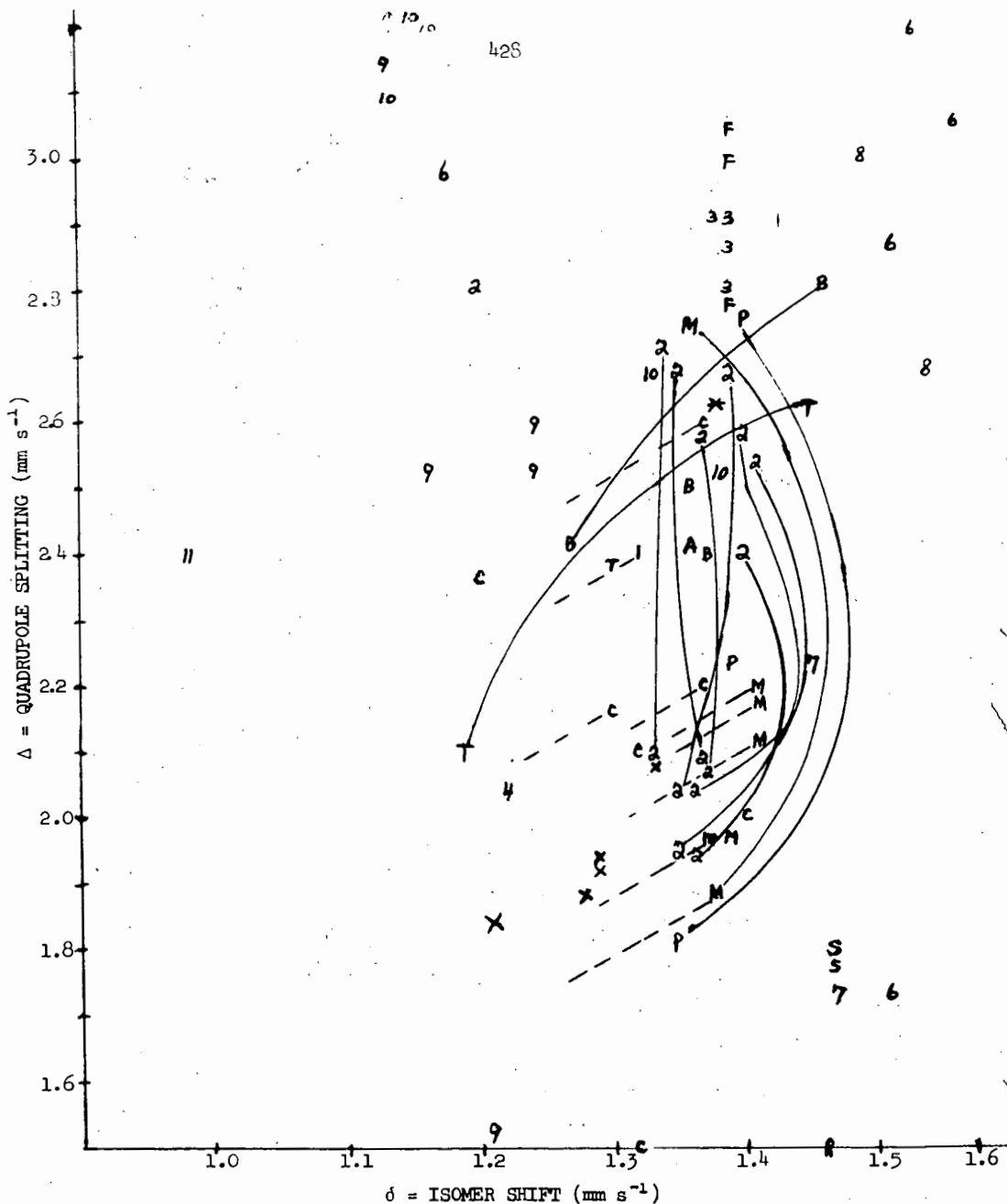


Figure 3. Enlarged section of Figure 2, showing quadrupole splitting versus isomer shift relative to sodium nitroprusside for two-line ferrous spectra. Lines connect pairs of points which are observed together in the same mineral or compound. Dashed lines indicate that a ferric spectrum is associated with the plotted ferrous point. Synthetic compounds: 1-ferrianite (synthetic mica), 2-synthetic pyroxenes, 3-synthetic olivines, 4-welding glass 5-germanium spinel, 6-oxy-salts, 7-carboxylates, 8-halides, 9-pyridine complexes, 10-phenanthroline complexes, 11-ferrous hemoglobin. Natural materials: A-actinolite, B-biotite, C-clay minerals, F-fayalite and olivine, M-clinopyroxenes, P-orthopyroxenes, R-ankerite, S-siderite, T-tourmaline, X-tektites, *-non-pyrite iron in coal.

CONCLUSION

In summary, several coal samples contain a form of iron which exhibits a hitherto unobserved Mössbauer spectrum, in addition to the well-known pyrite spectrum. The non-pyrite iron is ferrous, in a high-spin configuration, in octahedral symmetry, and apparently in a rather well-defined state. Comparisons with known compounds suggest that this iron may be bound in the coal macerals to heterocyclic nitrogen aromatic groups, though a clay-like silicate mineral or gel is a possibility. Mössbauer spectrometry can at the very least indicate the most suitable coal samples for further studies of this iron by chemical and other methods. It should ultimately permit unambiguous identification of the iron in coal with synthetic compounds or analogs. We intend to pursue this line of investigation.

ACKNOWLEDGEMENTS

We wish to thank Drs. Maurice Deul and Bryan C. Parks of the Bureau of Mines for their assistance in obtaining some of the coal samples. We are especially indebted to Mr. Michael Toia for the construction and maintenance of the Mössbauer spectrometer. The work at Carnegie Institute of Technology was performed under the auspices of the U.S. Atomic Energy Commission under contract AT(30-1)-844; Report No. NYO-844-69.

REFERENCES

- (1) Brooks J.D. and Sternhell S. (1957) Brown coals. I. Oxygen containing functional groups in Victorian brown coals. Australian J. Appl. Sci. **8**, 206-221.
- (2) Brooks J.D., Durie R.A. and Sternhell S. (1958) Chemistry of brown coals. II. Infrared spectroscopic studies. Australian J. Appl. Sci. **9**, 63-80.
- (3) Elofson R.M. (1957) Infrared spectra of humic acids and related materials. Can. J. Chem. **35**, 926-931.
- (4) Dutcher R.R., White E.W. and Spackman W. (1964) Elemental ash distribution in coal components--Use of the electron probe. Proc. 22nd Ironmaking Conf., Iron and Steel Div., Metallurgical Soc. of A.I.M.M.E., 463-483.
- (5) Herzenberg C.L. and Toms D. (1966) Mössbauer absorption measurements in iron-containing minerals. J. Geophys. Res. **71**, 2661-2677.
- (6) Pecull T.E. (1966) Thesis Georgia Institute of Technology, A study of iron in clay minerals using Mössbauer spectroscopy; Pecull T.E., Wampler J.M. and Weaver C.E. (1966) Mössbauer analysis of iron in clay minerals. Abstracts, 15th Ann. Clay Min. Conf. (Pittsburgh, Oct. 1966), 32-3.
- (7) Hafner S. and Kalvius M. (1965) Mössbauer studies of FeS minerals with the NiAs-type structures. Abstract DJ5, Bull. Am. Phys. Soc. (II) **10**, 1112.
- (8) Temperley A.A. and Lefevre H.W. (1966) The Mössbauer effect in marcasite structure iron compounds. J. Phys. Chem. Solids **27**, 85-92.
- (9) Pollak H., deCoster M. and Amelinckx S. (1962) Mössbauer effect in biotite. Phys. Stat. Sol. **2**, 1653-1659.
- (10) deCoster M., Pollak H. and Amelinckx S. (1963) A study of Mössbauer absorption in iron silicates. Phys. Stat. Sol. **3**, 283-288.
- (11) Marzolf J.G., Dehn J.T. and Salmon J.F. (1966) The study of oxidation states and ordering phenomena in tektites and iron bearing silicates using the Mössbauer effect. Symposium on the Mössbauer Effect sponsored by Nuclear Science and Engineering Corporation (New York, Sep. 1966).
- (12) Whitfield H.J. and Freeman A.G. (1966) Mössbauer studies of amphiboles. Abstracts, International Conference on Hyperfine Nuclear Spectroscopy at Victoria University (Wellington, Oct. 1966).
- (13) Avrahami M. and Golding R.M. (1966) Mössbauer spectroscopy as a tool in analytical chemistry. Abstracts, International Conference on Hyperfine Nuclear Spectroscopy at Victoria University (Wellington, Oct. 1966).
- (14) Hryniewicz A.Z., Kubisz J. and Kulgawczuk D.S. (1965) Quadrupole splitting of the 14.4-keV gamma line of ^{57}Fe in iron sulphates of the jarosite group. J. Inorg. Nucl. Chem. **27**, 2513-2517.
- (15) Imbert P., Gerard A. and Wintenberger M. (1963) Étude des sulfure, arséniosulfure et arsénure de fer naturels par effet Mossbauer. Compt. Rend. Paris **256**, 4391-4393.

- 5) Sprenkel-Segel E.L. and Hanna S.S. (1964) Mössbauer analysis of iron in stone meteorites. Geochim. Cosmochim. Acta 28, 1913-1931.
- 6) Gerard A. and Delmelle M. (1964) Effet Mössbauer et caractère ionique des atomes de fer dans les météorites Orgueil et Cold Bokkweid. Compt. Rend. Paris 252, 1756-1759.
- 7) Fluck E., Kerler W. and Neuwirth W. (1963) The Mössbauer effect and its significance in chemistry. Angew. Chem. Internat. Ed. 2, 277-287.
- 8) Wertheim G.K. (1964) Mössbauer Effect, Principles and Applications. Academic Press, Inc., New York.
- 9) Goldanskii V.I. (1964) The Mössbauer Effect and its Applications in Chemistry. Consultants Bureau, New York.
- 10) Herber R.H. (1965) Introduction to Mössbauer spectroscopy. J. Chem. Educ. 42, 130-137.
- 11) DeBenedetti S., Barros F. deS. and Hoy G.R. (1966) Chemical and structural effects on nuclear radiations. Ann. Rev. Nucl. Sci. 16, 31-83.
- 12) Herber R.H. and Hayter R.G. (1964) Mössbauer effect in cis-trans isomers. J. Am. Chem. Soc. 86, 301-302.
- 13) Spijkerman J.J., Ruegg F.C. and DeVoe J.R. (1965) Standardization of the differential chemical shift for Fe⁵⁷, Mössbauer Effect Methodology, pp. 115-120. Plenum Press, New York.
- 14) Thiessen G. (1945) Chemistry of Coal Utilization (Ed. H.H. Lowery), Vol. 1. John Wiley, New York.
- 15) Mitra G.B. (1954) Identification of inorganic impurities in coal by the X-ray diffraction method. Fuel 33, 316-330.
- 16) Eckhause M., Harris R.J., Shuler W.B. and Welsh R.E. (1966) Measurement of the lifetime of the 14.4-keV level of ⁵⁷Fe. Proc. Phys. Soc. London 89, 137-138.
- 17) Obenshain F.E., Roberts L.D., Coleman C.F., Forester D.W. and Thomson J.O. (1965) Hyperfine structure of the 14.4-keV γ -ray of ⁵⁷Fe in hydrated ferric ammonium sulfate as a function of the magnetization of the salt. Phys. Rev. Lett. 14, 365-369.
- 18) Wignall J.W.G. (1966) Mössbauer line broadening in trivalent iron compounds. J. Chem. Phys. 44, 2462-2467.
- 19) Margulies S. and Ehrman J.R. (1961) Transmission and line broadening of resonance radiation incident on a resonance absorber. Nucl. Instr. Meth. 12, 131-137.
- 20) Epstein L.M. (1962) Mössbauer spectra of some iron complexes. J. Chem. Phys. 36, 2731-2737.

- (32) Gibb T.C. and Greenwood N.N. (1966) The Mössbauer spectrum of the tetrachloroferrate(II) ion. J. Chem. Soc. London, 6989-6991.
- (33) Kündig W. and Bömmel H. (1966) Some properties of supported small α -Fe₂O₃ particles determined with the Mössbauer effect. Phys. Rev. 142, 327-333.
- (34) Muir A.H. Jr., Ando K.J. and Coogan H.M. (1965) Mössbauer Effect Data Index, Issue 5. North American Aviation Inc., Thousand Oaks, California.
- (35) Golding R.M., Mok K.F. and Duncan J.F. (1966) Magnetic susceptibility and Mössbauer results of some high-spin iron (II) compounds. Inorg. Chem. 5, 774-775.
- (36) Duncan J.F. and Mok K.F. (1966) A Mössbauer study of iron (II)-1,10-phenanthroline-complexes. J. Chem. Soc. London, Sec. A, 1493-1496.
- (37) König E. and Madeja K. (1967) $^5T_2-^1A_1$ Equilibria in some iron (II)-bis(1, 10-phenanthroline) complexes. Inorg. Chem. 6, 48-55.
- (38) Lang G. and Marshall W. (1966) Mössbauer effect in some haemoglobin compounds. Proc. Phys. Soc. London 87, 3-34.
- (39) Mathur H.B., Sinha A.P.B. and Yagnik C.M. (1965) The Mössbauer spectra of spinel oxides containing ferrous ion. Solid State Commun. 3, 401-403.
- (40) Frank E. and Abeledo C.R. (1966) Mössbauer effect in iron (III) dithiocarbamates. Inorg. Chem. 5, 1453-1455.

REACTIONS OF COAL AND RELATED MATERIALS IN MICROWAVE DISCHARGES IN H₂, H₂O AND Ar

Yuan C. Fu and Bernard D. Blaustein

U. S. Bureau of Mines, Pittsburgh Coal Research Center,
4800 Forbes Avenue, Pittsburgh, Pennsylvania 15213

INTRODUCTION

Recent investigations on the reaction of carbon in a high frequency discharge have shown that it produces methane, acetylene and minor amounts of other hydrocarbons in the hydrogen discharge,^{1-3/} but produces primarily an H₂-CO mixture downstream from a water discharge.^{3/} Similar work with respect to coal, however, is almost non-existent except that carried out by Letort et al.^{4/} and by Pinchin.^{5/} Though some work on coal in a plasma jet^{6-9/} has been reported, the characteristic of those reactions is generally the thermal decomposition of coal by rapid heating to high temperatures in an inert atmosphere.

In a microwave-generated discharge, hydrogen or water vapor can be excited or dissociated into atoms, ions and electrons at temperatures much lower than those attained in a plasma jet. The present study is concerned with the reactions of various coals, a polynuclear hydrocarbon, and graphite, in microwave discharges in H₂, water vapor and Ar. The results are compared in terms of the product yield and distribution in each type of discharge. Differences observed between the reactions of the various coals and the other materials suggest that the amount and type of volatile material, carbon content, and the type of the carbonaceous material, as well as the type of the gas discharge, are all factors affecting the product yield and distribution. The difference between coal and graphite in their behavior toward water vapor in the microwave discharge is of particular interest. In the water discharge, the graphite yields almost no hydrocarbons but only an H₂ + CO mixture while the coal yields appreciable amounts of C₂H₂ and CH₄ in addition to H₂ + CO. Experiments using D₂O and Ar discharges indicate that the D₂O and the water actually do participate in the reactions with coal to form hydrocarbons. It is also demonstrated that the C₂H₂ yield from coal in the hydrogen discharge can be drastically increased by condensing at a low temperature part of the primary products formed during the discharge reaction.

ACKNOWLEDGEMENTS

The authors wish to thank Dr. Irving Wender for his valuable discussions, Gus Pantages for his technical assistance, A. G. Sharkey, Jr. and Janet Shultz for their mass spectrometric analyses, and John Queiser for his infrared analysis.

EXPERIMENTAL

The experiments were carried out in a static system with the discharge produced by a Raytheon microwave generator in the air-cooled Ophthos coaxial cavity at 2450 Mc/sec. Chemical analyses and origins of the vitrains of the different coals used are given in table 1. All the vitrains were -200 mesh. Ultra purity spectroscopic graphite powder (325 mesh, United Carbon) and chrysene (C₁₈H₁₂) were used for comparison. As reactant gases, a 9.7:1 H₂-Ar mixture, H₂O-Ar mixtures and Ar were used. The H₂ and Ar were obtained from cylinders and passed through a liquid N₂ trap prior to storage. The water vapor was obtained from distilled water degassed in high vacuum.

In the experimental procedure, a known weight of graphite or coal powder was placed in a cylindrical Vycor tube (ID = 11 mm, vol = 32 ml) and degassed in a high vacuum at an elevated temperature (150°C for graphite and 100°C for coal) for a half to one hour to remove the moisture and the air adsorbed on the carbon. A known pressure of the reactant gas or gas mixture measured by a Pace Engineering pressure

transducer was then introduced into the reactor tube. For the H₂-Ar mixture, a known pressure of the water vapor was first introduced to the reactor containing the degassed carbon, and then a known pressure of the argon was introduced while the water was condensed in the end of the tube by dry ice and acetone. The portion of the tube cooled by the dry ice was so small compared to the total volume that no correction on the pressure reading seemed to be necessary. The discharge was then produced with the carbon in the discharge zone. The gaseous products were analyzed by mass spectrometer.

The solid product obtained from the high volatile bituminous coal in the H₂ discharge was analyzed by infrared spectrometer. The sample was obtained either by scraping the reactor wall or by solvent (benzene or acetone) extraction. In some instances, a reactor consisting of a tube divided by a fritted Vycor disc was used. The coal was placed on the disc and KBr powder was introduced on the other side of the disc. During the discharge, the lower end of the tube was immersed in liquid N₂, thus permitting the condensable low volatile products to pass through the disc and be adsorbed on the surface of the KBr powder. This was later removed, pressed into a pellet, and examined by infrared analysis.

TABLE 1. - Analysis of vitrains (moisture free basis, percent)

	C	H	N	S	O (by diff.)	Volatile matter	
Anthracite ^{1/}	91.06	2.49	0.96	0.83	2.89	1.77	6.1
Low volatile aminous ^{2/}	89.57	4.67	1.25	.81	2.17	1.53	20.2
bituminous ^{3/}	81.77	5.56	1.71	.97	5.87	2.06	39.2
Lignite ^{4/}	66.45	5.40	.31	1.40	22.84	3.06	44.0

^{1/} Dorrance Mine, Lehigh Valley Coal Co., Luzerne County, Pennsylvania.

^{2/} Pocahontas No. 3 Bed, Buckeye No. 3 Mine, Page Coal and Coke Co., Stephenson, Wyoming County, West Virginia.

^{3/} Bruceton, Pittsburgh Bed, Allegheny County, Pennsylvania.

^{4/} Beulah-Zap Bed, North Unit, Beulah Mine, Knife River Coal Mining Co., Beulah, Mercer County, North Dakota.

RESULTS AND DISCUSSION

All results were obtained from experiments using 5 mg of the carbonaceous material in each discharge at 35 watts of power input. For consistency, an initial total pressure of about 25 mm was used for most runs, but in the runs with H₂O vapor it was varied in the range of 12 to 25 mm. The time of the discharge reaction was intended to be 60 seconds in most runs, but the discharge would not sustain itself in some runs. It is suspected that the solid product (probably polynuclear hydrocarbons) formed may tend to draw away the electrons in the discharge to form negative ions and create a shortage of energetic species in the gas phase. However, under the experimental conditions employed, a large part of the reaction occurred within 30-60 seconds, and prolonged treatment resulted only in some change in the product distribution and a little increase in the extent of the gasification. A few runs were made for as long as 3 minutes.

Hydrogen-Argon and Argon Discharges

In preliminary runs with graphite in an H₂ discharge, we attempted to interpret the data on the basis of the hydrogen balance before and after reaction. It appears, however, that appreciable amounts of hydrogen were consumed in the formation of solid product or were taken up by the carbon. Therefore, to allow

interpretation of the data, Ar was introduced into the reactant gas as an internal standard. The presence of Ar in the system gives no noticeable effect on product type or distribution.

Table 2 summarizes the results obtained from the reactions of each material in microwave discharges in an H₂-Ar (9.7:1) mixture and in Ar. In the Ar discharge, coal is partially gasified to give H₂, CO, and C₂H₂ as the major gaseous products, CO₂, CH₄, and minor amounts of other hydrocarbons (C₂ and C₃ hydrocarbons, biacetylene and benzene were detected), in addition to a solid product and residual char. In the H₂-Ar discharge, the percent of carbon forming gaseous hydrocarbons is increased as compared with the Ar discharge; the total amount of carbon gasified is also increased. In this discharge, C₂H₂, CO, and CH₄ are the main constituents of the gaseous product, and minor amounts of other hydrocarbons are also formed as in the Ar discharge. Comparison of the several 60-second runs indicated that the net amount of hydrogen remaining after the reaction was decreased, except for high volatile bituminous coal and lignite. Besides that converted to hydrocarbons, part of the hydrogen was probably consumed in the formation of solid product or was taken up by the coal residue. With high volatile bituminous coal and lignite, gasification was extensive and resulted in a net increase of hydrogen.

The percent of carbon converted to gaseous hydrocarbons increases with the volatile matter of coal as shown in figure 1, suggesting that a rapid release of the volatile matter and its subsequent gas phase reaction in a discharge may be the determining factors. Figure 1 includes the data for graphite. Lignite, with the highest volatile matter, however, gave only small amounts of hydrocarbons in both discharges. The high oxygen content of the lignite results in higher yields of carbon oxides and water but apparently inhibits hydrocarbon formation. Water vapor, in a discharge, can reverse the reactions of hydrocarbon formation by reacting with the hydrocarbon species to form carbon oxides and hydrogen.^{10/}

Chrysene did not behave particularly different from coal in both discharges; the extent of gasification was appreciably small, approximately the same as that for anthracite. Interestingly, the carbon contents of the chrysene and the anthracite are also close to each other and are much higher than the other coals.

For coal in general, the higher the carbon content the lower the volatile matter. The extent of the reaction of graphite with H₂ was very much smaller under comparable conditions, probably due to the absence of volatile matter. The main products from graphite were CH₄ and C₂H₂; however, the hydrogen balance indicated, for example, that with an initial pressure of the H₂-Ar mixture of 25 mm Hg, the percentage of the initial hydrogen present in each component of the product is H₂, 77.6; CH₄, 9.2; C₂H₂, 3.3; C₂ + C₃ hydrocarbons, 1.6; and the remainder (8.3%) was apparently consumed in the formation of polymer or was taken up by the graphite.^{11/}

It is interesting to note that C₂H₂ accounted for 75-92% of the gaseous hydrocarbons produced from coal in both discharges. Hydrogasification or carbonization of coal usually gives CH₄ as the major hydrocarbons. It has been suggested that, in a microwave hydrogen discharge system, transport of carbon from the solid to the vapor phase takes place by bombardment of the carbon by energetic ions and electrons, and that the gaseous carbon species could react with H atoms or CH species to form hydrocarbons.^{2,3/} A similar mechanism appears to apply to the system containing coal except that H and CH species would also be evolved from the coal in addition to gaseous carbon species, even in the absence of an initial hydrogen. The predominance of C₂H₂, however, is also observed in rapid heating of coal by various high temperature methods such as plasma jet,^{6-9/} laser beam^{12/} and flash heating,^{13/} etc. A comparison of our experimental results with those obtained with an Ar plasma jet by Bond et al.^{7/} indicates that the percentage of carbon converted to C₂H₂ in our system is somewhat lower, but the effect of volatile matter on the hydrocarbon

yield is quite similar. The conversion of carbon to C_2H_2 for the high volatile bituminous coal (VM = 39.2%) in table 2 is 9.2% in the H_2 -Ar discharge as compared to 12.5% in the Ar plasma for a coal of similar volatile matter content.

TABLE 2. - Reactions of coal and related materials
in microwave discharges of H_2 and Ar

Material	Pressure, mm		Time, sec	Yield x 10 ⁴ , mole/g of solid					Percent of C present as	
	H ₂	Ar		H ₂	CH ₄	C ₂ H ₂	CO	CO ₂	Gaseous products	Gaseous hydrocarbons
hvab	22.7	2.3	60	63.9	4.7	31.1	21.1	0.2	13.6	10.4
	22.7	2.3	60	53.6	10.2	28.6	20.2	.2	13.1	10.3
	23.4	2.4	60	12.5	4.5	27.0	23.6	.4	12.8	9.4
	22.8	2.4	90	1/	3.9	29.8	22.2	.2	13.1	9.9
	21.8	2.3	105	1/	4.8	21.0	16.9	.2	9.9	7.4
	21.9	2.3	110	1/	3.6	20.0	16.0	.2	9.4	7.0
	-	25.7	17	3.3	.1	1.2	7.1	.1	1.5	.4
	-	24.0	60	56.4	.9	13.4	23.0	.2	7.7	4.3
	-	23.6	180	44.0	1.1	16.5	22.6	.2	8.7	5.3
lvb	23.8	2.5	34	1/	4.1	15.6	7.3	.1	6.1	5.1
	21.6	2.2	60	1/	3.8	17.5	8.1	.1	6.7	5.6
	-	23.5	60	19.3	.3	3.6	7.7	trace	2.1	1.1
Lignite	21.6	2.2	60	25.4	2.1	9.3	66.2	3.5	16.7	4.1
	22.6	2.3	180	22.9	2.1	7.7	80.3	1.8	18.3	3.4
	20.7	2.1	180	26.0	2.1	7.3	69.2	1.7	16.1	3.3
	-	24.7	32	50.4	.7	6.9	61.7	3.2	14.1	2.7
	-	23.0	60	18.4	.6	5.0	68.4	3.2	15.1	2.1
Anthracite	21.6	2.2	60	1/	4.2	8.3	4.0	trace	3.6	3.1
	22.6	2.4	60	1/	4.6	9.6	3.0	trace	3.9	3.4
	-	24.0	60	.3	trace	trace	2.0	.1	.3	-
Chrysene	22.7	2.4	10	1/	6.5	12.8	2.0	trace	4.6	4.4
	20.0	2.0	30	1/	10.4	5.8	trace	trace	3.4	3.4
	-	22.0	30	18.6	.8	2.6	trace	trace	.9	.9
Graphite	22.4	2.3	60	1/	3.5	2.5	trace	trace	1.2	1.2
	22.6	2.4	60	1/	3.4	1.8	trace	trace	1.0	1.0

1/ Net decrease of hydrogen was indicated.

Solid Product

The solid product obtained from coal is brownish and is similar to that usually observed from the thermal treatment of coal. No appreciable amount of solid product was formed from anthracite or from lignite. Though the extent of the gasification for the chrysene was not appreciable, the original white powder was instantaneously converted to a brown solid upon the initiation of both discharges. The infrared spectra of the solid product and the residual char obtained from the high volatile bituminous coal in the H_2 -Ar discharge showed the usual aliphatic C-H bands and some weak aromatic bands which are typical of pitch and coal.

Effect of Cooling by Liquid Nitrogen

Since the indications are that the water formed can retard the hydrocarbon formation and that the hydrocarbons produced may undergo further destructive reactions, it can be expected that a rapid quenching of the primary products should give a pronounced effect on the result. Experiments were carried out in a reactor consisting of the

tube divided by a fritted Vycor disc. The coal was placed on the disc, and was subjected to reaction in the H_2 discharge while the lower end of the tube was cooled in liquid N_2 . Though the process of condensing water and some hydrocarbons at this temperature is diffusion controlled, the effect is pronounced, as shown in table 3. For both the bituminous coal and the lignite, the yield of the hydrocarbons, C_2H_2 in particular, was greatly increased. The amount of H_2 remaining and the amount of CO produced after the reaction were also decreased. Therefore, the increase of hydrocarbon yield can be attributed mainly to subsequent hydrocarbon formation by reaction of H_2 and CO; this hydrocarbon yield is greatly enhanced by rapid removal of H_2O formed.

Water-Argon Discharge

There is a marked difference between the products obtained from graphite and coal in a water discharge. In the discharge in H_2O -Ar mixtures, as shown in table 4, graphite yields hydrogen and CO but practically no hydrocarbons; while the coals yield an appreciable amount of C_2H_2 and some CH_4 in addition to H_2 and CO. The amounts of H_2 and carbon oxides produced in the reaction with graphite were stoichiometric. The extent of gasification was also much greater for the coals than for the graphite. The active hydrogen species produced in the water discharge did not react further with the graphite or the CO formed from it to produce significant amounts of hydrocarbons. This is further evidence demonstrating that the presence of water vapor retards hydrocarbon formation.

For the reaction of a given coal in a H_2O -Ar discharge, an initial H_2O pressure of less than 12 mm Hg appears to give the optimum gasification and hydrocarbon production. Higher initial H_2O pressures cause a decrease in both gasification and hydrocarbon production. So long as the H_2O pressure is not at its highest values, more hydrocarbons are formed than in the Ar discharge. (Also, with the higher initial H_2O pressures, the discharge could not be initiated readily and would not sustain itself for as long as 60 seconds, perhaps due to too large an increase in the total gas pressure in the reactor.) The data seem to indicate that 60 seconds may have been too long a period for the maximum production of hydrocarbons. The formation of the hydrocarbons should be a maximum at the time when a plateau of the extent of coal gasification is attained, and prolonged treatment probably allows the remaining H_2O vapor to diffuse into the discharge zone, giving an adverse effect. It was also noticed that, at an initial H_2O pressure of less than 12 mm, the hydrogen content of the products exceeded that which could possibly be derived from the stoichiometric amount of the H_2O initially present.

These results seem to indicate the following. The active hydrogen species formed in the H_2O discharge participate in the reactions which lead to the formation of hydrocarbons from (some of) the species derived from the coal. This occurs despite the retarding effect of H_2O on hydrocarbon formation. (If the H_2O pressure is too high, this latter effect decreases the hydrocarbon yield.) Presumably, the coals when gasified supply enough CH species to allow hydrocarbons to be formed, even though the active oxygen species present react with some of the gaseous carbon and CH species. On the other hand, graphite produces negligible amounts of CH species in a H_2O -Ar discharge, and therefore cannot produce hydrocarbons since the reaction of the CO formed with the active hydrogen species is retarded by the H_2O present.

Lignite, with its high volatile matter content, was extensively gasified but gave a relatively low hydrocarbon yield, presumably due to the inhibition by its high oxygen content. For lignite, the production of CO_2 was also higher in the H_2O -Ar discharge than in the H_2 -Ar or Ar discharge. Again, the extent of gasification for chrysene was rather small.

TABLE 3. - Effect of cooling at reactor end by liquid nitrogen

Material	Pressure, mm H ₂ -Ar mixture (9.7:1)	Time, sec	Yield x 10 ⁴ mole/g of solid						Percent of C present as		
			H ₂	CH ₄	C ₂ H ₂	C ₂ H ₄	C ₂ H ₆	CO	CO ₂	Gaseous products	Gaseous hydrocarbons
HVA-bituminous	23.0	60	2/	8.2	22.6	3.2	2.4	8.6	0.4	11.1	9.8
	24.6	60	2/	4.9	23.8	2.3	1.7	7.6	.2	10.0	8.9
Lignite	24.5	180	2/	4.5	51.8	5.5	3.6	13.7	.5	20.4	18.3
	25.9	60	2/	2.8	17.0	.7	.7	38.0	3.6	14.8	7.3
	23.8	180	20.8	2.0	25.2	.7	.7	39.6	5.0	18.2	10.1

1/ Peaks attributed to HCN was neglected.
 2/ Net decrease of hydrogen was indicated.

TABLE 4. - Reactions of coal and related materials in microwave discharges of H₂O-Ar mixtures

Material	Pressure, mm H ₂ Ar	Time, sec	Yield x 10 ⁴ mole/g solid						Percent of C present as	
			H ₂	CH ₄	C ₂ H ₂	C ₂ H ₄	CO	CO ₂	Gaseous products	Gaseous hydrocarbons
hvab	18.1	7.6	17.3	0.5	8.6	28.4	2.1	7.3	2.8	
	18.0	5.7	25.8	.8	10.2	30.0	1.0	8.0	3.4	
	12.3	6.9	40.0	.8	16.5	42.6	.7	11.7	5.3	
	12.0	8.0	70.0	1.7	22.7	36.0	.7	12.8	7.3	
	11.2	7.7	34.0	1.2	18.2	39.0	1.0	11.8	5.9	
	10.5	8.2	56.4	2.0	24.4	44.8	2.0	14.8	7.9	
	7.9	8.6	102	2.0	23.0	38.6	.7	13.2	7.1	
	7.3	6.4	24.2	.9	15.8	27.0	.8	10.1	5.2	
	6.6	9.3	42.8	1.6	23.5	28.7	.8	11.9	7.6	
	11.2	6.7	180	115	1.9	15.4	60.0	.6	14.2	5.3
	18.4	7.3	25	13.8	.4	4.6	21.2	2.4	4.6	1.4
	10.0	7.7	60	20.9	1.1	13.6	25.8	.5	7.6	4.0
	Lignite	17.5	5.7	63.8	3.7	trace	52.6	16.6	13.4	.9
	Anthracite	11.0	8.8	89.0	1.5	10.0	87.2	5.0	20.9	4.1
		7.3	5.0	45.4	.6	10.4	42.4	.8	8.7	3.0
Chrysene	8.2	6.6	30.4	2.0	6.4	7.4	.2	3.0	2.0	
Graphite	16.3	5.4	24.2	trace	trace	19.4	3.0	2.8	-	
	18.9	5.9	37.8	trace	trace	28.8	5.4	4.1	-	

Deuterium Oxide-Argon Discharge

It is of interest to obtain further evidence as to whether water is actually involved in the reaction with coal to form hydrocarbons in addition to the production of $H_2 + CO$. The gaseous product obtained from the reaction of the high volatile bituminous coal in a D_2O -Ar mixture was analyzed by the high resolution mass spectrometer. At a resolution of 1 part in 20,000, precise masses for doublets and in some instances triplets that occurred at the same nominal masses could be used to identify completely deuterated, monodeuterated and nondeuterated species present in the product. For example, peaks due to C_2H_2 (mass = 26.0156), C_2D (26.0141) and CN (26.0031) were observed at the nominal mass of 26 and peaks due to C_2D_2 (28.0282), N_2 (28.0061) and CO (27.9931) were observed at the nominal mass of 28. The whole spectrum up to the nominal mass of 44 contained peaks attributed to all species present including minor amounts of oxygenated and N-containing compounds, but the major products were H_2 , HD , D_2 , C_2H_2 , C_2HD , C_2D_2 and partially deuterated methanes in addition to D_2O , DHO , H_2O and carbon oxides. Thus it is apparent that D_2O is initially dissociated into D , OD and possibly an active oxygen species which in turn recombine to give D_2O and D_2 , or react with the active species derived from coal such as H , CH , C_1 , C_2 and CO , etc., to give DHO , HD , CO , CO_2 and deuterated hydrocarbons.

CONCLUSIONS

In the microwave discharges of H_2 , H_2O and Ar, coal is gasified to give gaseous hydrocarbons and carbon oxides plus a solid product and residual char. Hydrogen is also produced either by dissociation of the water vapor or by devolatilization of the coal in the H_2O and/or Ar discharges. But, in most cases in the hydrogen discharge, hydrogen is consumed rather than produced (except for hvab coal and lignite). The yield of the hydrocarbons is highest in the hydrogen discharge and that of carbon oxides is highest in the water discharge. Both the hydrogen and the water discharges give greater extents of gasification and yield more hydrocarbon products than the Ar discharge, indicating the occurrence of gas phase reactions of H , OH , and active oxygen species with the active species derived from the coal. The gasification of coal in the water discharge is of particular interest because it produces $H_2 + CO$ (~ 1:1) plus C_2H_2 and CH_4 . The high oxygen content of the lignite results in a higher yield of carbon oxides but apparently inhibits the hydrocarbon formation in the discharge. The hydrocarbon yield from the lignite or other coals in the hydrogen discharge, however, can be increased dramatically by rapidly condensing part of the product species produced, especially H_2O , during the discharge reaction.

C_2H_2 accounts for as much as 92% of the gaseous hydrocarbons produced, and, excepting for lignite, the amount of the hydrocarbons is related to the volatile matter of coal. The extent of gasification, however, is increased with the volatile matter content of coal including lignite. Thus, if the hydrocarbons are formed by the recombination of the species derived from the volatile material and other species present in the discharge, another interesting study would be to employ a flow system in which coal is devolatilized by ordinary means and the evolved gases are subsequently reacted in a discharge.

REFERENCES

1. Blackwood, J. D. and McTaggart, F. K. Reactions of Carbon with Atomic Gases. *Australian J. Chem.*, 12, 533 (1959).
2. Shahin, M. M. Reaction of Elementary Carbon and Hydrogen in High-Frequency Discharge. *Nature*, 195, 992 (1962).
3. Vastola, F. J., Walker, P. L. Jr., and Wightman, J. P. The Reaction Between Carbon and the Products of Hydrogen, Oxygen and Water Microwave Discharges. *Carbon*, 1, 11 (1963).

4. Letort, M., Boyer, A. F., and Payen, P. Attempting Hydrogenation of Coal with Atomic Hydrogen. *Bull. Soc. Chim. France*, 1589 (1963).
5. Pinchin, F. J. The Reaction of Coals with Atomic Hydrogen. Private Communication.
6. Bond, R. L., Galbraith, I. F., Ladner, W. R., and McConnell, G. I. T. Production of Acetylene from Coal, Using a Plasma Jet. *Nature*, 200, 1313 (1963).
7. Bond, R. L., Ladner, W. R., and McConnell, G. I. T. Reactions of Coal in a Plasma Jet. *Fuel*, 45, 381 (1956).
8. Graves, R. D., Kawa, W., and Hiteshue, R. W. Reactions of Coal in a Plasma Jet. *Ind. Eng. Chem.*, 5, 59 (1966).
9. Kawana, Y., Makino, M., and Kimura, T. Formation of Acetylene from Coal by Argon Plasma. *Kogyo Kagaku Zasshi*, 69, 1144 (1966).
10. Blaustein, B. D. and Fu, Y. C. Formation of Hydrocarbons from $H_2 + CO$ in Microwave-Generated Electrodeless Discharges. Paper to be presented at 153rd National ACS Meeting, Miami Beach, Fla., April 1967.
11. Montet, G. L. Retention of Protons by Graphite. *Proc. Fourth Conf. on Carbon*, Pergamon, New York, pp. 159-164 (1960).
12. Sharkey, A. G., Shultz, J. L., and Friedel, R. A. Gases from Flash and Laser Irradiation of Coal. *Nature*, 202, 988 (1964); *Coal Science, Advances in Chemistry Series 55*, R. F. Gould, Editor, Am. Chem. Soc., Washington, pp. 643-649 (1966).
13. Rau, E. and Seglin, L. Heating of Coal with Light Pulses. *Fuel*, 43, 147 (1964).

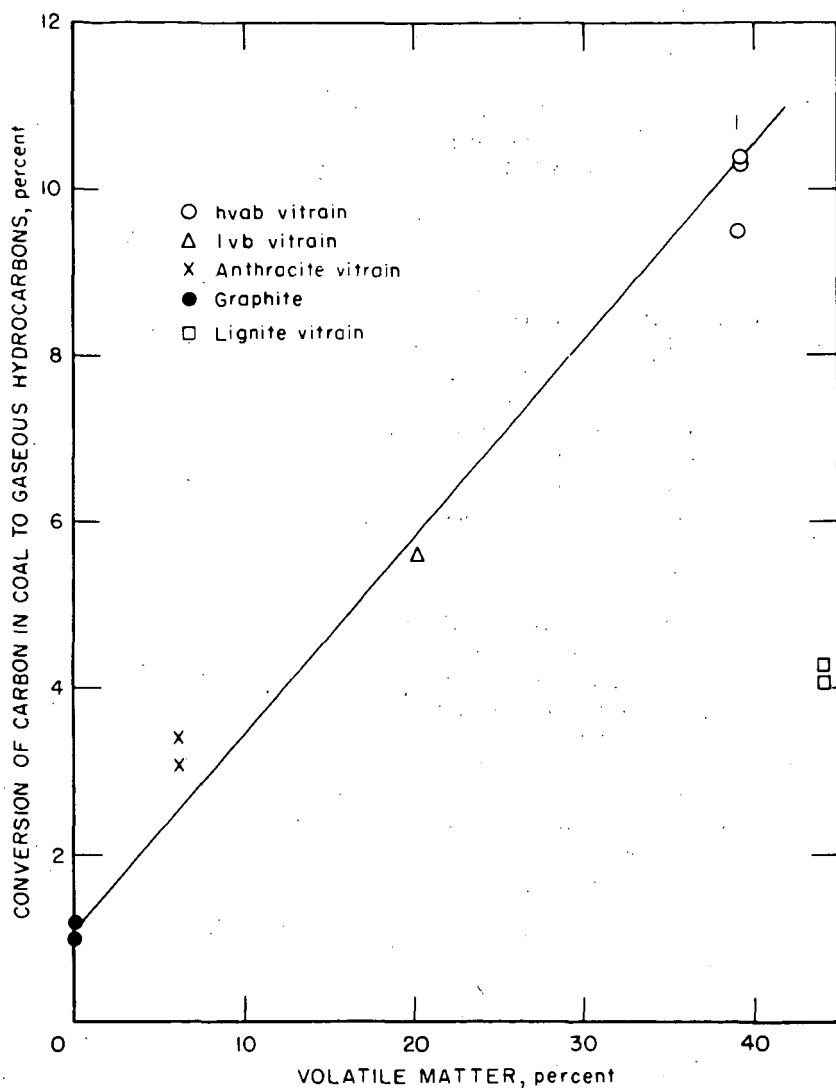


Figure 1 - Effect of volatile matter on yield of hydrocarbons in H_2 -Ar discharge (60 second run)

12-29-66

L-9741

CHEMICAL REACTIONS IN A CORONA DISCHARGE I. BENZENE

M. W. Ranney¹
Wm. F. O'Connor

Department of Chemistry
Fordham University
New York, New York 10458

INTRODUCTION

Corona discharges (silent) have been used to initiate chemical reactions for well over 150 years with much of the early work being confined to inorganic gases.² However, the only commercially significant development over the years has been the process for synthesizing ozone by subjecting oxygen to a corona discharge³ (ozonizer). Most early investigators encountered serious difficulties in studying the interaction of high voltage electricity with organic molecules. Equipment was unreliable and dangerous, and the complexity of the reaction product mass precluded definitive performance evaluation. Since World War II, technology has advanced to the point where high frequency power can be generated and controlled at reasonable cost and many new dielectric materials such as fused quartz, alumina and mica mat are available.⁴ Modern analytical techniques afford the opportunity to determine the composition of the product mix.

Corona electrons are accelerated by the applied voltage to an energy level of 10-20 electron volts, which is sufficient to break the covalent bond. This represents a very efficient approach when compared with high energy radiolysis (m.e.v. range) where the actual chemical work is effected by secondary electrons with an energy of 10-25 e.v., formed after a series of energy-dissipating steps. Potentially, corona energy can deliver electrons to the reaction site at the desired energy level to give products which are not readily obtainable by more conventional means. The energy available in the corona discharge is somewhat above that commonly encountered in photochemistry (up to 6 e.v.).

Bertholot reduced benzene to C_6H_8 in 1876 in what appears to be the first exposure of an aromatic compound to the corona discharge.⁵ Losanitsch obtained the following products from benzene in an electrical discharge: $(C_6H_6)_2$, biphenyl, (C_72H_96) and $(C_6H_6)_{90}$.⁶ Benzene vapor treated at 300° in an ozonizer tube gave resinous products with a 6/4 carbon-hydrogen ratio.⁷ Linder and Davis exposed benzene vapor to 37,000 volts and found biphenyl, gaseous products and evidence of polymerization.⁸ The early work with benzene reactions in various types of electrical discharges is reviewed in considerable detail by Glocker and Lind.² Brown and Ripper investigated the hydrogenation of benzene flowing down the walls of an ozonizer tube and found 1,3- and 1,4-cyclohexadiene, biphenyl, and a resinous mass which gave an infrared spectrum consistent with polystyrene.⁹

In recent years, benzene has been subjected to direct electrode discharge¹⁰ and glow discharges induced by microwave¹¹ and radiofrequency¹² energy. In this paper, we report some of our observations for the reaction of benzene in a corona discharge.

APPARATUS

The corona reactor system used in this study is shown in Figure 1 and the reactor details are given in Figure 2. The system is designed to run at atmospheric or reduced pressure and, with slight modification, under recycle conditions. The use of the threaded rod center electrode affords a more uniform and higher treating potential than is obtained with a cylindrical electrode.¹³ The electrode threads concentrate surface irregularities thereby eliminating severe discharge points. The copper electrode serves as a cooling coil and affords direct observation of the corona. In a typical run, the benzene reservoir temperature is set at 55°, the helium is adjusted to 100 ml/min. and after a two minute purge, an electrical potential of 15,000 volts is applied. A brilliant blue corona is established, the intensity being a function of helium flow, pressure, benzene content and the applied voltage. Benzene traverses the corona reactor as a vapor and is condensed by the cold water trap and collected. Yellow solids gradually deposit in the flask at the bottom of the reactor and eventually adhere to the dielectric surfaces in the reactor. Some benzene and the more volatile reaction products are condensed in the -70 and -195° traps. See experimental section for further details.

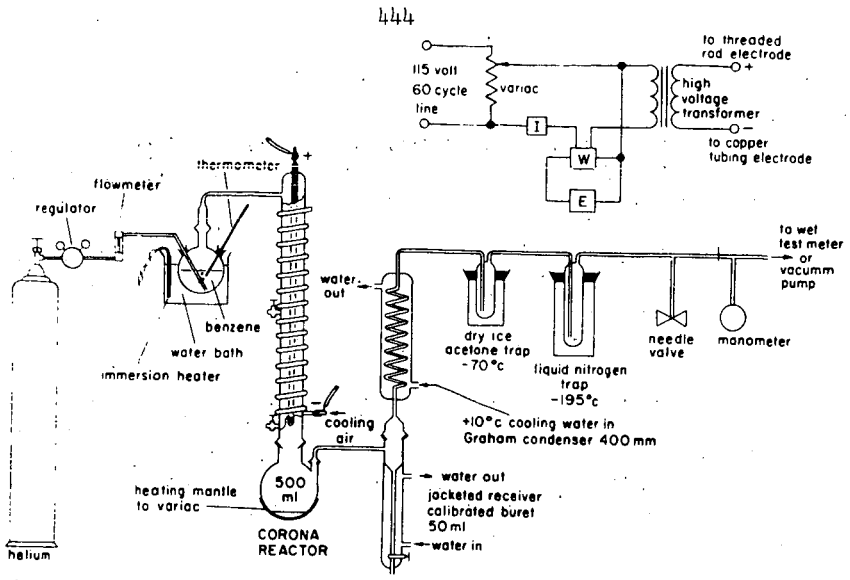
RESULTS AND DISCUSSION

The excitation of benzene vapor in a corona discharge provides an 8.5% conversion to identifiable products. The major products are a benzene soluble polymer (6%), a benzene insoluble polymer (0.7%), biphenyl (0.3%), and acetylene (1%). The composition of the product mix obtained is given in Table 1. The overall yield obtained under our experimental conditions is similar to that produced in a radiofrequency glow discharge¹² (10%, with longer residence time) and somewhat higher than Streitwieser obtained using a microwave¹¹ induced glow discharge (5%). The corona discharge gives a considerably higher proportion of polymer than is obtained from these other energy sources. Benzene substitution products such as toluene, phenylacetylene and ethylbenzene were observed in the microwave discharge but were not noted in this study or in the radiofrequency investigation. The high yield of fulvene in the radiofrequency discharge is surprising in view of its tendency to polymerize or add oxygen under rather mild conditions. The sum of the carbon and hydrogen analyses for the polymeric fraction obtained by Stille in the glow discharge of benzene (86-94 per cent) suggests some fixation of oxygen and/or nitrogen during discharge or product work-up.¹² The pressure for these electrodeless glow discharge studies was of the order of 20 mm. or less, while the corona reactor was operated at atmospheric pressure. Schüller, using an electrode discharge in benzene, obtained products similar to those produced in the microwave glow discharge.¹⁰

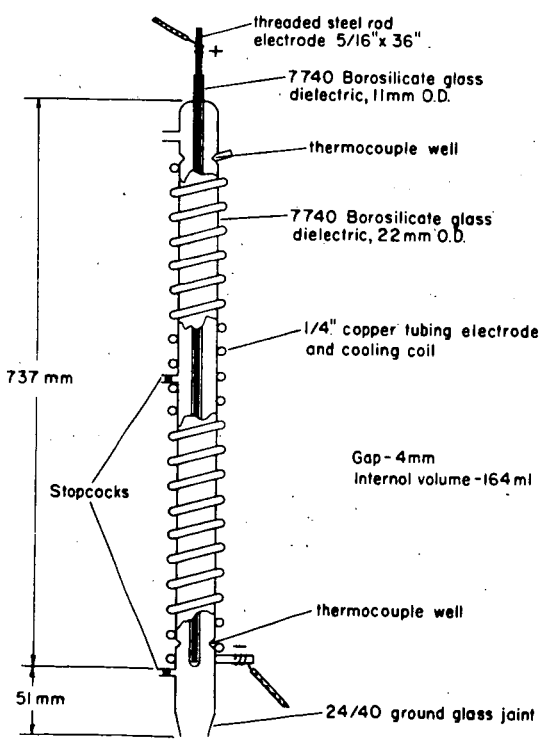
The reaction products obtained in this study are roughly categorized as the benzene fraction, biphenyl fraction and polymeric material for purposes of discussion. After initial studies indicated that the components of the -70 and -195° traps were similar to those in the benzene trap, these samples were combined. The acetylene content of the low temperature traps was determined by weight loss prior to mixing with the benzene.

Benzene Fraction

The exposed benzene, as collected in the cold traps, is bright yellow. The following reaction products have been identified in this fraction: 1,3-cyclohexadiene, 1,4-cyclohexadiene, fulvene and cyclohexene. The approximate per cent yield for each of these constituents is given in Table 2. The data were determined using a 100 foot



CORONA REACTOR SYSTEM
Figure 1



DETAIL OF CORONA REACTOR
Figure 2

TABLE 1

Product Distribution in the Corona Discharge of Benzene, 15KV

Product	Yield-Per Cent Benzene Exposed	Yield-Per Cent of Product Mix	Radiofrequency ^(c) Yield, Per Cent
Benzene insoluble polymer	0.7	8.2	N.D. ^(d)
Benzene soluble polymer (a)	6.0	70.5	5.0 ^(e)
Biphenyl	0.3	3.5	2.0
o-, m-, and p-Terphenyl	0.1	1.2	N.D.
Phenyl, benzyl substituted cyclopentenes ^(b)	0.3	3.5	N.D.
1,3-and 1,4-Cyclohexadiene	0.1	1.2	N.D.
Fulvene	0.01	0.1	1.0
Acetylene	1.0	11.8	2.0 ^(f)
TOTAL	8.5	100.0	10.0

(a) Polymer fraction includes materials from 250 molecular weight and up.

(b) Includes several phenyl and benzyl substituted cyclopentenes similar to biphenyl and o-terphenyl in vapor pressure. See discussion.

(c) See reference No. 12.

(d) N. D. -- not determined.

(e) Benzene and toluene soluble polymer.

(f) Acetylene 1%, allene 1%.

support-coated open tubular column with a squalane liquid phase and appropriate calibration standards (Figure 3). No significant change is noted in the cyclohexane content when compared with starting benzene. The increase in the methyl cyclopentane peak is ascribed to its higher vapor pressure thus affording some accumulation of this material in the benzene distillate and a concomitant depletion in the benzene feed stock. Cyclohexene is produced in very low yield, as expected, because of the degree of hydrogenation required during its short residence time in this single pass reactor.

The reduction of benzene to the cyclohexadienes is interesting as 1,3-cyclohexadiene is thermodynamically unstable with respect to benzene, cyclohexene and cyclohexane.¹⁴ The synthesis of 1,3-cyclohexadiene under these conditions is analogous to the conversion of oxygen to ozone which also represents an energetically unfavorable process. The momentary energy input and the rapid removal of the activated species from the reaction zone affords this material in low yield. As expected, the more stable 1,4-cyclohexadiene is produced in higher yield (3/1). Additionally, 1,3-cyclohexadiene would be expected to polymerize at a rapid rate under these conditions. The thermodynamic instability of 1,3-cyclohexadiene is demonstrated by its gradual disappearance from the sample after a few days standing at room temperature. The yields of both the 1,4- and 1,3-cyclohexadiene are somewhat higher than previously reported by Brown and Rippere.⁹ The yields reported by these workers after 24 hours exposure to a 15 KV corona discharge in a counter-current hydrogen stream were 0.02 and 0.01 per cent respectively. The major variable in technique which likely accounts for this difference in yields is the use of benzene vapor in our work, versus the hydrogenation of a thin liquid benzene film running down the annular dielectric surface by Brown and Rippere.

The ultraviolet spectrum for the benzene fraction was obtained by running differentially against pure benzene in isooctane. A broad absorption band with a maximum at 258 μ is ascribed to the 1,3-cyclohexadiene. An additional absorption at 242 μ and a tailing into the visible region with a broad maximum at 360-370 μ is also observed. These spectral features are consistent with those reported for fulvene, the non-aromatic isomer of benzene.¹⁵ Blair and Bryce-Smith found fulvene in the photochemical irradiation of benzene in what appears to be the first direct conversion of an aromatic hydrocarbon to a non-aromatic hydrocarbon.¹⁶ Fulvene co-distilled with benzene, but could be separated from benzene using the 100 ft. squalane column (Figure 3). Fulvene prepared by the method of Meuche gave the same retention time and spectral features.¹⁷ Additional evidence for assignment of the fulvene peak included its disappearance from the chromatogram after the sample was refluxed with maleic anhydride (color disappears) or exposure to a free radical catalyst. The Diels-Alder reaction product with maleic anhydride was isolated and hydrolyzed to give the adduct, 7-methylene-5-norbornene -2, 3-dicarboxylic acid. The melting point and infrared data for this adduct were identical with the sample prepared using fulvene synthesized from cyclopentadiene and formaldehyde.¹²

The formation of the 1,3,5-hexatrienyl diradical has been suggested as an intermediate in the photochemical decomposition¹⁸ and the radiofrequency discharge¹² of benzene. Material isolated in the photochemical excitation gave a UV spectrum similar to 1,3,5-hexatriene, but displaced by 7.5 μ and, more disturbing, the investigators were able to separate the material from benzene by fractional distillation. No experimental evidence was given in the radiofrequency study. In our work, 1,3,5-hexatriene could not be detected (less than 100 ppm) in the benzene fraction using the squalane column. No spectral evidence was noted in the ultraviolet although the region of interest is complicated by the presence of 1,3-cyclohexadiene.¹⁹

The unidentified peak in the chromatogram (Figure 3) gives a negative test for an acetylenic hydrogen (ammoniacal cuprous chloride solution) and does not disappear after the sample is subjected to free radical catalysis for several hours. Thus, the open chain, acetylenic isomers of benzene, hexa-1, 3-diene-5-yne, 1,4-hexadiyne, 1,5-hexadiyne and 1,5-hexadien-3-yne do not appear to account for this peak. The possibility of valence isomers of benzene such as bicyclo (2.2.0) hexa-2, 5-diene, "Dewar benzene", were excluded based on the observation that the peak was stable to prolonged heating at 100°. The valence isomers would be expected to convert to benzene under such conditions.²⁰

TABLE 2

Product Distribution in Discharged Benzene Fraction (a)

<u>Product</u>	<u>Yield % Benzene Exposed</u>
1,3-Cyclohexadiene	0.03
1,4-Cyclohexadiene	0.09
Fulvene	0.01
Cyclohexene	0.01
Unidentified	0.02

(a) Quantitative data obtained by GLC using squalane column and appropriate calibration standards.

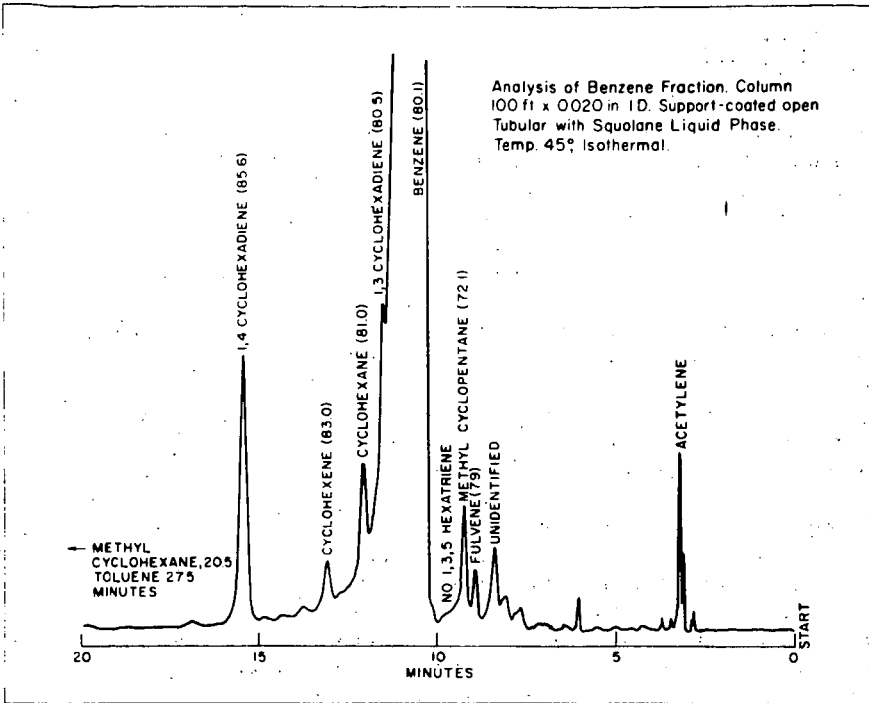


Figure 3

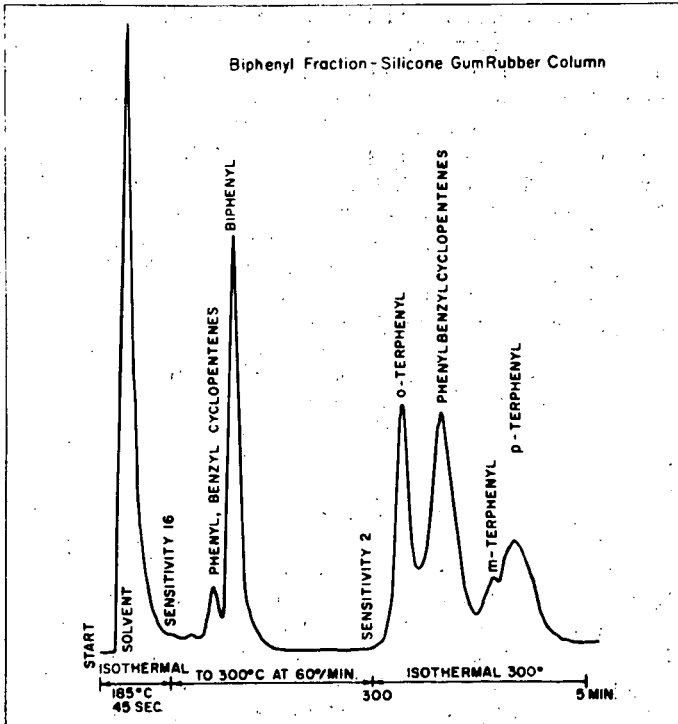


Figure 4

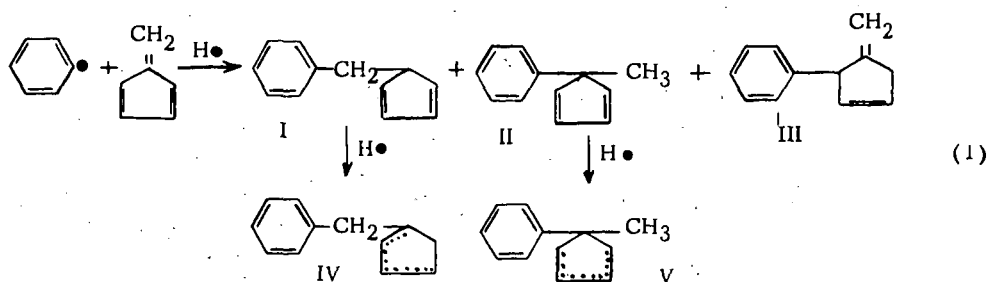
Biphenyl Fraction

The low molecular weight compounds, soluble in isooctane and hot methanol, were primarily biphenyl and o-, m-, and p-terphenyl. These products were identified by gas-liquid chromatography using a silicone gum rubber column (Figure 4) and a Carbowax 20M column with appropriate standards. The peaks were trapped and analyzed by infrared and NMR spectroscopy for confirmation. Biphenyl was present in sufficient quantity to be readily detected in the initial infrared spectrum and was isolated by sublimation. Quantitative data, obtained using the silicone column with appropriate calibration curves are presented in Table 3. With the possible exception of biphenyl, the yields are very low considering the overall conversion noted. The o-, m- and p-terphenyl ratio (1/0.4/1) indicates a preference for the para position beyond that expected for random attack.

If hydrogenation of the polyphenyls by hydrogen radicals generated "in situ" is to be considered a primary reaction mechanism, one would expect to see components corresponding to the possible hydrogenated species of biphenyl and the terphenyls. This does not appear to be the case, however, as no significant peak can be ascribed to a hydrogenated o-terphenyl compound. The small peaks before biphenyl and after o-terphenyl in the chromatogram (Figure 4) actually include four or more components present in small proportions which have not been completely identified. The first peak, (eluted before biphenyl) amounting to less than 0.1 per cent of the total yield, was initially ascribed to a mixture of the possible hydrogenation products of biphenyl. On the Carbowax column at lower temperatures this peak is eluted between phenylcyclohexane and 1-phenylcyclohexene. Initial infrared examination of this peak after trapping indicated an intriguing similarity with the peak (s) noted after o-terphenyl and with the polymer fractions. The possibility that this component was a low molecular weight precursor to polymer formation prompted further study. Infrared indicates a phenyl substituted aliphatic compound containing some olefinic unsaturation, and the spectrum is not consistent with the anticipated phenyl cyclohexenes. Careful examination of the spectrum indicates that the following phenyl substituted compounds are not present on the basis of the indicated missing absorptions - phenyl cyclohexane (1010, 1000, 888, 865 cm^{-1}), 1-phenylcyclohexene (922, 805 cm^{-1}), and 3-phenylcyclohexene (855, 788, 675 cm^{-1}).²¹ The spectrum is consistent with a non-conjugated benzylcyclopentene system with absorptions at 1070, 1030, and 960 cm^{-1} and the expected aromatic substitution bands.²¹ Two additional absorptions are noted, one at 850 cm^{-1} which may be attributed to vinyl protons and a phenyl substitution band at 730 cm^{-1} . This likely results from biphenyl contamination, but it is interesting to note that benzylidenecyclopentane has an absorption at 732 cm^{-1} with the remainder of the spectrum being similar to the benzylcyclopentenes.

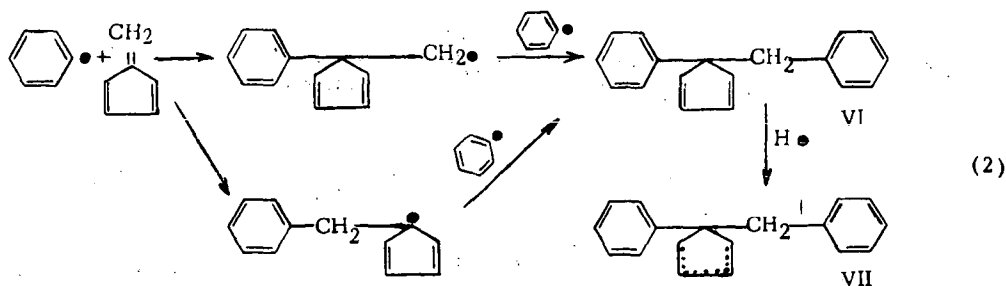
NMR data provides strong evidence for a rigid ring system (non-olefinic protons poorly resolved 1-3 ppm), non-conjugated olefinic protons at 5.7 ppm and phenyl protons at 7.1 ppm. The olefinic protons are complex, giving a closely-spaced doublet superimposed on a broad absorption, suggesting the presence of both ring and exocyclic unsaturation. Additional sharp proton resonances are noted at 1.2 ppm (methyl) and a doublet at 2.7 ppm which is attributed to benzylic protons. The lack of olefinic protons downfield from 5.7 ppm would rule out the benzylidene compounds and likely any similar structures wherein the unsaturation is conjugated with the phenyl moiety. The olefinic protons in cyclopentadiene are found at 6.42 ppm and were not obvious in this fraction. However, absorptions due to a minor component could have escaped detection because of limited sample size. The difficulty encountered in isolating the components of this peak precludes definite structural assignments, but the reaction of phenyl radicals with fulvene followed by H radical termination and hydrogenation to give

phenyl or benzyl substituted cyclopentenes is clearly indicated. The following reaction scheme is proposed to account for the experimental observations:

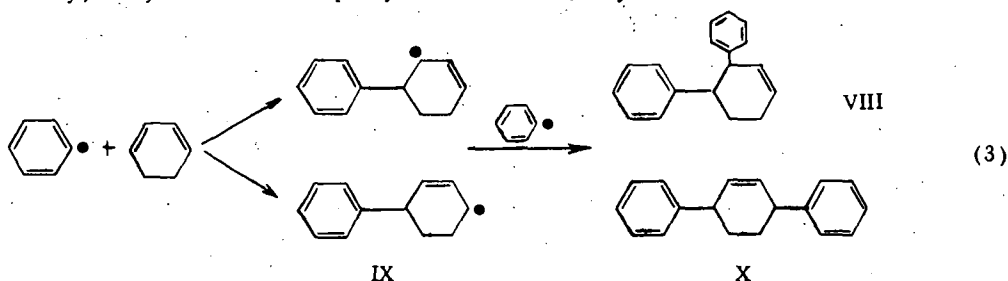


The inherent complexity of the product mix is illustrated by IV above which could be 1-, 3- and 4-benzylcyclopentene. Preliminary mass spectral data for this sample, as isolated from the chromatographic separation, indicates m/e values of 156 and 158, corresponding to the cyclopentadienes I, II and the cyclopentenes IV, V. Ring substituted compounds such as III would also have a mass of 156. Mass 91, corresponding to the benzyl radical is prominent as is mass 77, the phenyl radical, although this would be expected to arise from the biphenyl (154) contamination. Other features of the spectrum are being evaluated. The low yield is reasonable in view of the limited probability for radical termination and hydrogenation compared with the high reactivity of these olefins (or the diene precursors) under the reaction conditions. The glow discharge work of Schüller indicates the absence of any products with vapor pressure similar to biphenyl¹⁰ and the other related literature generally does not give details beyond biphenyl analysis and gross polymer properties.

The peak after *o*-terphenyl (Figure 4) actually consists of 3-4 components when analyzed by varying the chromatographic conditions. This peak has the same retention time as diphenyl fulvene and is in the same general range as noted for a commercially available hydrogenated terphenyl, Monsanto HB-40. This complex peak was trapped (with trace *o*-terphenyl contamination) as a yellow liquid which gave an infrared spectrum identical to the polymer fractions and very similar to the peak before biphenyl. Again, phenylbenzylcyclopentenes are indicated and the spectrum bears little resemblance to the hydrogenated terphenyl spectrum. The NMR spectrum in carbon tetrachloride showed aromatic protons at 7.1 ppm, a broadened olefinic proton resonance at 5.7 ppm and non-olefinic protons from 0.8-3.5 ppm with poor resolution. These extremely complex olefinic and non-olefinic resonances are typical of protons in a fixed ring system such as cyclopentene. The integration for these resonances allows approximation of an average structure containing a cyclopentene ring system substituted with one phenyl and one benzyl group. The reactions appear analogous to those responsible for the components of the peak before biphenyl with termination being with a phenyl radical rather than the hydrogen radical. The mass spectrum for this material as trapped from the chromatographic analysis shows prominent peaks at mass 232 and 234 corresponding to VI and VII below. The benzyl and phenyl radical peaks are also evident at mass values of 91 and 77 respectively. Evaluation of the final structure details is continuing. The following is believed to be representative of the many reactions which are possible under the experimental conditions, to give a variety of closely related compounds:



The actual structural definition must await isolation of sufficient quantities of the components for NMR studies under various conditions. The possibility of a hydrogenated p-terphenyl was carefully considered, but the only structure even remotely consistent with the infrared and NMR data would require that the center ring of p-terphenyl be non-aromatic with mono-substituted phenyl groups attached. Such a material could be formed by preferential hydrogenation of the center ring of p-terphenyl (statistically unlikely) or by the reaction of phenyl radicals and 1,3-cyclohexadiene as follows:



This mechanism requires the formation of hydrogenated ortho terphenyl derivatives such as VIII, which were not noted by gas-liquid chromatography or infrared.

TABLE 3

Biphenyl Fraction (a)

	Yield % Exposed Benzene	Yield % Reaction Products
Biphenyl	0.30	3.5
o-Terphenyl	0.05	0.6
m-Terphenyl	0.02	0.2
p-Terphenyl	0.05	0.6
Benzyl and phenyl cyclopentenes (C ₁₂)	0.05	0.6
Phenylbenzylcyclopentenes (C ₁₈)	0.25	2.9
TOTAL	0.72	8.4

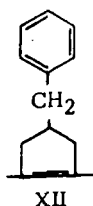
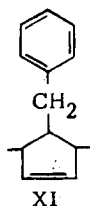
(a) Quantitative data were obtained by GLC, using a silicone gum rubber column with appropriate standard calibration curves based on peak height.

Polymeric Products

The material which adheres to the glass dielectric surface in the reactor is a high melting solid ($>320^\circ$), insoluble in benzene and all common solvents. The infrared spectrum and the carbon-hydrogen ratio are essentially the same as noted for the benzene soluble material. The benzene soluble polymer was fractionated into three molecular weight ranges based on solubility in isoctane. The polymers are all yellow with the intensity increasing as the molecular weight decreases. The ultraviolet spectrum for the low molecular weight polymer shows a gradual tailing into the visible region. The physical property data for the polymeric fractions are summarized in Table 4.

Infrared data indicate that the polymeric fractions are structurally similar to the low molecular weight products identified as benzyl and phenyl substituted cyclopentenes. The infrared evidence already presented for the low molecular weight products is applicable to the polymeric products and need not be repeated. The data are consistent with an average repeating unit containing the cyclopentene ring structure substituted with phenyl or benzyl groups. NMR data for the polymers were obtained in carbon tetrachloride at the cell holder temperature (40°). The spectrum obtained for the 300 molecular weight polymer fraction is presented in Figure 5. The extreme broadening of the proton resonances is associated with the complex, long range proton coupling in a rigid system and the motional averaging commonly noted in polymers.²² Scanning the same sample at 90° in tetrachloroethylene did not significantly improve the resolution. The NMR spectrum of the polymer in pyridine (Figure 5) gives some improvement in the high field proton resolution, indicating a doublet at 2.6 ppm (benzylic protons) and a complex methyl proton resonance. The spectra are similar to those obtained for the low molecular weight precursors containing unresolved ring protons. The NMR spectra generally eliminate polymer formation by way of phenyl and hexatrienyl radicals as suggested for the radiolysis of benzene.²³ The aliphatic proton portion of the spectrum is very similar to that reported for cyclopentadiene polymers by Davies and Wassermann.²⁴ The cyclopentadiene polymers had a molecular weight range of 1200-2300, a λ max. at 320-360 m μ and non-olefinic proton to olefinic proton ratio of approximately 3/1.

The data are consistent with polymer formation by way of phenyl radical (or excited benzene) reaction with the fulvene produced to give phenyl or benzyl substituted cyclopentadienes which then polymerize to give a polycyclopentene chain with pendant phenyl and/or benzyl groups. The average non-olefinic to olefinic proton ratio of 2.9 indicates that the many possible structures similar to XI (5/2) predominate over the alternate type structures, XII (7/0),²⁴ assuming our analogy to cyclopentadiene type polymers is valid.



(4)

Many similar structures must be considered, including those derived from phenyl attack on the ring with polymerization through the exocyclic vinyl group of fulvene.

TABLE 4

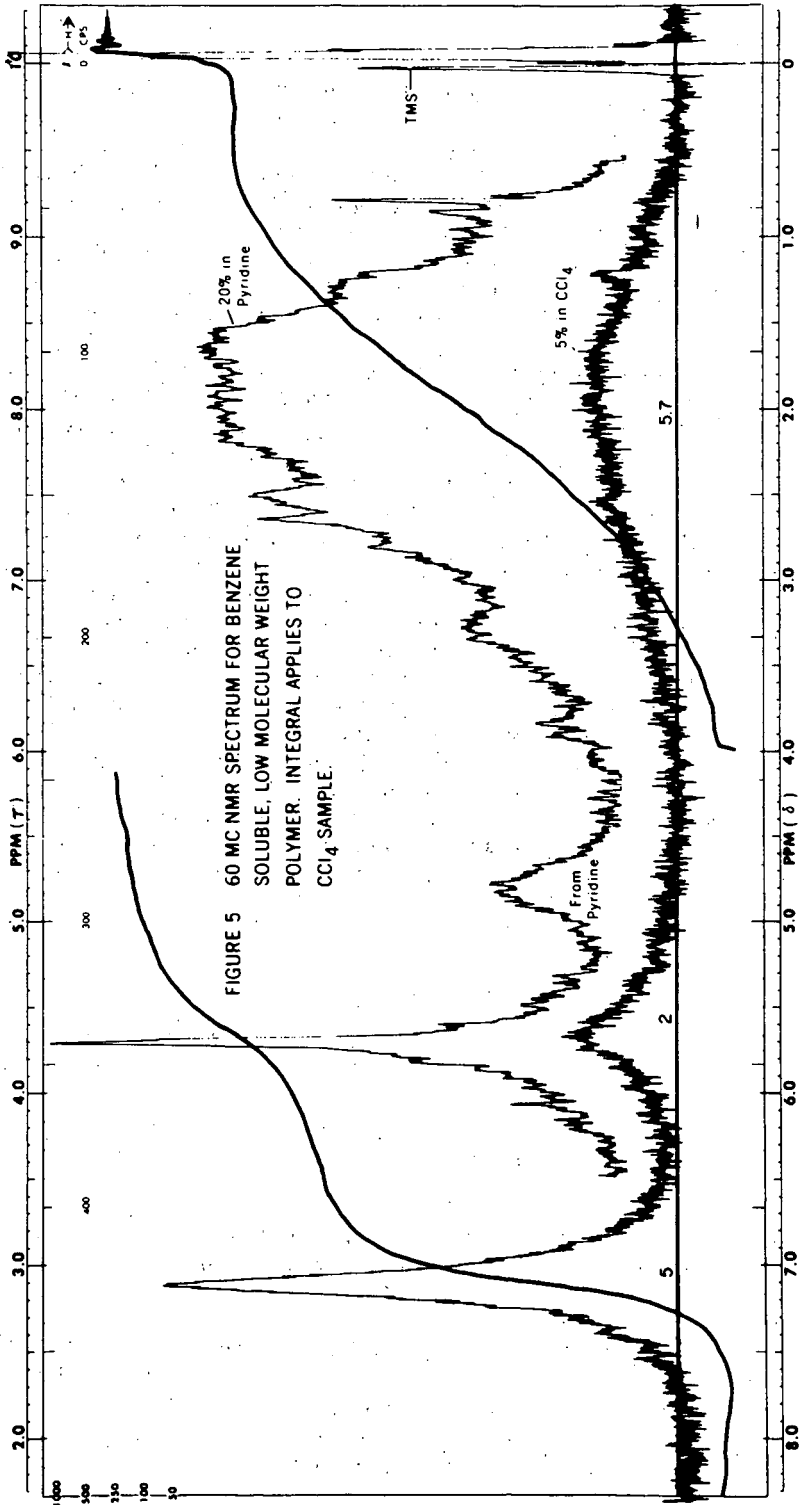
Properties of Polymers Produced
in Corona Discharge of Benzene

	% C	% H	C/H	M. W. (a)	Infrared cm ⁻¹	(b)		
						Aromatic	Protons Olefinic	Non-olefinic
Benzene insol.	86.95	7.17	1.01	---	755, 695	---	---	---
Benzene sol. 1	88.32	7.18	1.02	4360	755, 695	5	2	5.8
2	87.26	7.09	1.03	1555	755, 695	5	2	5.7
3	87.23	7.09	1.03	305	755, 695	5	2	5.7

452

(a) Vapor pressure osmometry in benzene solution.

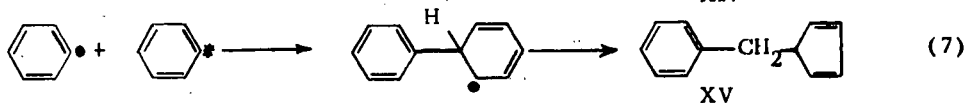
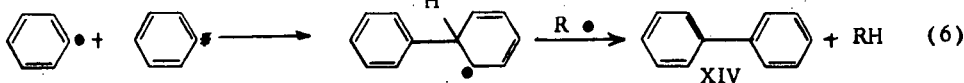
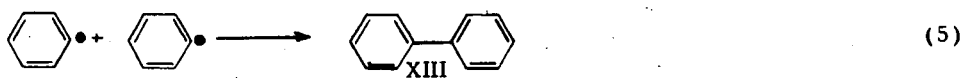
(b) Aromatic proton resonance assigned five protons.



Mechanism

The available evidence is thus not consistent with the generally proposed mechanism of polymer formation based on the random build-up of a poly (phenylene) chain accompanied by hydrogenation,⁹ or the interaction with the hexatrienyl diradical.²³ In the radiofrequency discharge of benzene, evidence was presented which clearly indicated that the polymer contained consecutive para linkages suggesting poly (p-phenylenes) as the predominant structure.¹² Schüller observed that the polymer (C/H 1.03, M.W. 503) was a phenyl substituted aliphatic chain based on infrared evidence.¹⁰ Patrick and Burton have demonstrated that hydrogen atoms are not involved to any significant extent in polymer formation when liquid benzene is irradiated with a 1.5 m.e.v. source.²⁴

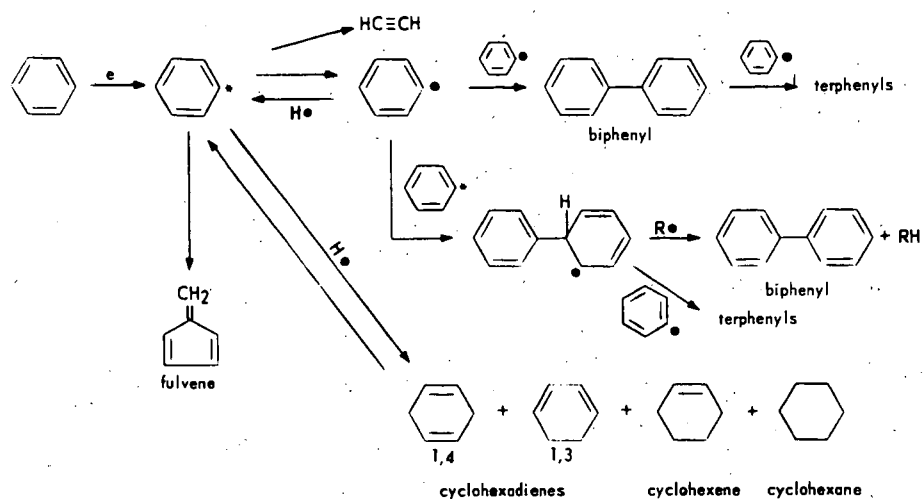
In the corona discharge many types of energy transfer are occurring, varying from photolysis (visible corona) to relatively high energy electrons responsible for fragmentation. The low yield of biphenyl in this single pass reactor suggests that phenyl radical production through loss of a hydrogen radical is not the primary reaction route leading to polymer formation. Considerable energy should be available to excite benzene to relatively high vibrational levels which would be somewhat below that energy required to actually separate the H radical. At any given time the number of these excited benzene molecules should greatly exceed the phenyl radical population. Fulvene is produced from benzene by ultraviolet energy (200 mμ, about 112 kcals, or 4.9 electron volts).²⁵ Thus, the formation of this benzene isomer with a resonance energy (11-12 kcals/mole) intermediate between benzene and 1,3 cyclohexadiene may be energetically favorable in the corona environment. Fulvene has been shown to polymerize rapidly under similar conditions with no reversion to benzene.²⁵ The uniformity of the phenyl (benzyl) - cyclopentene ratio throughout all polymer fractions makes it difficult to accept a mechanism based solely on random attack by phenyl radicals on the growing fulvene polymer. The initial synthesis of a monomeric unit comprised of the benzylcyclopentadiene system with subsequent diene type polymerization is consistent with all our observations. The phenyl radical produced in the discharge should collide with the nearest benzene molecule which will be excited to a relatively high vibrational energy level. The following reaction sequences are suggested for the phenyl radical:



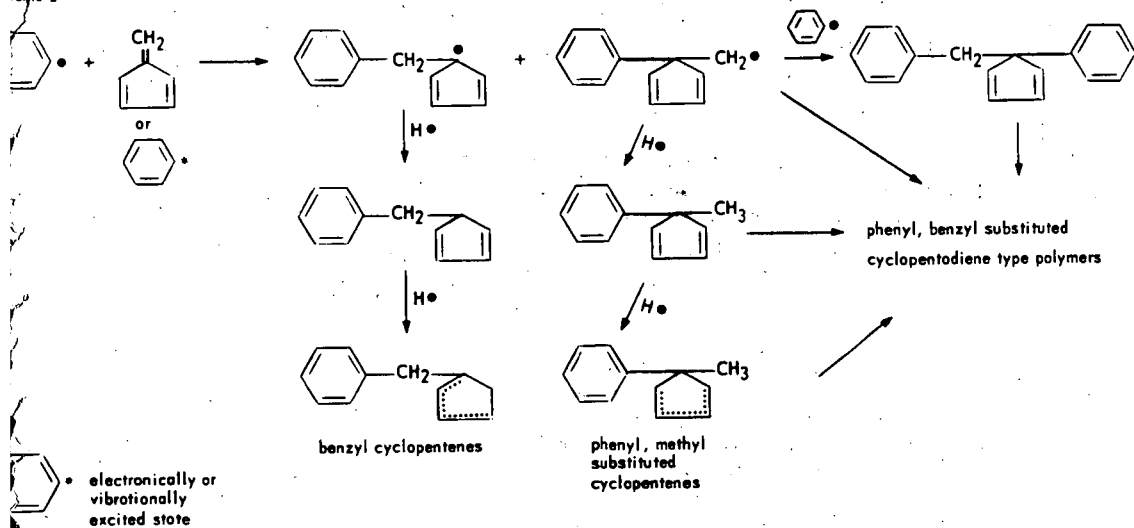
Reaction (5) is the typical termination reaction by radical coupling leading to biphenyl. The intermediate radical in (6) would be expected to lose hydrogen more readily than it would add to another benzene molecule to give polymer formation.²⁶ The possibility of ring contraction in the excited intermediate, accompanied by an intramolecular shift of a hydrogen atom is suggested in reaction (7). The benzylcyclopentadiene XV so obtained would be a very active monomer leading to the polymeric products observed. Although our data support polymer formation by the mechanism indicated, we cannot rule out participation by the cyclohexadienes and acetylene, both of these being noted in the benzene fraction and the low temperature traps.

FIGURE 6 PROPOSED REACTION MECHANISMS

Scheme 1



Scheme 2



The relatively low yield and the complexity of the reaction products does not allow an unequivocal designation of reaction mechanism or of the mode of energy transfer in the corona environment. However, where possible, we have proposed reaction mechanisms which are consistent with our results to date. These mechanisms are summarized in Figure 6. Studies are underway to obtain deuterium exchange data in the corona reactor, and mass spectral data are being evaluated. Investigation of the utility of corona chemistry will be extended to other volatile compounds.

EXPERIMENTAL

Materials: Fisher thiophene-free benzene contained trace quantities of methyl cyclopentane, cyclohexane and toluene. Chromatogram (squalane) of original material was used as reference for irradiated benzene evaluation under the same GLC conditions.

Reference materials for chromatographic identification were generally used as obtained from commercial sources. Most of these materials were of sufficient purity to identify the major peak. However, mono-phenyl fulvene, obtained from Aldrich, gave no peak on the silicone column and infrared indicated extensive hydroxyl and carbonyl absorptions. 1,3,5-hexatriene from Aldrich gave two major and two minor peaks on the squalane column. Infrared²⁷ indicated largely the trans isomer with only a small cis absorption at 818 cm^{-1} .

Fulvene was prepared by the method of Meuche.¹⁷ Infrared ($1662, 925, 890, 765\text{ cm}^{-1}$) and ultraviolet ($\lambda_1 = 242\text{ mu}, \lambda_2 = 360\text{ mu}$) were in good agreement with literature values.¹⁵

Reaction Conditions

The equipment used in these experiments was presented in Figures 1 and 2. Helium was bubbled through the benzene reservoir (55°) at 100 ml/min. to carry 4.2 gm. (0.054 moles) benzene through the corona reactor per hour. The reactor temperature was $45^\circ \pm 2^\circ$. A total of 101 gm. (1.3 moles) benzene was passed through the $15\text{ KV, 60 cycle, corona discharge}$ in 23.7 hours. A small helium purge was maintained throughout all sampling operations and necessary downtime to preclude oxidation.

Product Isolation and Analysis

At the conclusion of the run, the reactor was partially filled with benzene and refluxed on a steam bath for 2 hours. The benzene soluble material from the column was combined with the yellow brown solid which collected in the lower receiver. The insoluble material was swelled by benzene and generally loosened from the glass dielectric surface. This insoluble material was filtered off, washed several times with chloroform and dried overnight at 70° in a vacuum oven. The reactor was cleaned with a 5 per cent hydrofluoric acid solution to remove final traces of polymer after each run. Benzene insoluble polymer - 0.7 gm. yellow brown color, % C 86.95, % H 7.17, C/H 1.01.

The benzene containing all solid products from the reactor and pot residue was reduced to 30 ml. volume by vacuum distillation at 50° . Considerable foaming was encountered, requiring careful control of the distillation. The 30 ml. of

brown benzene solution was added to 300 ml. isooctane at room temperature. A yellow solid precipitated immediately and was collected by filtration. After several washings with hot methanol, the material was dried for 8 hours at 70° in a vacuum oven. Benzene soluble polymer - Fraction 1, 2.3 gm., M. W. 4360, %C 88.32, %H 7.18, C/H 1.02.

The isooctane-methanol solution was reduced to 100 ml. volume (all methanol removed) by vacuum distillation at 60°. The solution was a brilliant yellow color at this point. On cooling to room temperature, a small proportion of a deep yellow polymeric solid precipitated and was collected by filtration. After washing with hot methanol, this yellow material was dried at 70° for 8 hours in a vacuum oven. Benzene soluble fraction 2, 0.2 gm., M.W. 1555, %C 87.26, %H 7.09, C/H 1.03.

The isooctane-methanol soluble portion was reduced to 20 gm. by vacuum distillation and sufficient benzene added to insure solubility of all components. The per cent solids was determined for this sample, being careful to limit sublimation of biphenyl (about 2 hours at 70° in a vacuum oven). This sample contains the low molecular weight products and a yellow resinous polymer. Qualitative analysis for the low molecular weight components was accomplished by gas-liquid chromatography using the following liquid phases: silicone gum rubber, Carbowax 20 M, and Reoplex 400. Quantitative data were obtained on the silicone column (Figure 4) using calibration curves (peak height) prepared from appropriate standards. The concentration of the small peak eluted before biphenyl was estimated using the biphenyl calibration curve and the peak after o-terphenyl was estimated using a commercial hydrogenated terphenyl mixture (Monsanto HB-40) as a reference. The F & M 500 gas-liquid chromatograph equipped with a standard thermoconductivity detector was used for these analyses. These low molecular weight products (biphenyl, o-, m-, p-terphenyl and phenylcycloalkenes, M. W. up to ~250) amount to 0.72 gms. (See Table 3). Peak confirmation was provided by infrared and NMR analysis after fraction collection from the chromatographic separation.

The concentration of the low molecular weight resinous polymer was determined by subtracting the total biphenyl fraction weight from the total isooctane-methanol soluble material. A sample of this material was placed in the vacuum oven at 100° until the GLC trace indicated negligible biphenyl content and the molecular weight was determined. Benzene soluble fraction 3, 3.5 gm., M. W. 305, %C 87.23, %H 7.09, C/H 1.03. Prolonged heating at 150° in air gives a hard, brittle yellow film. Infrared analysis indicates oxidation is involved in the drying process.

The benzene fraction was initially examined by GLC using 100 ft. support coated open tubular columns containing Carbowax 1540 poly (ethylene glycol) and squalane (Figure 3) as the liquid phase. Quantitative data were obtained at 45° on the squalane column with a helium flow of 3.0 ml/min. The Perkin Elmer Model 380 gas-liquid chromatograph, equipped with a stream splitting device and hydrogen flame detector was used for these analyses. Peak identification was by comparison with commercial standards and the synthesized fulvene. Additionally, the benzene fraction was refluxed in pressure bottles with maleic anhydride, azobisisobutyronitrile, and ammoniacal cuprous chloride solution prior to chromatographic analysis to note peak changes due to adduct formation, polymerization or presence of acetylenic hydrogen. Acetylene content was estimated from weight loss of the -70° and -195° traps. The vapor space above those cold traps and the gas stream directly below the corona were analyzed by infrared using an 8 cm. gas cell. Although the study was not exhaustive, several samplings were made and only acetylene was detected.

Methylacetylene, allene and butadiene were not present in sufficient quantity to be detected.

The yellow benzene from several runs (1000 ml.) was fractionated and 900 ml. distillate obtained from 79-80°. The distillate was refluxed with maleic anhydride until colorless and the benzene removed at reduced pressure. Dilute sodium hydroxide solution was added and the resulting solution was extracted several times with chloroform. After acidification with dilute hydrochloric acid, the solution was extracted with ether. The ether was removed after drying to give a white solid which, on recrystallization from chloroform and pet ether, gave the adduct 7-methylene-5-norbornene-2, 3-dicarboxylic acid which melted at 146°-150°. The infrared showed maxima at 1553, 875 and 710 cm^{-1} , (lit ⁽¹²⁾ 1555, 874, 712 cm^{-1}). Fulvene was prepared in low yield (less than one per cent) from cyclopentadiene and formaldehyde with sodium ethoxide catalyst. ¹⁷ The adduct was prepared by adding maleic anhydride to the crude fulvene reaction product in Freon 113 (b.p. 47.6°) and refluxing until colorless. After removal of the solvent, hydrolysis and recrystallization yielded the adduct, m.p. 147-150°, which gave properties identical with the fulvene adduct obtained from the corona discharge. Bryce-Smith obtained a melting range of 105-110° for this adduct which was likely a mixture of the exo and endo isomers. ²⁵ Stille prepared the fulvene-maleic anhydride adduct with a melting point of 149-150° which may be a single isomer. ¹²

Through the courtesy of the Perkin Elmer Company at Norwalk, Connecticut, the discharged benzene was analyzed by combination of gas-liquid chromatography and mass spectroscopy. The peak attributed to fulvene gave a parent mass of 78 and fragments at m/e 77, 52, 51, 50 and 39 in good agreement with the literature. ¹⁷ Confirmation of other assignments was obtained by this technique and the one unidentified component on the squalane column gave a parent mass of 78.

Molecular weight and carbon-hydrogen determinations were made by Schwarzkopf Microanalytical Laboratories, New York, New York. Molecular weight was determined in benzene by vapor pressure osmometry.

LITERATURE CITED

- 1 Present address: Tarrytown Technical Center, Union Carbide, Tarrytown, New York.
- 2 G. Glockler and S. C. Lind, "The Electrochemistry of Gases and Other Dielectrics," John Wiley and Sons, New York (1939).
- 3 Ozone Chemistry and Technology, Advances in Chemistry Series No. 21, American Chemical Society (1959).
- 4 J. A. Coffman and W. A. Browne, Scientific American, 89, June (1965).
- 5 M. Bertholot, Compt. rend., 82, 1357 (1876).
- 6 S. M. Losanitsch, Bull. soc. stin. Bucharest, 233 (1914).
- 7 A. P. Davis, J. Phys. Chem., 35, 3330 (1931).
- 8 V. Karapetoff, W. H. Trebler, E. G. Linder, and A. P. Davis, Research Reports, Detroit Edison Company, Cornell Univ. (1928-32).
- 9 G. P. Brown, R. E. Rippere, Am. Chem. Soc., Div. Petrol. Chem., Preprints 2, No. 3, 149-54 (1957).
- 10 H. Schüller, K. Prchal, and E. Kloppenburg, Z. Naturforsch., 15a, 308 (1960).
- 11 A. Streitwieser, Jr., and H. R. Ward, J. Am. Chem. Soc., 84, 1065 (1962), 85, 539 (1963).
- 12 J. K. Stille, R. L. Sung, and J. Vander Kooi, J. Org. Chem., 30, 3116 (1965).
- 13 U. S. I. Chemicals, Polyolefin News, Feb. (1964).

- 14 G. J. Janz, *J. Chem. Phys.*, **22**, 751 (1954).
- 15 J. Thiec and J. Wiemann, *Bull. Soc. chim., France*, 177 (1956).
- 16 J. M. Blair and D. Bryce-Smith, *Proc. Chem. Soc.*, 1287 (1957).
- 17 D. Meuche, N. Neuenschwander, H. Schaltegger, and H. V. Schlunegger, *Helv. Chim. Acta*, **47**, 1211 (1964).
- 18 G. E. Gibson, N. Blake, and M. Kalm, *J. Chem. Phys.*, **21**, 1000 (1953).
- 19 G. F. Woods and L. H. Schwartzman, *J. Am. Chem. Soc.*, **70**, 3394 (1948).
- 20 E. E. Van Tamelen and S. P. Pappas, *J. Am. Chem. Soc.*, **85**, 3297 (1963).
- 21 E. L. Eliel, J. W. McCoy, and C. C. Price, *J. Org. Chem.*, **22**, 1533 (1958).
- 22 J. G. Powles, *Polymer*, **1**, 219 (1960).
- 23 W. N. Patrick and M. Burton, *J. Am. Chem. Soc.*, **76**, 2626 (1954).
- 24 A. G. Davies and A. Wassermann, *J. Polymer Sci.*, **4**, 1887 (1966).
- 25 H. J. F. Angus, J. M. Blair, and D. Bryce-Smith, *J. Chem. Soc.*, 2003 (1960).
- 26 G. A. Mortimer and L. C. Arnold, *J. Am. Chem. Soc.*, **84**, 4986 (1962).
- 27 J. C. H. Hwa, P. L. de Bonneville and H. J. Sims, *J. Am. Chem. Soc.*, **82**, 2538 (1960).

VAPOR PHASE DECOMPOSITION OF
AROMATIC HYDROCARBONS BY ELECTRIC DISCHARGE

Masayuki Kawahata

Research and Development Center
General Electric Company
Schenectady, New YorkIntroduction

Decomposition of organic compounds in presence of electric discharge generally involves fragmentation and polymerization induced by inelastic collision with high energy electrons. When hydrogen is added, active hydrogen atoms produced by electric discharge also participate in the decomposition reactions. The reaction mechanisms are complex involving excited molecules, free radicals, and ions.

In this laboratory hydrocracking of coal, coal volatiles and related materials by electric discharge in hydrogen was studied. It is postulated by Given¹ that coal (vitrinite) molecules contain aromatic and hydroaromatic structures and probably fused aromatic ring nuclei linked together by methylene or ethylene groups forming hydroaromatic rings. Many of the replaceable hydrogens in the structure are substituted by hydroxyl or carbonyl groups. Short alkyl groups and alicyclic rings may also be attached as side chains. In pyrolysis at 500 - 600°C., dissociation of hydroxyl groups and dehydrogenation of naphthenic rings take place. These acts lead to formation of OH and H radicals which in turn help to break the linkages between aromatic nuclei, forming smaller, partly aromatic volatile fragments, and at the same time leaving a more aromatic residual structure behind.

On the other hand, high pressure hydrogenation of coal gives partial or complete hydrogenation of the aromatic structure. When this is subsequently cracked, the light products tend to be aliphatic rather than aromatic hydrocarbons. It was thought that hydrocracking of coal by electric discharge might be somewhere between pyrolysis and high pressure hydrocracking. In the course of study it was thought important to test this hypothesis by subjecting several aromatic or hydroaromatic compounds to electric discharge in a hydrogen stream for better understanding of the process. Organic compounds selected were m-cresol, α -methylnaphthalene, tetrahydronaphthalene, decahydronaphthalene, and 9, 10-dihydrophenanthrene.

Experimental Apparatus and Procedures

The apparatus consisted of a vaporizer, a preheater, a discharge reactor, and a product collecting system. The organic compound was fed into the vaporizer at a certain rate and vaporized. Hydrogen was also

¹ P. H. Given, presented Am. Chem. Soc., January, 1963 in Cincinnati, Ohio

fed into the vaporizer at a certain flow rate and mixed with the organic vapor. The resultant mixture was then fed into the reactor through the preheater. The liquid products condensed in a water cooler were collected in a receiver and the gaseous products were collected in a liquid nitrogen trap. These products were analyzed by mass spectroscopy and vapor phase chromatograph employing a 6 ft. column of 10% silicone rubber, SE-30 and 60-80 Chromosorb P.

The discharge reactor was fabricated with quartz and was of a concentric tube design similar to an ozonizer. The inside of the inner barrier (40 mm OD and 38 mm ID) and the outside of the outer barrier (48 mm OD and 46 mm ID) were coated with conductive, transparent, tin oxide. The former was connected to the high voltage terminal and the latter to ground. In this arrangement the electric discharge was sustained in an annular space, 46 mm OD, 40 mm ID, and 200 mm long. The inside barrier tube was filled with stainless steel wool and a thermometer was placed in the center. This thermometer and three thermistors attached to the outside electrode were used to determine the reactor temperature. The reactor was insulated with glass wool, and the reactor temperature was maintained at approximately 300°C. for all the runs.

The electric discharge power was supplied by feeding the output of a 10,000 Hertz, 30 kilowatt inductor-alternator to the primary of a 50 kilovolt transformer and, in turn, to a tuned circuit, to the reactor and to the high voltage instrumentation. The electric discharge power was determined by measuring the area of parallelogram on the oscilloscope².

When making the run, hydrogen was fed into the reactor at a definite flow rate and the electric discharge was applied to heat the reactor. When the reactor temperature was stabilized at about 300°C., the feed of the organic compound was started. The discharge power sustained for the reaction was in a range from 140 to 170 watts.

Experimental Results and Discussions

For cresol-hydrogen mixtures, two runs were made using the empty reactor and three runs were made by filling the reactor space with porous or activated aluminum oxide grains. For all the runs, the reactor pressure maintained at 300 mm Hg. Experimental results, including product distribution, are listed in Table 1. The principal products were phenol, toluene, benzene, aliphatic hydrocarbons, carbon dioxide and water. Among the aliphatic hydrocarbons, acetylene was present in the largest amount and about 80% was unsaturates except for Run 5. In this run the concentration of unsaturates was 55%. This is probably due to a higher hydrogen concentration in the feed causing somewhat

² T. C. Manley, Trans. Am. Electro Chem. Soc. 84 83, 1943

more efficient hydrogenation. The bond energies of $C_6H_5-CH_3$ and C_6H_5-OH are 90 and 73 Kcal/mol. respectively. Despite this, it was observed that, in the products, phenol was in higher concentration than toluene.

Use of aluminum oxide packing in the discharge space was intended to investigate the possibility of increasing the energy yield. Narrowing the gaseous discharge gap with dielectric packings may cause the following two effects on the discharge: (1) increase of discharge current for the same discharge power dissipated, and (2) increase of gaseous space breakdown field strength, if the gap decreases beyond a certain limit. The exact nature of the electric discharge employed in this study is still debatable.^{3,4} However, it can be reasonably assumed that the primary reaction rate of the organic vapor with either high energy electrons or active hydrogen atoms may be dependent on discharge current density and field strength, if the system pressure and partial pressure of the reactant are constant. In electric discharge product of ozone, an increase in ozone concentration after filling the discharge gap with various dielectric packings is also reported by Morinaga and Suzuki.⁵ In this study for approximately the same concentration of cresol vapor, the use of aluminum oxide grains in the discharge space appeared to increase the energy yield somewhat, but not conclusively.

In all the runs, the formation of brown solid films was observed on the reactor wall or on the surface of the grains. These solid films were not analyzed but they were insoluble in methylethyleketone or toluene. It is presumed that they are indicating possibly highly cross-linked polymerized products derived from the cresol. The energy yield for film formation was estimated to be in a range from 30 to 50 g/KWH; considerably higher than that for the fragmentation products.

Experimental results for the polycyclic compounds are summarized in Table 2. Methyl-naphthalene vapor in hydrogen was tested under pressures of 760 and 74 mm Hg. The principal lighter products were aliphatic hydrocarbons, benzene and toluene. At the higher pressure the concentration of the lighter aliphatic hydrocarbons was in the order $C_2 > C_3 > C_4 > C_5$. At the lower pressure, however, this order was reversed. In both cases about 32 - 35% were unsaturates. The energy yield was approximately doubled by lowering the pressure.

For tetrahydronaphthalene, three experiments were made under different pressures. Among the lighter aliphatic hydrocarbons produced, the C_2 fraction was present in the largest amount, in which ethylene was in highest concentration followed by acetylene and ethane. The total percentage of unsaturates increased as the pressure decreased. This increase was essentially due to the increase in C_2 and C_3 unsaturates. As observed for methyl-naphthalene, the energy yield at 70 mm Hg was twice as high as that at 760 mm Hg. A considerably higher

³ R. W. Lunt, Advanced Chem. Series, "Ozone Chemistry and Technology", Am. Chem. Soc., p. 286 (1959)

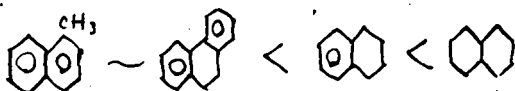
⁴ M. Suzuki and Y. Naito, Proc. Japan Academy, 28 469 (1959)

⁵ K. Morinaga and M. Suzuki, Bull. Chem. Soc., Japan 35 429 (1962)

energy yield than for the other two runs was observed at the intermediate pressure, 300 mm Hg.

When decahydronaphthalene was tested, one experiment was made under 760 mm Hg using 6.7% concentration in hydrogen. Another run was made under 300 mm Hg using 67% concentration. In the latter run, a higher energy yield was obtained. The product distribution was richer in the C₂ and C₃ fraction and also unsaturate concentration was higher.

One experiment was made to test dihydrophenanthrene in hydrogen. The gaseous products were essentially in the C₂ fraction; about 50% being unsaturated. Vapor phase chromatography of the liquid product showed two peaks. They were not identified but by the combined results of the VPC and mass spectroscopy one of the peaks was tentatively identified as butylbenzene. Biphenyl, which is a likely decomposition product, was not found. For the polycyclic aromatic and hydroaromatic compounds tested in this study, the energy yield from electric discharge hydrocracking for production of the lighter hydrocarbons was in the following order:



As observed in cresol runs, solid films were formed on the reactor wall, but they were not analyzed.

The number of experiments are not sufficient to permit drawing a concrete relationship between energy yield and molecular structure. The resonance energies of benzene, naphthalene, and phenanthrene are 39, 75, and 110 Kcal, respectively. It is reasonable to assume that the condensed aromatic ring structure absorbs large amounts of energy and requires high energy for cracking. The radiation effect on various polycyclic aromatic compounds were studied by Weiss et al⁶. They discussed correlations between the radiation stability and various structural factors. These include resonance energy, electron affinity, and ionization constant. Since there is a close similarity between radiation and electric discharge in principle, further information along this line would be helpful for a better understanding of the electric discharge hydrocracking process.

Elucidation of the reaction scheme in detail is beyond the scope of the this study. However, it was indicated that in electric discharge hydrocracking of aromatic or hydroaromatic hydrocarbons, dissociation of the side chains and rupture of the rings are followed by secondary reactions involving the decomposed species; this leads to the formation of aromatic or aliphatic lighter compounds. Energy requirement to form these lighter compounds appear to be too high for practical applications. The formation of the solid polymerized products, which takes

⁶ J. Weiss, C. H. Collins, J. Sucker, and N. Carciello, *Ind. Eng. Chem, Prod. Res. and Development*, 3, 73 (1964)

place in parallel with fragmentation, as seen for cresol runs, requires considerably less energy. Study on the formation of polymer films starting with various monomers and using the present discharge system presents an extremely interesting problem which is currently under investigation.

This is a part of the work supported by the Office of Coal Research, U. S. Department of Interior. The author is thankful for their generous support.

Table 1

Exp. No.	m-cresol Conc. %	Reactor packings	Organic Products Distributions, g/KWH			Energy Yield g/KWH	Unsaturates in Aliphatic %	
			Aromatic H/C	Aliphatic H/C	Phenol			
			C ₆	C ₇				
1	88.8	no	0.8	2.7	1.4	4.3	9.2	78
2	65.5	no	0.5	2.3	1.0	3.2	7.0	85
3	93.0	porous alumina	1.0	4.1	2.2	4.4	11.7	82
4	35.5	porous alumina	0.8	2.1	1.5	3.1	7.5	55
5	67.5	activated alumina	0.2	0.9	1.4	6.8	9.3	80

Electric Discharge Hydrocracking of m-cresol

Table 2

Exp. No.	Organic Vapor	Vapor Conc. %	Pressure mmHg	Energy Yield g/KWH	Product Distribution, Wt. %								
					C ₁	C ₂	C ₃	C ₄	C ₅	C _{6-C₉}	Unsaturated		
6		4.5	760	0.66	2	33	24	21	13	7	32		
7		5.8	74	1.2	8	5	24	29	40	2	35		
8		5.8	760	1.5	5	77	12	3	1	2	74		
9		7.3	300	8.8	1	78	16	3	1	2	85		
10		7.4	70	3.0	--	74	23	2	.5	.5	90		
11		6.7	760	3.9	4	38	20	10	7	21	49		
12		66.7	300	5.4	4	56	27	7	2	7	76		
13*		4.5	760	0.69	3	23	7	3	2	1	71**		

466

* The balance of the product distribution for this run (60%) was the heavier fractions which were not identified by VPC.

** Percentage of unsaturates in C₁-C₉ fractions

Hydrocracking of Polycyclic Aromatic and
Hydroaromatic Compounds

HYDROCARBONS AND CARBON FROM A ROTATING ARC HEATER

C. Hirayama and D. A. Maniero

Westinghouse Electric Corporation, Pittsburgh, Pa.

INTRODUCTION

A brief description of the rotating arc heater utilized in this work, and some preliminary hydrocarbon processing data, were described a year ago.¹ A more detailed description of the heater, and some of the operating characteristics have also been presented within the past year.² The arc heater consists essentially of water-cooled, toroidal electrodes, in which the arc is rapidly rotated as a result of interaction of the arc current with a magnetic field. The heater is a high current, low voltage device with a rating of 3 megawatts into the arc. Both alternating and direct current power operation are possible with this device. In contrast, most arc devices previously reported³ are of the long arc, high voltage type which are operated on d.c. only.

We wish to report, herewith, some of the results obtained more recently in the pyrolysis of methane at atmospheric and at slightly elevated pressures.

EXPERIMENTAL

The feed gas was commercial grade methane of 96 per cent purity which was injected into the heater at ambient temperature. The flow rate was controlled by regulating the pressure drop across a sonic orifice.

The arc heater was operated only on a.c. power at electrode separations of 0.38, 0.75 and 1.0 inch. The arc power with methane ranged from 550 to 2200 kilowatts, with thermal efficiencies between 25 and 76 per cent, depending on operating conditions. For operation at elevated chamber pressure, the nozzle was choked with a graphite plate which had an orifice of 0.5 or 0.75 inch diameter in the center of the plate. The chamber pressure was as high as 100 psig.

The heater was operated at two different field coil currents to determine arc rotation velocity on the degree of reaction.

The products of the reaction were quenched and collected through a water-cooled copper probe, 1/8 or 1/4 inch I.D., inserted about an inch inside of the nozzle. The product from the probe was first passed through a fiber filter (Purolater Co.) to separate the carbon, then collected at appropriate intervals in gas sampling tubes on a manifold, as previously described.¹

The gas analyses were made mass spectrometrically. A typical composition of a sample is shown in Table I; Table II shows the approximate material balance based on the H_2/C ratios of the feed and product gases. The only variation with operating conditions is in the relative concentration of the different species.

TABLE I. COMPOSITION OF GASEOUS PRODUCT, MOLE PERCENT

H_2	CO	CO ₂	CH ₄	C ₂ H ₂	C ₂ H ₄	C ₃ H ₄	C ₄ H ₂	C ₆ H ₆
77.68	1.27	0.09	5.81	13.58	1.01	0.12	0.32	0.14

TABLE II. MATERIAL BALANCE OF PRODUCTS IN MOLE PERCENT

H_2	CO	CO ₂	CH ₄	C ₂ H ₂	C ₂ H ₄	C ₃ H ₄	C ₄ H ₂	C ₆ H ₆	C
73.06	1.19	0.08	5.46	12.77	0.95	0.11	0.30	0.13	15.00

Electron micrographs were obtained on a number of the carbon samples by replicating an amyl acetate suspension on a carbon film. X-ray spectra were obtained by packing the soot into a disc-sample holder and irradiating with Cu K- α radiation. The sample packing and irradiation were kept as nearly identical as possible for all of the samples. The d-spacing and line intensity were compared against AUC graphite measured under identical conditions.

RESULTS AND DISCUSSION

As shown in Table II, the product consists of species which are expected from the high temperature pyrolysis of methane. The primary products are H_2 , C_2H_2 , and carbon, with varying concentration of CH_4 , depending on the degree of reaction. The diacetylene and benzene are formed from the polymerization of the acetylene; the methyl acetylene, although not an intermediate in the conversion of CH_4 to C_2H_2 , is known to be a minor product found in the pyrolysis of diacetylene.⁴ The C_2H_4 is an intermediate in the $CH_4 \rightarrow C_2H_2$ reaction. There is a slight error in the material balance since the hydrogen content of the soot was not taken into account because of sampling difficulty. The soot usually contains about one percent of hydrogen, and the presence of aromatic constituents is evident from the odor.

Considering the difficulty of obtaining exact experimental parameters during an experiment, quite good correlation was obtained between the degree of reaction and arc enthalpy, whereas the correlation was poor with respect to the net enthalpy increase of the gas. Figure 1 shows the relative degree of methane pyrolysis as a function of the arc enthalpy. The curves show the comparison between runs made at 2500 and 1500 amperes field coil current. The former effects an arc rotation velocity approximately 66 percent greater than that at the 1500 amps field coil current. There is a significantly steeper slope at higher arc rotation velocity, this result probably arising from the greater degree of mixing. Note that the curves saturate at high enthalpies, where the system is at equilibrium, or near equilibrium condition. A minimum just above the critical enthalpy (or initiation temperature).

The electron micrographs of the soot, quenched at the heater nozzle, at 25,500X magnification, Figure 2, shows spherical particles of less than 100 Å to approximately 5000 Å diameter. The nature of the background is not known at present, but blow-ups of the photomicrographs to approximately 153,000X suggests that the cloud consists of extremely fine, smokey carbon dust.

The d-spacings obtained from the x-ray diffraction of the soot varies between 3.45 and 3.49 Å, compared to 3.35 Å for pure, crystalline graphite. The lower value of 3.45 Å was obtained on the carbon collected from the high pressure runs, where the residence times were up to seven times longer than the runs at atmospheric pressure. The degree of crystallinity of the soot, based on the x-ray intensity, varied from two to ten percent of AUC graphite. The x-ray crystallinity, as suspected, is a function of the residence time.

It was of interest to plot the major product compositions on a semi-log plot, as a function of reciprocal arc enthalpy since the latter is proportional to the temperature in the gas. Figure 3 shows that the slopes for acetylene and hydrogen are approximately the same, whereas the slope for carbon is much steeper. The difference in slopes for carbon, as compared to C_2H_2 and H_2 , clearly shows the different mechanisms for the formation of these species.

REFERENCES

1. C. Hirayama and D. A. Maniero, "A New Rotating Arc Heater for Chemical Processing," Preprints, Div. of Fuel Chem., Am. Chem. Soc. Meeting, Pittsburgh, March 22-31, 1966, Vol. 10, No. 1, pp. 123-132.
2. D. A. Maniero, P. F. Kienest, and C. Hirayama, Westinghouse Engineer 26, 66 (1966). Also, same authors, paper presented at Electrochem. Soc. Nat. Meeting, Phila., Oct. 12, 1966.
3. See, for example, S. A. Miller, "Acetylene, Its Properties, Manufacture and Uses." Vol. I, Academic Press, New York, 1965, pp. 391-405.
4. K. C. Hou and H. B. Palmer, J. Phys. Chem. 69, 858 (1965).

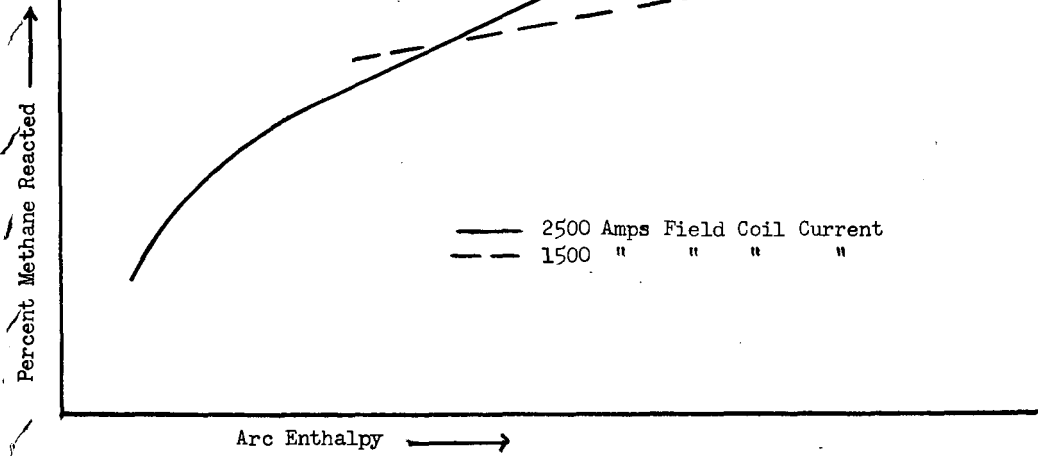


Fig. 1. Methane conversion as functions of arc enthalpy and arc rotation



Fig. 2. Electron micrographs of carbon at 25,500X

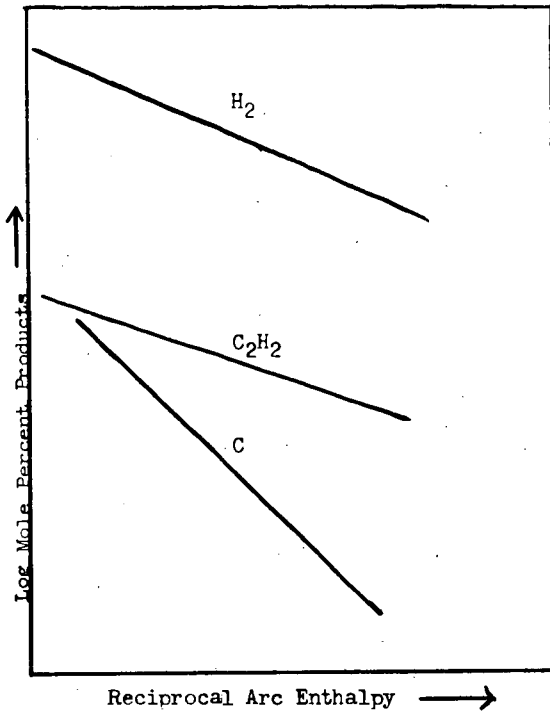


Fig. 3. Product composition as a function of reciprocal arc enthalpy

THE REARRANGEMENT OF METHANE AND METHYL CHLORIDE IN A MICROWAVE DISCHARGE

J. P. Wightman

Virginia Polytechnic Institute, Blacksburg, Virginia

N. J. Johnston

NASA - Langley Research Center, Hampton, Virginia

I. INTRODUCTION

In a previous paper(1) the rearrangement of a series of hydrocarbons including methane in a microwave discharge was reported. The work reported here is an investigation of the effect of the introduction of a functional group in methane on the nature of both the gaseous and solid products of rearrangement. Such measurements should ultimately support a model of the rearrangement mechanism in a microwave discharge. Methane and methyl chloride were passed separately in the absence of a diluent through a microwave discharge.

II. EXPERIMENTAL

A. Materials

Methane (ultrahigh purity grade) was obtained from the Matheson Co. and used without further purification. The following analysis was supplied with the methane: CO_2 - <5 ppm; O_2 - 5 ppm; N_2 - 19 ppm; C_2H_6 - 14 ppm; C_3H_8 - <5 ppm. Methyl chloride (high purity grade) was obtained from the Matheson Co. and used without further purification.

B. Apparatus and Procedure

The rearrangements were carried out in a high vacuum flow system. The power source for the microwave discharge was a Raytheon generator (Model KV-104) and was operated at a power level corresponding to about 40 r.f. watts at 2450 Mc. The generator was connected to an air-cooled cavity (Raytheon - KV series) by a coaxial cable. Two procedures were used depending upon whether an analysis of the gaseous products was being made or whether solid film was being deposited for subsequent analysis. In the former case, the parent gas was passed through a variable leak valve (Veeco - VL). The pressure in a typical experimental run was 0.15 torr at a mass flow rate of 1×10^{-5} moles/min. and a linear flow rate of 20 cm./sec. In the latter case, the parent gas was passed through a Teflon needle valve (Fischer-Porter). The pressure in a typical experimental run was 0.50 torr. Normal deposition time was 20 min.

The gaseous rearrangement products of methane and methyl chloride were determined using a mass spectrometer (Associated Electronics Industries - MS-10). The sampling volume was located about 140 cm. downstream from the discharge. After establishment of a constant flow rate, the parent gas stream was sampled. An off-on valve upstream from the discharge allowed the system to

be pumped down without altering the setting of the variable leak. Between analyses pumpdown resulted in faster attainment of steady state concentrations of rearrangement products. Flow was again started and the discharge initiated with a Tesla coil. After establishment of a constant flow rate the discharged gas stream was sampled.

The solid polymeric films were removed mechanically from the walls of the Pyrex tubing. The infrared spectra of the films of both gases were obtained using either a Perkin-Elmer 421 or 621 spectrophotometer. The electron spin resonance spectra of the neat films from both gases were obtained on a Varian ESR 6 spectrometer. Elemental analyses of both films were made by Gailbraith Labs.

III. RESULTS

A. Gaseous Products

1. Mass spectra

Selected peaks from the mass spectra of methane and methyl chloride obtained with the discharge on and off are shown in Figures 1a and 1b. The most significant features in the methane spectra (Figure 1a) were the increase in the $m/e = 2$ (H_2^+) peak and the decrease in the $m/e = 15$ (CH_3^+) peak when methane was passed through the discharge. Trace quantities of higher molecular weight hydrocarbons were also noted. The most significant features of the methyl chloride spectra (Figure 1b) were the increase in the $m/e = 2$ (H_2^+) peak, the appearance of the $m/e = 30$ ($C_2H_6^+$) peak and the decrease in the $m/e = 50$ (CH_3Cl^+) peak when methyl chloride was passed through the discharge. Further, HCl was noted when the liquid nitrogen cooled trap downstream from the discharge was opened.

B. Solid Films

A solid film was observed to form in the discharge region when either methane or methyl chloride was passed through the discharge. Both films were characterized in several ways.

1. Elemental analysis

Empirical formulas for the solid films were established by elemental analysis. The formulas for the solid films formed from methane and methyl chloride were $(CH_{1.5})_x$ and $(CH_{0.65}Cl_{0.045})_x$, respectively.

2. Infrared spectra

The infrared spectrum of the film obtained from methane is shown in Figure 2 where a neat sample was used. Peaks ascribed to the film were noted in the region of the following frequencies: 2900, 1700, 1450, 1380 and 880 cm^{-1} . The assignments of these frequencies follow those given by Jesch et al (2). The band at 880 cm^{-1} may be due to rocking vibration of $-CH_3$ in a multiple carbon atom chain. The band at 1380 cm^{-1} is characteristic of $-CH_3$ deformation. The band at 1450 cm^{-1} is characteristic of $-CH_2$ symmetric scissors vibration. The band at 1700 cm^{-1} was probably due to carbonyl formed on exposure of the film to air. The 2900 cm^{-1} band

is due to C-H stretching vibration.

The infrared spectrum of the film obtained from methyl chloride is shown in Figure 3 where a neat sample was used. The low intensity peaks were a characteristic of the methyl chloride films whether run as a neat sample or as a KBr pellet. Peaks ascribed to the film were noted in the region of the following frequencies: 2900, 1700, 1580, 1440 and 875 cm^{-1} . The peak at 1380 cm^{-1} observed in the methane film is absent in the methyl chloride film and a new peak at 1580 cm^{-1} is observed in the methyl chloride film.

3. Electron spin resonance

The electron spin resonance spectra of the films produced from methane and methyl chloride are shown in Figures 4a and 4b. A significantly larger free spin concentration on the order of one thousand times greater was noted in the case of the methyl chloride film. No fine structure was observed in the case of the methyl chloride film. g-values for both films were essentially identical to the value for pitch ($g = 2.000$).

4. Solubility studies

An extensive series of liquids were tested as possible solvents for the films prior to NMR measurements. Solubility of the methane film was observed only in the case of hexamethylphosphamide and concd. H_2SO_4 .

IV. DISCUSSION

Investigations of chlorinated hydrocarbons in a microwave discharge have not been reported in the literature previously. Swift et al (3) however have investigated the effect of an rf discharge on CCl_4 in the absence of a diluent. A number of chlorinated gaseous products were reported in addition to a chlorinated polymer. The present work indicated a limited number of gaseous products. The results are consistent with the argument that molecules in a microwave discharge are subjected to a greater degree of fragmentation than in an rf discharge thereby limiting both the number and the complexity of gaseous products.

From the previous work of Vastola and Wightman (1) the following postulate could be advanced: if a parent hydrocarbon has a hydrogen to carbon (H/C) ratio greater than about 1.6, a hydrogen saturated solid film will be produced on passage of the hydrocarbon through a microwave discharge in addition to hydrogen. Conversely, if a parent hydrocarbon has a (H/C) ratio less than about 1.6 a hydrogen deficient film will be produced and no hydrogen will be observed.

The present work is an attempt to test the validity of this postulate if a functional group is introduced into the hydrocarbon molecule. Methyl chloride was chosen since it represents a straightforward extension of the methane case. Methyl chloride has a (H/C) ratio of 3 and if the Cl is neglected, the formation of a hydrogen saturated film would be predicted. However, HCl was observed as a rearrangement product. Hence the Cl can not be neglected and yet assuming the limiting case of a 1:1 correspondence between CH_3Cl and HCl, the (H/C) ratio of the remaining fragment would be 2. Thus the formation of a hydrogen saturated film would still be predicted but which in fact was not observed.

Instead a hydrogen deficient film was produced. The formation of a hydrogen deficient film from a parent molecule which has a high enough (H/C) ratio to form a hydrogen saturated film can be attributed to two factors. In the first instance, Cl preferentially appears in the gas phase as is indicated by the low percentage of Cl in the film, the absence of a significant C-Cl absorption peak in the infrared spectrum (Figure 3) and the presence of HCl downstream from the discharge. The extension of this work to other functional groups is anticipated to determine if this is a general scheme. In the second instance, the tendency to form hydrogen in a microwave discharge is again noted in the case of methyl chloride as in the case of methane (Figures 1a and 1b). Apparently for hydrocarbons containing functional groups, the formation of hydrogen is favored even at the expense of the formation of a hydrogen deficient film. The formation of ethane observed as a product of the methyl chloride discharge could be due to the recombination of methyl radicals produced in the discharge.

Films formed in various types of electrical discharges have not been extensively characterized. The recent work of Jesch et al (2) described the infrared analysis of a series of films produced from hydrocarbons in a glow discharge. Direct comparison between the present results and those of Jesch et al is not possible since two different types of electrical discharges were used. The type of discharge used dramatically alters the nature of both the gaseous and solid rearrangement products as indicated above.

The properties of the film produced from methyl chloride are similar to those reported previously (1) for the hydrogen deficient films formed from acetylene, benzene and naphthalene. The color of the methyl chloride film was dark (brownish-black) characteristic of hydrogen deficient films in contrast to the light yellow methane film characteristic of hydrogen saturated films. The high electron spin concentration of the methyl chloride film had also been observed for the hydrogen deficient film from acetylene.

The films produced from both methane and methyl chloride appear to be highly cross-linked as evidenced by the negligible solubility in liquids used as solvents for other polymeric systems. The methyl chloride film contains a greater number of free electrons than the methane film indicative of a significant number of unsaturated valences in the methyl chloride film. The methyl chloride film appears to be characterized by a greater degree of unsaturation than the methane film. Highly unsaturated polymeric systems have been found difficult to analyze by infrared spectroscopy* which has also been noted in the present results. Definitive NMR work would be helpful in elucidating the nature of these polymeric films.

* private communication with Dr. Vernon Bell (NASA - Langley Research Center)

Acknowledgements - The authors would like to acknowledge the help of Dr. R. E. Dessy in obtaining the ESR spectra and the experimental assistance of Mr. R. O. McGuffin.

REFERENCES

- (1). F. J. Vastola and J. P. Wightman, *J. Appl. Chem.*, 14, 69 (1964).
- (2). K. Jesch, J. E. Bloor and P. L. Kronick, *J. Poly. Sci. A-1*, 4, 1487 (1966).
- (3). E. Swift, jr., R. L. Sung, J. Doyle and J. K. Stille, *J. Org. Chem.*, 30, 3114 (1965).

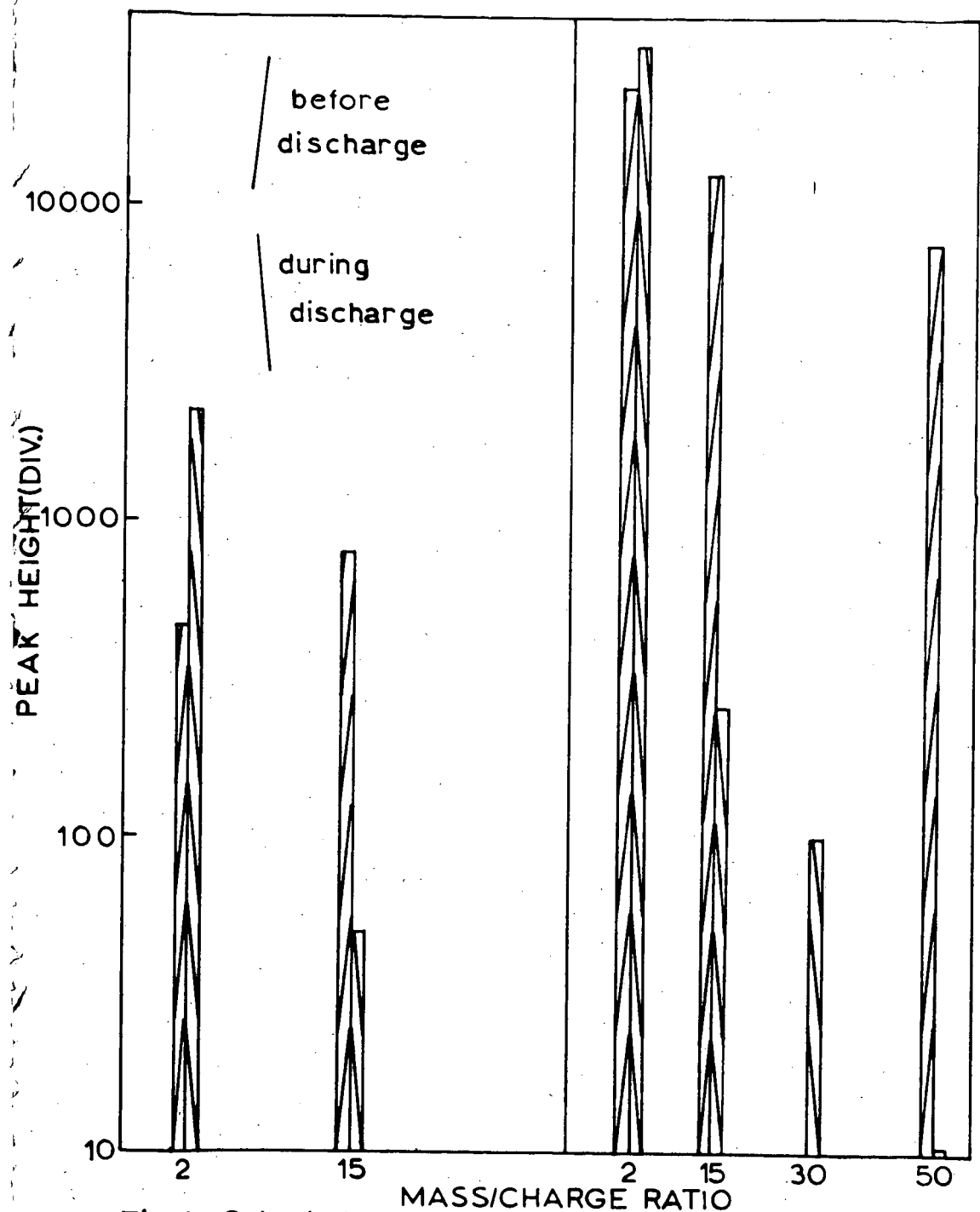
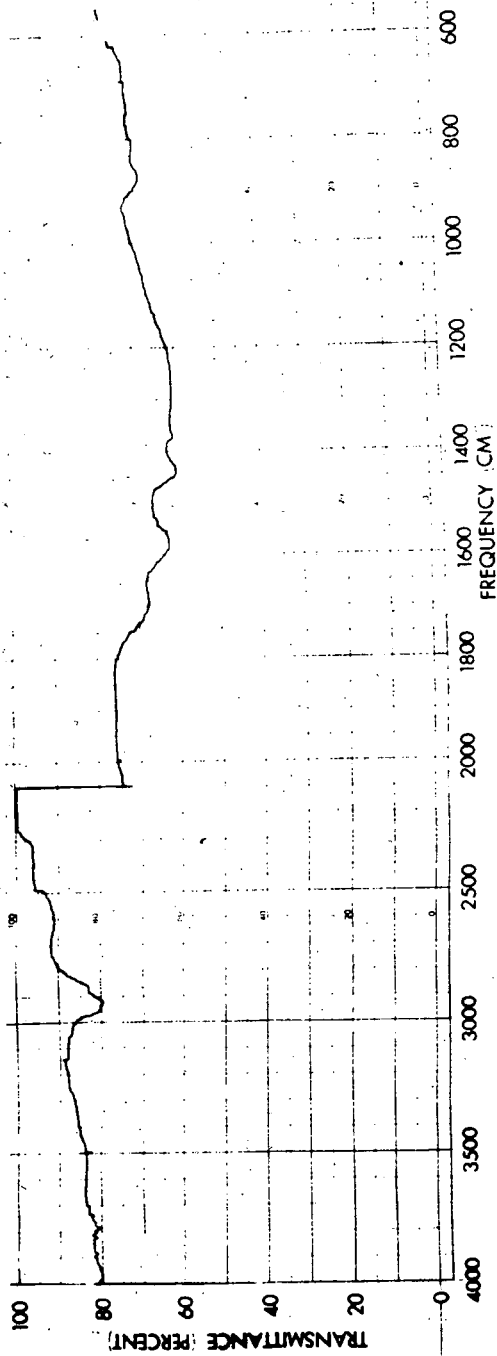


Fig. 1a. Selected peaks from Fig. 1b. Selected peaks from mass spectra of methane mass spectra of methyl chloride in a microwave discharge. mass spectra of methyl chloride in a discharge.



478

Fig.3. Infrared spectrum of polymer produced from methyl chloride.

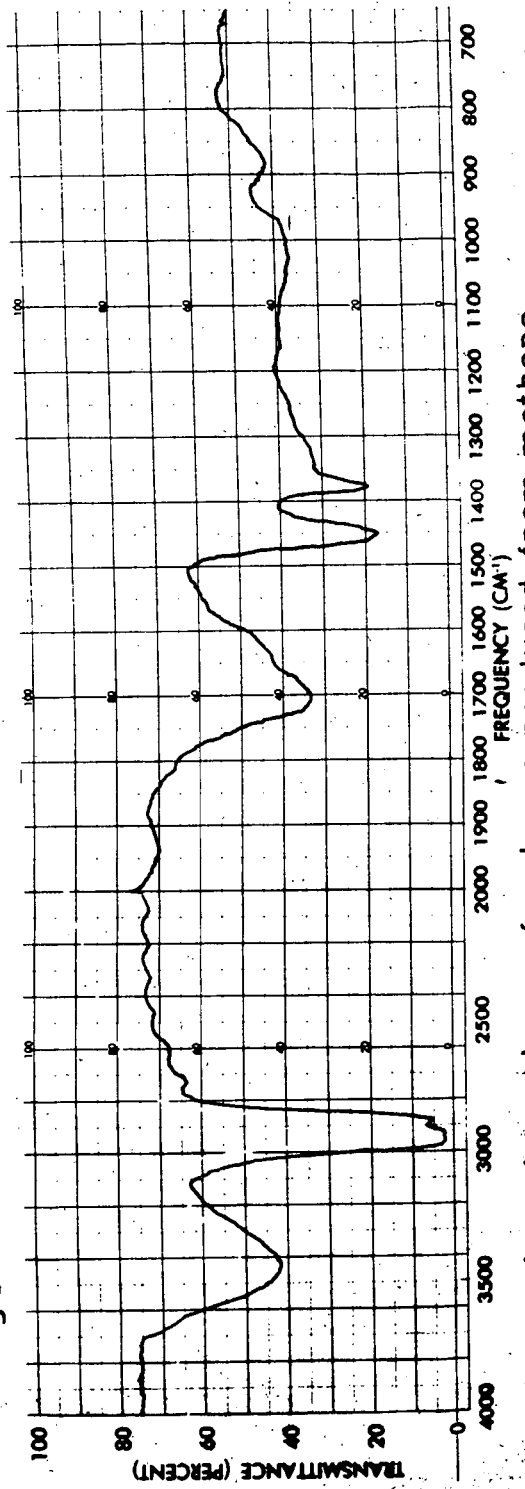


Fig.2. Infrared spectrum of polymer produced from methane.

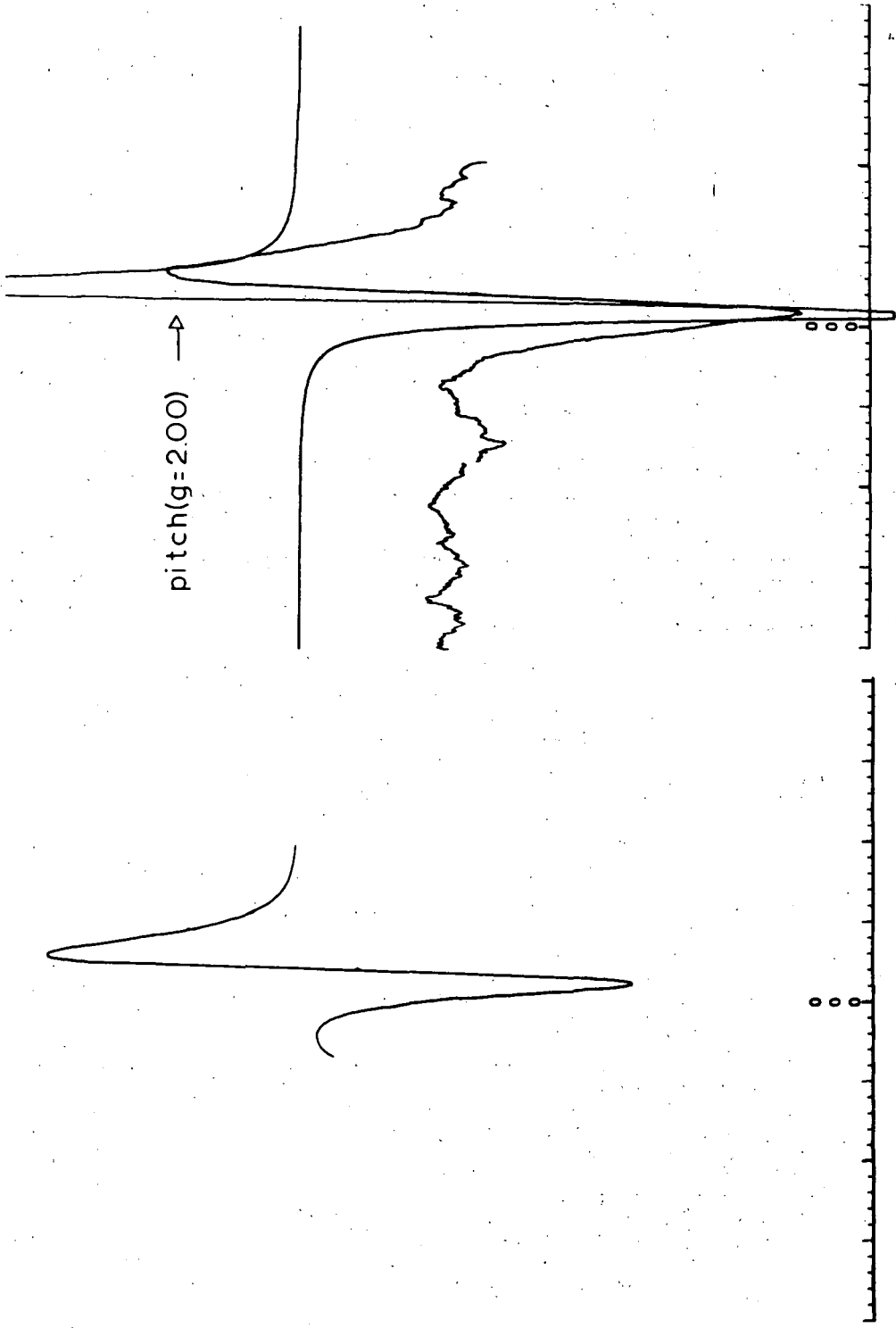


Fig.4b. ESR spectrum of polymer produced from methyl chloride.

Fig.4a. ESR spectrum of polymer produced from methane.

FATTY ACIDS AND n-ALKANES IN GREEN
RIVER OIL SHALE: CHANGES WITH DEPTH

Dale L. Lawlor and W. E. Robinson

Laramie Petroleum Research Center, Laramie, Wyoming

INTRODUCTION

Many papers have been published relating fatty acids to n-alkanes in ancient sediments. Breger (1) postulated that n-alkanes may be formed in sediments by beta-keto acid decarboxylation. Jurg and Eisma (5) demonstrated in the laboratory that a homologous series of n-alkanes can be produced by heating the C₂₂ fatty acid in the presence of bentonite. Cooper and Bray (2) suggested that odd-carbon-numbered n-alkanes and odd-carbon-numbered fatty acids may be produced from naturally occurring even-carbon-numbered fatty acids by a free-radical decarboxylation mechanism. Mair (7) and Martin and coworkers (8) have discussed the relationship between fatty acids and n-alkanes in petroleum genesis.

If fatty acids are converted to n-alkanes in sediments, a distributional relationship would likely be apparent between the two compound classes. Such a relationship would be most relevant if both the acids and the alkanes were indigenous to each sample taken from one geological formation. In this respect the Green River Formation is ideal for study of the relationship between fatty acids and n-alkanes. This formation represents 6 million years of accumulation of organic debris from a highly productive Eocene lake which existed approximately 50 million years ago. A 900-foot core representing 3 million years of the Green River Formation was sampled and the fatty acids were extracted and analyzed.

An earlier paper (6) presented a correlation between the carbon number distribution of the fatty acids and the carbon number distribution of the n-alkanes in the Mahogany zone portion of the Formation. The present paper tests the postulate that n-alkanes are formed from fatty acids by maturation processes resulting from the time differential existing between the bottom and the top of the core. The results showed that both maturation and changes in organic source material explain the differences in samples taken from several stratigraphic positions in the formation.

EXPERIMENTAL

Ten oil-shale samples were taken from the Green River Formation, nine from a 900-foot core (Equity Oil Co., Sulfur Creek No. 10), and one from the Mahogany zone. The stratigraphic positions and the oil yields of the 10 samples are presented in table 1. The samples were the same as those used by Robinson and coworkers (9) in a study of the distribution of n-alkanes at different stratigraphic positions within the formation.

The samples, ground to pass a 100 mesh screen, were treated with 10 percent hydrochloric acid to remove mineral carbonates and to convert salts of acids to free acids. Two-hundred grams of each of the acid-treated samples were refluxed with 400 ml of 7 percent borontrifluoride in methyl alcohol for 6 hours. This reaction converted free and esterified acids to methyl esters. The reaction mixture was cooled, filtered, and washed with methyl alcohol until the washing was clear. The filtrate was transferred to a separatory funnel, water was added, and the solution was extracted with successive portions of carbon tetrachloride until the solvent was colorless. The carbon tetrachloride solution of the methyl esters was dried overnight using anhydrous sodium sulfate. The fatty acid methyl esters were isolated from the carbon tetrachloride solution by urea adduction.

TABLE 1. - Stratigraphic position and pyrolytic oil yields of the oil-shale samples

Sample Number	Stratigraphic position, feet from surface	Approximate pyrolytic oil yield, gallons per ton of shale
0	830	60
1	1036-1056	35
2	1056-1081	34
3	1152-1178	42
4	1236-1241	48
5	1450-1462	39
6	1597-1628	35
7	1668-1696	37
8	1786-1825	28
9	1884-1924	20

Fatty acid methyl esters were further purified by thin layer chromatography using silica gel. The thin layer plate was developed with a mixture of n-hexane, ethyl ether, and acetic acid (90/10/1). The adsorbant zone where esters occur was scraped from the plate and extracted with a solution of 10 percent methyl alcohol in carbon tetrachloride. The solvent was removed from the methyl esters by evaporation at room temperature under a stream of nitrogen. The carbon number distribution of these isolated fatty acid methyl esters was determined by mass spectrometry using the intensity parent peak as a measure of the quantity.

Carboxyl and ester contents were determined for the 10 shale samples by analytical procedures developed by Fester and Robinson (4).

RESULTS AND DISCUSSION

The fatty acid distribution with depth (table 2), shows that the predominant acid at various stratigraphic depths within the formation is not constant. The sample number, percentage, and chain length of the predominant acid of the samples are: No. 0, 16.2, C₃₀; No. 1, 14.1, C₂₄; No. 2, 21.7, C₂₈; No. 3, 9.8, C₂₈; No. 4, 16.6, C₂₄; No. 5, 9.2, C₂₈; No. 6, 12.8, C₁₄; No. 7, 12.6, C₁₄; No. 8, 12.1, C₂₈; and No. 9, 23.9, C₂₈. The C₂₈ acid is the predominant acid in five of the samples, and is among the three most abundant acids in all the other samples except samples 1 and 4 where it is present in small amounts. The C₂₀ acid content in samples 5 through 9, despite being more abundant in nature than the C₁₉ and C₂₁ acids, is less than the C₁₉ and C₂₁ acids in these samples. The C₁₈ acid is quite low in samples 1 and 2 relative to the other eight samples. The C₃₂ acid is present in large amounts only in sample No. 0. There appears to be no consistent relationship between the acids of one sample to that of another sample. This lack of relationship may be due to differences in source material or environmental changes rather than maturation changes.

Significant differences are apparent in the relative distribution of the fatty acids and the n-alkanes from published data (3,9), shown in figures 1 and 2, where the data from four samples are plotted for comparative purposes. These particular samples were chosen because they represent three stratigraphic levels below the Mahogany zone sample approximately equi-distant from each other. If maturation of sediments causes decarboxylation of fatty acids to form n-alkanes, a relationship between the distribution of the two components would be expected. Except for sample No. 0, little similarity is evident. Since the distributions correlate poorly, either the original postulate is untrue and n-alkanes are not produced from fatty acids having one more

TABLE 2. - Carbon number distributions of fatty acids

Carbon Number	Fatty acids, wt percent of total									
	Sample number									
	0	1	2	3	4	5	6	7	8	9
14	5.1	7.1	2.8	6.3	2.3	8.0	12.8	12.6	11.4	6.5
15	3.0	3.4	2.8	6.3	2.8	7.2	2.1	6.3	8.1	3.7
16	2.7	7.1	2.4	5.6	4.0	5.8	6.4	7.8	9.4	5.4
17	2.0	4.0	1.9	4.9	2.9	5.1	5.9	4.3	2.4	2.0
18	3.4	2.6	2.1	4.2	4.2	5.4	8.0	7.4	7.4	6.1
19	2.4	3.4	1.8	3.5	3.8	4.0	4.3	3.6	2.0	2.0
20	2.7	8.2	1.9	2.8	4.5	2.9	4.2	2.9	2.0	1.3
21	2.4	7.1	2.2	2.8	5.6	3.6	4.8	3.6	2.0	1.7
22	7.4	8.8	3.6	4.9	9.7	5.8	11.6	8.3	10.7	13.0
23	4.7	4.7	4.4	5.6	12.5	5.8	3.8	4.7	3.4	3.3
24	7.1	14.1	6.2	4.2	16.6	3.3	8.0	6.3	8.7	12.0
25	3.7	7.6	5.0	3.5	8.3	2.5	3.8	3.4	2.7	2.6
26	12.1	11.8	13.3	8.4	11.8	6.5	4.9	5.9	4.7	5.2
27	2.7	2.6	8.2	6.3	3.7	8.0	2.7	4.9	3.4	3.7
28	11.1	4.2	21.7	9.8	4.0	9.2	9.8	8.5	12.1	23.9
29	2.7	1.3	5.7	4.2	1.2	4.3	1.5	2.9	2.7	2.4
30	16.2	1.3	8.6	7.7	1.1	5.8	2.5	3.2	2.7	2.8
31	1.7	0.4	2.5	4.2	0.3	4.0	0.8	1.6	2.0	1.3
32	7.1	0.4	2.9	4.9	0.5	3.3	0.9	1.6	2.0	1.1

carbon atom or other factors are more significant. One factor to consider is that the fatty acids recovered from the lower portions of the core may not be representative of the acids originally present since they may be residual acids from selective maturation.

Groups of even numbered acids vary in abundance as shown graphically in figures 1 and 2. Sample No. 0 has predominant acid peaks between C₂₆ and C₃₀, sample No. 4, between C₂₂ and C₂₆, sample No. 6, between C₂₂ and C₂₈, and sample No. 9, between C₂₂ and C₂₈. The latter two samples show the greatest overall similarity.

The carboxyl content of the shale generally decreases with depth, table 3, beginning with sample No. 0 having 23.6 mg of carboxyl per gm of organic carbon and ending with sample No. 9 having 4.8 mg of carboxyl per gm of organic carbon. This general decrease in carboxyl content with depth, and a corresponding increase in the n-alkane content, as shown by Robinson and coworkers (9), implies that the fatty acids may have been converted to n-alkanes by decarboxylation.

The ester content of the samples, table 3, did not show a trend; this is in contrast to the trend shown by the acids. Random distributions found for the ester samples reflect more accurately changes in organic source material than do the acid distributions.

Maturation changes are evident in the decreasing amount of carboxyl content with depth, the increasing amount of n-alkane content with depth, and the decreasing ratio of odd to even-carbon-numbered n-alkanes. Source material or environmental changes are evident in the variations in the amount and carbon number of the dominant fatty acids, and n-alkanes and the random distribution of ester content with depth.

TABLE 3. - Carboxyl and ester contents of the 10 shale samples

Sample Number	Carboxyl, mg/gm carbon	Ester, mg/gm carbon ^{1/}
0	23.6	36.6
1	18.3	22.2
2	10.1	33.9
3 ^{2/}	--	--
4	3.8	26.7
5	6.7	17.9
6	4.0	37.1
7	4.7	26.0
8	4.9	42.9
9	4.8	29.0

^{1/} Calculated as COOH

^{2/} Insufficient sample.

CONCLUSIONS

The postulate that fatty acids from the organic debris in the Green River Formation may form n-alkanes of one less carbon atom was found to be subject to question. Relatable fatty acid and n-alkane distributions were shown to be present in the younger portions of the Formation but the older portions showed little relation.

Maturation and organic source material differences may account for the observed distributions of fatty acids in sections of Green River Formation oil shale. Evidence of maturation is found in the decreasing amount of odd-carbon-numbered n-alkanes and in the decreasing amount of carboxyl content with depth. Evidence of organic source material differences is found in the inconsistent distribution of the predominant fatty acids from sample to sample.

The ester content is not related to the free-acid content, indicating different formative histories.

REFERENCES

1. Breger, I. A. Diagenesis of Metabolites and a Discussion of the Origin of Petroleum Hydrocarbons. *Geochim. et Cosmochim. Acta*, v. 19, 1961, pp. 297-308.
2. Cooper, J. E., and E. E. Bray. A Postulated Role of Fatty Acids in Petroleum Formation. *Geochim. et Cosmochim. Acta*, v. 27, 1963, pp. 1113-1127.
3. Cummins, J. J., and W. E. Robinson. Normal and Isoprenoid Hydrocarbons Isolated from Oil-Shale Bitumen. *J. Chem. Eng. Data*, v. 9, 1964, pp. 304-307.
4. Fester, J. I., and W. E. Robinson. Oxygen Functional Groups in Green River Oil Shale and Trona Acids. Ch. in "Advances in Chemistry Series." American Chemical Society, Washington, D.C. (1966), pp. 22-31.
5. Sarg, J. W., and E. Eisma. Petroleum Hydrocarbons: Generation from Fatty Acids. *Science*, v. 144, 1964, pp. 1451-1452.

6. Lawlor, D. L., and W. E. Robinson. Division of Petroleum Chemistry, Am. Chem. Soc., Detroit, Mich., April 1965, Petroleum Division General Papers No. 1, 1965, pp. 5-9.
7. Mair, B. J. Terpenoids, Fatty Acids and Alcohols as Source Materials for Petroleum Hydrocarbons. *Geochim. et Cosmochim. Acta*, v. 28, 1964, pp. 1303-1321.
8. Martin, R. L., J. C. Winters, and J. A. Williams. Distributions of n-Paraffins in Crude Oils and Their Implication to Origin of Petroleum. *Nature*, v. 199, 1963, pp. 110-114.
9. Robinson, W. E., J. J. Cummins, and G. U. Dinneen. Changes in Green River Oil Shale Paraffins with Depth. *Geochim. et Cosmochim. Acta*, v. 29, 1965, pp. 249-258.

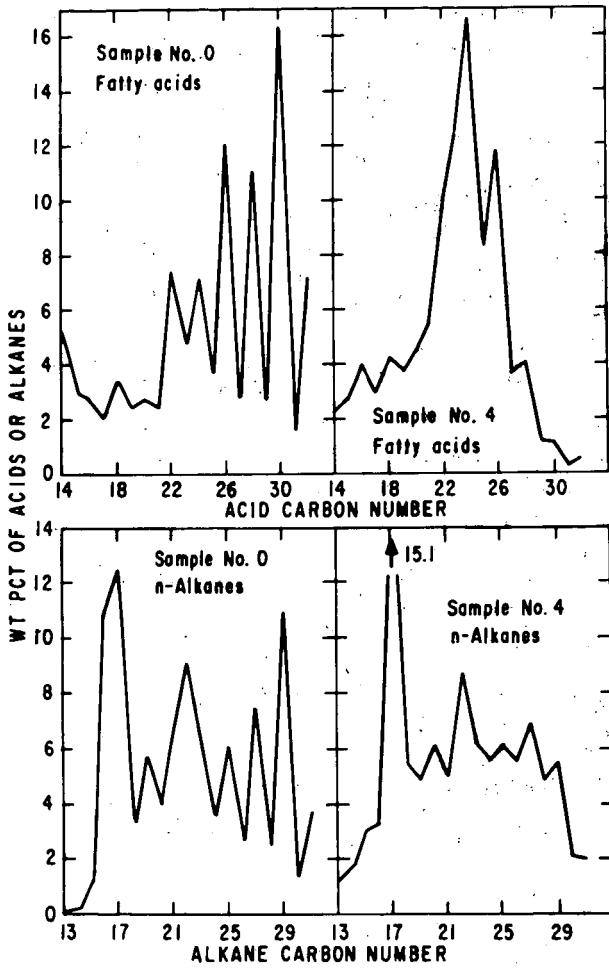


Figure 1. Comparison between fatty acid and n-alkane distributions, Sample Nos. 0 and 4

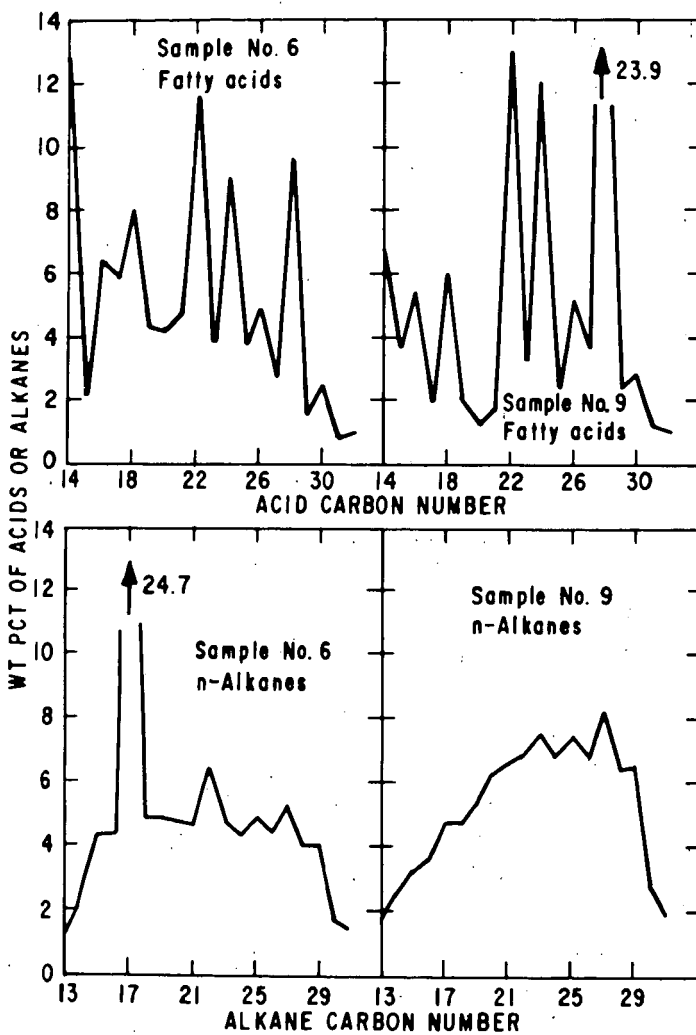


Figure 2. Comparison between fatty acid and n-alkane distributions, Sample Nos. 6 and 9

ELECTRICAL PROPERTIES OF IODINE COMPLEXES OF ASPHALTENES

Gustave A. Sill and Teh Fu Yen

Mellon Institute
Pittsburgh, Pennsylvania 15213

INTRODUCTION

Polynuclear aromatic hydrocarbons generally form charge-transfer complexes with halogens. Some of the fused aromatic hydrocarbons, e.g., perylene, violanthrene, yield solid complexes exhibiting extremely good semiconduction (1,2,3) while others, e.g., coronene, show only fair to poor semiconduction (4). A number of charge-transfer complexes of aromatic containing polymers have been investigated for possible differences in electrical properties (5,6,30).

A polymeric dielectric may be converted to a polymeric semiconductor by increasing the aromaticity of the insulator, followed by complex formation with a halogen (7,8). The increase in aromaticity can be effected by radiation--e.g., cyclization of polyethylene and followed by dehydrogenation (7); or by heat--e.g., pyrolysis or graphitization to a pyropolymer (8). The resulting products when treated with iodine exhibit a wide range of interesting electrical properties.

From a structural standpoint asphaltene (9) are considered to consist of two-dimensioned fabrics of condensed aromatic rings, intermingled with short aliphatic chains and fused naphthenic ring systems (10). X-ray diffraction (11,12) and ESR investigations (13) have indicated that these aromatic systems tend to form stacks of graphite-like layers surrounded by a disorganized zig-zag chain structure of saturated carbons. Morphologically they may be considered as a highly associated "multipolymer" (14), the

molecular weight of which can vary from a few thousand (unit or particle weight) to a few million (micelle weight) (15). The aromatic centers, roughly 15\AA in diameter, are considered to be pericondensed (23,18). It has been demonstrated that asphaltics can form charge-transfer complexes, due to the presence of such aromatic systems (20).

Most polynuclear aromatic compounds form well defined crystals, the iodine complexes of which are stable and stoichiometric in composition. Asphaltics are mesomorphic (17) owing to the random distribution and isotropic orientation of the structural units, and it is to be anticipated, therefore, that the conduction mechanism will be different from that of the crystalline environment (due to diffusion and phonon processes) (16). Since there is a difference in the conduction mechanism between crystalline and amorphous aromatics, one would like to know whether the mesomorphic nature of asphaltics would retard or inhibit the conductivity, and if so to what extent.

The aims of this research were two-fold. The first was simply to observe where asphaltenes fall in the conductivity range and to determine the extent to which conductivity can be enhanced by iodine complex formation. The second was a more general study of the electrical properties of asphaltics as another approach to a better understanding of their structure. To the authors' best knowledge, there is no published work on the electrical characteristics of these materials. Iodine may be visualized as a tracer or indicator for condensed aromatic systems, even when buried in a matrix of paraffinic or cycloparaffinic material. It was thought, therefore, that iodine complex formation and its effect

on the overall electrical properties of the asphaltene might yield independent information of the size and distribution of the aromatic centers in these multipolymers.

EXPERIMENTAL

Resistance Measurements

A General Radio type 1230A electrometer was used for specimens with resistance less than 10^{12} ohms (ambient temperature), and a Cary model 31 electrometer was used for specimens of higher resistance. In each case a glass vessel equipped with a ball joint and appropriate electrostatic shielding was coupled to the head of the electrometer (Fig. 1). Each specimen (approximately $1 \times 0.5 \times 0.1$ cm) was pelleted with a Beckman KBr press at 7.09×10^3 kg/cm² between two pieces of 52 mesh platinum screen. The pellet was degassed for eight hours and the electrical measurements made in a vacuum of 5×10^{-4} Torr. Using the high resistance leak method, a standard resistor served as calibrating reference (21); data were taken under conditions of both falling and rising temperature, a minimum of 30 minutes being allowed for equilibration at 10° levels. Upon completion of the temperature dependence measurements, the physical dimensions of the specimen block were obtained with a travelling microscope (10X) with an x,y micrometer attachment (0.0001 cm precision).

Preparation of Sample

The asphaltene sample was prepared by our standard procedure (9). Two native asphaltenes were investigated, one from the Boscan crude oil from Venezuela (Sample VY), the other from the Baxterville crude from

Mississippi (Sample GS). Stock solutions in benzene of iodine and of the individual asphaltenes were made up in fixed concentration and samples of varied composition prepared by mixing appropriate quantities of these stock solutions at room temperature and lyophilizing at reduced pressure to yield powdered solids with a homogeneous iodine distribution. These samples were analyzed before and after the electrical measurements for %I by ignition in oxygen, reduction with hydrazine sulfate, and potentiometric titration of the resulting iodide with AgNO_3 using a Beckman model K automatic titrator. Usually there was no observable loss of free iodine during electrical measurements; 10-15% loss of iodine was found after degassing. The iodine values used in the present work are those values obtained after completion of the electrical measurements for the entire specimen.

Treatment of Data

The resistance values along with the corresponding temperature data and dimensions of the specimen were key punched on IBM cards and evaluated on an IBM 7090-1401 digital computer system. Given A, the area of the cross section, and L, the length of the specimen, the resistivity, ρ , can be evaluated from the resistance, R, as follows: $\rho = AR/L$. The temperature dependence of the resistivity is then evaluated by the relationship:

$$\rho_T = \rho_0 \exp (\epsilon/2kT),$$

where k is Boltzman's constant, ϵ is the energy gap in eV and ρ_0 is the resistivity extrapolated to $\frac{1}{T} = 0$. By use of a California Computer Products 30-in. plotter (300 steps; 1/500-in. per step) the temperature dependence data were fitted to straight lines (Fig. 2) as given by the equation

$$\log \rho = \log \rho_0 + \epsilon / (2kT \ln 10)$$

From the digital output, $\rho_{25^\circ\text{C}}$ and ϵ can be obtained. The applied voltage was limited to values under 10 V; in this region Ohm's law was followed.

The temperature range examined was from ambient to 90°C .

There is error involved in any single measurement of resistance, owing to systematic errors in the electrometer; errors also enter in the measurement of the dimensions of the specimen. That the results were not influenced by such systematic errors is evident from the two sets of data for two different preparations of an asphaltene (VY)-iodine complex, as given in Table I. The uncertainties in the per cent iodine and sample size may be judged from the variations in the independent measurements. Despite these variations, the resistivity at 25°C and the energy gap are within ca. 5% of the mean values.

Infrared Analysis

Differential IR spectra were obtained from a scan of an iodine-containing asphaltene versus a reference asphaltene at equal asphaltene concentration in CS_2 (the iodine-containing sample is normalized to 100% asphaltene for purposes of comparison) using a Beckman IR-12 instrument. A control scan of asphaltene in CS_2 solution against itself also was made for each sample.

X-ray Diffraction

A Norelco x-ray diffractometer equipped with a $\text{CuK}\alpha$ radiation source and a geiger tube detector was used to study the asphaltene-iodine system. In order to record the shift of the d-spacing due only to change in mass absorption coefficients, adamantane was added to an asphaltene-iodine complex (24% I) and to the original asphaltene. Strong (111) and (200) reflections due to the adamantane mixed with the VY asphaltene were

found at 5.7 and 4.9Å; for the VY asphaltene-iodine complex shifts were observed to 5.5 and 4.7Å, respectively. The spacing is reproducible to $\pm 0.2\text{\AA}$.

Electron Spin Resonance

ESR spectra were taken with a Varian V-4502 x-brand EPR spectrometer system in conjunction with a 12-inch magnet and a "Fieldial." The relative intensity observed was used as a guide for the spin concentration of the asphaltene (VY)-iodine complexes and native asphaltene (VY) (13).

RESULTS

All asphaltene-iodine samples studied gave repeatable linear relations in the temperature range investigated as shown in Fig. 2. There is no significant deviation from Ohm's law through the range 2.5 to 97 V as indicated by Fig. 3 in the temperature interval 313° to 372°K.

The native asphaltenes (Points 1, Fig. 4) fall generally in the insulator range. Upon the addition of iodine the resistivity falls, a to b, then increases sharply, b to c, and finally drops, c to d, as iodine content rises. Both complexes appear to yield curves of similar shape. The gap energy values for the asphaltene-iodine complexes are plotted versus their iodine contents (Fig. 5). The smallest energy gap measured in each case was $\sim 0.5\text{eV}$, but the absolute minimum is uncertain. These minima (points b) correspond to the sharp transitions of resistivity shown in Fig. 4.

Scanning in the far IR region revealed no C-I stretching frequencies for those iodine complexes for which ρ was determined. However, the differential IR measured in the $700\text{-}1200\text{ cm}^{-1}$ did show an additional band at

1080 cm^{-1} (Fig. 6), and freshly prepared asphaltene-iodine complexes in CS_2 also exhibited an enhancement in absorption in the region of 1000 to 1150 cm^{-1} , which is generally ascribed to complex formation.

The x-ray spectrograms in the region $2\theta = 2 - 42^\circ$ of the asphaltene (VI)-iodine system yielded an amorphous pattern with broad halos as shown in Fig. 7. For samples with an iodine content of less than 5 per cent, the 3.5Å band still appeared as a shoulder. In the meantime a new band was formed at around 8.7Å. At higher iodine contents (>10%), the 3.5Å band has apparently disappeared and the 8.7Å band became clearly visible. There is a general overall decrease of total intensity as %I increases since the iodine itself absorbs an increasingly large fraction of the diffracted x-rays. In the present case, the noise level coupled with the intensity reduction has made the disappearance of the 3.5Å shoulder difficult to detect.

In general, the ESR spectra obtained from the asphaltene-iodine samples indicated an increase in free radical concentration with increase in iodine content. The increase in relative intensity for an asphaltene (VI)-iodine complex containing 20% I over the corresponding native asphaltene is about 3.8 fold.

DISCUSSION

In all the samples studied, including both native asphaltenes and their iodine adducts, a negative temperature coefficient of resistivity was obtained. The linearity of $\log \rho$ vs. reciprocal T is substantiated by the plots shown in Fig. 2. The resistivity is inversely related to the concentration of the charge carriers (holes and electrons), but the fact that the number of charge-carriers increases exponentially with temperature does not enable a choice to be made between electronic or ionic conduction

mechanisms. However, the voltage dependence for the current at a relatively low electric field is linear, indicating that Ohm's law is valid (Fig. 3). This adherence to Ohm's law supports the belief that the conduction is electronic (19).

The fact that the asphaltene-iodine sample exhibits (Fig. 6) strong enhancement of absorption near 1080 cm^{-1} suggests that an iodine molecule forms a donor-acceptor complex with the aromatic portion of the asphaltenes. It is known that the iodine molecule forms such a charge-transfer complex with benzene and other alkylated benzenes, and that these complexes, in general, exhibit bands from 992 cm^{-1} to 1200 cm^{-1} (24,25). Arguing from analogy, it is plausible that the complex assumes the axial model (model A of Mulliken) while the acceptor molecule is sitting perpendicular to the plane of the aromatics (26). Further, our failure to locate any C-I stretching frequencies in the $400\text{-}600\text{ cm}^{-1}$ region supports the view that iodination of the asphaltene samples did not occur.

Most charge-transfer complexes of iodine with aromatics are crystalline. An exception to this is the violanthrene-iodine system, which x-ray diffraction indicates to be amorphous (2). X-ray results also indicate a low degree of order for the asphaltene-iodine complexes. If the acceptors (I_2) are homogeneously distributed in the host matrix (asphaltene), these systems may be considered analogous to the impurity or valence-controlled semiconductor systems. Disappearance of the 3.5\AA spacing of the (002) band means that the layered structure of asphaltene must have been altered (Fig. 7). The 4.6\AA γ -band, due to the saturated carbon in the structure, did not change in the complexing process.

The new band at 8.7\AA then may be due to the expansion of the aromatic interplanar distance to allow for complexing by the iodine molecule. In the case of the perylene-iodine systems, the spacing found at 10.7\AA was interpreted (5) as the distance between perylene molecules when iodine molecules were sandwiched between the aromatic layers. The present observed value of 8.7\AA can be viewed as the sum of the interplanar distance (5.5\AA) and the iodine length ($4 \times 1.53\text{\AA}$). The picture of these interlinked layers resembles that of an intercalation compound of graphite (Fig. 6).

Referring again to Fig. 4, the room temperature resistivities for the two native asphaltenes are seen to be in the insulator range ($>10^{14}$ Ohm). Upon addition of the iodine, the resistivity decreases about six decades or a million fold. This is essentially the same behavior as that observed for polymeric charge-transfer complexes such as poly(vinylpyridium TCNQ) and its derivatives. These polymeric salts are dependent upon the TCNQ concentration which at best increases the conductivity six decades. Here we have to point out that it is not easy to prepare a polymeric charge-transfer complex with good semiconduction. Slough (5) made a number of polymeric complexes from aromatic-containing polymers, with acceptors such as tetracyanoethylene, chloranil, etc., and found the conductivities of these complexes were not measurably higher than those of the original polymeric donors. These mesomorphic materials may lack the order of the π -systems needed to open a path for charge carriers. More likely, the aromatic systems are too small to form stable charge-transfer complexes.

For pure polynuclear aromatic hydrocarbons, donor-acceptor complexes, especially the iodine complexes (2,3), exhibit increases in conductivity of 12 to 16 decades when compared to the parent hydrocarbon.

The enhancement in conduction by the addition of iodine can be illustrated by comparison of the complexes with a valence controlled semiconductor, a typical example being nickel (II) oxide doped with lithium oxide (22). In Fig. 9 a comparison is made between this system and the aromatic-iodine complexes. The trends in resistivity with the concentration of impurity are quite similar.

Asphaltenes contain fused ring aromatics, the peripheral hydrogens of which are substituted heavily by short chain alkyl groups (23). Owing to the relatively large porportion of methyl groups (20%) and the large average layer diameters ($L_a \sim 15\text{\AA}$), the asphaltic molecule can be viewed as a typical aromatic donor (D); halogens such as iodine can behave as an acceptor (A). Through charge-transfer by overlapping of the molecular orbitals of the two moieties, the dative structure (D^+A^-) should result in which asphaltene is the positive ion.

Fig. 4 clearly indicates that the increase of conductivity follows two different paths, the first a to b, is the path followed for small increments of iodine, terminating at b with fixed composition (VY, 15.5%; GS, 10.0%); the other, c to d, is for higher percentages of iodine. Line bc represents the transition state. The curve cd may be extrapolated to a resistivity value of 5.8×10^6 ohm-cm, corresponding to that for pure I_2 (27). The same results were found (23) for violanthrene-iodine system with a minimum corresponding to a 2:1 iodine-violanthrene molar ratio for the complex. Apparently b in Fig. 4 corresponds to a stoichiometric ratio of

a stable complex where conductivity is at a maximum. It is assumed that for iodine contents less than that corresponding to the minimum the amount is insufficient to form the complex. At bc the resistivity is highly sensitive to the number of iodine molecules. When c is passed, excess iodine acts as an impurity in the stoichiometric complex. The transition at b is also reflected by the energy gap plot in Fig. 5. The same fixed composition (VY, 15.5%; GS, 10.0%) is obtained in either plot. At these minima, the energy gap value is ca. 0.5eV suggesting favorable conditions for conduction.

A number of aromatic-iodine complexes have been reported (2,3) and from their phase diagrams (either temperature or density vs. mole per cent of iodine) the complexes are found to be stoichiometric (29). For example perylene-iodine can have 2:3, or 1:3; pyranthrene-iodine is 1:2; violanthrene-iodine is 1:2; pyrene-iodine is 1:2. In all cases for peri-type aromatics the ratio of I_2 to aromatic is higher than unity. Since the diameter of the aromatic system in asphaltics falls in the range 8-15Å (12), the system would be comparable in size to violanthrene or perylene.

Assuming the composition at the transition (VY, 15.5%; GS, 10.0%) is stoichiometric, then for any given ratio of aromatic and iodine, the molecular weight of the asphaltene can be calculated. We have taken the liberty of calculating this weight for VY and GS asphaltenes based on sample ratios of I_2 :asphaltene of 2:1, 3:2 and 1:1. Since all layers contain the aromatic moieties and the sample is free of wax contamination, the molecular weight obtained is that of the unit sheet weight (weight of an average sheet containing both aromatic and saturated carbon atoms). These

values are listed in Table II. Next, provided aromaticity is also known (f_a for VY, 0.35; for GS, 0.51), the disk weight (weight of aromatic carbon atoms in a single sheet) and the layer diameter also can be approximated. These values are also listed in Table II. Experimental values for the VY and GS asphaltenes from a previous paper (15) are included. It is of interest that the unit weight values obtained from GPC, mass spectrometry, x-ray diffraction and the electron microscopic measurements agree in general magnitude with the weights obtained by the present method. Deviations of the disk weight of GS calculated from resistivity from that obtained by mass spectrometry may be due to the polydispersity of the GS asphaltene (e.g., M_w/M_n for VY is 1.27; for GS, 1.74 (15)).

From Table II, the asphaltene-iodine complexes formed appear to correspond to an I_2 :asphaltene ratio of about 1.5:1. This composition is shown in model A of Fig. 8. Actually aromatic disks of the size present in asphaltenes should be able to accommodate more than one molecule of iodine.

Finally the increase in the free spins, as demonstrated by the EPR spectra, may be indicative of an increase in carrier concentration (2). The nature of these charge carriers will have a strong bearing on the conduction mechanism and will be the subject of a separate investigation.

ACKNOWLEDGMENT

The authors thank Mr. Timothy R. Drury, Mellon Institute, Research Services, for his technical assistance; and Mrs. Marianne P. Hoy and Dr. Sidney S. Pollack, Mellon Institute, Research Services for the x-ray diffraction work.

This work was sponsored by Gulf Research & Development Company as part of the research program of the Multiple Fellowship on Petroleum.

REFERENCES

- (1) Inokuchi, H., and Akamatu, H., *Solid State Physics*, 12, 03 (1961).
- (2) Uchida, T., and Akamatu, H., *Bull. Chem. Soc. (Japan)*, 35, 981 (1962).
- (3) Uchida, T., and Akamatu, H., *Bull. Chem. Soc. (Japan)*, 34, 1015 (1961).
- (4) Labes, M. M., Sehr, R. A., and Bose, M., "Proceedings of the Princeton University Conference on Semiconductors in Molecular Solids," Princeton, N. J., 1960.
- (5) Slough, W., *Trans. Faraday Soc.*, 58, 2360 (1962).
- (6) Bakh, N. A., Vannikov, A. V., Grishina, A. D., and Nizhnil, S. V., *Russian Chemical Rev.*, 34, 736 (1965).
- (7) Vannikov, A. V., and Bakh, N. A., *Doklady Akad. Nauk., S. S. S. R.*, 159, 230 (1963).
- (8) McNeill, R., Suidak, R., Wardlaw, J. H., and Weiss, D. E., *Aust. J. Chem.*, 16, 1056 (1963).
- (9) The asphaltene fraction of a crude oil or refinery residue is a brown-to-black, amorphous, powdery, solid material, insoluble in n-pentane but soluble in benzene; see Ref. 11 for sample preparation.
- (10) Yen, T. F., and Erdman, J. G., *A. C. S., Div. Petroleum Chem., Preprints*, 7, No. 1, 5 (1962).
- (11) Yen, T. F., Erdman, J. G., and Pollack, S. S., *Anal. Chem.*, 33, 1587 (1961).
- (12) Yen, T. F., and Erdman, J. G., in "Encyclopedia of X-rays and Gamma-rays" (G. L. Clark, Ed.), Reinhold Publishing Co., New York, N. Y., 1963, p. 65.
- (13) Yen, T. F., Erdman, J. G., and Saraceno, A. J., *Anal. Chem.*, 34, 694 (1962).
- (14) The word "multipolymer" refers to a polymer with a very large number of different building blocks, say ca. 100. Simpler structures can be referred to by more specific terms, as for example, "copolymer" (2 blocks) or "terpolymer" (3 blocks).

- (15) Dickie, J. P., and Yen, T. F., to be presented at A. C. S., Div. Petroleum Chemistry, Symposium on "Modern Instrumental Methods for the Analysis of Petroleum Fractions," Miami Beach, 1967.
- (16) LeBlanc, Jr., O. H., J. Chem. Phys., 37, 916 (1962).
- (17) Yen, T. F., Erdman, J. G., and Hanson, W. E., J. Chem. Eng. Data, 6, 443 (1961).
- (18) Yen, T. F., and Dickie, J. P., A. C. S., Div. Petroleum Chem., Preprints, 11, No. 3, 49 (1966).
- (19) Seamon, D. A., Adv. Polymer Sci., 4, 317 (1965).
- (20) Yen, T. F., and Erdman, J. G., A. C. S., Div. Ana. Chem., Abstracts, Detroit, Michigan, 1965, p. 29B.
- (21) This is essentially a method using voltage drop across a standard resistor (potential drop method); see Ref. 26 for example.
- (22) Morin, F. J., in "Semiconductors" (N. B. Hannay, Ed.), Reinhold Publishing Co., New York, N. Y., 1959, p. 600.
- (23) Yen, T. F., and Erdman, J. G., A. C. S., Div. Petroleum Chem., 7, No. 3, 99 (1962).
- (24) Haller, W., Jura, G., and Pimentel, G. C., J. Chem. Phys., 22, 720 (1954).
- (25) Ferguson, E. E., Spectrochim. Acta, 10, 123 (1957).
- (26) Ferguson, E. E., J. Chem. Phys., 25, 577 (1956).
- (27) Rabinowitsch, M., Z. Physik. Chem., 119, 82 (1926).
- (28) Akamatu, H., Inokuchi, H., and Matsunaga, Y., Bull. Chem. Soc. (Japan) 29, 213 (1956).
- (29) Kommandeur, J., and Singer, L. S., in "Symposium on Electrical Conductivity in Organic Solids," (H. Kallmann and M. Silver, Ed.) Interscience, New York, N. Y., 1961, p. 325.
- (30) Hatano, M., Nomori, H., and Kambara, S., A. C. S., Div. Polymer Chem., Preprints, 2, No. 2, 848 (1964).

TABLE I

Resistivity and Gap Energy Measurements
 from Asphaltene (VI)-Iodine Complexes

Sample No. ^a	Iodine	A. (cm)	L. (cm)	$\rho_{25^\circ\text{C}} \times 10^{-12}$ (ohm-cm)	ϵ (eV)
23	17.1	1.262 ₈	0.099 ₄	1.75 ₆	1.74 ₂
25	16.8	1.266 ₄	0.103 ₃	1.61 ₄	1.82 ₅
27	17.2	1.259 ₂	0.119 ₂	1.77 ₆	2.00 ₇
24	15.8	1.267 ₅	0.102 ₇	2.15 ₅	1.95 ₀
28	15.7	1.276 ₆	0.051 ₉	2.06 ₃	1.75 ₃
29	15.8	1.147 ₉	0.048 ₀	2.25 ₄	1.81 ₄

(a) Same numbers used in curves of Fig. 4; Sample Nos. 23, 25, and 27 are from one preparation; Sample Nos. 24, 28, and 29 are from another preparation.

TABLE II

Determination of the Molecular Weight and Aromatic Sheet Size
of Native Asphaltenes by Various Physical Methods

Physical Methods	Unit Weight ^a		Disk Weight ^b		Layer Diameter (Å) ^c	
	VY	GS	VY	GS	VY	GS
<u>Resistivity Calculation</u>						
I ₂ :Asphaltene						
2:1	2770 ^d	4570	969 ^e	2330	14.6 ^f	22.6
3:2	2080	3430	727	1750	12.6	19.5
1:1	1380	2290	484	1170	10.3	16.0
GPC (M _n) ^{g,h}	3160	3780	-	-	-	-
<u>Mass Spectrometry^h</u>						
(Mean)	-	-	634	543	-	-
<u>X-ray Diffraction^h</u>						
(L _a)	-	-	-	-	11.9	17.0
<u>Electron Microscope^{h,i}</u>						
(Particle weight)	3440	4030	-	-	-	-

(a) Weight of a single sheet containing both aromatic and saturated carbon atoms (see J. P. Dickie and T. F. Yen, A. C. S., Div. Petroleum Chem., Preprints, Miami meeting, April, 1967).

(b) Weight of aromatic carbon atoms in a single sheet.

(c) Diameter of aromatic cluster; see T. F. Yen, J. G. Erdman, and S. S. Pollack, Anal. Chem., 33, 1587 (1961).

(d) Calculated based on $254t^{-1}R$ (100- t) where R is the ratio of I₂ to asphaltene and t is the %I corresponding to the transition in resistivity and gap energy.

(e) Calculated from $f_a \times$ (unit weight).

(f) $L_a = (2.62 C_A)^{1/2}$, C_A from disk weight without contribution of hydrogens.

(g) From gel permeation chromatography data on the native asphaltene, number average molecular weight.

(h) Experimental data from J. P. Dickie and T. F. Yen, A. C. S., Div. Petroleum Chem., Preprints, Miami meeting, April, 1967.

(i) J. P. Dickie and T. F. Yen, A. C. S., Div. Petroleum Chem., Preprints, 11, 39 (1966).

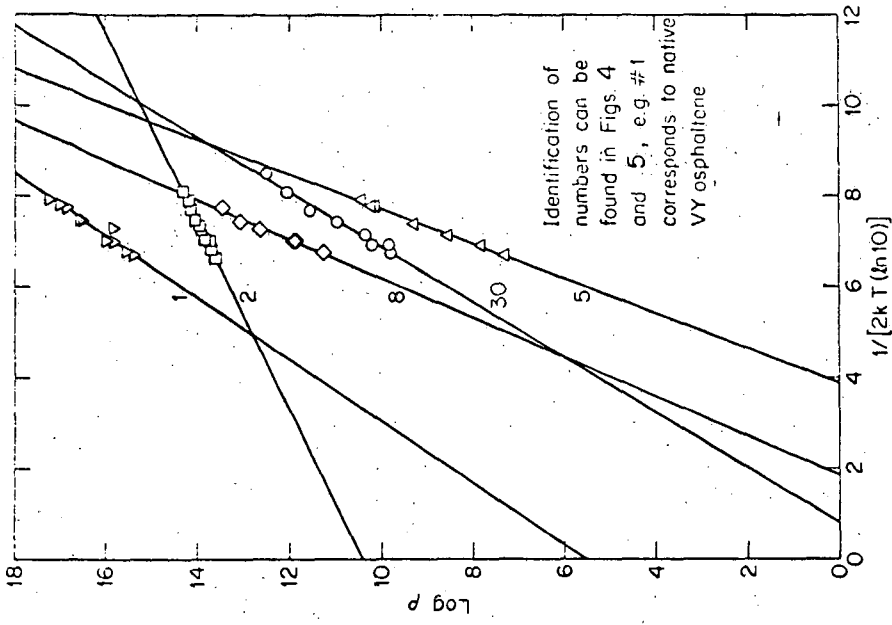


Fig. 2-Temperature Dependence of Resistivity for the Asphaltene-Iodine System.

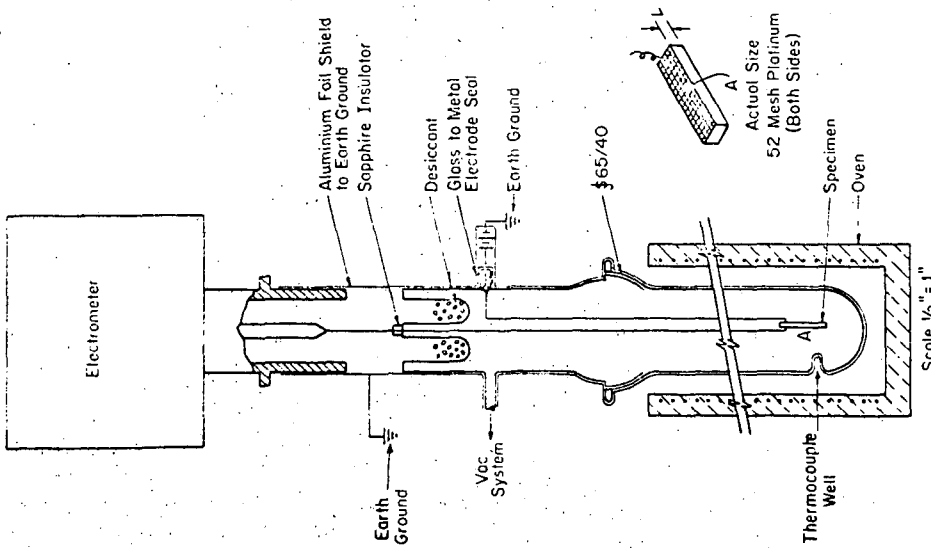


Fig. 1-Apparatus for Resistance Measurement

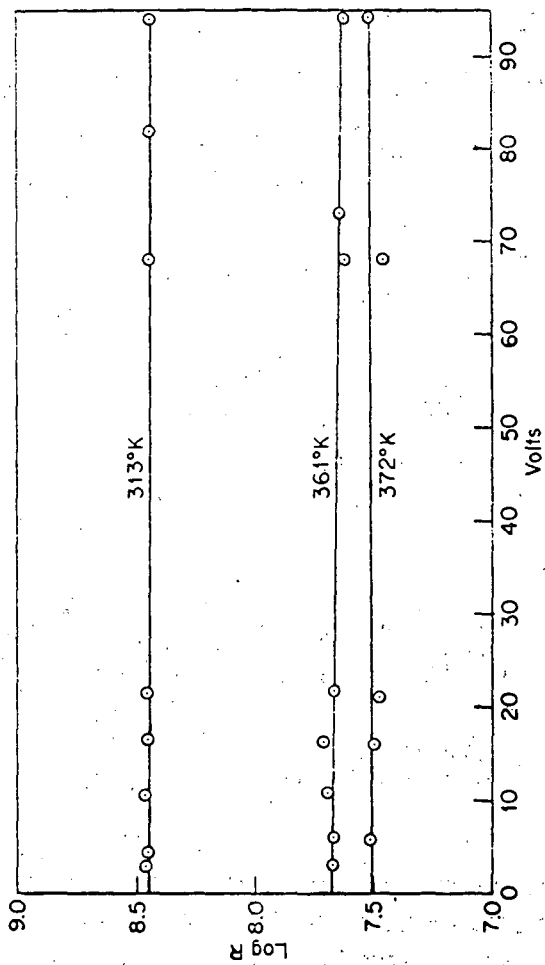


Fig. 3—Voltage Dependence of Resistance for an Asphaltene-Iodine Complex (1% = 11).

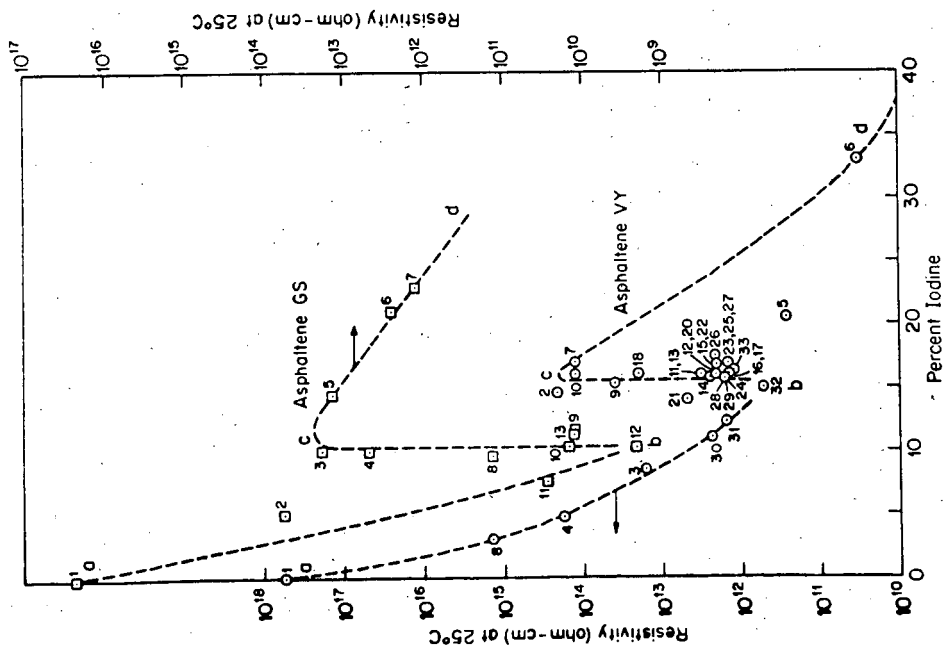


Fig. 4-Resistivity of the Asphaltene-Iodine Complex as a Function of Iodine Content.

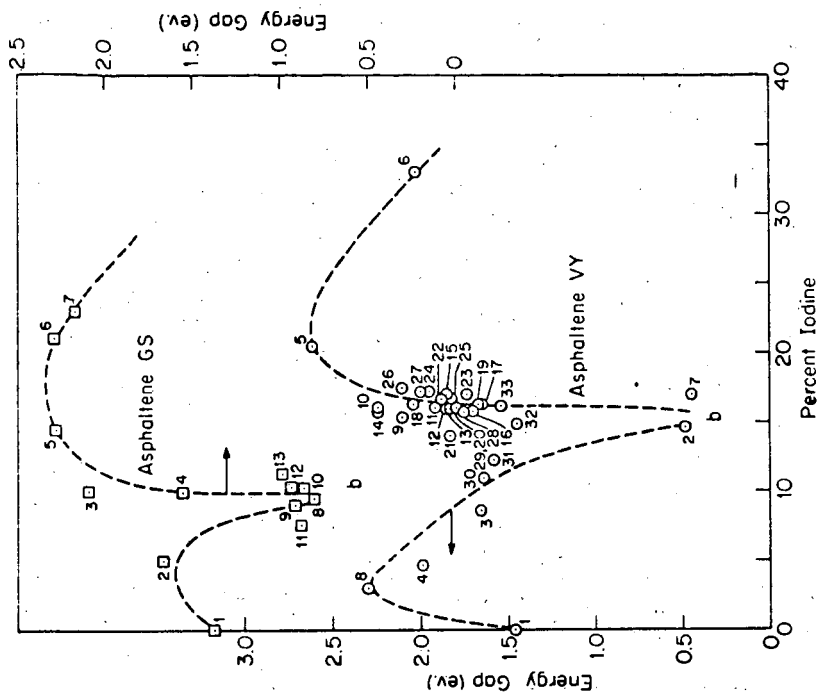


Fig. 5-Gap Energy of the Asphaltene-Iodine Complex as a Function of Iodine Content.

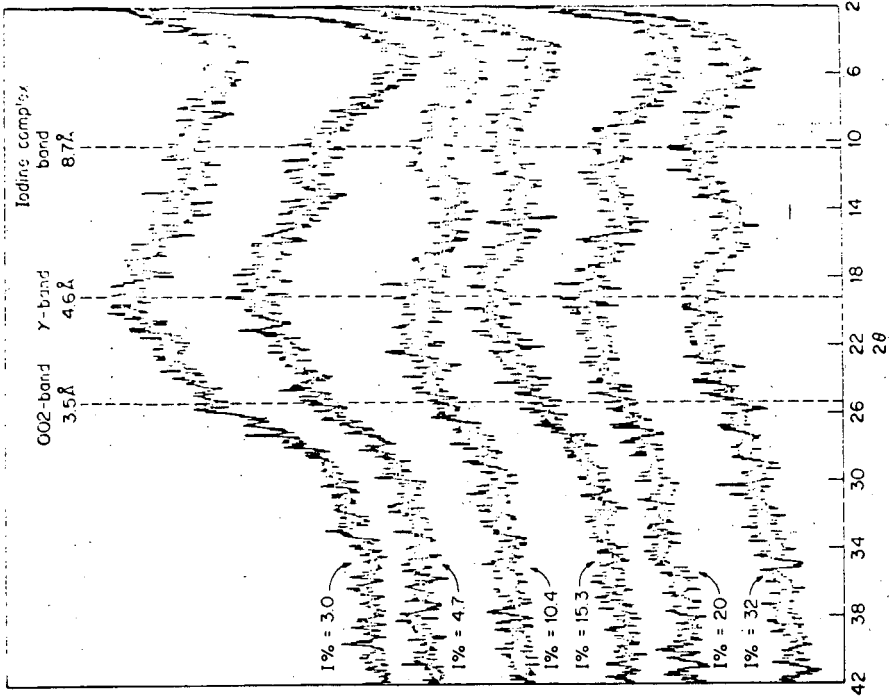


Fig. 7 - X-Ray Patterns of the Asphaltene (VY)-Iodine System

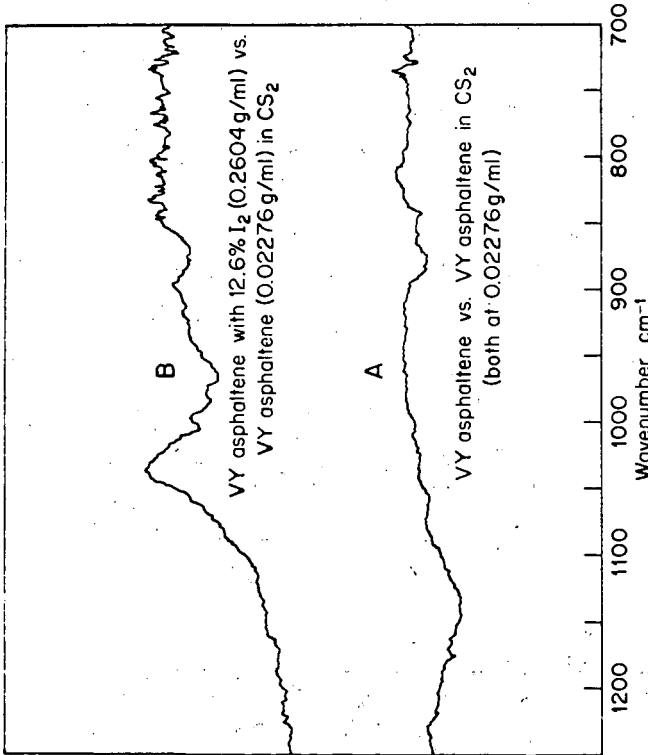


Fig. 6 - Differential Infrared Spectra of Asphaltene-Iodine Complex.

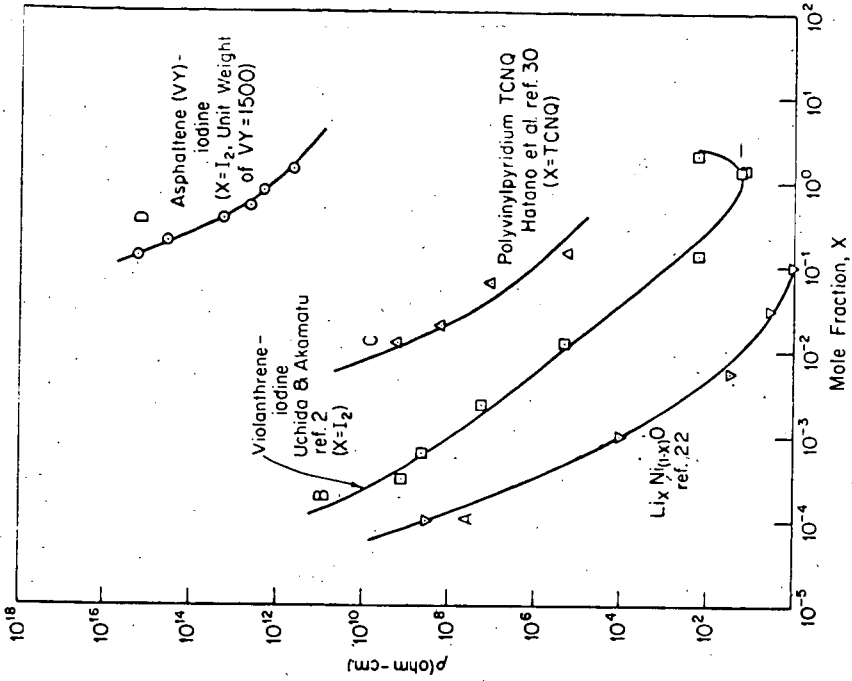


Fig. 9-Aromatic-Iodine Complexes Vs. a Valence Controlled Semiconductor with Resistivity as a Function of Impurity Content.

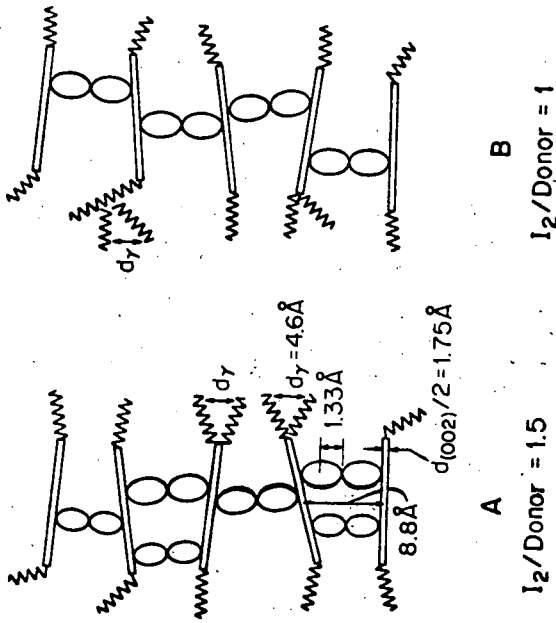


Fig. 8-Proposed Model of Asphaltene-Iodine Complexes
 A, 2 Asphaltene $\cdot 3 \text{I}_2$; B, Asphaltene $\cdot \text{I}_2$.

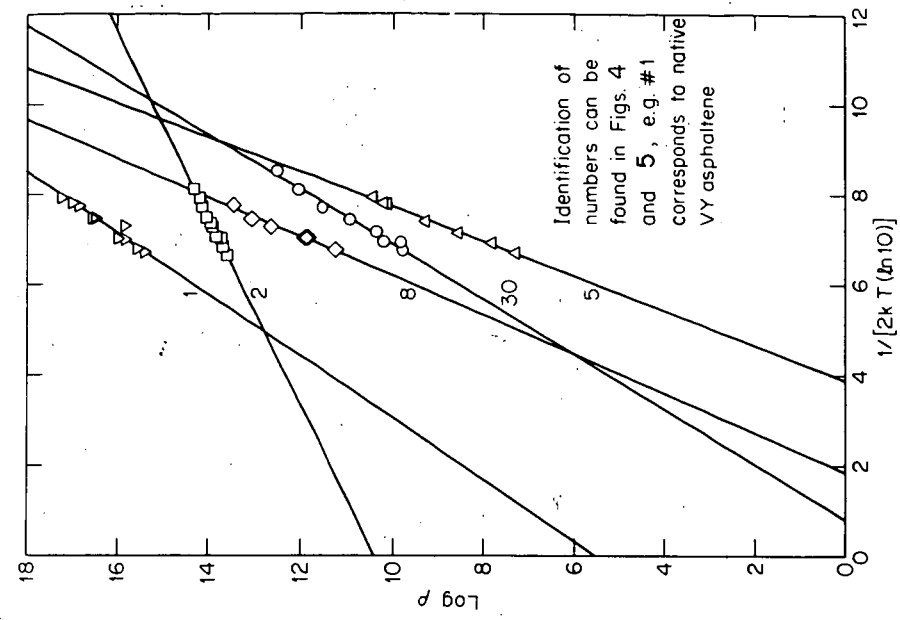


Fig. 2-Temperature Dependence of Resistivity for the Asphaltene-Iodine System.

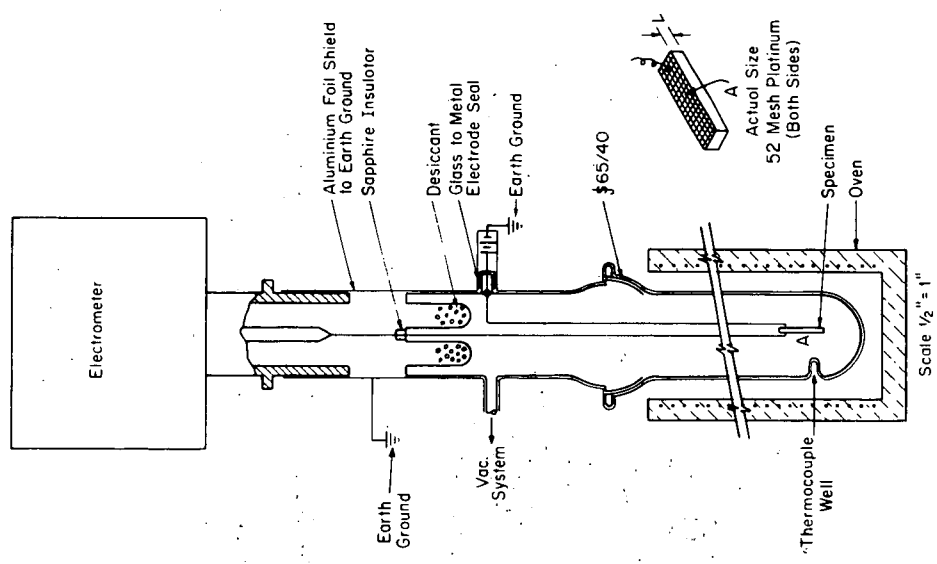


Fig. 1-Apparatus for Resistance Measurement

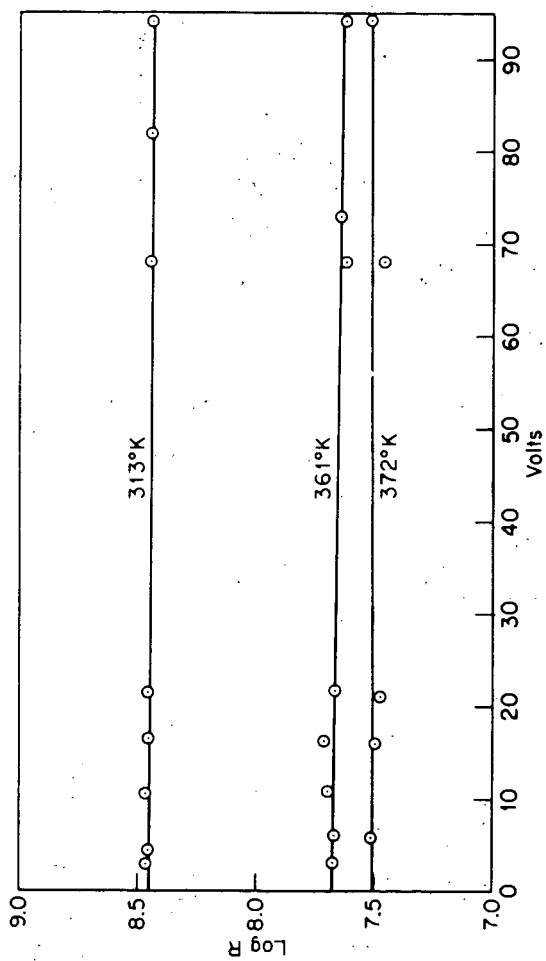


Fig. 3-Voltage Dependence of Resistance for an Asphaltene-Iodine Complex (1% = 11).

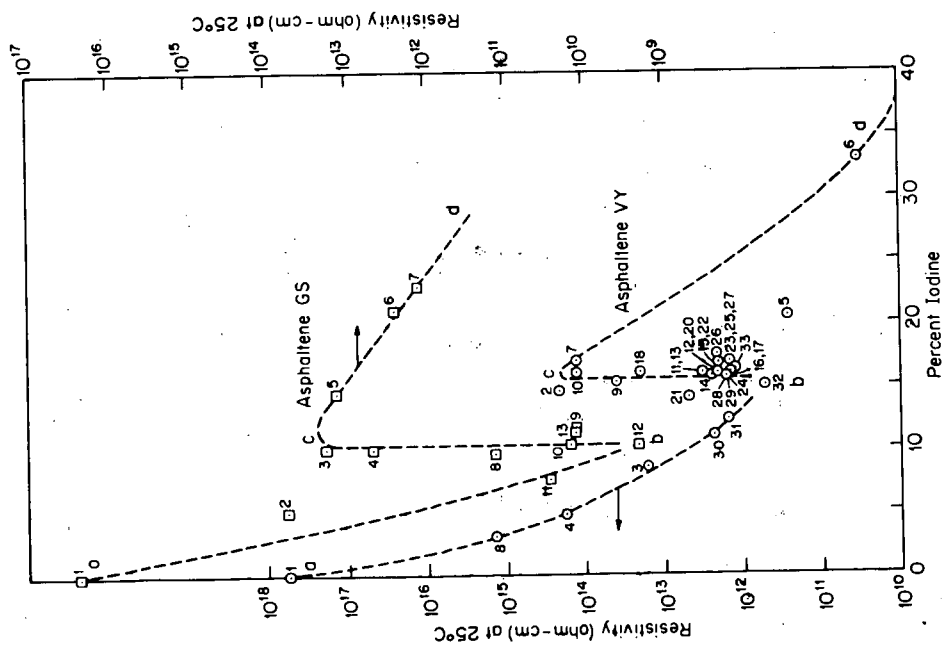


Fig. 4-Resistivity of the Asphaltene-Iodine Complex as a Function of Iodine Content.

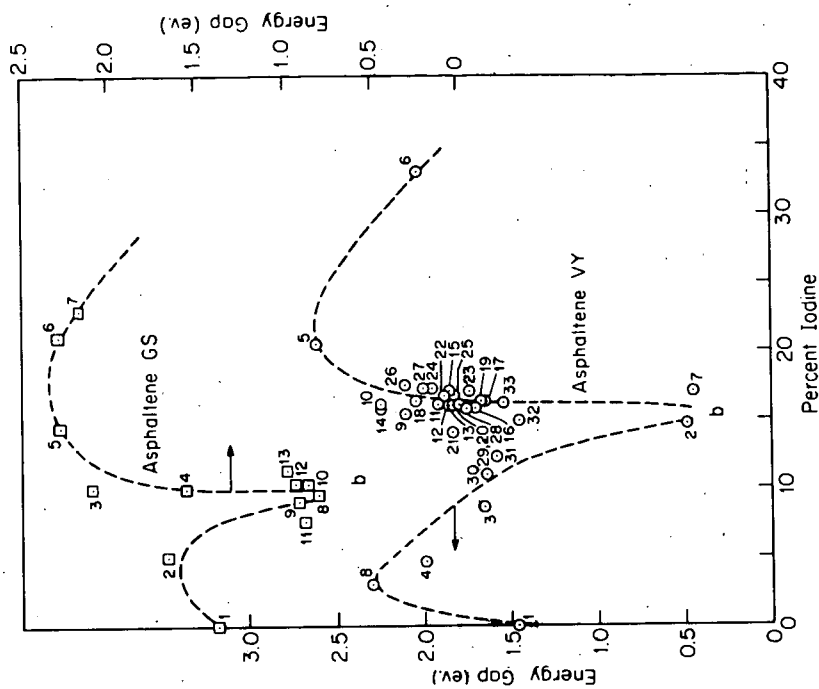


Fig. 5-Gap Energy of the Asphaltene-Iodine Complex as a Function of Iodine Content.

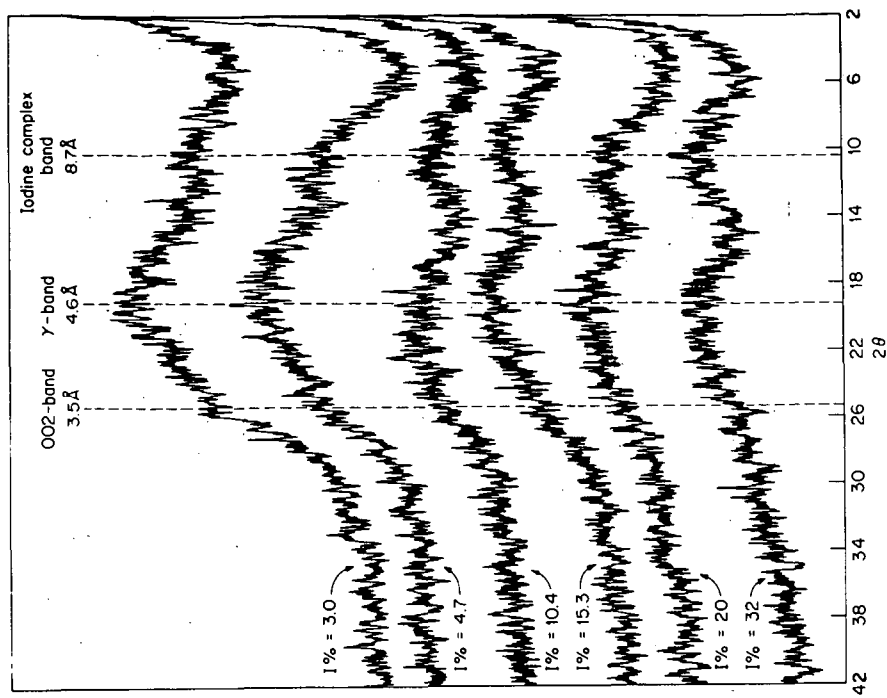


Fig. 7 - X-Ray Patterns of the Asphaltene (VY)-Iodine System

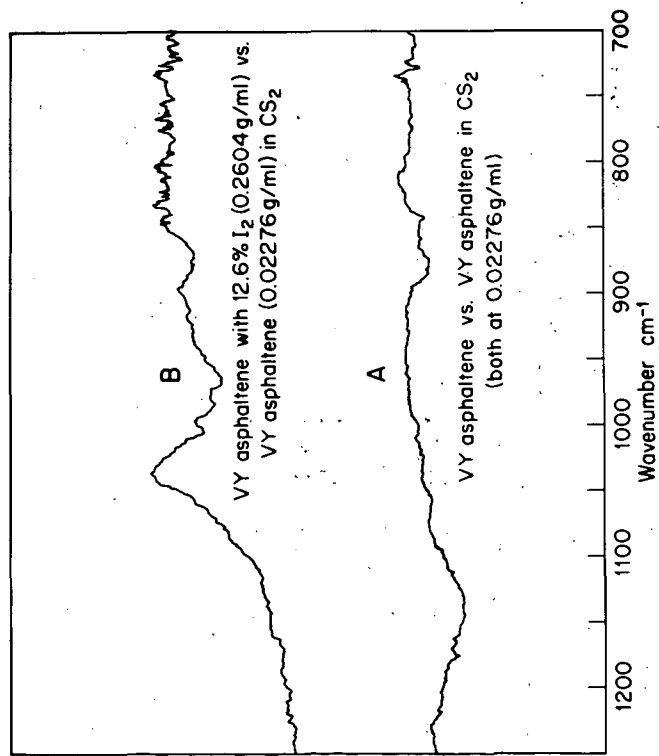


Fig. 6 - Differential Infrared Spectra of Asphaltene-Iodine Complex.

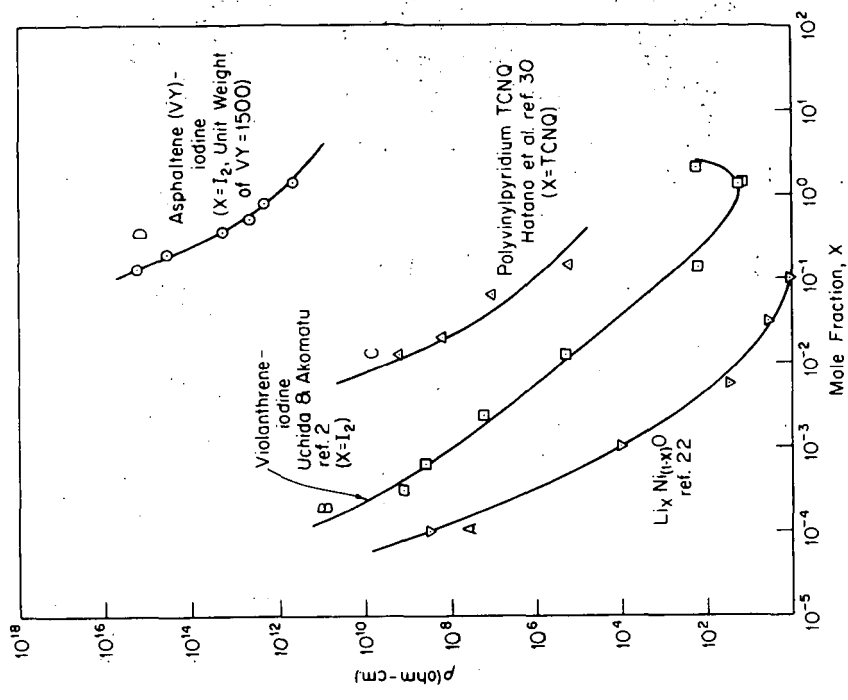


Fig. 9--Aromatic-Iodine Complexes Vs. a Valence Controlled Semi-conductor with Resistivity as a Function of Impurity Content.

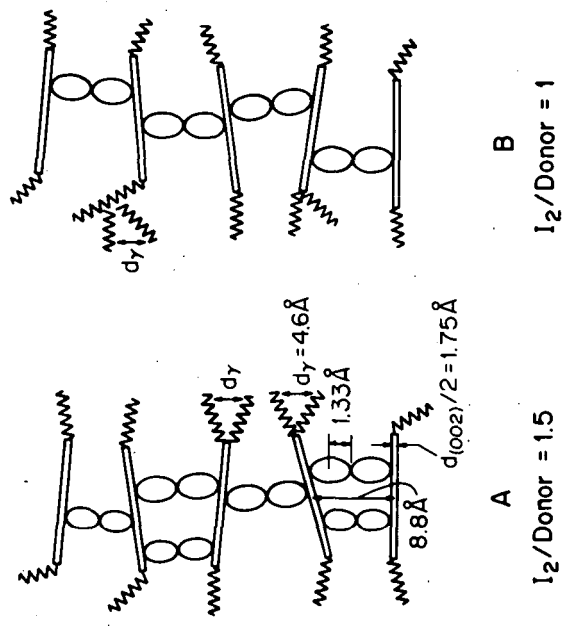


Fig. 8--Proposed Model of Asphaltene-Iodine Complexes
 A, 2 Asphaltene $\cdot 3 I_2$; B, Asphaltene $\cdot I_2$.

THE ELECTRON SPIN RESONANCE SPECTRA OF CELLULOSE CHARS TREATED WITH HALOGENS*

Evidence for Donor-Acceptor Complexes in Coals and Chars

R. M. Elofson and K. F. Schulz

Research Council of Alberta
Edmonton, Alberta

INTRODUCTION

Coals and low- and medium-temperature chars have been shown to be paramagnetic by bulk magnetic susceptibility measurements^{1,2,3} and by electron spin resonance studies^{4,5,6}. If due care is taken to eliminate errors, reasonable agreement in the estimate of the number of unpaired electrons present can be obtained⁷. While there is agreement on the existence of paramagnetic centres in these materials, the origin and nature of these free radicals is not understood^{8,9,10,11,12}. It is the purpose of this article to present new evidence to suggest that these unpaired electrons arise from donor-acceptor forces present in these materials.

One way of studying the nature of free radicals is by observing the behavior of the electron spin resonance signals when the substrate is treated with adsorbed gases and other reagents. Early workers in the field found that paramagnetic gases such as oxygen affected only the spin-lattice relaxation times of chars prepared at from 300° to 500°C. For chars prepared in the 550° to 800° temperature range, however, reversible line broadening occurred with an apparent decrease in free radical concentration at higher oxygen pressures. Removal of oxygen restored the original signal, which indicated that the phenomenon was due to physical and not chemical processes. Halogens were at first found to have no effect on coals and chars and the oxygen effect was attributed to spin broadening due to the paramagnetism of the oxygen molecules. Similar results to oxygen were obtained with nitric oxide.

In 1963 Wynne-Jones¹³ and co-workers found that e.s.r. signals in chars obtained by heating polyvinylidene chloride (saran) were affected by adsorption of halogens. These workers noted that IBr, ICl, I₂, Br₂, and Cl₂ caused partial or complete reduction in spin concentration at constant line width. The original signal was not restored by outgassing in vacuo at room temperature but could be partially restored by reheating the specimen at 100°C in vacuo. Since, as mentioned above, no halogen effect had been obtained on coals or more common chars, these authors attributed the susceptibility to halogens of these saran chars to a high degree of porosity. Reinvestigation of the interaction of a series of cellulose chars with iodine, bromine and hydrogen iodide in this laboratory has shown pronounced effects on the electron spin resonance of some of these materials.

EXPERIMENTAL

Cellulose chars were prepared by first charring cellulose powder (Whatman Cellulose Powder, Standard Grade) in an autoclave at 195°-200°C under nitrogen. Subsequently this char

* Contribution No. 360 from the Research Council of Alberta, Edmonton, Alberta.

was heated under nitrogen in a Vycor tube to the desired temperature and held at temperature for one hour. Aliquots of the chars were then treated with a large excess of 0.1 M solutions of iodine or bromine in carbon tetrachloride. After standing in the solutions for twenty-four hours, the samples were washed once with carbon tetrachloride and dried. Samples for e.s.r. measurements were placed in 3 mm. o.d. glass tubes and evacuated.

Samples to be treated with hydrogen iodide were placed in open 3 mm. o.d. tubes placed in the cavity of the spectrometer and purged with purified nitrogen. Gaseous hydrogen iodide (Matheson) was passed directly over the sample in the cavity. Excess hydrogen iodide was removed after treatment by subsequent purging with nitrogen.

Electron spin resonance measurements were performed with a Varian Model 4500 electron spin resonance spectrometer fitted with a TE102 cavity and a 100 Kc modulation attachment. Saturation phenomena were avoided by working at 10 db attenuation and checks for saturation were made. Line widths and spin concentrations were measured from first derivative curves, generally by direct inspection but in the case of very wide and very narrow signals resort was made to graphical integration. A standard 500° cellulose char, used for calibration, was standardized against DPPH, CuSO_4 and a Varian Standard char. The amount of sample was always less than 10 mg. and asymmetric line shapes were not observed, indicating the absence of serious skin effects.

RESULTS

In Figures 1 and 2 are summarized the results of iodine and bromine treatment on line width and spin concentration as measured at room temperature. The untreated chars prepared at 625° and 650° show a marked decrease in line width as compared with those prepared at higher or lower temperature — an effect attributed to exchange⁴. It is seen that both iodine and bromine remove this intense narrowing in the 625° and 650° chars. Neither has a significant effect on the 300° to 500° chars but both broaden further the signal from the 700° char. The broadening due to bromine is not as great as that due to iodine and for the 600° char, in particular, the broadening effect of the bromine is minimal. The effect on spin concentration shows that line broadening is accompanied by a considerable drop in concentration in both the bromine and iodine treated chars.

Measurements made at 78°K showed that whereas the signals for the 300° to 500° chars were broadened somewhat, those from the iodine- and bromine-treated chars in the 600° to 700° range were narrowed. Washing the iodine-treated chars with cold 0.1 M sodium thiosulfate solution restored the original narrow signals. This showed that no chemical reaction had occurred to alter the signals.

Treatment of a series of chars with hydrogen iodide gas for sixty hours resulted in reduction of the signal strength and broadening of the signals as shown in Table I. The broadening for the 300°, 400° and 500° chars was moderate but that of the exchange narrowed chars (600° to 700°) was extensive. Cold 0.1 M sodium thiosulfate produced no further change in the signals but refluxing for twenty-four hours with thiosulfate restored the original signals^{1,4}. The restored signals of the 600°, 625°, 650° and 700° chars were sensitive to air whereas the restored signals of the 300°, 400° and 500° chars were not. The e.s.r. signals of the untreated chars refluxed with 0.1 N $\text{Na}_2\text{S}_2\text{O}_3$ were unchanged.

TABLE I

Effect of Hydrogen Iodide on Free Radical Content of Chars

Electron Spin Resonance Signals

spins/g in vacuo and width in gauss*

Char Temperature	Untreated	HI Treatment 60 hours	Na ₂ S ₂ O ₃ 0.1 M Refluxed 24 hours
300	2.1 × 10 ¹⁸ 4.9	2.0 × 10 ¹⁷ 7.9	8.3 × 10 ¹⁷ 5.76
400	2.3 × 10 ¹⁹ 6.1	5.3 × 10 ¹⁸ 8.3	2.6 × 10 ¹⁹ 6.3
500	5.1 × 10 ¹⁹ 4.8	3.3 × 10 ¹⁹ 5.9	5.4 × 10 ¹⁹ 4.1
600	1.4 × 10 ²⁰ 0.45	1.3 × 10 ¹⁹ 19.1	1.4 × 10 ²⁰ 0.49
625	1.3 × 10 ²⁰ 0.40	1.7 × 10 ¹⁹ 22.4	9.8 × 10 ¹⁹ 0.49
650	1.0 × 10 ²⁰ 1.4	4.8 × 10 ¹⁹ 41.0	1.0 × 10 ²⁰ 1.2
700	7.4 × 10 ¹⁹ 1.4	1.2 × 10 ¹⁹ 43	7.2 × 10 ¹⁹ 2.0

* Width measured between points of maximum slope.

DISCUSSION

Two aspects of these results must be considered – the interaction with the halogens which are typical electron acceptors and the interactions with hydrogen iodide. In agreement with Wynne -Jones and co-workers, we are of the opinion that iodine, and to a lesser extent bromine, can form donor-acceptor complexes with the chars and in so doing affect the e.s.r. signals. Presumably the iodine and bromine act as acceptors and aromatic ring systems of the char act as donors in these complexes. The low-temperature chars, 300° to 500°, having few aromatic ring systems as large or larger than four or five rings¹⁵, are not affected by iodine or bromine. The 600° char apparently has a high enough donor ability – low enough ionization potential – to interact with iodine but not sufficient to react definitely with bromine, which is a much weaker acceptor. Both bromine and iodine readily form complexes with the 625°, 650° and 700° chars. The fact that the signals of the halogen affected chars are narrowed on cooling to 79°K is also indicative of donor-acceptor interaction between halogens and aromatic moieties¹⁶. It is possible that lack of porosity is sufficient explanation of the failure of the 300° to 500° chars to be affected by iodine¹³. However, the difference between iodine and bromine on the 600° char suggests that the electrophilicity and not the size of the adsorbed molecule is important.

The line broadening at 79°K of the 300°, 400° and 500° chars treated with halogens is not only indicative of no complex formation between halogen and the aromatic system but also suggests that the initial signals of these chars are due to complexes between quinonoid acceptors and carbocyclic donors¹⁶. This is further borne out by the effects of hydrogen iodide on these chars. Treatment of all the chars with hydrogen iodide causes a reversible reduction in the number of spins/g. Aromatic hydrocarbons would not be expected to show such reversible behavior^{17,18}, but electron acceptors such as quinones, which have been shown by Given and Peover¹⁹ to be present in coals and related materials, would interact with hydrogen iodide. A reasonable explanation is that the e.s.r. signals of these chars are associated with acceptor moieties. These acceptor or quinonoid moieties apparently exist in the 300° to 500° chars as well as the 600° to 700° chars, since the signals are all reduced reversibly by hydrogen iodide. Since the halogen treatments suggest that the free radicals of the 600° to 700° chars, and probably of the 300° to 500° chars as well, are associated with aromatic centres, the presence of both donor and acceptor moieties associated with free radicals in the untreated chars is indicated. Hence, we suggest that the free radicals in the 600° to 700° chars are due to donor-acceptor complexes between aromatic donors and quinonoid acceptors. It is likely that the signals in the 300° to 500° chars are similar in nature but the aromatic centres are too small to form complexes with iodine or bromine.

Russian workers²¹ reached similar conclusions, but only by a process of elimination, in order to account for the free radicals in a series of polyarylene polyacetylenes that had been heated to various temperatures. They concluded that complexes with charge-transfer were the only possible explanation after eliminating in turn the presence of paramagnetic ion impurities, radicals arising in the process of polymerization, and the existence of a triplet ground state. The first reference to charge-transfer complexes in coals or chars was made by Schuyer²² to explain why the molar increment of refractive index per gram of aromatic carbon (I_M/C_{ar}) decreases in the range between ninety per cent carbon and graphite. Some of the semiconductor properties of anthracites and chars were also explained on the basis of such a model.

In order to illustrate the relative importance of charge-transfer complexes in these chars a plot has been made in Figure 3 of the number of free radicals vs. carbon content. There has also been plotted the reciprocal of crystallite size in no./g. vs. carbon content calculated from the work of Hirsch¹⁵ and van Krevelen²³ assuming that there is an average crystallite height of three graphitic layers and that there is no unordered material. It should be noted that the average height of the crystallites would be somewhat less than three in the low temperature chars and possibly somewhat greater than three in the higher temperature chars. In any event, it is seen that in the 600° to 650° range the number of crystallites closely approximates the number of free radicals, accounting for the results of Schuyer²². In fact these latter chars are apparently composed of little but charge transfer complexes in close proximity to one another which explains the intensive exchange narrowing of the e.s.r. signals of these materials. The decrease in free radicals at higher temperatures is at least in part due to the decrease in number of crystallites at higher charring temperatures.

Extending the conclusions on cellulose chars to coal and related materials, suggests that e.s.r. signals in all these materials result from donor-acceptor complexes which, while reaching a maximum of importance in anthracites and 600° to 700° chars, may still be of significance in lower rank coals and humic acids. Such a conclusion finds support from a number of other aspects of the behavior of coal and humic acids. Charge-transfer forces between coal and solvent can be used to explain the order of effectiveness of coal solvents. Thus catechol and anthracene oils, which are donor molecules, are very effective in extracting or dispersing coal or humic materials. Charge-transfer equilibria can also rationalize the failure of coal extracts once dried to redissolve completely in the original solvent used for extraction. Free

radicals in coals and chars are physically affected by oxygen, as indicated by line broadening of the e.s.r. signal, but are stable to chemical attack. Such behavior could be explained as due either to spin-spin coupling of the oxygen molecule with the free electron of the charge-transfer complex or to formation of new donor-acceptor complexes between aromatic centres and oxygen²⁴.

The so-called molecular weight of humic acids and coal extracts should be re-examined in the light of the concept of donor-acceptor complexes. Thus molecular weight determinations of humic acids in catechol²⁵, a substance conceivably capable of breaking up donor-acceptor complexes of humic acids, resulted in a low molecular weight estimate. Determinations on apparently similar material in sulfolane, a poor complexing agent, produced very much higher estimates of molecular weight²⁶.

Finally, coals and related materials have a well-known broad absorption band at 1600 cm^{-1} in the infrared region which has defied interpretation. Donor-acceptor phenomena have been shown to produce strong and broad absorption in this region^{27,28} in aromatic systems, as shown in Figure 4, and hence may be the cause of this band in coal and chars.

REFERENCES

1. Honda, H., and Ouchi, K., Rep. Resources Inst. Japan No. 1, 1952.
2. Adamson, A.F., and Blayden, H.E., Proc. of the 3rd Conference on Carbon (1957), Pergamon Press, London, 1959, p. 147.
3. Berkowitz, N., Cavell, P.A., and Eloffson, R.M., Fuel 40, 279 (1961).
4. Ingram, D.J.E., and Bennett, J.E.P., Oil Mez. 45, 545 (1954).
5. Uebersfeld, J., Etienne, A., and Combrisson, J., Nature 174, 614 (1954).
6. Winslow, F.H., Baker, W.O., and Yager, W.A., J. Am. Chem. Soc. 77, 4751 (1955).
7. Akamatu, H., Mrozowski, S., and Wobschall, D., Proc. of the 3rd Conference on Carbon (1957), Pergamon Press, London, 1959, p. 135.
8. Singer, L.S., Spry, W.J., and Smith, W.H., Proc. of the 3rd Conference on Carbon (1957), Pergamon Press, London, 1959, p. 121.
9. Ingram, D.J.E., Free Radicals as Studied by Electron Spin Resonance, Butterworths, London, 1958, p. 213.
10. Uebersfeld, J. and Erb, E., Proc. of the 3rd Conference on Carbon (1957), Pergamon Press, London, 1959, p. 103.
11. Antonowicz, K., Proc. of the 5th Conference on Carbon (1961), Pergamon Press, London, 1963, p. 61.
12. Mrozowski, S., Proc. of the 4th Conference on Carbon (1959), Pergamon Press, London, 1960, p. 271.

13. Campbell, D., Jackson, C., and Wynne-Jones, W.F.K., *Nature* 199, 1090 (1963).
14. Toland, W.G., U.S. Patent 2,856,424 (1958).
15. Hirsch, P.B., *Proc. Roy. Soc. (London)*, A226, 143 (1954).
16. Bose, M., and Labes, M.M., *J. Am. Chem. Soc.* 83, 4505 (1961).
17. Mitchell, H.K. and William, R.J., *J. Am. Chem. Soc.* 60, 2723 (1938).
18. Deno, N.C., Freedman, N., Hodge, J.D., MacKay, F.P. and Saines, G., *J. Am. Chem. Soc.* 84, 4713 (1962).
19. Given, P.H., and Peover, M.E., *J. Chem. Soc.* 394 (1960).
20. Voet, A.C. and Teter, A.C., *Amer. Ink Maker* 38, No. 9, 94 (1960).
21. Dulov, A.A., Slinkin, A.A., Rubinshtein, A.M., and Kotlyarevski, I.L., *Izvestia Akad. Nauk S.S.S.R. Seriya Khim.* No. 11, p. 1910 (1963).
22. Schuyer, J., *Brenn. Chemie.* 37, 74 (1956).
23. van Krevelen, D.W. and Schuyer, J., *Coal Science*, Elsevier Publishing Co., London (1957), p. 176.
24. Tsubomura, H., and Mulliken, R.S., *J. Am. Chem. Soc.* 82, 5966 (1960).
25. Polansky, T.S., and Kinney, C.R., *Fuel* 31, 409 (1952).
26. Wood, J.C., Moschopedis, S.E., and Elofson, R.M., *Fuel* 40, 193 (1961).
27. Elofson, R.M., Anderson, D.H., Gutowsky, H.S., Sandin, R.B., and Schulz, K.F., *J. Am. Chem. Soc.* 85, 2622 (1963).
28. Sandin, R.B., Elofson, R.M., and Schulz, K.F., *J. Org. Chem.* 30, 1819 (1965).

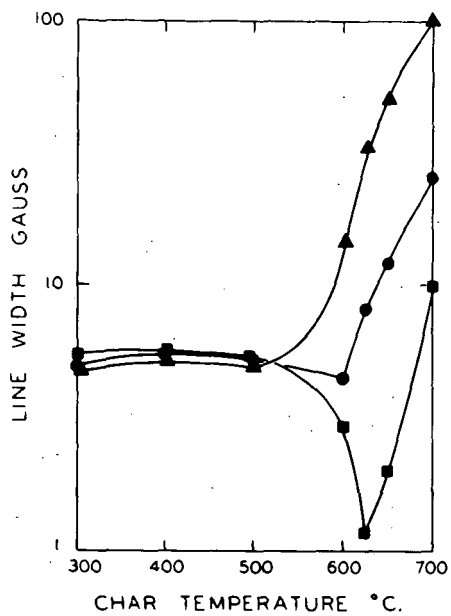


Figure 1.

Effect of I₂ and Br₂ on line widths of cellulose chars measured in vacuo at room temperature.

- no treatment
- ▲ treated with 0.1 M I₂ in CCl₄
- treated with 0.1 M Br₂ in CCl₄

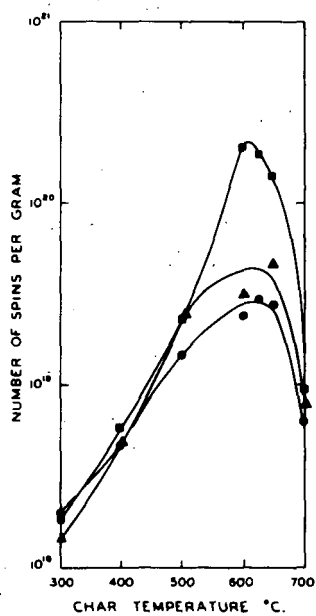


Figure 2.

Effect of I₂ and Br₂ on spin concentrations in cellulose chars measured in vacuo at room temperature

- no treatment
- ▲ treated with 0.1 M I₂ in CCl₄
- treated with 0.1 M Br₂ in CCl₄

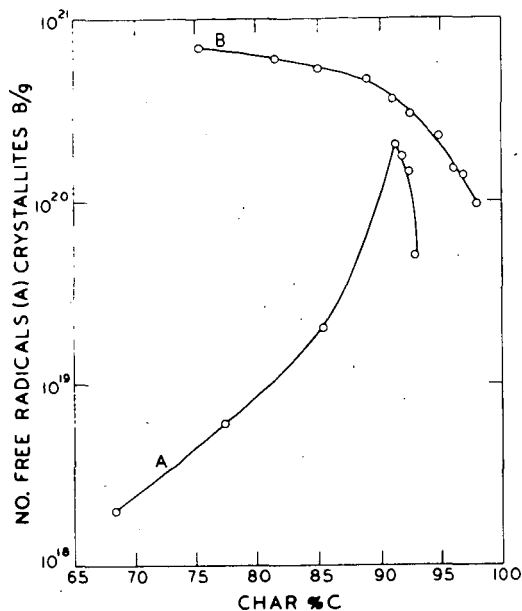


Figure 3.

Comparison of the number of free radicals with the size of crystallites in cellulose chars.

- A. number of free radicals per gram vs. Carbon content
- B. number of crystallites possible per gram vs. Carbon content

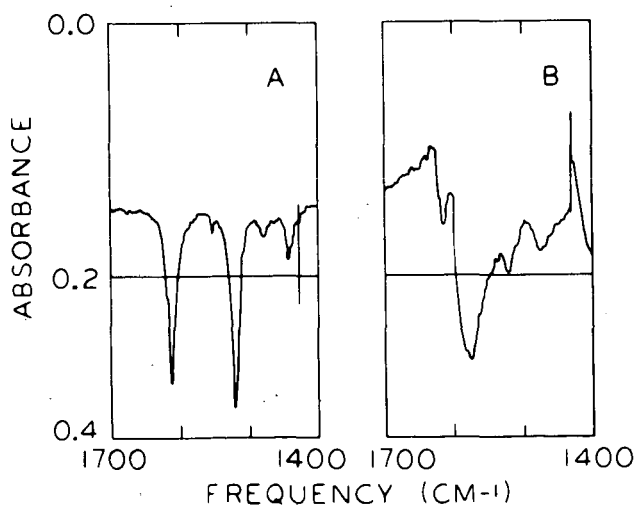


Figure 4.

The influence of charge transfer forces on infrared spectra.

- A. Tetrakis [p-dimethylaminophenyl] ethylene in fluorolube mull
- B. Iodine complex of tetrakis [p-dimethylaminophenyl] ethylene in fluorolube mull

INFRARED SPECTRA OF OXYGEN-18 LABELED CHARs

R. A. Friedel

Pittsburgh Coal Research Center, Bureau of Mines,
U.S. Department of the Interior, Pittsburgh, Pa.

R. A. Durie and Y. Shewchuk

Commonwealth Scientific and Industrial Research Organization,
Chatswood, New South Wales, Australia

SUMMARY

Chars of four O-18 labeled compounds were prepared. Infrared spectra were examined for isotopic shifts. On the basis of a few published results on pure compounds the shifts for C=O¹⁸ at 1600 cm⁻¹ were expected to be -20 cm⁻¹ or more. The observed shifts are less than 5 cm⁻¹; this result may indicate that chelated carbonyls are not involved. However, very strong hydrogen bonding as in chelated, conjugated carbonyl structures may be responsible for the small shifts. An O¹⁸-labeled chelate is being prepared at the CSIRO laboratories in order to investigate this point.

IntroductionChars

Since the early work at the Bureau of Mines on carbohydrate chars^{1,2/} the infrared spectra of chars ($\leq 500^\circ$ C) of various chemicals have been studied.^{3,4,5/} Spectral investigations of structure of chars have included studies of the effect of elemental constitution; the effect of introducing oxygen into chars of hydrocarbons indicated that spectral absorption bands, particularly the intense 1600 cm⁻¹ band, were attributable to oxygenated structures.^{4,6,7/} Isotope-labeling of chars has been utilized; a successful study of deuterium labeling was carried out by comparing infrared spectra of chars of an aliphatic hydrocarbon and a corresponding deuterocarbon. From this study definite evidence was obtained for assignment of the 730-910 cm⁻¹ absorption bands to CH out-of-plane aromatic vibrations.^{6,7/} Also, further indications were found that the most intense band in char spectra, 1600 cm⁻¹, was attributable to oxygenated structures.

A more direct investigation of the specific structures responsible for the 1600 cm⁻¹ band seemed desirable. Charring of compounds labeled with oxygen-18 was judged to be a direct method with good chances for success. Three structures were considered on the basis of their intense absorption, near 1600 cm⁻¹, to be possible sources of the 1600 cm⁻¹ band in chars:

(1) Carbonyl groups in ketones, quinones, or conjugated chelate structures should show a shift to low frequency in going from C=O¹⁶ to C=O¹⁸; (2) aromatic nuclei should produce no change in spectral frequency; (3) aromatic nuclei with enhanced intensities due to oxygenated substituents on the ring should not undergo any appreciable frequency shift in the 1600 cm⁻¹ region; a shift should occur in the C-O stretch region at 1100 cm⁻¹.

Coals

Studies of the 1600 cm^{-1} band in char spectra may produce information on the origin of the same band in the spectra of coals. Spectral data from chars of carbohydrates would be particularly applicable for comparison with coal spectra as carbohydrate chars produce spectra nearly identical to spectra of coals.^{1,2/} Unfortunately O^{18} -labeled carbohydrates are not available.

Information on the intense 1600 cm^{-1} band in coals has been obtained in studies of absorption intensities for many pure compounds in an effort to determine what structures could produce the 1600 cm^{-1} absorption.^{8/} The principal type of structure found to have sufficient intensity is the conjugated chelated carbonyl group. These groups can only produce the 1600 band if all or nearly all of the oxygen in the coal is in the form of hydroxyl chelated carbonyl groups.

O^{18} -Labeled Compounds

The minimum spectral shift in the infrared spectra for a labeled carbonyl group ($\text{C}=\text{O}^{18}$) relative to an unlabeled group ($\text{C}=\text{O}^{16}$) is -40 cm^{-1} , on the basis of the simple ratio of the reduced masses. Hooke's law for the stretching vibration of $\text{C}=\text{O}^{16}$ is: $\nu_{16} = \frac{1}{2\pi c} \sqrt{\frac{k}{\mu_{16}}}$, where

$$\mu_{16} = \frac{m_{\text{C}} + m_{\text{O}^{16}}}{m_{\text{C}}m_{\text{O}^{16}}}; \quad \nu = \text{frequency, cm}^{-1}; \quad k = \text{constant};$$

For $\text{C}=\text{O}^{18}$ the same equation applies; dividing,

$$\frac{\nu_{16}}{\nu_{18}} = \sqrt{\frac{\mu_{16}}{\mu_{18}}} = \sqrt{1.05}$$

$$\text{or } \nu_{18} = \frac{\nu_{16}}{\sqrt{1.05}}$$

For $\nu_{16} = 1600 \text{ cm}^{-1}$, $\nu_{18} = 1560 \text{ cm}^{-1}$; $\Delta\nu = -40 \text{ cm}^{-1}$. If this 1600 cm^{-1} band in a char or coal spectrum is due to a simple carbonyl structure, the corresponding labeled carbonyl group should produce an absorption band shifted to 1560 cm^{-1} . If the stretching vibration of the carbonyl structure is complex the simple value obtained from the reduced mass calculation will differ somewhat from 40 cm^{-1} . A ketone investigated by Karabatsos^{9/} showed an appreciable deviation; 2,3-dimethyl-3-pentanone- O^{18} shows a shift of 31 cm^{-1} instead of the expected 40. This shift is in the neighborhood predicted by Francis^{10/} for a mixed vibration composed of about 80 percent $\text{C}=\text{O}$ stretch and 20 percent $\text{C}-\text{C}$ stretch. With conjugation the shift does not change for the benzenoid carbonyl compounds: Benzoic acid, two benzoates, benzophenone, and benzoquinone.

	$\Delta\nu, \text{ cm}^{-1}$
Benzoic acid (monomer)	-32 ^{11/}
Methylbenzoate	-31 ^{11/}
Cinnamyl nitrobenzoate	-30 ^{12/}
Benzophenone	-30 ^{13/}
p-Benzoquinone	-30 ^{14/}
Benzoylchloride	-25 ^{11/}
Benzamide	-24 ^{15/}

The decreased shift for benzamide is attributable to greater participation of other groups of the molecule in the carbonyl vibration.^{15/} Apparently the same explanation may be given for the decreased shift observed for benzoylchloride. It is surprising that the shifts observed indicate no particular increase due to conjugation with an aromatic ring. (A large effect due to ring conjugation is observed by comparison of the spectra of nitromethane- O^{18} and nitrobenzene- O^{18} .^{16,17/}) Future investigations of more aliphatic ketones may produce different results.

The only published indication of the effect of conjugated chelation is on benzoic acid dimer:

	$\Delta\nu, \text{ cm}^{-1}$
Benzoic acid dimer	-20
Benzoic acid monomer	-32

Thus hydrogen bonding is seen to produce a significant decrease in the O^{18} shift of a conjugated carbonyl system. It was anticipated that the spectra of chars having carbonyl groups enriched in O^{18} may show shifts for the 1600 cm^{-1} band of -20 to -30 cm^{-1} . Such shifts in char spectra would be measurable, even though absorption bands are broad.

Experimental

On the initiation of this work only three usable O^{18} -labeled organic compounds were commercially available. They were investigated in the following order: Linoleic acid, phenol, and benzoic acid; sodium phenate and sodium benzoate- O^{18} were also prepared and charred. First the unlabeled compounds were charred under various conditions in order to determine the most favorable condition for producing intense 1600 cm^{-1} bands. Temperatures required to eliminate the absorption of monosubstituted benzenes in order to produce coal-like absorption bands in the $730\text{-}900 \text{ cm}^{-1}$ aromatic band region were usually so high that other spectral details, including the 1600 cm^{-1} band, were weakened.

Samples of O^{16} compounds were placed in a glass tube or a steel bomb, sealed or unsealed, in vacuo or under nitrogen. Amounts of sample used were 50-100 mg because of the scarcity of O^{18} samples. Pyrolysis temperatures were varied from 350° C to 620° C ; times were varied from 1 to 58 hours.

Linoleic acid- O^{18}

Two samples were investigated: (a) A sample of 22 percent O^{18} -enriched acid (kindly given by Dr. A. Miko, of the Yeda Research and Development Co., Rehovoth, Israel), and (b) a commercial sample of 38 percent enriched acid. The best conditions found for obtaining 1600 cm^{-1} bands were 400° C , 2 hours, under 1 atmosphere of nitrogen in a sealed pyrex tube. The 22 percent enriched sample was donated, with the warning that polymerization probably had occurred; it is also possible that polymerization occurred in the 38 percent enriched sample. Yeda has taken linoleic acid- O^{18} off the market.

Phenol- O^{18} , 86 percent

Pyrolysis of phenol of 86 percent O^{18} enrichment was carried out at temperatures near 550° C for about 18 hours in a sealed tube under nitrogen.

Sodium phenate

The O^{18} -labeled phenate was not prepared because of insufficient phenol- O^{18} . Sodium phenate- O^{16} was prepared from ordinary phenol and charred. Conditions were similar to those used for phenol.

Benzoic acid- O^{18} , 95.6 percent

Conditions were similar to those used for phenol.

Sodium benzoate- O^{18}

A nitrogen atmosphere and a temperature of 500° C were used. Pyrolysis times were about 24 hours.

In all samples except the sodium phenate and sodium benzoate, char was obtained in the form of a thin film on the walls of the sealed tube. These films were sufficiently thin to give spectra of good quality directly; data obtained from such films was qualitative or semi-quantitative as thicknesses of the film varied considerably. In all cases spectra were also obtained by means of KCl pellets which were better for quantitative absorption measurements.

Spectra were determined first on gases produced. Then the samples were washed with hexane and/or benzene and the spectra of the soluble products were obtained. The benzene-insoluble char was then investigated.

Ultimate analyses of all of the chars are given in table 1.

Results and Discussion of Results

Results obtained on the four substances investigated show that the spectral shifts are very small or negligible (table 2); no shift was definitely detectable for any of the chars. In figure 1 the spectra of chars from benzoic acid- O^{16} and - O^{18} are given; they are practically identical, including the positions of the two 1600 cm^{-1} bands.

1600 cm^{-1} bands were obtained in all chars but in no case were they intense bands. This is a possible indication that carbonyl groups may not have been involved. For linoleic acid and benzoic acid it is nearly certain that no oxygen-containing group could be an important contributor to the 1600 cm^{-1} band, as the oxygen contents of the chars were found to be negligible. Hydrocarbon structures could have produced the weak bands found.

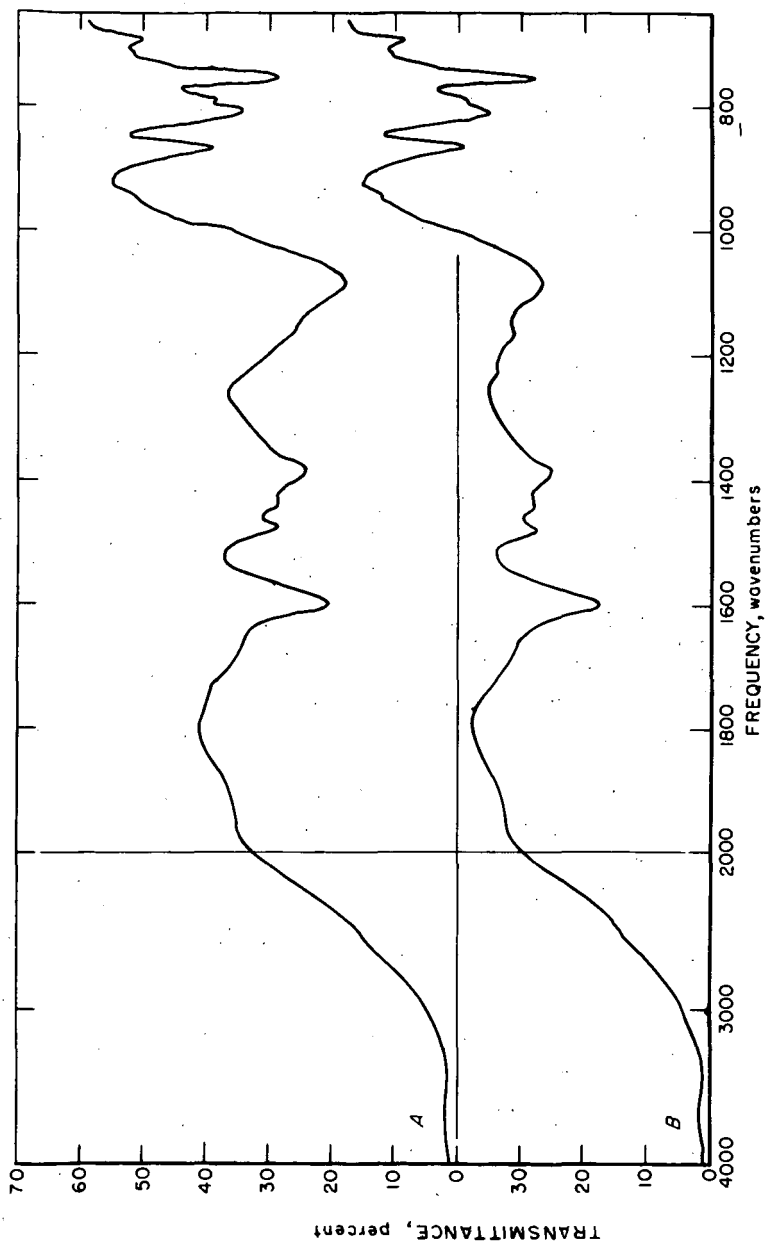


Figure 1. Infrared spectra of chars prepared from 50 mg heated at 550 C for 72 hours. KCl pellets, 2 percent in 100 mg KCl. Curve A, benzoic acid; curve B, benzoic acid-O₁₈.

Table 1.- Ultimate analyses of chars

	C	H	O	State
Benzoic acid	96.2	3.8	< 0.5	Film
Benzoic acid	70.08	2.86	(6.35) ^{2/}	Powder
Benzoic acid- O^{18}	95.17	3.89	1.35	Film

Sodium benzoate	93.00	3.71	3.88	Powder
Sodium benzoate- O^{18}	91.47	3.22	2.60	Powder ^{3/}

Phenol	71.80	3.35	20.0	Powder
Phenol	93.26	3.46	3.42	Film
Phenol- O^{18}	91.20	3.81	3.73	Film.

Sodium phenate	76.76	2.98	19.4	Powder

Linoleic acid ^{1/}	95.9	3.7	0.4	Powder

1/ O^{18} -labeled chars were not analyzed.

2/ Very small sample; oxygen analysis dubious.

3/ Ash, 3.5 percent, apparently due to a trace of glass from vial opening.

Table 2.- Negative spectral shifts of oxygen-18 labeled chars

	Spectral shift, cm ⁻¹ ^{1/}
Linoleic acid- O^{18} (22 and 36 percent)	< 5
Phenol- O^{18} (86 percent)	< 5
Benzoic acid- O^{18} (95.6 percent)	< 5
Sodium benzoate- O^{18}	< 5

1/ Bands were broad. Small shifts were difficult to measure accurately.

The phenol chars also showed no shift from 1600 cm^{-1} , even though one char contains 20 percent oxygen. It is not surprising if the pyrolysis of phenol at 550°C does not produce carbonyl groups. The 1600 cm^{-1} band observed in the spectrum of the phenol char must be due to aromatic absorption enhanced by oxygen-containing substituents on the aromatic rings (ethers and phenols).

The char of sodium benzoate also shows a negligible shift. It was the most likely possibility for producing an isotope shift, as the elimination of oxygen encountered in the chars of linoleic and benzoic acid does not occur for the char of sodium benzoate. The sizeable percentage of oxygen present in the char, 4 percent, is likely to exist in the char as carbonyl groups of some sort; even so, no appreciable shift is observed.

The lack of appreciable shift in the spectra of O^{18} -labeled chars may be attributable to extremely strong association (chelation, or other). With the sizeable oxygen content of some of these chars there are presumably some carbonyl groups present. Unfortunately no O^{18} -labeled pure compounds having very strong hydrogen-bonding have been investigated. As mentioned above, the spectrum of benzoic acid- O^{18} shows a smaller shift for the associated dimer acid (-20 cm^{-1}) than for the free monomer (-32 cm^{-1}).¹⁰ These results are for a rather weakly associated acid dimer; the vibration of the C=O group in the dimer obviously involves participation of other groups in the molecule. For a more strongly hydrogen-bonded chelate, as acetylacetone, the participation of other groups in the molecule would be greater and the shift probably would be less. On this basis the small shifts in chars are explainable. Certainly the negligible shift observed for chars does not exclude the presence of C=O groups in structures producing the 1600 cm^{-1} band. In order to investigate the effect of strong chelation on the C= O^{18} shift preparation of dibenzoylmethane, $\text{H}_5\text{C}_6\text{-CO}^{18}\text{-CH}_2\text{-CO}^{18}\text{-C}_6\text{H}_5$, is being carried out at the CSIRO laboratories. Little or no C= O^{18} shift is expected. If an appreciable shift is observed for this compound it will be necessary to conclude that chars do not contain strongly chelated carbonyls.

Further studies will be carried out on labeled chars as other O^{18} -containing compounds become available. It is expected that prices of these compounds will decrease greatly, for cheaper methods of preparation are being developed.^{18/}

References cited

1. Friedel, R. A., and M. G. Pelipetz. Infrared Spectra of Coal and Carbohydrate Chars. *J. Opt. Soc. of Am.*, v. 43, No. 11, November 1953, pp. 1051-1052.
2. Friedel, R. A., and J. A. Queiser. Infrared Analysis of Bituminous Coals and Other Carbonaceous Materials. *Anal. Chem.*, v. 28, 1956, pp. 22-30.
3. Friedman, S., R. Raymond, L. Reggel, I. Wender, and R. A. Friedel. Chemistry and Structure of Coal. Formation of Coallike Chars From Pure Organic Compounds. Abstracts, Am. Chem. Soc. meeting, Dallas, Texas, April 1956.
4. Friedel, R. A. Spectra and the Constitution of Coal and Derivatives. Proc. 4th Carbon Conf., Univ. of Buffalo, Pergamon Press, London, 1960, pp. 320-336.
5. Brown, T. H., and Turkevich, J. A Study of the Low-Temperature Carbonization of d-Glucose Using Electron Magnetic Resonance and Infrared Absorption. Proc. 3rd Conf. on Carbon, Pergamon Press, London, 1959, pp. 113-120.

6. Friedel, R. A., and H. Retcofsky. Spectral Studies of Coal. Proc. 5th Biennial Conf. on Carbon, The Pennsylvania State Univ., Pergamon Press, London, 1963, v. 2, pp. 149-165.
7. Friedel, R. A. The Use of Infrared Spectra of Chars in Coal Structure Research. Applied Optics, v. 2, No. 11, Nov. 1963, pp. 1109-1111.
8. Friedel, R. A., R. A. Durie, and Y. Shewchuk. The Origin of the 1600 Wavenumber Absorption Band in the Infrared Spectra of Various Coal Vitrains. To be published.
9. Karabatsos, G. J. Infrared Spectra of Isotopically Labelled Compounds. I. Diisopropyl Ketones. J. Org. Chem., v. 25, 1960, pp. 315-318.
10. Francis, S. A. Intensities of Some Characteristic Infrared Bands of Ketones and Esters. J. Chem. Phys., v. 19, 1951, pp. 942-948.
11. Pinchas, S., D. Samuel, and M. Weiss-Brodsky. Infrared Absorption of O^{18} Labelled Benzoic Acid, Benzoylchloride, and Methylbenzoate. J. Chem. Soc., 1961, p. 2382.
12. Braude, E. A., and M. Turner. O^{18} Isotope Effect on Infrared Spectra of Benzophenone. Chem. and Ind. 1955, p. 1223.
13. Halman, M., and S. Pinchas. The Isotope Effect of O^{18} on the Infrared Spectrum of Benzophenone. J. Chem. Soc., 1958, p. 1703.
14. Becker, E. D., E. Charney, and T. Anno. Molecular Vibrations of Quinones. VI. A Vibrational Assignment for p-Benzoquinone and Six Isotopic Derivatives. Thermodynamic Functions of p-Benzoquinone. J. Chem. Phys., v. 42, 1964, pp. 942-944.
15. Pinchas, S., D. Samuel, and M. Weiss-Brodsky. Infrared Absorption of O^{18} -Labelled Benzamide. J. Chem. Soc., 1961, p. 1688.
16. Pinchas, S. and M. Halman. The Infrared Absorption of O^{18} -Labelled Nitromethane. J. Chem. Soc., 1960, p. 1242.
17. Pinchas, S., D. Samuel, and B. L. Silver. The Infrared Absorption Spectrum of O^{18} -Labelled Nitrobenzene. Spectrochim. Acta, v. 20, 1964, p. 179.
18. Richter, W. J., M. Senn, and A. L. Burlingame. Convenient Labelling Technique for Mass Spectroscopy: Acid Catalyzed Deuterium and Oxygen-18 Exchange Via Gas-Liquid Chromatography. Tetrahedron Letters, No. 17, 1965, pp. 1235-1239.

Recovery of Nitrogen Bases with
Weak Acids

by

T. F. Johnson, P. X. Masciantonio
and J. H. Schelling

Applied Research Laboratory
United States Steel Corporation
Monroeville, Pennsylvania

Introduction

The recovery of nitrogen bases is of particular interest in chemical plants that operate in conjunction with coal-carbonization facilities. Traditionally, nitrogen bases such as ammonia, pyridine, and quinoline have been recovered by processes that involve acid extraction followed by neutralization with caustic soda or lime.^{1,2)} Such processes have inherent disadvantages with regard to excessive consumption of acids and bases as well as concomitant waste-disposal problems.

Recently, several processes have been developed for nitrogen-base recovery by regenerative cyclic techniques. For example, recovery of ammonia from coke-oven gas and pyridine from coke-oven light oil have been reported.^{3,4,5)} These processes for recovery of nitrogen bases are characterized by the use of an aqueous acid solution for the extraction step followed by a high-temperature stripping, or springing, operation that liberates the nitrogen bases and simultaneously regenerates the acid extractant. The selection of an appropriate acid extractant for a particular nitrogen-base system is an important factor in designing or developing a regenerative process. Previously reported studies^{3,4,5)} have demonstrated that monoammonium acid phosphate is a suitable extractant for ammonia recovery, whereas either phosphoric acid or monopyridinium sulfate is adequate for pyridine recovery. However, the theory for selection of appropriate reagents for regenerative nitrogen-base recovery has not been developed and, consequently, the general applicability of this recovery technique has not received significant attention. It is the object of this paper to demonstrate that readily available thermodynamic data can be used to determine the feasibility of a regenerative technique for recovery of particular nitrogen bases. The discussion is based on the behavior of particular acids during the extraction and springing operations. Data are also presented on the extraction and springing steps for recovery of pyridine and quinoline from coal-tar fractions.

Discussion of the Regenerative Technique

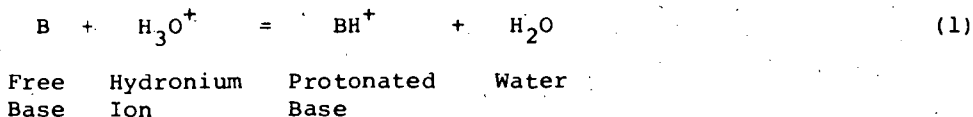
The general scheme for a regenerative recovery process for

* See References.

nitrogen bases involves three steps: a) extraction, b) separation, and c) regeneration. The system can be seen in Figure 1 as a generalized flow diagram. Usually, nitrogen bases are recovered from streams in which they are present in low concentrations (about 0.1 to 5%), such as coke-oven light-oil streams.

Selection of Reagents for Regenerative Systems

The selection of an appropriate acidic extractant for a particular nitrogen base is the initial problem encountered in developing a regenerative process. Although such factors as solubility, volatility, decomposition, and side reactions must be considered, the acid component essentially must be strong enough to effect efficient removal of the nitrogen base from the hydrocarbon stream during the extraction step and yet be sufficiently weak to allow decomposition of the resultant acid salt during the regeneration step. Therefore the values of the equilibrium constants at the springing and extraction temperatures (K_{T_2} and K_{T_1}) for the following reaction are of significance in determining whether the regenerative technique is feasible.



The temperature dependence of the equilibrium constant follows the expression

$$\ln \frac{K_{T_2}}{K_{T_1}} = \frac{-\Delta H}{R} \left(\frac{1}{T_2} - \frac{1}{T_1} \right) \quad (2)$$

where

ΔH = the heat of reaction, and
 R = the gas constant.

It is desirable that the ratio (K_{T_2}/K_{T_1}) be less than unity for a regenerative system (ΔH , the heat of reaction, must be negative).

In an effort to develop suitable parameters for the selection of reagents for regenerative systems, the ionization equilibria of acids and bases have been examined.

In a discussion of acid-base systems, the following equations are applicable. Acid extraction of a nitrogen base (B) from a hydrocarbon stream involves the equilibrium reaction



which can be represented by an equilibrium constant

$$K_e = \frac{[\text{BH}^+]}{[\text{B}][\text{H}_3\text{O}^+]} \quad (4)$$

The ionization constant of the base involves the equilibrium



expressed by an ionization constant

$$K_b = \frac{[BH^+][OH^-]}{[B]} \quad (6)$$

By using the ionization constant for H_2O

$$K_w = [OH^-][H_3O^+] \quad (7)$$

and combining Equations 4, 6, and 7, the following expression is obtained to show the concentration of protonated base in an aqueous extract.

$$[BH^+] = \frac{K_b}{K_w} [B][H_3O^+] \quad (8)$$

The dependence of $[BH^+]$ on $[H_3O^+]$ can be represented in terms of the strength of any acid (HA) by using the equilibrium dissociation constant of the acid.



$$K_a = \frac{[H_3O^+][A^-]}{[HA]} \quad (10)$$

$$[H_3O^+] = \left([HA] K_a \right)^{1/2} \quad (11)$$

Combining (11) with (8) gives

$$[BH^+] = \frac{K_b}{K_w} K_a^{1/2} [HA]^{1/2} [B] \quad (12)$$

Equation 12 indicates that, for a given concentration $[B]$ and strength (K_b) of base, the concentration $[BH^+]$ can be increased by increasing the strength of acid (K_a).

$$[BH^+] \propto K_a^{1/2} \quad (13)$$

A similar discussion of the regeneration step is pertinent. The reaction involved is



The equilibrium constant for the reaction can be represented as

$$K_r = \frac{[B][H_3O^+]}{[BH^+]} \quad (15)$$

and can be expressed in terms of Equation 8 to give

$$K_r = \frac{K_w}{K_b} = \frac{[B][H_3O^+]}{[BH^+]} \quad (16)$$

Therefore

$$[B] = \left(\frac{K_w}{K_b}\right)^{1/2} [BH^+]^{1/2} \quad (17)$$

$$[B] \propto K_b^{-1/2} \quad (18)$$

Thus, for a given concentration $[BH^+]$ in the aqueous extract, the concentration $[B]$ of base is high for bases of low base strength (K_b).

From Equations 12 and 17, the following generalizations can be made concerning the selection of an acid and a base for recovery of nitrogen bases by a regenerative process. To get good extraction, maximize $[BH^+]$ by using an acid with as large a value for K_a as is possible, consistent with other requirements of the process. To get good regeneration, maximize $[B]$ (a base with a small K_b value should be involved).

Accordingly, suitable systems appear to involve an acid extractant with a large K_a value and a nitrogen base with a small K_b value. Consistent with the above, the ΔpK was examined as a useful guide in selecting components for regenerative systems,

where

$$pK = -\log K \quad (19)$$

$$\Delta pK = (pK_b - pK_a), \text{ and} \quad (20)$$

ΔpK is expressed as the absolute value of $(pK_b - pK_a)$. It is anticipated that the larger the ΔpK of a system, the better it will function in a regenerative recovery process. Therefore it appears that recovery of nitrogen bases is facilitated by combinations of relatively weak bases and relatively strong acids or relatively strong bases and weak acids.

Systems for Recovery of Ammonia and Pyridine Bases

As mentioned above, several processes have previously been reported for recovery of ammonia and pyridine bases from coke-oven product streams. The data on ammonia and pyridine are consistent with the discussion presented above, Tables I and II. Experimentally it has been demonstrated that, although ammonia can be recovered in a regenerative manner using monoammonium phosphate, neither phosphoric acid nor sulfuric acid can be used ($H_2PO_4^-$ is suitable for NH_3 recovery, whereas H_3PO_4 , HSO_4^- , and H_2SO_4 are not applicable).

It has also been shown that pyridine can be recovered successfully with either H_3PO_4 or HSO_4^- ; however, neither $H_2PO_4^-$ nor H_2SO_4 can be employed.

The use of the parameter ΔpK does not appear to fit the observed behavior of all the systems examined. However, the elementary ionization equilibrium theory explains certain inconsistencies with ΔpK values. For example, in general, (1) systems in which both components have pK values greater than about 6 are not useful since interaction is too weak to effect extraction, (2) systems in which both components have pK values less than about 6 are not useful since interaction is too strong for dissociation of the acid-base salt during regeneration, and (3) when either component is a strong acid or a strong base, the system is not applicable because interaction is too strong for regeneration of the reagent.

Recovery of Pyridine and Quinoline from Coal-Tar Fractions

A regenerative system for recovery of pyridine from coal-tar fractions has been examined on the basis of the above consideration of ΔpK . Values of ΔpK for the pyridine - HSO_4^- and pyridine - H_3PO_4 systems are 6.85 and 6.64, respectively, Table II. Each system was examined to determine the behavior of these acids in the extraction and regenerative steps. Data on the quinoline regenerative recovery system are presented for comparison. Ionization data on quinoline ($K_b = 6.3 \times 10^{-10}$, $pK = 9.87$) suggest that either HSO_4^- or H_3PO_4 could be used as the extractant. The respective values of ΔpK are 7.95 and 3.22. Since HSO_4^- gives a larger value of ΔpK , the recovery of quinoline with quinolinium acid sulfate solution as the extractant was examined for comparison.

Experimental

Data on the extraction of pyridine and quinoline bases were obtained by using conventional laboratory equipment consisting of a stirred 1-liter 3-neck flask equipped with a bottom outlet stopcock. Single-stage extraction tests were conducted over the temperature range 0 to 55 C. The data on the pyridine - sulfuric acid system are presented in Table III, and data on the pyridine - phosphoric acid and the quinoline - sulfuric acid systems appear in Tables IV and V, respectively. The extraction data indicate that the nitrogen bases can be concentrated in the aqueous phase by the extraction technique.

To examine the vapor-liquid equilibrium data for the pyridine - phosphoric acid system, the pyridine - sulfuric acid system, and the quinoline - sulfuric acid system, solutions were prepared of various strengths of acid and concentration of the respective nitrogen bases. Acid strengths covered the range 20 to 40 percent and base-to-acid mole ratios varied from 0.6 to 1.9.

An Othmer equilibrium still was used to determine concentrations of pyridine and quinoline in the vapor and liquid phases for the various sample solutions.

Discussion

The Othmer equilibrium data indicate that pyridine concentration

in the vapor increases with increasing concentration of acid (consistent with Equation 17) and, at a given level of acid strength, with increasing pyridine-to-acid mole ratio, see Figures 2 and 3, Tables VI and VII.

Although it was expected that quinoline should behave similar to pyridine, such was not the case. Quinoline was realized in the distillate of the Othmer still; however, the quinoline concentration is significantly lower than pyridine for a given mole ratio of base to acid. Two factors, low vapor pressure and low solubility, cause problems in the quinoline system. Because of the relatively poor solubility of quinoline in water (0.08 g/100 ml at 25 C), recovery of quinoline as a distillate product depends on the limitations of a steam distillation system. Accordingly, the distillate composition is a function of the vapor pressure of quinoline at the boiling point of the mixed liquid phase. Because of the low volatility of quinoline, only about 2 weight percent quinoline is realized in the distillate during the regeneration step. Thus, typical Othmer equilibrium data are not realized for quinoline.

Therefore, although quinoline can be recovered by a cyclic regenerative process, the system is not analogous to the pyridine system. The quinoline system appears suitable on the basis of ΔpK data, but other factors such as solubility and volatility must be considered for practical application.

Summary

A method for selecting reagents for recovery of weak bases from hydrocarbon streams has been developed, based on thermodynamic ionization equilibrium constants. An acid can be selected for recovery of a given base according to the value of ΔpK calculated for the system. Experimental data have been presented on the pyridine - sulfuric acid system, the pyridine - phosphoric acid system, and the quinoline - sulfuric acid system and demonstrate the utility and limitations of the method.

The technique should also be applicable to development of systems for recovery of acids from effluent streams by extraction with selected nitrogen base reagents. When it is required to effectively remove nitrogen impurities in conjunction with a subsequent refining operation on a hydrocarbon stream, a regenerative process may also be applicable; however, provision must be made for adequate removal of nitrogen bases by using a sufficient number of extraction stages.

References

1. H. H. Lowry, "Chemistry of Coal Utilization," Vol II John Wiley & Sons, Inc., New York, 1945.
2. P. J. Wilson and J. H. Wells, "Coal, Coke and Coal Chemicals," McGraw Hill, N. Y., 1950.

3. H. L. Stewart, U. S. Patent 2,410,906, November 12, 1946.
4. R. D. Rice, U. S. Patent 3,024,090, March 6, 1962.
5. G. D. Kharlampovich and R. I. Kudryashova, Coke and Chemistry (USSR),
2, 29, (1964).

Table I

Data on Regenerative Recovery Systems
for Nitrogen Bases¹⁾

<u>Nitrogen Bases</u>	<u>Extractant</u>	<u>K_a</u>	<u>K_b</u>
NH ₃	(NH ₄)H ₂ PO ₄	6.23 x 10 ⁻⁸²⁾	1.79 x 10 ⁻⁵
NH ₃	H ₃ PO ₄	7.52 x 10 ⁻³³⁾	1.79 x 10 ⁻⁵
NH ₃	(NH ₄)HSO ₄	1.20 x 10 ⁻²²⁾	1.79 x 10 ⁻⁵
NH ₃	H ₂ SO ₄	-4)	1.79 x 10 ⁻⁵
Pyridine	(PyH)H ₂ PO ₄	6.23 x 10 ⁻⁸²⁾	1.71 x 10 ⁻⁹
Pyridine	H ₃ PO ₄	7.52 x 10 ⁻³³⁾	1.71 x 10 ⁻⁹
Pyridine	(PyH)HSO ₄	1.20 x 10 ⁻²²⁾	1.71 x 10 ⁻⁹
Pyridine	H ₂ SO ₄	-4)	1.71 x 10 ⁻⁹

- 1) Handbook of Chemistry and Physics, 44th Ed., Chemical Rubber Publishing Co., Cleveland, Ohio, 1963.
- 2) K_a for second hydronium-ion dissociation.
- 3) K_a for first hydronium-ion dissociation.
- 4) Completely dissociated.

Table II

ΔpK Values for Acid-Base Systems

<u>Systems</u>	<u>ΔpK</u>	<u>Suitability of System</u>
NH ₃ -(NH ₄)H ₂ PO ₄	2.46	Yes
NH ₃ -H ₃ PO ₄	2.63	No
NH ₃ -NH ₄ HSO ₄	2.83	No
NH ₃ -H ₂ SO ₄	*	No
Pyridine-(PyH)H ₂ PO ₄	1.55	No
Pyridine-H ₃ PO ₄	6.64	Yes
Pyridine-(PyH)HSO ₄	6.85	Yes
Pyridine-H ₂ SO ₄	*	No

* ΔpK Not applicable.

Table III

Extraction of Pyridine Bases from Light Oil
With Pyridinium Sulfate Solution*

<u>Test No.</u>	<u>Mole Ratio of Pyridine to H₂SO₄</u>	<u>Pyridine in Washed Light Oil, %</u>	<u>Pyridine in Extract, %</u>
1	1.68	0.15	29
2	1.67	0.12	29
3	1.63	0.08	28
4	1.54	0.05	27

* In each test, light oil containing 0.44 percent of P-bases was washed with a lean pyridinium sulfate solution (mole ratio 1.05) prepared by adding crude P-bases to a 30 weight percent sulfuric acid solution.

Table IV

Extraction of Pyridine Bases from Light Oil
(30 Percent Phosphoric Acid at 55 C)

<u>Test No.</u>	<u>Mole Ratio of Pyridine to H₃PO₄</u>	<u>Pyridine in Light Oil, %</u>	<u>Pyridine in Washed Light Oil, %</u>	<u>Pyridine in Extract, %</u>
1a)	1.0	5.67	0.44	19.5
2a)	1.0	2.10	0.40	19.2
3a)	0.70	4.60	0.24	14.5
4a)	0.92	4.60	0.59	18.1
5b)	0.95	4.60	0.58	18.6

a) One-stage wash.

b) Two-stage wash.

Table V

Extraction of Quinoline from a Tar Fraction
With Sulfuric Acid^{1,2)}

<u>Test No.</u>	<u>Mole Ratio of Quinoline to H₂SO₄</u>	<u>Quinoline in Washed Oil, %</u>	<u>Quinoline in Acid Extract, %</u>
1	1.46	1.59	36.7
2	1.41	2.06	35.7

1) Tar fraction contained 12.1 weight percent quinoline bases.

2) Extractant contained 30 weight percent H₂SO₄.

Table VI

Pyridine Concentrations in Vapor at Equilibrium With
Refluxing H₂SO₄ Solutions - Othmer Still Data

<u>Initial H₂SO₄ Concentration, wt %</u>	<u>Mole Ratio of Pyridine to H₂SO₄</u>	<u>Pyridine Content of Vapor, wt %</u>
20.4	1.63	4.7
19.9	1.95	21.1
30.9	1.60	10.4
30.4	1.81	23.8
30.6	1.98	41.6
40.3	1.60	21.3

Table VIII

Pyridine Concentrations in Vapor at Equilibrium With
Refluxing H₃PO₄ Solutions - Othmer Still Data

Initial H ₃ PO ₄ Concentration, wt %	Equivalent Ratio of Pyridine to Acid	Pyridine Content of Vapor, wt %
10.45	0.60	0.54
10.44	0.80	2.08
10.41	0.98	6.86
19.88	0.40	0.0
20.42	0.60	0.87
20.40	0.81	4.72
20.34	0.97	13.84
31.20	0.60	1.11
30.38	0.80	6.52
31.08	0.98	21.46
30.98	0.99 ^{a)}	19.92
31.06	0.99 ^{b)}	21.65 ^{c)}

- a) Pyridine contained 23.4 percent picoline.
 b) Pyridine replaced with picoline.
 c) Analyzed as picoline.

D. M. Mason

Institute of Gas Technology
Chicago, IllinoisINTRODUCTION

Luminescence is the emission of nonequilibrium or nonthermal radiation as opposed to incandescence. A number of materials have been observed to luminesce when placed in a flame. This phenomenon, called candoluminescence, must be distinguished from thermoluminescence - in which a material is excited by radioactivity or other means but luminesces only when raised to a higher temperature - and from incandescence and luminescence of the flame itself. The blue luminescence of an aerated methane flame is an example of the latter. Candoluminescence is of interest from two standpoints - that of obtaining a better understanding of flames and flame-solid interactions, and secondly the possibility, though remote, of developing a new method of gaslighting. The work reported here was supported in part by the American Gas Association.

Candoluminescence has been known and studied for many years. It was probably first reported by Balmain in 1842 (3) in his description of the material boron nitride, which he was the first to prepare. Apparently the phenomenon was not recognized with other materials until it was reported by Donau in 1913 (5). The subject was reviewed by L. T. Minchin in 1938 (8) and by E.C.W. Smith in 1941 (11).

The materials that luminesce in flames share the characteristics of phosphors generally; that is, they are comprised of a colorless crystalline host or matrix material into which a small concentration of foreign atoms or ions, called the activator, is incorporated. The radiation is typically continuous and extends over only a small wavelength range, thus having a definite color. The color is usually characteristic of the activating ion and can also be obtained with other means of excitation, such as ultraviolet light or cathode rays.

Excitation by a hydrogen flame has been used in most studies of candoluminescence, although Tiede and Buescher reported that, in addition to hydrogen, flames of ethyl alcohol, hydrogen sulfide, and carbon disulfide excited the luminescence of boron nitride (14). Excitation by the flame of city gas has also been reported (9).

The existence of the phenomenon at relatively low temperatures has not been seriously questioned. The temperature range here is from the temperature attained when a flame impinges on a thin film of phosphor spread on a cool metal support up to a bright red heat. This upper limit is based on the observation of Tiede and Buescher (14) that blue luminescence occurred when a flame touched boron nitride in a carbon boat heated electrically to redness.

E. L. Nichols (10) claimed that at much higher temperatures he had observed light outputs from materials heated in an oxyhydrogen flame that were several times greater than the light output from a blackbody at the same temperature. Apparently this work was inspired by the

limelight which was produced by heating a cylinder of lime with an oxyhydrogen flame. The fact that a fresh portion of the lime had to be brought to the flame from time to time was interpreted to mean that something other than thermal radiation was involved (8). Neunhoeffer (9) reports that the natural chalks from which the lime was prepared contain rare earths. If this were known to Nichols, it would no doubt have suggested to him that the rare earths were activators in a luminescence process. However, the work of later investigators indicated that the limelight was similar to the light of the Welsbach mantle in that both are only excited thermally.

Nichols applied his "phosphors" on ceramic adjacent to a uranium-oxide-coated area and heated both areas evenly with an oxyhydrogen flame. Observations were made of both areas with an optical pyrometer; the uranium oxide was taken to behave essentially as a blackbody and to have the same temperature as the companion material. Many mixtures of colorless oxides with small amounts of rare earths, or with some other elements that were also regarded as activators, had a greater emittance than uranium oxide. E.C.W. Smith (11) repeated some of Nichols's experiments and obtained similar emittance readings. He then proceeded to determine or approximate the actual temperature of the two coatings - a matter of some difficulty. By means of thermocouples made of extremely fine wires, he was able to show large differences in the temperatures of the two coatings - differences sufficient to conclude that at incandescence temperatures there was no emission other than thermal. This conclusion has been confirmed by Sokolov and his co-workers (12), (13).

In hydrogen flames, at least, recombination of hydrogen atoms is generally accepted as the major source of energy for the low-temperature excitation (1), (7); earlier Donau (5) and Nichols (10) considered an oxidation-reduction mechanism, and Neunhoeffer (9) thought that electrons in the flame were responsible. Smith, and Arthur and Townend (1), (2) investigated this question with phosphors composed of calcium oxide activated with manganese, antimony, or bismuth. They found that:

1. Activated oxides that luminesce in hydrogen flames also luminesce when subjected to the action of hydrogen atoms produced in an electrical discharge. When subjected to the latter action and heated electrically, the color of the luminescence approached the color produced in the flame. Presumably, the temperature of the heated oxides approached the temperature of oxides in the flame.
2. The intensity of hydrogen flame luminescence increases when the hydrogen is burned under reduced pressure. This effect was presumed to be caused by a decrease in the number of three-body collisions. These collisions remove hydrogen atoms by recombination.
3. The luminescence is strongest in hydrogen, erratic and very faint in town gas, and absent in carbon monoxide flames. It is also absent in methane and ethylene flames tested at pressures from atmospheric to 10 cm Hg.
4. The luminescence is extinguished when small amounts of hydrocarbon gases or vapors are added to the hydrogen.

According to recent studies of flame mechanisms, hydrogen atoms are present in the methane-air flame as well as in the hydrogen flame (15). Thus it appeared reasonable to search for phosphors that candoluminesce in the methane-air flame. This search and the study of the characteristics of this phenomenon were the objectives of our investigation.

PROCEDURES

Preparation of Phosphors

Materials

Rare earths were obtained as 99.9% pure oxides from Lindsay Chemical Division of American Potash and Chemical Corporation. Other chemicals were research grade.

Calcium Oxide Phosphors

Calcium and rare earth nitrate solutions were prepared and mixed in the required amounts. The mixed nitrate solution was slowly poured into hot ammonium carbonate solution with stirring. The precipitate was filtered, washed with hot ammonium carbonate solution, dried at 100°C, and ignited at 900°C for 30 minutes. The pure rare earth oxides were prepared by precipitation from the nitrate in the same manner.

Yttrium Europium Tungstate - $(Y_{0.9}Eu_{0.1})_2O_3WO_3$ - and Gadolinium Europium Molybdate - $(Gd_{0.8}Eu_{0.2})_2O_3.MoO_3$

The required amounts of the oxides (tungstic acid in the case of tungsten) were mixed, heated in a platinum crucible at 1000°C for 2 hours, ground with mortar and pestle, and reheated at 1000°C for 2 hours. The X-ray patterns of the two products showed that in both a new phase had been formed.

Screening Tests

Mounting strips about 2 cm wide and 10 cm long were made of insulating fire brick and of copper sheet. Phosphor powder, thick enough to hide the surface of the strip, was pressed on to it with a spatula. The nearly vertical face of the strip was observed as it was passed through a methane-air flame (bunsen burner) and a hydrogen diffusion flame in a dark room.

Spectra

Three different methods of mounting the phosphors were used in obtaining the spectra. When we wished to observe the effect of temperature, the phosphor was applied as a paste to a silicon carbide rod. Pastes made with monomethyl ester of ethylene glycol seemed to adhere after drying somewhat better than those made with other liquids. The silicon carbide rod, about 6 mm in diameter, was held between two water-cooled electrical terminals to allow the electrical current passing between the terminals to heat the silicon carbide rod and the phosphor.

When hydrogen was used as a fuel, the phosphor could be coated dry on the fritted disk of a gas-dispersion tube. The fritted disk was operated as a porous-plate burner (Figure 1) without primary air. Known amounts of other gases could be added to the hydrogen.

The phosphor was coated on a water-cooled copper plate when a methane-air flame was to be used. The plate was 1 in. square x 1/4 in. thick with two 1/4-in. copper tubes soldered to the back for cooling water. Plating the face with silver was found to be necessary to prevent slow poisoning of the phosphor by the copper. The phosphor was settled onto the plate from a water suspension. The plate was mounted facing upwards at about 45° to the horizontal and the flame of a National Welding Equipment Co. Type-3A blowpipe was directed downward onto it.

A Beckman DK-2 spectrophotometer with an IP 28 photomultiplier was used to record spectra. The backplate of the lamp housing was removed to allow direct entrance of the radiation from the excited phosphor into the spectrophotometer. A slit opening of 0.4 mm without an auxiliary light-gathering system gave sufficient energy. Varying light intensity from the flickering of the flame was troublesome and made it necessary to use the highest time constant and the slowest recording rate of the instrument. The porous-plate burner gave the steadiest radiation.

RESULTS

Screening tests to discover phosphors that candoluminesce in methane-air flames or in hydrogen flames were run on a number of commercial phosphors and on others prepared in our laboratories. The latter were principally rare earths - pure and in calcium oxide. The phosphors were spread on fire-brick slabs and on copper strips - the latter to hold down the temperature of the phosphor at least momentarily - and tested by impingement in both hydrogen and methane-air flames. Several phosphors that candoluminesce in both flames were found. Detailed results are shown in Tables 1 and 2. These results should be regarded as tentative rather than conclusive.

A few additional phosphors not listed in the tables were tested. Three General Electric silver-activated zinc sulfides (Nos. 118-2-3, 118-2-11, and 118-3-1) showed emission in the blue. Their spectra, obtained with a hydrogen diffusion flame on a fritted glass disk, showed that the emission was the band spectrum of S₂ and that no candoluminescence was present (6). The S₂ was undoubtedly formed by decomposition of the phosphor. Zinc sulfide activated by silver and copper showed both candoluminescence and the band spectrum of S₂ (Figure 2). A boron nitride sample from Carborundum Co., Electronics Division showed weak, green luminescence in hydrogen and methane flames. Two recently developed rare earth phosphors, (Y_{0.9}Eu_{0.1})₂O₃·WO₃ and (Gd_{0.8}Eu_{0.2})₂O₃·MoO₃ were prepared and tested (4). Both luminesced red in hydrogen and methane flames on the fire-brick strip.

Light emission in some of the screening tests may have had a source other than candoluminescence. The emission from magnesium germanate was probably thermal. This is indicated by the color of the emission (white to yellowish white), by the absence of a maximum of emission intensity with increasing temperature of the phosphor, and by equal emission when the phosphor is heated to the same temperature with or without the flame. For this test, the phosphor was mounted on the electrically heated silicon carbide rod, and temperature equivalence was indicated by the emission of the phosphor at 2.25 microns. Light

Table 1. LIGHT EMISSION OF YTTRIUM OXIDE AND RARE EARTHS (Pure and in CaO) IN HYDROGEN AND METHANE-AIR FLAMES

Element	Atomic No.	Symbol	Metal Conc in CaO, wt %	Light Emission				Color
				With H ₂		With CH ₄ -Air		
				On Cu Strip	On Fire Brick	On Cu Strip	On Fire Brick	
Yttrium	39	Y	0.2 1.0 PO*	Trace Trace Weak	Weak Trace Trace	Nil Nil Trace	Nil Nil Nil	Violet Violet Green and Orange
Lanthanum	57	La	0.2 1.0 PO	Trace Trace Weak	Weak Trace Trace	Nil Nil Nil	Nil Nil Nil	Lavender Lavender Green and Orange
Praseodymium	59	Pr	0.2 1.0 PO	Trace Trace Nil	Strong Strong Trace	Nil Trace Nil	Strong Strong Nil	Red Red Red
Neodymium	60	Nd	0.2 1.0 PO	Trace Trace Nil	Trace Weak Trace	Nil Nil Nil	Nil Nil Nil	Violet Lavender Red
Samarium	62	Sm	0.2 1.0 PO	Trace Trace Nil	Trace Trace Nil	Trace Nil Nil	Trace Trace Nil	Orange Orange --
Gadolinium	64	Gd	0.2 1.0 PO	Trace Trace Strong	Trace Weak Strong	Nil Nil Trace	Nil Nil Weak	Violet Violet Red
Dysprosium	66	Dy	0.2 1.0 PO	Trace Trace Nil	Trace Weak Nil	Nil Nil Nil	Nil Nil Nil	Lavender Blue --
Holmium	67	Ho	0.2 1.0 PO	Trace Trace Nil	Trace Weak Trace	Nil Nil Nil	Nil Nil Trace	Aqua to Blue Aqua Red
Erbium	68	Er	0.2 1.0 PO	Trace Trace Nil	Trace Weak Trace	Nil Nil Nil	Nil Nil Nil	Blue White Red
Ytterbium	70	Yb	0.2 1.0 PO	Trace Trace Nil	Trace Trace Nil	Nil Nil Nil	Nil Trace Nil	Lavender Red --

* Pure oxide.

emission in a few cases may be caused by decomposition of the phosphor, as was shown in the case of the silver-activated zinc sulfides.

The manganese-activated zinc phosphate (Sylvania No. 151) phosphor appeared to give the most intense luminescence emission in methane-air flames of any tested, and, accordingly, its light emission was investigated further. When the phosphor was coated on a fritted disk and the disk used as a porous-plate burner, a steady emission was obtained with a hydrogen diffusion flame. However, no emission could be obtained in this manner when the fritted-disk burner was fed with pure methane or with a methane-air mixture. Only when the phosphor was brought into a Bunsen flame was the light emission observed. We do not know the cause of this effect. A greater concentration of hydrogen atoms in the hydrogen flame may play a role. The high diffusivity and other properties of hydrogen that cause its flame to burn closer to the solid surface may be of equal or greater importance.

Spectra recorded with the Beckman DK-2 spectrophotometer were used to compare the light emission of this phosphor in the hydrogen flame with its emission in the methane-air flame. The phosphor was coated on a silicon carbide rod for this experiment. No significant difference other than that of the emission from the flame itself was observed (Figure 3).

The effect of temperature on the light emission of the phosphor was investigated by electrically heating the silicon carbide rod. With a methane-air flame impinging on the phosphor-coated rod, and with the spectrophotometer focused on the rod near one of its water-cooled ends, the light emission increased to a maximum with an increase in electrical heating, then decreased to near extinction with further heating. This agrees with the observation of Neunhoeffler (9) that the hydrogen flame candoluminescence of calcium oxide impregnated with various activators exhibits temperature maxima.

When the phosphor was heated to a still higher temperature, thermal emission appeared. When the emission of the phosphor was corrected for the emission of the flame, no essential difference in emission at high temperatures with and without the flame was evident. These experiments indicated that the low-temperature light emission experienced with this phosphor is candoluminescence, but that candoluminescence is not involved in the high-temperature emission.

This phosphor was the only one of several tested that luminesced in a carbon monoxide flame. The question of excitation in this flame by high-energy species other than hydrogen atoms was not pursued.

Spectra of the luminescences from several phosphors excited by hydrogen burning on the surface of a sintered glass disk were obtained, and the effect of the addition of small amounts of carbon monoxide and methane to the fuel was observed. The phosphors were calcium silicate activated with lead and manganese (Sylvania No. 290), calcium oxide activated with ytterbium, calcium oxide activated with praseodymium, and calcium oxide activated with samarium. The spectra obtained from the first three of these phosphors when they are excited with pure hydrogen burning on a fritted disk are shown in Figure 4. The Sylvania No. 290 phosphor emits with a broad peak in the green. Praseodymium-activated calcium oxide shows two peaks - one at 595 millimicrons (yellow) and a weaker one at 490 millimicrons (blue-green). Ytterbium-

547
activated calcium oxide also shows two peaks - one at 375 millimicrons, which is in the ultraviolet. Samarium-activated calcium oxide also emits with a similar peak in the ultraviolet and another at 570 millimicrons (yellow), as shown in Figure 5.

The effect of the addition of small amounts (1 to 10 volume percent) of carbon monoxide or methane to the hydrogen burning on the fritted disk was different for each of these phosphors. Luminescence of the Sylvania No. 290 phosphor was substantially unchanged with addition of as much as 10% of the carbon monoxide or methane. Luminescence of the praseodymium-activated calcium oxide was not greatly affected by addition of 1% of the carbon monoxide or methane, but decreased rapidly with greater amounts. Only about 10% of the original intensity was obtained with 6% carbon monoxide or 8% methane. The luminescence of the ytterbium-activated calcium oxide was even more strongly quenched by the addition of carbon monoxide or methane. With these phosphors, only the intensity of the luminescence was affected.

With samarium-activated calcium oxide, the spectral distribution of the luminescence was also affected, as shown in Figure 5. Upon the addition of carbon monoxide, emission by this phosphor in both wavelength regions decreased in intensity, and, at about 3% carbon monoxide, emission in the 375-millimicron region had virtually disappeared. The 570-millimicron peak, however, was replaced by two narrower emission bands with peaks at about 560 and 595 millimicrons. With further addition of carbon monoxide the intensity of this emission increased to a maximum several times more intense than the original peak emission, then decreased. These effects were not observed upon the addition of methane to the flame. The variation of the intensity of the luminescence in the two cases is shown in Figure 6.

At a late stage of the work, phosphors were deposited by settling from a water suspension onto a water-cooled copper plate. A few spectra were obtained in this way with methane-air excitation.

Enhancement of the luminescence from the manganese-activated zinc silicate (Sylvania No. 161) by the cooling of the copper plate was very pronounced. (Figure 7).

ACKNOWLEDGMENT

The author wishes to thank the American Gas Association for their support and for permission to publish these results. John Hasenberg did most of the experimental work. Peter Mrdjin identified the S₂ bands in the spectra of the zinc sulfide phosphors.

1. Arthur, J. R. and Townend, D.T.A., "Fundamental Aspects of Combustion - Some Reactions of Atomic Hydrogen in Flames," J. Inst. Fuel 26, 44-51, 61 (1953) July.
2. Arthur, J. R. and Townend, D.T.A., "Some Reactions of Atomic Hydrogen in Flames," in U.S. Natl. Bur. Standards, Circ. 523, "Energy Transfer in Hot Gases," 99-110. Washington, D.C.: Govt. Print. Office, 1954.
3. Balmain, W. H., "Observations on the Formation of Compounds of Boron and Silicon With Nitrogen and Certain Metals," Phil. Mag. 21, 270-77 (1842).
4. Borchardt, H. J., "Rare Earth Phosphors," J. Chem. Phys. 38, 1251 (1953) March 1.
5. Donau, J., "New Kind of Luminescence of Alkaline Earth Preparation, Especially Calcium Preparations Which Contain Bismuth or Manganese Brought Out by the Hydrogen Flame; as Well as the Detection of Traces of the Latter," Monatsh. 34, 949-55 (1913).
6. Gaydon, A. G., The Spectroscopy of Flames, 244. New York: John Wiley, 1957.
7. Gorban, A. N. and Sokolov, V. A., "On the Question of the Physico-Chemical Nature of Candoluminescence," Opt. Spectr. (U.S.S.R.) English Transl. 7, 164-65 (1959) August.
8. Minchin, L. T., "Luminescence of Oxides Under Flame Excitation," Trans. Faraday Soc. 35, 163-70 (1939); "Luminescence of Substances Under Flame Excitation," Trans. Faraday Soc. 36, 505-06 (1940).
9. Neunhoeffler, O., "The Hydrogen Flame as a Source of Electrons," Z. Physik. Chem. 197, 179-85 (1951).
10. Nichols, E. L., Howes, H. L. and Wilber, D. T., "Cathodo-luminescence and the Luminescence of Incandescent Solids," Carnegie Inst. Publ. No. 348 (1928).
11. Smith, E.C.W., "The Radiation From Solid Substances Under Flame Impact: Part 1," Institution of Gas Engineers Comm. 237. London, 1941; Gas J. 233, 202-05, 247, 250-51, 256, 293, 298 (1941).
12. Sokolov, V. A., "Candoluminescence From the Viewpoint of the Vavilov-Wiedemann Criterion and of Contemporary Physicochemical Ideas," Izv. Akad. Nauk. U.S.S.R., Ser. Fiz. 26, 514-17 (1962).
13. Sokolov, V. A., Grozina, I. S. and Gorban, A. N., "The Nature of Candoluminescence of Calcium Oxide," Izv. Tomskogo Politekhn. Inst. 95, 253-56 (1958).
14. Tiede, E. and Buescher, F., "Inorganic Luminescent Phenomena. II. Luminous Boron Nitride (Balmain's Aethogen and the Flame Excitation of Luminescence)," Ber. 53B, 2206-14 (1920).

15. Wise, H. and Rosser, W. A., "Homogeneous and Heterogeneous Reactions of Flame Intermediates," in Ninth Symposium (International) on Combustion, 733-42. New York: Academic Press, 1963.

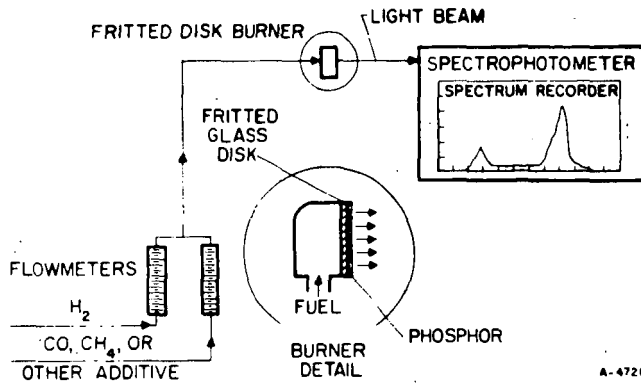


Figure 1. SCHEMATIC REPRESENTATION OF THE POROUS BURNER APPARATUS FOR LIGHT EMISSION STUDIES

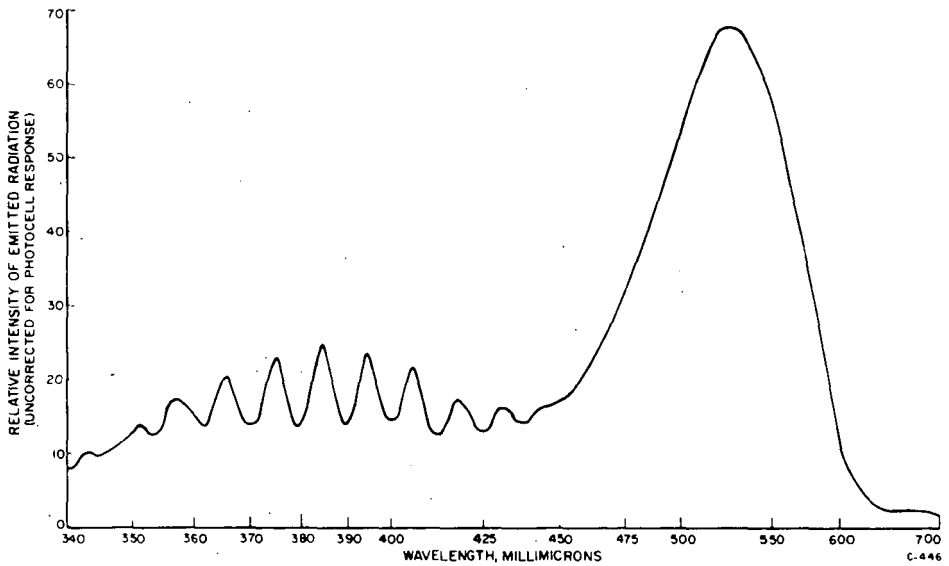


Figure 2. EMISSION SPECTRUM OF ZnS:Cu:Ag EXCITED BY A HYDROGEN DIFFUSION FLAME

15. Wise, H. and Rosser, W. A., "Homogeneous and Heterogeneous Reactions of Flame Intermediates," in Ninth Symposium (International) on Combustion, 733-42. New York: Academic Press, 1963.

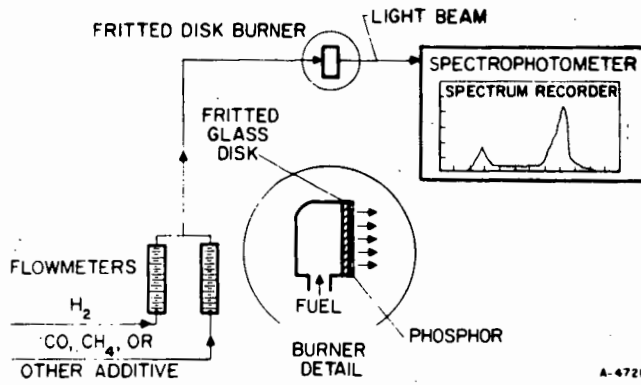


Figure 1. SCHEMATIC REPRESENTATION OF THE POROUS BURNER APPARATUS FOR LIGHT EMISSION STUDIES

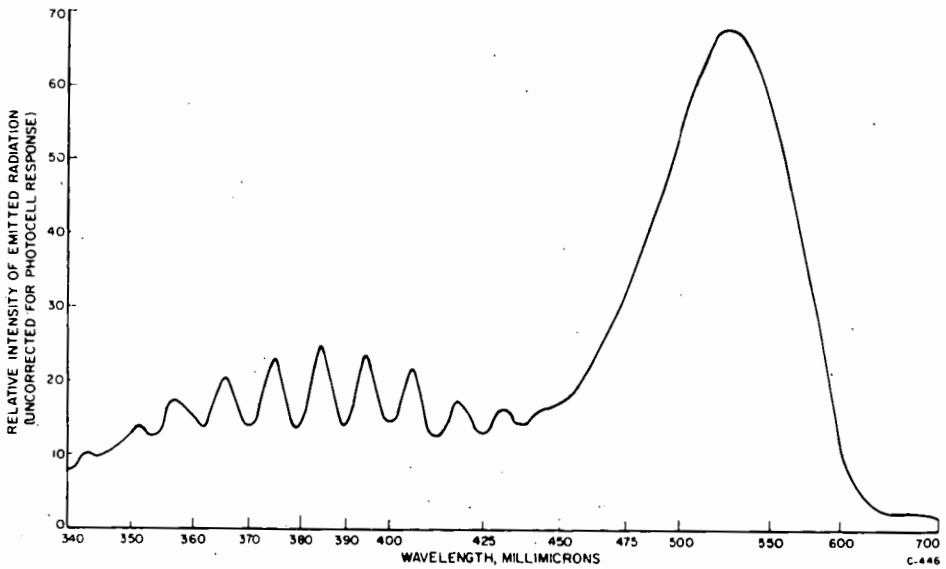


Figure 2. EMISSION SPECTRUM OF ZnS:Cu:Ag EXCITED BY A HYDROGEN DIFFUSION FLAME

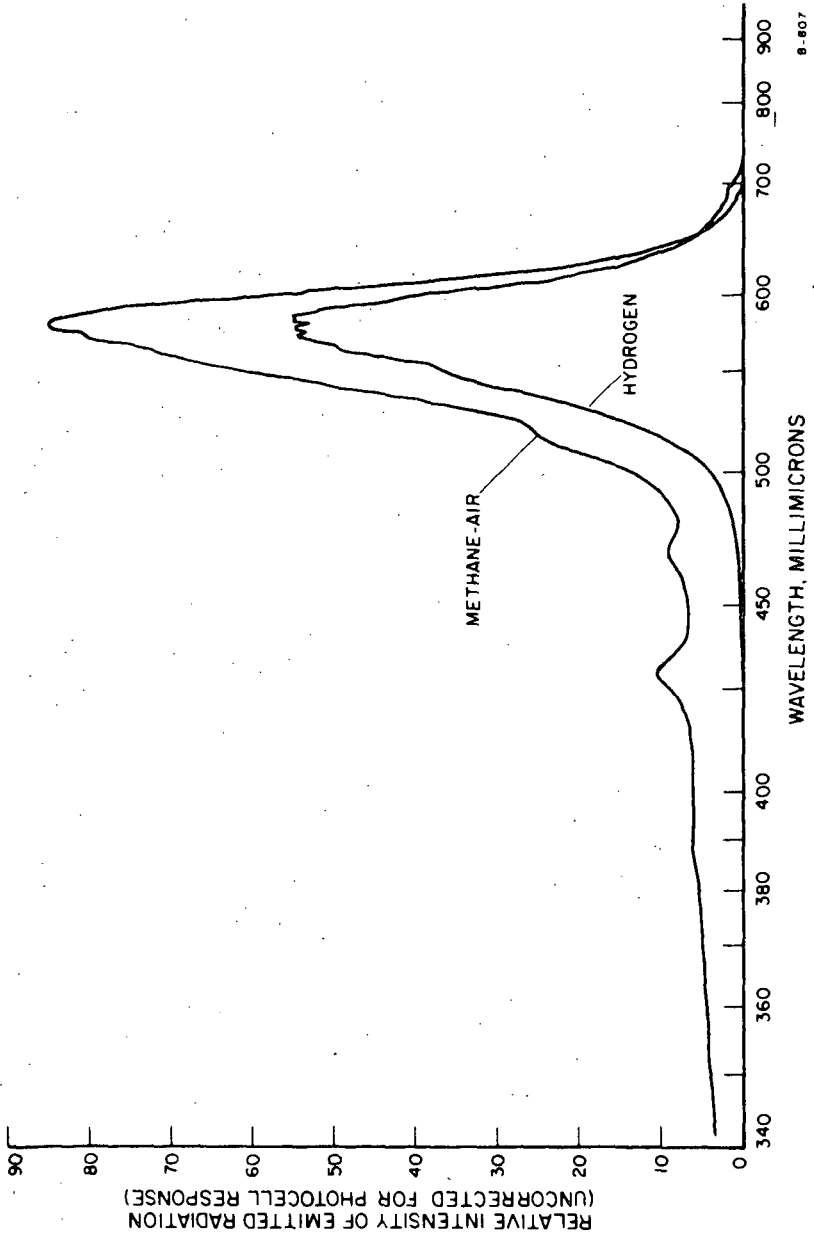


Figure 3. EMISSION SPECTRA OF SYLVANIA NO. 151 PHOSPHOR EXCITED BY HYDROGEN AND METHANE-AIR FLAMES

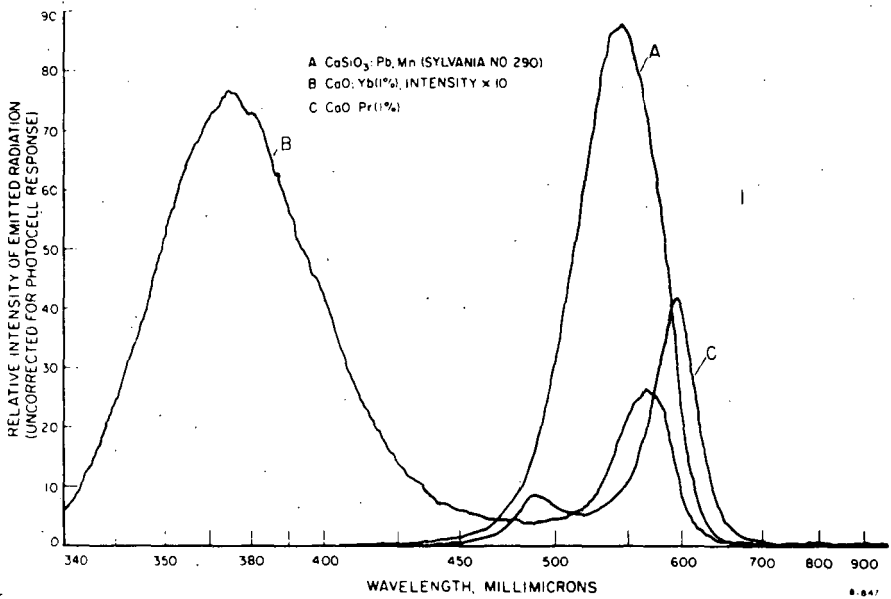


Figure 4. EMISSION SPECTRA OF PHOSPHORS EXCITED BY A HYDROGEN DIFFUSION FLAME

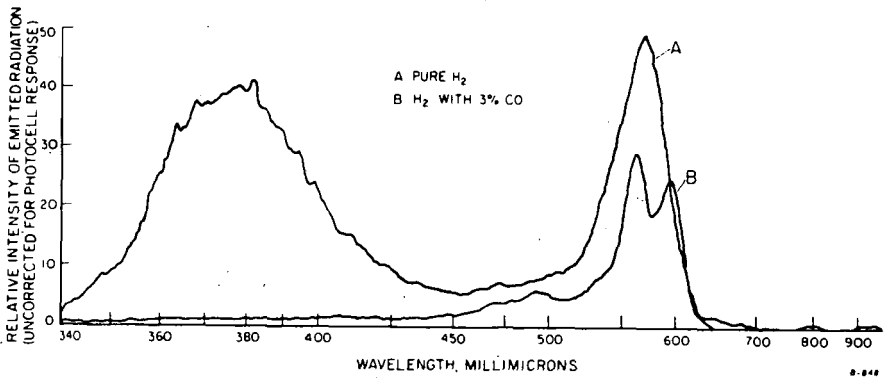


Figure 5. EFFECT OF CARBON MONOXIDE ON THE EMISSION SPECTRUM OF SAMARIUM-ACTIVATED CALCIUM OXIDE

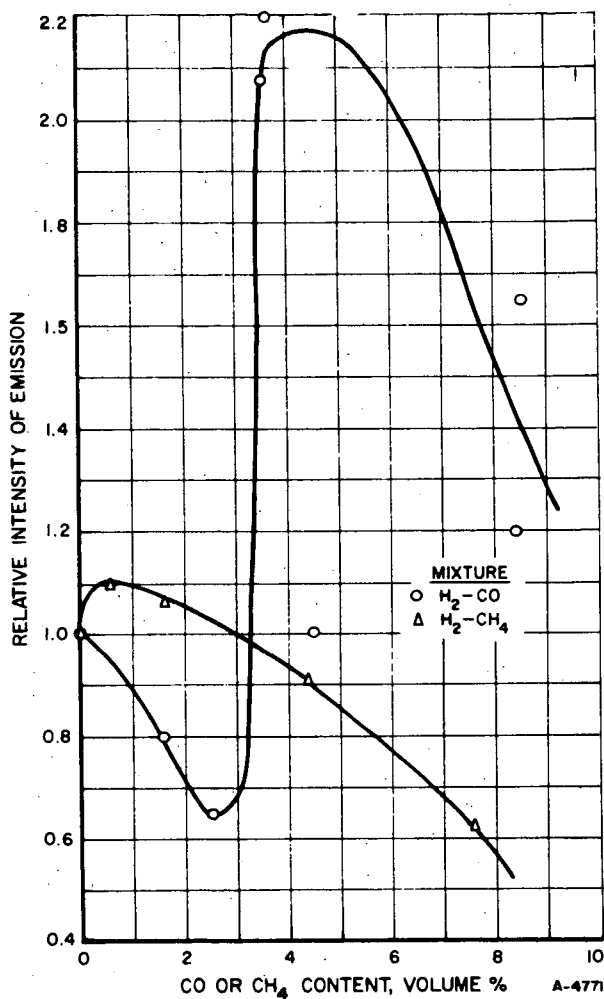


Figure 6. EFFECT OF FUEL COMPOSITION ON THE CANDOLUMINESCENCE OF SAMARIUM-ACTIVATED CALCIUM OXIDE

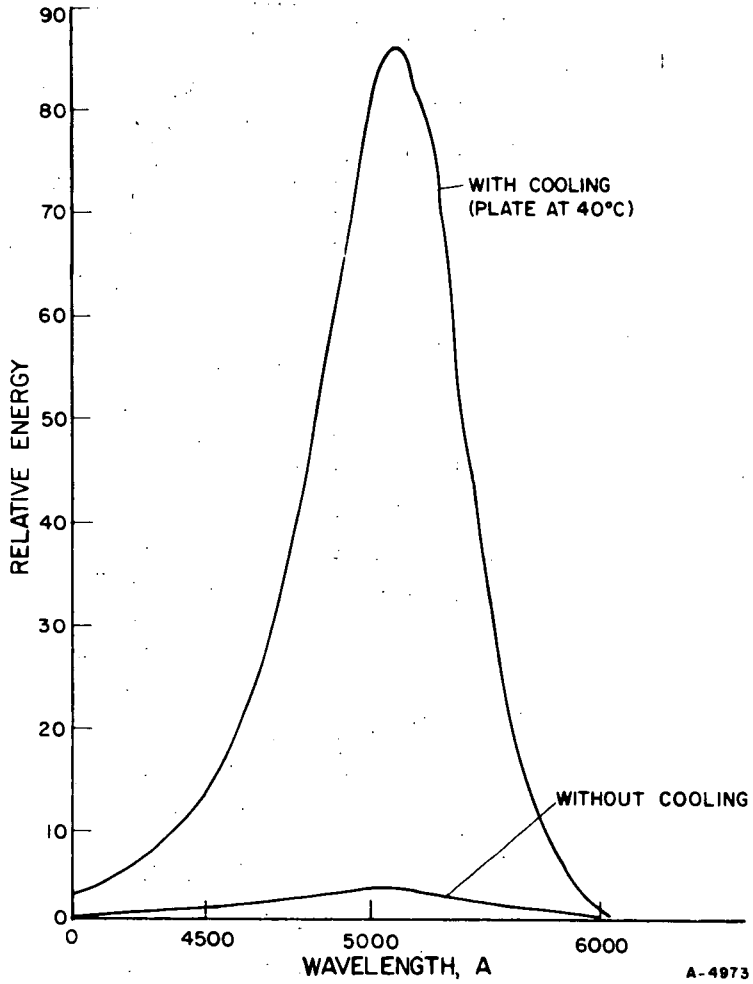


Figure 7. THE EFFECT OF TEMPERATURE ON THE EMISSION SPECTRUM OF SYLVANIA NO. 161 PHOSPHOR EXCITED BY A METHANE-AIR FLAME

A RAPID, SIMPLE METHOD FOR THE DETERMINATION
OF THE THERMAL CONDUCTIVITY OF SOLIDS

Neal D. Smith
Fay Fun
Robert M. Visokey

UNITED STATES STEEL CORPORATION
Research Center
Monroeville, Pennsylvania

The rational design of equipment such as shaft coolers, heaters, and rotary kilns for the heating and cooling of solids requires that the thermal properties of the solids be known. Thermal conductivity is one of these properties that to measure necessitates elaborate equipment and time-consuming techniques.

A rapid, simple method has been developed for determining the thermal conductivity of solids. The solids can be either porous or non-porous and of either high or low conductivity. If high-conductivity materials are tested, then both the thermal conductivity and heat capacity can be simultaneously measured by the method.

The procedure involves preparing a cylindrical briquette of the test solid that has a thermocouple located in the center. This briquette is heated to a constant temperature after which it is suspended in an open-end glass tube and cooled by a known flow of nitrogen or any other nonreactive gas. The thermal conductivity is then computed from a digital computer comparison of the cooling curves for the test solid versus a reference solid of known thermal properties and similar size that has undergone the same heating and cooling cycle. The method was validated by using the known thermal properties of lead, aluminum, and silver and computing the theoretical cooling curves. The theoretical curves were in close agreement with the experimentally measured cooling curves for these materials.

Theory

The mathematical basis for determining thermal conductivity by the described method is discussed in a paper by Newman¹⁾ and is summarized as follows. Consider a cylindrical briquette as shown in Figure 1. The differential equation for unsteady state heat transfer by conduction in the x-direction is (see nomenclature for definition of the variables):

$$\frac{\partial t}{\partial \theta} = \alpha \left(\frac{\partial^2 t}{\partial x^2} \right) \quad (1)$$

For a briquette of thickness $2a$, the central plane being at $x = 0$ and assuming:

- 1) uniform temperature at the start of cooling of the initially hot briquette

then $t = t_0$ when $\theta = 0$ (2)

2) the final temperature of the briquette will be the temperature of the surroundings:

therefore $t = t_s$ when $\theta = \infty$ (3)

3) there is no heat flow across the central plane because of symmetry:

consequently $-k \left(\frac{\partial t}{\partial x} \right) = 0$ at $x = 0$ (4)

The heat balance on the briquette surface is made by equating heat transferred to the surface by conduction with heat transferred from the surface by convection. In differential form, the heat balance is:

$$-k \left(\frac{\partial t}{\partial x} \right) = h (t - t_s) \text{ at } x = \pm a \quad (5)$$

Newman¹⁾ showed that the solution to Equations (1) through (5) expressed in terms of a dimensionless temperature ratio Y_x is:

$$Y_x = \frac{t - t_s}{t_0 - t_s} = 2 \sum_{n=1}^{\infty} A_n e^{-(\beta_n^2 X_a)} \cos(\beta_n \frac{x}{a}) \quad (6)$$

where $A_n = \frac{m_a}{(1 + \beta_n^2 m_a^2 + m_a) \cos \beta_n}$ and

β_n are defined as the first, second, third, etc., roots of the transcendental equation:

$$\beta_n \text{TAN } \beta_n - 1/m_a = 0 \quad (7)$$

The surface to solid thermal resistance ratio, m_a , is defined as:

$$m_a = k/ha \quad (8)$$

and X_a is defined as: $X_a = \alpha \theta / a^2$ (9)

where the thermal diffusivity is: $\alpha = k/\rho C_p$ (10)

Similarly, considering radial heat transfer, the radial briquette heat balance is

$$\frac{\partial t}{\partial \theta} = \alpha \left[\frac{\partial^2 t}{\partial r^2} + \frac{1}{r} \frac{\partial t}{\partial r} \right] \quad (11)$$

The initial condition equation is:

$$t = t_0 \text{ WHEN } \theta = 0 \quad (12)$$

The final temperature equation is:

$$t = t_s \text{ WHEN } \theta = \infty \quad (13)$$

The boundary condition equations are:

$$-k \left(\frac{\partial t}{\partial r} \right) = 0 \text{ AT } r = 0 \quad (14)$$

and
$$-k \left(\frac{\partial t}{\partial r} \right) = h(t - t_s) \text{ AT } r = R \quad (15)$$

Solving Equations (11) through (15) gives:

$$\frac{t - t_s}{t_0 - t_s} = 2 \sum_{n=1}^{\infty} A_n e^{-(\beta_n^2 X_r)} J_0(\beta_n \frac{r}{a}) = Y_r \quad (16)$$

where

$$A_n = \frac{m_r}{(1 + \beta_n^2 m_r^2) [J_0(\beta_n)]} \quad (17)$$

and β_n are the first, second, third, etc., roots of the equation:

$$\beta_n J_1(\beta_n) - 1/m_r J_0(\beta_n) = 0 \quad (18)$$

The surface to solid thermal resistance ratio, m_r is

$$m_r = k/hR \quad (19)$$

and

$$X_r = a\theta/R^2 \quad (20)$$

The complete differential equation for the case shown in Fig. 1 is:

$$\frac{\partial t}{\partial \theta} = a \left(\frac{\partial^2 t}{\partial r^2} + \frac{1}{r} \frac{\partial t}{\partial r} + \frac{\partial^2 t}{\partial x^2} \right) \quad (21)$$

and the solution to Equation (21) is:

$$Y = \frac{t - t_s}{t_0 - t_s} = Y_r \cdot Y_x \quad (22)$$

If the center temperature defined at $r = 0$, $x = 0$ is t_c , then eqn. 22 becomes:

$$Y_c = \frac{t_c - t_s}{t_0 - t_s} = Y_r \cdot Y_x \quad (23)$$

where Y_r and Y_x are evaluated at $r = 0$ and $x = 0$.

The preceding mathematical analysis shows that the rate of cooling, or change in center temperature for a cylindrical briquette is a function of time (θ), density (ρ), thermal conductivity (k), the surface heat transfer coefficient (h), specific heat (C_p) and the briquette dimensions as expressed by Equation (23).

The experimental technique can now be described in terms of the previous discussion. If the change in center temperature with time is measured experimentally for a material of known thermal and physical properties (standard briquette), the surface heat transfer coefficient can be calculated from Equation (23), since it is the only unknown.

The surface heat transfer coefficient (h) is a function of the flow rate of the cooling gas and the geometry and size of the briquette. It is independent of all other physical, thermal, or chemical properties of the briquette. Therefore, any other briquette having similar dimensions and cooled at the same flow rate will have the same value for (h).

Once (h) has been determined using the standard briquette, the thermal conductivity of any test material can be determined from Equation (23) since all other variables are known.

A computer program has been written which through an iterative process determines the best value of (h) which makes the calculated values for the dimensionless temperature ratio equal to the experimental values obtained when the standard briquette is cooled.

With (h) determined, another computer program is run for the test specimen. Thermal conductivity is now the unknown variable and through another iterative scheme, the best value for (k) that makes the calculated and experimental values for the temperature ratios equal is found.

The input data for both programs consist of density, specific heat, time, briquette dimensions, and several experimental values for the temperature ratio. The output from the first program (standard) is the best value for (h). Using this value for (h), the second program used to determine the k value for any test material. If a highly conductive material is tested, then it is possible to determine its heat capacity since the solid thermal resistance will be small compared to the surface thermal resistance. A transient heat balance can be written for the test solid cooling in a stream of coolant gas.

$$V\rho C_p \frac{dt}{d\theta} = hA(t - t_s) \quad (24)$$

In the above equation, $t = t_c$ since the thermal gradient in the solid is neglected. Integrating Equation (24) and using the dimensionless temperature ratio, Y_c gives:

$$Y_c = \exp(hA/\rho C_p V)\theta \quad (25)$$

Thus, if the internal solid thermal resistance is negligible, a plot of the experimental Y_c versus θ data on semilog paper should be linear as shown by Equation (25). The heat capacity, C_p , can be calculated from the slope of the line for Y_c versus θ since (h) is the same as for the standard briquette and the density, ρ , and total surface area, A , for the test material are also known.

Materials and Experimental Work

A primary advantage of the transient technique for determining thermal conductivities is the ease and swiftness with which the experiment can be conducted.

In so far as sample preparation is concerned, any solid that can be briquetted, cast, or fabricated around a centrally located rigid

thermocouple ($x = 0$; $r = 0$) may be tested. Finished test sample cylinders should be approximately one inch in diameter, and one-half inch in height; however, other dimensions can be used.

Experimental Apparatus

The experimental apparatus (see Figure 2) consists simply of a 3-inch diameter glass tube approximately 3 feet in length. One end of the tube is completely stoppered except for a one-half inch circular opening through which the coolant gas flows. The other end of the tube is open to the atmosphere. A small electric furnace is used to heat the briquette, and an automatic single point temperature recorder connected to the embedded thermocouple is used to measure the center temperature of the briquette.

Experimental Procedure

The experimental procedure is the same for both the standard and test briquettes. Either the standard (aluminum was chosen since its thermal properties are well established), or the test briquette is connected to the temperature recorder by way of the thermocouple leads. The briquette is heated until the center temperature has reached a constant, predetermined value. The briquette is then quickly removed from the furnace and suspended in the cooling tube with the cooling gas flowing at a constant rate. The briquette is usually cooled to the temperature of the cooling gas within 20 minutes.

Data Processing

For the standard briquette, the experimental dimensionless temperature ratio versus time data points for the standard briquette along with the known thermal properties are used to calculate the surface coefficient, h , in the following manner. A digital computer program is written to compute Y_c from Equations (6) through (23). By iteration and assuming various values of (h), the computed values of Y_c can be made to converge on each of selected experimental Y_c versus θ data points. Thus, for a selected data point, the best experimental (h) is that which when used in Equations (8) and (19) results in equal values for the computed and experimental Y_c values.

For low conductivity test materials, the same method is used to determine the best experimental value of k by using the h determined for the standard and the other properties of the test material. If the test material is a good conductor as discussed in the theory section, then experience has shown that h should be computed from the experimental cooling curve and then this value is used to compute k by the same method as for low conductivity test materials.

Discussion and Results

Three briquettes of aluminum, lead and silver were made to test the validity of the experimental technique since their thermal properties were available from the literature as shown in Table I. Sintered, dense hematite (Fe_2O_3) and a briquette of porous carbon made from a partially devolatilized coal were used as test materials. For these materials, all properties except the thermal conductivities shown in Table I were previously measured. Cooling curves for each briquette were measured for a nitrogen flow rate of 0.9 scfm. Surface heat transfer coefficients for lead, silver and aluminum were calculated by the method discussed in the data processing section. For these materials, the literature conductivity values were used to calculate the surface coefficient. Table I shows that the calculated or experimental h values for each metal are nearly identical. This result is consistent with the theoretical basis of the experiment and may be considered as establishing the validity of the method. Also as additional evidence, aluminum was chosen as the standard and k values for lead and silver were calculated using the h value for aluminum. Table I shows that the calculated or experimental k values were within 0.5 percent of the literature values. The conductivities for hematite and porous carbon were calculated using aluminum as the standard. Figure 3 shows the experimental data points with the solid lines calculated from the theory. Note that the line for the carbon is curved whereas those for the metals and hematite are linear. As discussed previously, a linear cooling curve is obtained if the surface to solid thermal resistance ratios are relatively large. Note that for the metals, lead which has the lowest conductivity and thermal diffusivity cooled the fastest. This result is explained by examination of eqn. (25) which shows that for similar gas flows and briquette dimensions, the rate of cooling for different materials is determined by the heat content, ρC_p . It can be seen in Table I that the heat content for lead is the lowest of all metals tested.

Summary

A rapid, simple method for determining thermal conductivity for a solid has been developed. The solid can be either porous or non-porous and of either high or low conductivity. If high conductivity materials are tested, then both conductivity and heat capacity can be simultaneously measured from one cooling experiment. The method was validated by using the known thermal properties of lead, aluminum, and silver and the experimental cooling curves in a comparison with the computed results.

References

1. Newman, A. B., Industrial and Engineering Chemistry, Vol. 28, 1936, pp. 545-548

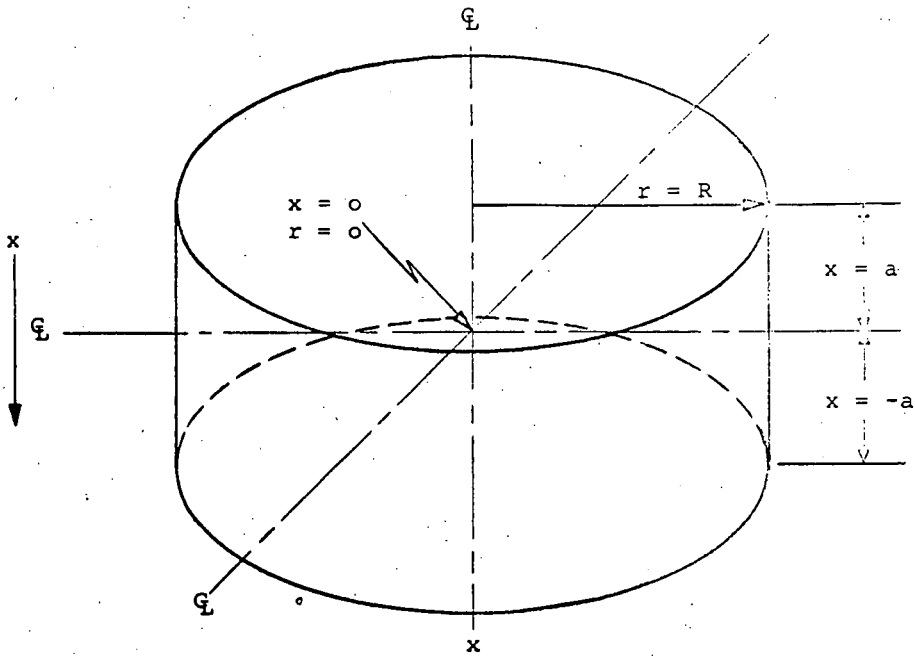
Nomenclature

- a = Half height of briquette; ft
 A = Area; ft²
 A_n = Coefficient in infinite series solution for temperature distribution in Briquette
 C_p = Specific heat; BTU/lb °F
 H = Overall heat transfer coefficient; BTU/hr ft² °F
 h = Surface heat transfer coefficient; BTU/hr ft² °F
 k = Thermal conductivity; BTU/hr ft² °F/ft
 m_a = Axial surface resistance; dimensionless
 m_r = Radial surface resistance; dimensionless
 Q = Heat flux; BTU/hr
 R = Maximum radius of briquette; ft
 r = Radius of briquette; ft
 s = Half width of infinite plate; ft
 t = Temperature; °F
 t_c = Temperature at center of briquette; °F
 t_o = Initial temperature of briquette; °F
 t_s = Temperature of cooling gas; °F
 x = Distance of direction; ft
 X_o = $\frac{a\theta}{\alpha^2}$ Dimensionless time parameter for axial component
 X_r = $\frac{a\theta}{r^2}$ Dimensionless time parameter for radial component
 Y_x = Symbol for temperature ratio, axial component; dimensionless
 Y_r = Symbol for temperature ratio, radial component; dimensionless
 α = $(k/\rho C_p)$ Thermal diffusivity; ft²/hr
 θ = Time; minutes or hours
 ρ = Density; lb/ft³

Table I
THERMAL AND PHYSICAL PROPERTIES FOR THE BRIQUETTES

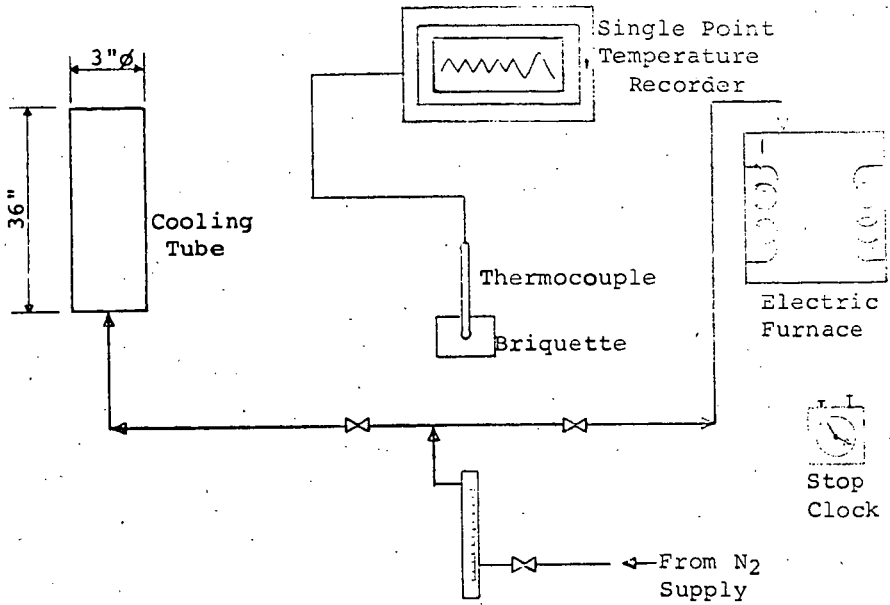
	Aluminum	Silver	Lead	Hematite	Porous Carbon
a	.01842	.02059	.01842	.01842	.01958
R	.04208	.04210	.04117	.04208	.04121
ρ	168.50	655.20	707.43	306.00	75.0
C_p	.2273	.0578	.0306	.2090	.2360
ρC_p	38.30	39.31	21.65	63.95	17.70
h (experimental)	5.58	5.70	5.60	5.58	5.58
k (experimental)		240.3	18.99	12.10	.0307
k (literature)	121.7	240.0	19.00	none	none
α (experimental)	3.178*	6.113	.8770	.1892	.00173

* Average of literature sources



STANDARD CYLINDRICAL BRIQUETTE

Figure 1



EXPERIMENTAL APPARATUS

Figure 2

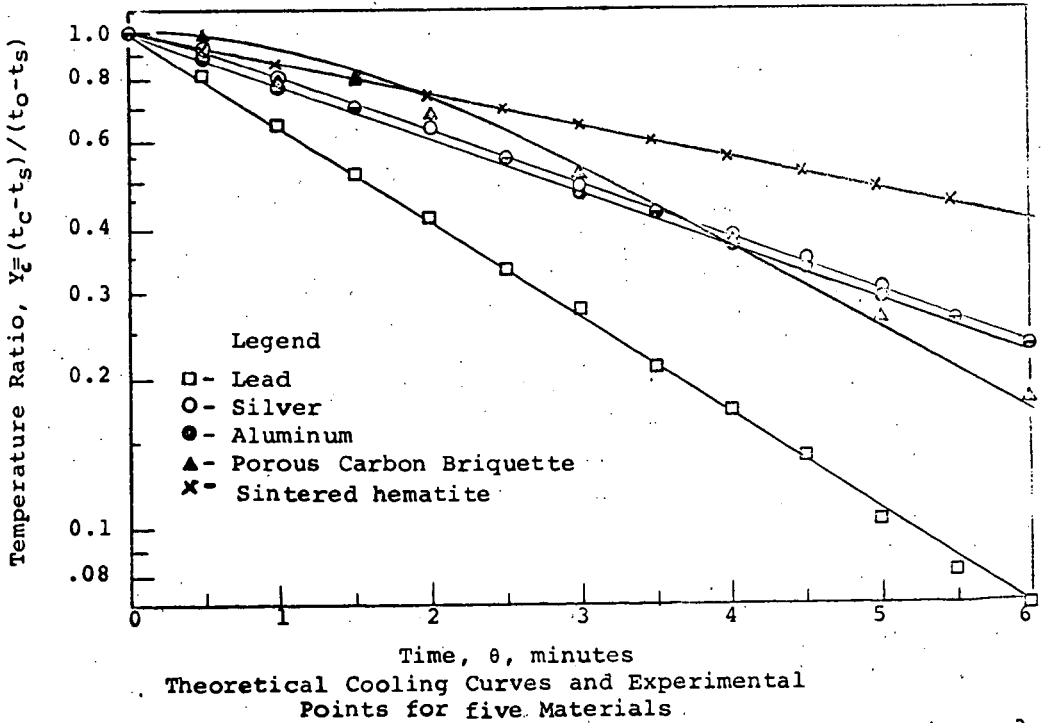


Figure 3